THE UNIVERSITY OF MICHIGAN

INDUSTRY PROGRAM OF THE COLLEGE OF ENGINEERING

COLLAPSE OF A CAVITATION BUBBLE IN VISCOUS, COMPRESSIBLE LIQUID -- NUMERICAL AND EXPERIMENTAL ANALYSES

Richard D. Ivany

A dissertation submitted in partial fulfillment
of the requirements for the degree of
Doctor of Philosophy in the
University of Michigan
Department of Nuclear Engineering
1965

April, 1965

IP-699

Doctoral Committee:

Professor Frederick G. Hammitt, Chairman
Associate Professor Julian R. Frederick
Associate Professor Terry Kammash
Associate Professor Herman Merte, Jr.

ACKNOWLEDGEMENTS

The financial support of grants from the National Aeronautics and Space Administration and from the National Science Foundation in this work is appreciated.

The conception of this work by Professor F. G. Hammitt and his assistance in carrying it out is appreciated.

Thanks also are due M. J. Robinson for his assistance in the operation and fabrication of the equipment and to D. M. Ericson who fabricated some of the pressure measuring equipment.

The Industry Program of the College of Engineering and especially D. Danford deserves particular credit for the preparation of this manuscript.

TABLE OF CONTENTS

TABLE OF CONTENTS (CON'T)

LIST OF FIGURES

LIST OF FIGURES (CON'T)

LIST OF FIGURES (CON'T)

LIST OF FIGURES (CON'T)

NOMENCLATURE

B	Constant in Equation of State (Equation 37)
c	Sonic Velocity
h	Enthalpy (Equation 27)
H	Enthalpy at Bubble Wall
n	Constant in Equation of State (Equation 37)
P	Liquid Pressure at Bubble Wall
p	Pressure in liquid near wall
p_o	Pressure inside bubble
p_∞	Pressure in liquid far from bubble
R	Bubble radius
R_o	Initial Bubble Radius
r	Radius to point in liquid near bubble
t	Time
U	Radial Velocity of bubble wall
u	Radial Velocity of liquid near bubble
$\vec{V}$	Vector liquid velocity
Z	Characteristic quantity (Equation 41)
ρ	Liquid density
μ	Liquid shear viscosity
σ	Liquid surface tension
L	Latent heat
ρ_v	Vapor density
p_v	Vapor pressure

T	Temperature
C_p	Specific heat of liquid
κ	Thermal diffusivity

Normalized Quantities for Incompressible Equations

(denoted by primes)

$R' = R/R_o$		Bubble Radius
$r' = r/R$		Radius to point in liquid
$t' = t/R_o\sqrt{\frac{p_\infty(R_o)-p_o(R_o)}{\rho}}$		Time
$U' = U\sqrt{\frac{p_\infty(R_o)-p_o(R_o)}{\rho}}$		Bubble wall velocity
$p' = \frac{p}{p_\infty(R_o)-p_o(R_o)}$		Pressure in liquid near bubble wall
$\sigma' = \frac{\sigma}{R_o[p_\infty(R_o)-p_o(R_o)]}$		Surface tension
$\mu' = \frac{4\mu}{R_o\sqrt{\rho(p_\infty(R_o)-p_o(R_o))}}$		Liquid Viscosity

I. INTRODUCTION AND LITERATURE SURVEY

A. Introduction

Cavitation bubbles referred to herein are approximately spherical cavities or voids within a body of liquid where the behavior of the interface of a bubble is governed primarily but not completely by the inertia and pressure of the liquid. The bubbles are formed by suitably superheating the liquid by means of lowering the liquid static pressure below the vapor pressure while the bulk liquid temperature remains essentially constant. The behavior of the interface after the bubble is formed and starts to collapse and the behavior of the liquid adjacent to the interface are the main concerns here.

A cavitating venturi was used in the work described here, but there are many other hydraulic machines where similar liquid conditions exist to form cavitating flows. Among these are pumps, high speed marine propellers, spillways and turbines at dams, hydrofoils, etc. If other conditions are considered, where bubbles are formed by superheating the liquid by raising its temperature to the boiling point while maintaining essentially constant pressure, then the applications when such conditions occur become innumerable. Among these are the multitudes of boiling heat transfer applications, where the analysis concerns single vapor bubbles growing in liquid at saturation temperatures and pressures. A third area of investigation involves single bubbles containing mostly gas other than the vapor of the liquid in which they exist. Such bubbles may grow from solutions of gas in liquid as in carbonated beverages or by injection of gas bubbles into the liquid as in injection cooling used in cryogenics work.

Some situations in which bubble behavior has recently become particularly important involve nuclear reactors and nuclear particle research. The application of nuclear reactors to high temperature liquid metal Rankine-cycle power plants for use in space has initiated considerable effort in cavitation research in regard to both cavitation damage in pumps, valves, etc. and cavitation effects upon performance of such components. High power density reactor cores, especially in fast reactors, require liquid metal coolants to effectively remove the heat. The performance of liquid metals in such situations where cavitation might occur cannot be reliably predicted on the basis of any known scaling laws, and in high performance systems cavitation damage may occur. For example, in the Fermi sodium cooled fast breeder reactor, pitting was observed on the fuel element nozzle seats of the core support plate. A study indicated that mis-seating of the nozzles permitted sodium flow across the seats through a convergent-divergent passage as a venturi and that, very likely, cavitation damage occurred.

The related areas of bubble dynamics in the nucleation and growth of vapor and/or gas bubbles in radiation fields becomes important when considering homogeneous liquid reactors and the evolution of radiolytic gases, especially during transient power operation. In water cooled solid fuel reactors, the associated problem of bubble growth by heat transfer at the fuel surface, with the attendant nuclear reactivity effect, especially for rapid transient conditions, is closely related to the pure cavitation bubble dynamics problems. The nucleation of bubbles in a supersaturated liquid by passage of nuclear particles, as in the

familiar bubble chamber, is also a related bubble-dynamics phenomenon. While all these areas of bubble investigation are related, the relative significance of the various physical parameters involved changes with the application, and only those parameters important in single cavitation bubbles will be considered here.

B. Historical Recognition of Cavitation

One of the first references to the fact that rotating hydraulic machinery might promote localized low pressure regions, in water which would result in voids or cavities was made by Leonhard Euler in 1754[1]. In 1894 Reynolds[2] considered the sound from a kettle of water as it was heated to boiling. He concluded that the "harsh hiss" which occurs at about 10°F below the boiling point comes from vapor bubbles which are formed at the heated bottom kettle surface and then rise and collapse suddenly in the colder water above. The hiss represents many bubbles, each of which gives a sharp click when it collapses. He then presented further evidence on the source of the hissing noise from pipes at room temperature by demonstrating that water flowing through a small glass tube venturi type restriction also produced a hissing. This noise coincided with the appearance at the restriction of a white spot which Reynolds attributed to a fog of air-vapor bubbles formed in the low pressure region. The hissing he attributed to the collapse of these bubbles in the higher pressure liquid downstream of the restriction.

In 1895 Sir John Thornycroft and S. W. Barnaby[3], in England, presented a paper on the screw trials of the new torpedo-boat destroyer, Daring, in which they postulated that the reason for her poor performance

was the inefficiency and loss of power caused by the formation of cavities in the water. R. E. Froude initiated the use of the work "cavitation" to describe this phenomenon. Barnaby[4] discussed the later trials of the Daring in 1898. By increasing the blade surface area by 45 percent, the same speed could be obtained as with the original screws, 24 knots, but with the horsepower reduced from 3700 to 3050, indicating the magnitude of the effect of cavitation on performance. At the same r.p.m., the speed was increased to 28.4 knots.

In January, 1894, Sir Charles Parsons[5] formed a syndicate to test applications of steam turbines to marine propulsion, and the ship Turbinia was started. In a recent review of Parson's work, L. C. Burrill[6] indicates that even before the Turbinia was built, or cavitation was recognized, Parsons anticipated that the high speed of the turbine drive would require several fine pitched screws on a shaft in order to obtain a sufficient blade area to provide the required thrust. The initial trials of the Turbinia were unsuccessful in that power consumption was excessive for the low ship speed attained. After considerable experimentation with various configurations, Parsons decided on three separate shafts each with three screws, and driven by three turbines. In conjunction with these experiments, Parsons ran a two inch diameter model screw in water within a few degrees of boiling, and photographically observed the formation of cavities behind the leading edge of the screw near the blade tip. At higher r.p.m., a complete vapor cavity was formed with almost all the power going into maintaining the

cavity. Thus, Parsons identified and solved the problem of cavitation on performance on high speed screws, and developed one of the first model tunnels for investigating cavitation of marine propellers.

In addition to loss of performance, another phenomenon became apparent as marine propulsion units became more powerful and operated at higher speeds. With propellers, and also with other rotating hydraulic machinery, the total vapor or cavity volume present for a noticeable loss in performance may be significant. But even if the performance is not noticeably affected, bubbles may form on the low pressure side of the blade and collapse as they move into the higher pressure region on the blade. The mechanical action of the bubbles collapsing on the blade surface causes pitting of the surface when the blade is on the verge of cavitation. In a paper presenting the results of a very extensive investigation into the possible causes of severe cases of propeller damage, Sir Charles Parsons and S. S. Cook[7] came to the firm conclusion that the damage was mechanical in nature and was caused by collapsing cavities. A. T. Quelch in the discussion of this paper said the large propellers his company made for the ocean liners Lusitania and Mauretania were quickly eroded two or three inches in depth. So rapid was the destruction that the blades would have had to be replaced two or three times a season. His conclusion on the damage was also that it was mechanical in nature and caused in part by streams of bubbles coming from cavitation off forward brackets and impinging on the propellers.

From the time of these first investigations on marine cavitation in the early twentieth century, innumerable situations have developed

where cavitation either is an unwanted phenomenon contributing to damage and loss of performance or is intentionally promoted and beneficial use made of the phenomenon. Many reviews consider the varied aspects of cavitation and erosion, vibration, noise etc.[8,9,10,11,12] Only those aspects of cavitation concerning the behavior of single bubbles will be considered here. No attempt will be made to theoretically extrapolate the results to liquid flows having so many bubbles that interaction between them may perturb the single bubble analysis. Also, large non-spherical, oscillating, attached cavities will not be considered. These restrictions will not greatly limit the value of the analysis as applied to cavitation damage, because the current major hypotheses for the damage involves the behavior of single bubbles.

C. Review of Theoretical Bubble Analyses

Besant[13] presented one of the earliest theoretical analyses on the motion of the liquid during the collapse of an empty spherical void or bubble. Rayleigh[14] gave a solution for this problem, which gives the velocity and pressure of the liquid, assuming the liquid is incompressible, inviscid, and has zero surface tension. The solution predicts infinitely high velocities for the liquid at the bubble wall as the radius of the bubble approaches zero. He also solved the problem for a bubble containing gas which is isothermally compressed as the bubble collapses and thus the gas arrests the bubble wall motion, and prevents infinitely high velocities. Cook[7] also solved the problem of spherical collapse, and assumed that the bubble wall struck a rigid concentric sphere after collapsing part way, thereby eliminating the

difficulty of an infinite liquid velocity. At the instant of contact he introduced liquid compressibility into the problem and calculated the resulting pressure on the rigid sphere. Lamb[15] has also presented Rayleigh's results, and has gone further to obtain the motion of an expanding bubble where there is internal gas at a pressure greater than the liquid pressure. In this expanding bubble, Lamb[16] used an adiabatic gas expansion from an initially high pressure to represent a submarine explosion.

Beeching[17] considered a Rayleigh type analysis and included the effect of surface tension at the bubble wall as well as both adiabatic and isothermal compression of gas within the bubble. His conclusion on surface tension was that it was negligible unless the pressure differential between the liquid far from the bubble and the constant assumed internal pressure were very small.

Noltingk and Neppiras[18] considered cavitation in an incompressible liquid caused by ultrasonic vibration. In this case they gave numerical solutions for the Rayleigh type equations with surface tension for an alternating pressure in the liquid away from the bubble which caused the bubble to oscillate when it contained a compressed gas. For a given ultrasonic frequency, the initial radius of the bubble will determine whether or not the bubble collapses completely during one cycle of the imposed pressure field. Or, for a given initial bubble size, a bubble resonant frequency can be calculated. If the ultrasonic pressure frequency is greater than the bubble resonant frequency the bubble will

oscillate irregularly during collapse and expansion, and if the ultrasonic frequency is less than the bubble resonant frequency, the bubble will collapse completely during one cycle.

Poritsky[19] presented the first analysis of single bubble collapse which considered liquid viscosity. As in the Rayleigh analysis he assumed an incompressible liquid. In the Rayleigh solution, the velocity at the bubble wall for a given value of the ratio of bubble radius to initial radius can be obtained for any initial bubble size or liquid pressure from a single solution to the suitably normalized differential equation. However, the introduction of surface tension and/or viscosity introduces a scaling effect into the equation through two normalized parameters containing the surface tension and viscosity. Poritsky, and also Shu[20] in a note to his paper, found that if the surface tension is zero there is a limiting value of the viscosity parameter which if exceeded will prevent the wall velocity from becoming infinite and instead will cause the collapse to slow down; and will make the collapse time infinite. When the effect of surface tension is included, all bubbles collapse in a finite time.

All the work mentioned here so far has neglected the effects of heat transfer from condensing vapor or heated, compressed gas inside the bubble during collapse, and the effects of mass transfer by diffusion of gas, between bubble and liquid. Such effects are of predominate importance in situations of bubble growth or collapse involving heating of liquids during boiling. They are of importance here also, even though inertia of the liquid is usually considered the controlling factor, in

that they limit and determine the minimum bubble radius during collapse and also the maximum liquid velocities and pressures. Silver[21] presented one of the first analyses which considered the effect of the condensation of the vapor inside a collapsing bubble. He assumed that the rate of collapse was dependent only on the rate at which the vapor condensed on the bubble wall and the rate of removal of the latent heat from the wall into the cooler liquid, thereby ignoring the liquid inertia effects which governed collapse in the Rayleigh case. His analysis eliminated the possibility of infinite velocities and pressures, but left some question as to the validity of the assumptions and of the results obtained therefrom. Eisenberg[8] states that Silver's results can be taken as a lower limit on the collapse rate of a vapor filled cavity, and have significance in that regard.

Plesset[22] has analysed the rate of evaporation or condensation into a typical bubble collapsing in water, and states that if the velocity of the wall as it moves inward is appreciably less than the velocity corresponding to the rate of condensation of vapor on the liquid surface as determined from equilibrium conditions, then the pressure within the bubble may be considered constant at the vapor pressure of the water. In other words as the bubble wall moves inward all the vapor in the volume displaced condenses on the bubble wall. For water at 72°F he estimates that the maximum wall velocity for this condition to hold is ~500 feet per second, which is considerably below the maximum possible calculated velocities, but within the range of velocities which can be observed photographically before the bubble becomes too small to see. Plesset[23] later considered the entire field of bubble dynamics including

heat transfer effects, gas diffusion and bubble instability in a resume report. He points out that the probability that a vapor molecule which strikes a liquid surface will stick to it is only 0.04 for water at 0°C. Using a modified approach to that above he obtains the "characteristic velocity" for either evaporation or condensation at only about 26 feet per second using the above probability of condensation of 0.04. In any event, it would appear that the finite condensation rate and therefore the compression of the vapor can be significant in retarding the collapse for rapidly collapsing vapor filled bubbles, especially in the later stages of collapse.

Novotny[24] verified that the damage to metal specimens, oscillated by a magneto-striction device in various liquids, was strongly dependent on vapor pressure. Assuming the validity of the usual hypothesis that cavitation damage is caused by the stresses developed on the specimen during bubble collapse, he indicates that the collapse is far less violent for liquids near their boiling point or for liquids with high vapor pressures. His conclusion on this point was that a higher vapor pressure inside the bubbles prevented the bubble from collapsing so rapidly, and therefore also prevented sufficiently high liquid pressures from developing to cause damage to the adjacent solid specimens.

The effects of surface tension on liquid vapor pressure and bubble surface temperature have not been extensively considered in relation to bubble collapse. Silver[21] took account of the increase of energy available from the decreasing bubble surface area and considered this energy in the heat transfer from the vapor to the liquid. As the

bubble collapses, the energy available, which is released at the surface, is equivalent to the energy required to form a new liquid surface, beyond that energy necessary to overcome hydrostatic pressure. Becker, Roellig and Wilson[25] also consider this surface contribution to total bubble energy in a review of several authors' work on nucleation of bubbles. They point out that most analyses ignore, in the energy balance describing bubble expansion from assumed micro-bubbles, the energy necessary to maintain the surface temperature constant during isothermal expansions. The curvature of the liquid surface forming the bubble wall has also been ignored in its affect on the equilibrium vapor pressure within the bubble. Most analyses have assumed that the equilibrium vapor pressure within a small bubble was the same as the vapor pressure over a large plane surface, which is the value reported in the saturation pressure-temperature tables for liquids. Sir William Thomson[26] and also later Keenan[27] and Paul[28] have shown that the equilibrium vapor pressure of a pure substance over a curved liquid surface such as in a capillary tube or a bubble is a function of the radius of curvature of the liquid surface. The vapor pressure inside a bubble of radius r is given by Paul[28] and by Keenan[27] as

$$\ln \frac{p}{p_{sat}} = - \frac{2\sigma}{r \rho_l R T}$$

where p is the vapor pressure over the concave surface and p_{sat} is the saturation vapor pressure for a flat surface at temperature T. The following table gives some values for the ratio p_{sat}/p in water at $68^{\circ}F$.

r (inches)	$\frac{p_{sat}}{p}$
10^{-3}	1.000043
10^{-4}	1.00043
10^{-5}	1.0043
10^{-6}	1.0427
10^{-7}	1.519
10^{-8}	65.5

By comparison, the wavelength of light in the visible spectrum is from 1.58×10^{-5} in. to 2.76×10^{-5} in., and a spherical drop of liquid water with radius 10^{-6} in. contains 2.29×10^{6} molecules. A reference bubble used in the later numerical analysis has an initial radius of 50 mils or 5×10^{-2} in. When the bubble has collapsed to one thousandth its initial radius, or to 5×10^{-5} in., then $p/p_{sat} = 1.00084$. Therefore, in the range of the calculations, the effect is small, but may be appreciable when considering nucleation phenomena from groups of liquid molecules.

The fact that liquids can support considerable tension, or the equivalent that they can be superheated above the stable boiling point without boiling, has received consideration in regard to the nucleation of bubbles. Reynolds[29] described experiments with a column of mercury in 1877 in which he was able to support a 59 inch column with atmospheric pressure. He then connected a vacuum pump to remove the

atmospheric pressure, so that the column of mercury had a tension at the top of nearly two atmospheres without breaking the column. Considerable care was required in cleaning the glass tube to permit this high tension. Reynolds noted that even though a liquid will support large tension, it is not necessary to provide large stresses to fracture it. In the same manner a piece of cloth may be easily torn from one edge and yet may support tension. Fisher[30] has calculated the fracture strength of pure liquids and found that the calculated values are always greater by a very large amount than the maximum experimental values. The premature failure is associated with impurities in the liquids, where a solid material in the liquid can act as a site for nucleation. Harvey[31] has also shown that gas in crevices in solids acts as nucleation sites in liquids, and is the cause of fracture strengths lower than theoretically predicted.

Nucleation of bubbles also occurs from microbubbles of gas which may be driven under pressure into cracks in solids or into solution. Zivi[32] has discussed the voids formed in the water moderator-coolant by nucleation of bubbles in the Spert III nuclear reactor transient tests as reason for the reactivity decrease observed. The sites for nucleation could have been either gas in the pores of the fuel plates which did not fill with water when the fuel was immersed in the water, or microbubbles from radiolytic gas produced, or gas dissolved in the water, which then migrated to the fuel surface and adhered by surface tension. The increase in fuel temperature caused these bubbles to expand and displace moderator, leading to a shutdown mechanism. Many other authors also consider the

formation of bubbles from preferred nucleation sites, both in cavitation and in boiling heat transfer. The main object here in this regard will be to use the information which is available on nucleation to predict the possible gas and/or vapor content of the cavitation bubble and thereby to more closely calculate the mechanisms involved in the collapse of the bubble after it is already formed.

D. Statement of Bubble Dynamic Problem

1. General Theoretical Analysis

The theoretical analysis is concerned with the behavior of a typical cavitation bubble in liquid. Assume that a perfectly spherical void exists within a body of liquid, and that it is maintained by some imaginary thin, hard shell, in a motionless state. At some instant (from which time is measured from zero) the hard shell instantaneously disappears, and the surrounding liquid, moving under the pressure differential between the liquid and the void, flows inward to fill the void. At all times the void or collapsing bubble is assumed to maintain its spherical shape. In real situations, of course, the bubble would have grown from a small nucleus to its maximum size as the result of lowering the liquid pressure. Therefore, in comparing the theoretical presentation with the experimental facts, it is assumed that there is no difference in the manner of collapse of a bubble which has grown from a small nucleus and a bubble which was artificially created for analytical convenience, provided only that the conditions which exist inside the real bubble and in the surrounding liquid at time zero and during collapse are reproduced

in the theoretical analysis. The desired information is the variation of the bubble radius as a function of time and the velocity of the bubble wall as the bubble collapses. Also desired is the velocity and pressure distribution in the liquid adjacent to the bubble at any instant of time during the collapse as a function of distance away from the bubble wall and into the liquid. The manner in which these quantities change as the physical parameters change will be investigated.

2. Liquid Conditions

Assume an infinitely large body of static liquid with a small, perfectly spherical void within it. The condition of infinite size is required to eliminate the influence that solid or free surfaces can have on the motion of the collapsing bubble, and is a common assumption in many bubble collapse analyses.

Birkhoff and Zarantonello[33] considered an oscillating bubble near a rigid surface and showed that the effect of the surface is to cause the bubble to migrate towards the solid boundary. Most of the migration takes place when the radius is small. Herring[34] considered the motion of underwater explosion bubbles and also verified the influence of a nearly rigid surface.

In regard to cavitation damage, several authors consider the collapse of bubbles which are attached to a solid surface and appear initially as hemispherical bubbles. Oza[35] considered the collapse of a hemispherical bubble, where there is only radial velocity. He took account of the viscosity of the liquid by assuming a parabolic velocity distribution along a perpendicular to the surface, so that the circle

of bubble contact on the solid was fixed at its original size. Therefore the bubble collapsed with the top of the hemisphere approaching the surface; and the bubble assuming a disc like shape. Naude and Ellis[36,37] showed photographs of bubbles collapsing on solid surfaces, and also concluded that the collapse was not of a spherical hemisphere. They found, as in Oza's analysis, that the hemisphere collapsed to a disc-like shape and then the center of the bubble disc was penetrated by a liquid jet which then struck the solid surface. A theoretical analysis for incompressible liquid, with no viscosity effect like Oza had used, indicated that with irrotational flow, a perturbation of the surface could cause the type of collapse which was photographed. The solid was a photoelastic material, so the stress in the solid when the jet struck the surface could be observed. They concluded that cavitation damage was due to the action of this jet of liquid. Kornfeld and Suvarov[38] had previously also come to a similar conclusion regarding cavitation damage.

Recently, Shutler and Mesler[39] performed experiments with spark generated bubbles adjacent to solid surfaces and came to the opposite conclusion - namely, that it was not the liquid jet which caused the observed damage on their solid specimens. They observed small dents from bubbles at their minimum volume and believed that the damage was surely caused by a pressure pulse from a collapsing cavity at its minimum volume. They further observed that a second solid boundary perpendicular to the first caused the bubbles to collapse asymmetrically. Therefore,

there is still some question as to whether cavitation damage is caused by attached hemispherical cavities, or by more distant completely spherical bubbles, or by both.

The magnitude of the effect of the adjacent boundary on the bubble collapse is somewhat uncertain, and the proximity of the venturi wall to the experimentally observed bubbles in the present investigation may affect them. It will be assumed for purposes of analysis that the bubble considered is separated and independent from the venturi wall.

The theoretical analysis will be compared with experimental photographic results of bubbles in a cavitating venturi, where the liquid environment of the bubble is far from static. There is slip in the venturi between the liquid and the bubble, with the bubble traveling at a greater axial speed than the liquid in the constant cross section throat of the venturi. In low velocity, gas-liquid tests, Smissaert[40] correlates slip ratio, (ratio of gas velocity to liquid velocity) with surface tension and dynamic viscosity of several different liquids as well as velocity, temperature, and pressure. Vogrin[41] also observed slip ratios on the order of 10 or more in two-component flow in a converging-diverging nozzle. Many other investigations also exist in the literature regarding the effects of slip in various specialized cases and these are merely cited as typical. One effect of the slip on the collapse of the bubble may be through its effect on the circulation of the bubble contents and the more rapid removal of heat from the liquid in the vicinity of the bubble wall. Lamb[42] gives estimates of the velocities of gas or vapor inside, and of the liquid outside, a constant

diameter bubble in a known force field, such as a bubble rising in a liquid in a gravity field. The effect of slip will not be explicitly applied here to the theoretical analysis.

It will be assumed in the analysis, that there is no gravitational or other body forces acting on the liquid in which the bubble is collapsing. Especially in liquid metals, there may be electric and/or magnetic field effects. Elliott[43] considers a magnetohydrodynamic cycle for nuclear-electric power conversion in which electric force fields are of importance. An interesting effect of the opposite type, namely the influence of cavitation bubbles on a magnetic field, was reported by Clark[44]. In working with the undesired cavitation in cryogenic liquid systems for rocket propulsion, it was found that when cavitation occurred, a magnetic field is generated in the region. This magnetic field is detected with appropriate sensing coils and used as an indication of cavitation inception. The author also described apparatus used for detecting a magnetic field which was generated where helium gas bubbles in liquid oxygen or water collapse on a surface. He indicated a possible mechanism whereby the magnetic field generated by collapsing bubbles and the subsequent eddy currents contributed to cavitation damage. No attempt has been made here to consider either the effect of an external electro-magnetic field on cavitation bubbles or to measure the field generated by collapsing bubbles if indeed such a field exists.

Gravitational effects may also be appropriately ignored in the venturi where the cavitation bubbles are small and other pressure

and velocity effects are predominate on the bubble behavior. However, in applications such as boiling heat transfer, the bouyancy of the bubbles on a hot surface may significantly affect their behavior.

In their investigation on the collapse of vapor-gas bubbles in liquid near the boiling point, Florschuetz and Chao[45] eliminated the effect of gravity by letting their entire experimental apparatus fall freely as a bubble was injected and collapsed in a tank of liquid. However, when the pressure rise in their experimental equipment was greater than about 30 cm Hg, they observed unstable collapse. In a typical manner, a jet of liquid appeared to pass down through the bubble, strike the bottom surface and cause shattering. Underwater explosions[34,46] are also strongly affected by bouyancy because of the greater bubble size and therefore greater pressure differential from top to bottom, and because of the longer time of collapse and therefore greater time for bouyancy effect to be felt. Gongwer[91] discusses high speed photographs of a four foot diameter underwater bubble formed by an explosive specially selected to produce a minimum of permanent gas upon detonation. Throughout most of the collapse of the bubble there appear porcupine-like streaks extending radially from the surface, attributed to debris on the surface. The fact that these streaks are straight radial lines indicated a verification of the assumption of perfectly radial flow surrounding the bubble. Since the bubble was in a relatively shallow pool of water, however, the final collapse of the bubble showed a rapid upward motion of the bubble center. In the extreme instance of large gas-filled bubbles in water, the initially spherical shape distorts into a torus-shaped

void. Walters and Davidson[47] describe experiments on gas bubbles rising in static water where the bubble assumes a mushroom shape and then breaks into a small spherical-cap bubble with a large toroid below.

Some consideration of the probable conditions in the experimental venturi used here indicated similar effects. A liquid particle leaving the experimental venturi throat would suddenly start slowing down in the diffuser if uniform single phase flow existed, and the velocity depended only on flow area. The maximum deceleration experienced by a liquid particle under such ideal conditions would occur at the throat exit. The liquid velocity $V(Z)$ at a distance Z inches downstream of the throat exit for a 1/4" throat opening is given by

$$V(Z) = V_T \left\{ \frac{1/4}{1/4 + (2 \tan 3^\circ) Z} \right\}$$

The liquid acceleration is then

$$\frac{d^2Z}{dt^2} = \frac{dV}{dZ}\frac{dZ}{dt} = - \frac{V_T^2 (2 \tan 3^\circ)^2}{16\left[1/4 + (2 \tan 3^\circ) Z \right]^3}$$

At a typical throat velocity, V_T = 74.6 ft/sec, the acceleration at the throat exit would be

$$\frac{d^2Z}{dt^2} = -2.79 \times 10^4 \frac{ft}{sec^2} = -867.\ g's$$

where the negative sign indicates the acceleration is directed upstream. However, as indicated later, the velocity is probably not uniform across the flow in the diffuser when cavitation is present, so the calculated negative acceleration does not occur at the throat exit. A jet of liquid leaves the throat and slows down abruptly at a location downstream of the throat exit, so the deceleration is probably still very large. Near the termination of the cavitation and within a very short distance the static liquid pressure (as shown later) surrounding a bubble moving with liquid velocity rises sharply. The time rate of change of pressure can be 10,000 $lbf/in^2/sec$. The very steep pressure gradient on even a small bubble may cause asymmetric collapse, which was observed here as a flattening of the bubble in the direction of flow. Plesset[22] has reported the spherical growth and collapse of bubbles from cavitation in the varying pressure field over an ogive in a water tunnel, based on pictures by Knapp and Hollander.[57] A more complete description of the venturi bubbles observed here will be given later, but the assumption of spherical symmetry for single bubbles even in a large pressure gradient is assumed for the present analysis to make the mathematics at all tractable.

3. Boundary Conditions in Liquid

The usual assumption, in bubble dynamics analyses, is that the pressure very far from the bubble is specified and is spherically symmetrical about the bubble. The narrow venturi throat which may be only a few times as large as the bubble diameter, and the changing

pressure gradients transverse to as well as along the direction of flow, may cause asymetries in the liquid pressure around the bubble. During the final portion of the bubble collapse, however, theory indicates that collapse occurs so rapidly that pressure changes more than a few original bubble diameters away will not affect the collapse. Therefore, local pressure fluctuations near the bubble will be assumed negligible for the present in the theoretical presentation.

Pressure variations in the axial direction as a bubble moves through the venturi can be measured. Wall taps placed at various positions along the direction of flow are used to obtain the pressure variation around the bubble, and this variation will be assumed to change symmetrically about the bubble, as if the bubble were in a static liquid where the liquid pressure had the same time variation as would be felt by a point which moves along the venturi with the same axial velocity as the bubble. Photographs of bubbles give the bubble axial position and therefore venturi pressure, as a function of both time and bubble radius. This pressure variation can then be used in calculations of bubble behavior as the boundary condition for the pressure at infinity.

4. Boundary Conditions Inside the Bubble

It will be assumed that whatever the conditions of pressure, temperature, or gas and vapor concentrations which exist inside the bubble, they are uniform throughout the bubble with no radial variations. Trilling[48] investigated the collapse and rebound of a gas bubble, and concluded that the pressure variation at the bubble wall,

when the shock waves in the gas as the bubble collapsed were included, was virtually the same as if the gas were compressed uniformly and isentropically. Therefore, it will be assumed that internal radial pressure variations will not significantly affect the collapse behavior.

Hickling[49] considers the temperature rise of various gases inside bubbles during a non-adiabatic collapse as a means of explaining the observed variations in intensity of the visible radiation from ultrasonically formed cavitation bubbles in liquid with several different dissolved gases. This phenomenon of sonoluminescence has been observed by many persons and in many different liquids.* Chambers[50] reported varying intensities of luminescence from 14 pure liquids and from some solutions for vibratory cavitation at 8900 cycles per second. He indicated the light intensity was proportional to the product of viscosity and dipole moment and inversely proportional to liquid temperature. Jarman,[51] in a discussion of the many and varied proposed mechanisms for sonoluminescence, concluded, in a modification of his previously reported results,[52] that it might possibly arise from microshocks within the collapsing cavities. Jarman and Taylor[53] give one of the few published reports of (very faint) sonoluminescence in a flowing system; namely tap water in a cavitating venturi. Hickling[49] concluded in his analysis that the light was from gas within the bubble which became incandescent when compressed very rapidly, due in most cases, to the

*It was observed here using glycerin, mixed with a few drops of water, oscillated by an ultrasonic horn at 20KC and about 2 mil amplitude. A faint bluish light was clearly visible to the naked eye in a darkened room. However, no light could be seen in a dark room from tap water cavitating in a venturi with throat velocities up to 200 ft/sec.

presence of various impurities. The variation in intensity with dissolved gas was caused by different thermal conductivities of the gases, and therefore different amounts of heat transferred from the gas to the bubble wall and dissipated in the liquid, thereby varying the maximum temperature of the gas near the bubble wall. Therefore, the radial variation in temperature within a gas bubble can be significant, and as Hickling shows, the smaller the initial bubble size the more pronounced is the thermal conduction effect on radial temperature variations.

In the venturi used here, the gas within the bubble presumably comes from the initial gas present in whatever nucleus initiated the growth, and also perhaps to a slight extent from gas diffusion from the liquid into the bubble during bubble growth. Treaste[54] calculated the length of time for bubble growth using several theoretical models in an attempt to predict the time delay for the appearance of cavitation in a water tunnel after the pressure is lowered to the point where it is known that cavitation will eventually occur. He used two previously published analyses. The first model assumed a large relative velocity between bubble and liquid, thereby contributing to air diffusion and subsequent bubble growth. The second assumed bubble growth by diffusion from a static liquid, neglecting the velocity transport. The first predicted bubble growth times which were several orders of magnitude less than his observed cavitation delay times, thereby indicating a possibly significant effect on the growth or collapse of bubbles as a function of the slip ratio between the bubble and liquid. The growth times

reported for the first analysis, including velocity transport, however were more nearly comparable to the growth times observed here for single bubbles growing in the venturi.

The effects of gas diffusion before and during bubble collapse will be considered in greater detail later, when a specific procedure is developed to be used in a numerical analysis to represent the pressure variation inside the bubble during collapse. Throughout this analysis, as stated above, the physical properties of the bubble contents will be assumed uniform at any instant of time, but may vary with time. As the bubble becomes very small, the question of whether or not the continuum approach is valid becomes important, especially for the gas or vapor inside the bubble. Hickling[49] states that he considered that even though the mean free path of gas molecules may be comparable to the bubble dimension, there are so many gas molecule collisions that the continuum approach is still valid. It is sufficient for the present, to state that the initial conditions inside the bubble may be estimated from the venturi conditions and the pressure variation inside the bubble can be specified as a function of bubble radius, and perhaps also bubble wall velocity. The analysis will hence assume that such a function is available, and can be varied to suit the conditions.

II. HYDRODYNAMIC EQUATIONS

A. Preliminary Introduction

The general equations of hydrodynamics have been discussed by many authors, with application to the problem of a collapsing or expanding spherical void in liquid.

The method of presentation, the assumptions made for the appropriate physical application, and the means of mathematical approximation or solution, when possible, have varied considerably. It will be desirable here, to present some of the more conventional analyses in detail in order to better interpret the numerical and experimental results which follow.

While some of the detail might be thought to be more appropriate in a purely mathematical summary as an appendix, its inclusion here permits a convenient and hopefully beneficial means of bringing out important differences among a few of the many other bubble dynamics analyses, and of indicating any particular value of the present analysis by comparison.

The imcompressible liquid analysis will be presented first, followed by the compressible analysis, and then both will be followed, in Chapter III, by the numerical solutions obtained here.

B. Equations of Flow and the Rayleigh Solution

The continuity equation for a compressible fluid can be written

$$\frac{D\rho}{Dt} + \rho \, \mathrm{div}\, \vec{V} = 0 \qquad (1)$$

where: ρ = fluid density, $\vec{V}$ = velocity vector, t = time and where:

$$\frac{D\rho}{Dt} = \frac{\partial \rho}{\partial t} + \text{grad } \rho \cdot \vec{V}$$

is the total derivative,[55] or the variation in density at a point moving with the fluid. For an incompressible fluid, the density is constant, so at any instant of time, Equation (1) gives

$$\text{div } \vec{V} = 0 \tag{2}$$

Equation (2), when expressed in a spherical coordinate system[56] and assuming spherically symmetric flow, is

$$\frac{\partial u}{\partial r} = -\frac{2u}{r} \tag{3}$$

where u = radial particle velocity

r = radius

Since Equation (3) is valid for any instant of time there is only one independent variable r, and since the flow is spherically symmetric there is only one dependent variable u so that (3) is an ordinary differential equation which is simply solved by separation of variables. Using the boundary conditions of velocity $u = U$ and of radius $r = R$ at the bubble wall, the solution to Equation (3) is, as also given by Rayleigh,

$$u = \frac{R^2}{r^2} U \tag{4}$$

The general Navier-Stokes equation of motion for viscous, compressible fluid flow in the absence of external body forces is

$$\frac{DV}{Dt} = -\frac{1}{\rho}\,\text{grad}\,p + \frac{\mu}{\rho}\left[\nabla^2\vec{V} + \frac{1}{3}\,\text{grad}(\text{div}\,\vec{V})\right] \qquad (5)$$

where p = pressure

μ = shear viscosity

For an inviscid fluid, the last term is zero, and for spherically symmetric inviscid flow Equation (5) becomes[56]

$$\frac{\partial u}{\partial t} + u\frac{\partial u}{\partial r} = -\frac{1}{\rho}\frac{\partial p}{\partial r} \qquad (6)$$

Equation (4) is substituted into Equation (6) to eliminate the partial derivative in time, giving an equation with r as the only independent variable. After separation of variables the equation is integrated using the boundary conditions that

$$\lim_{r\to\infty} p(r) = p_\infty$$

and $u = 0$ as r approaches infinity, and using the fact that $U = dR/dt$. The result is essentially a solution in Lagrangian coordinates, where the motion of a particle of liquid is followed, namely a particle on the bubble wall. The bubble wall radius as a function of time is thus

$$R\frac{d^2R}{dt^2} + \frac{3}{2}\left(\frac{dR}{dt}\right)^2 = -\frac{\left(p_\infty(t) - P(t)\right)}{\rho} \qquad (7)$$

where $P(t)$ = liquid pressure at bubble wall, or

$P(t)$ = pressure within bubble also, if surface tension and viscosity are zero

$p_\infty(t)$ = liquid pressure far from bubble

Therefore, the pressure at infinity, $p_\infty(t)$, and the pressure within the bubble $p_o(t)$ (which is equal to the liquid pressure $P(t)$ at the wall, here) may vary in time in Equation (7).

Rayleigh[14] presented a solution to this equation for a variable internal gas pressure in the bubble, assuming Boyle's law held during collapse. Lamb[16] considered an equivalent expression for an expanding bubble, where he assumed an adiabatic gas expansion and found an analytic solution for the particular case of $\gamma = 4/3$, where the bubble pressure varied as $(Ro/R)^{3\gamma}$. Noltingk and Neppiras[18] considered the case of a gas filled bubble in an oscillating pressure field, $p_\infty(t)$, and used numerical methods to obtain a solution of Equation (7). If then the pressure differential, $(p_\infty(t) - p_o(t))$, is a known function of time, sometimes the analytic solution is possible, and if it is constant, the analytic solution is definitely possible.

Equation (7) may be written

$$2R^3U\frac{dU}{dR} + 3R^2U^2 = -\frac{2(P_\infty(R) - P_o(R))R^2}{\rho} \qquad (8)$$

Therefore, the condition of incompressibility or constant density expressed by Equation (4), which may be interpreted as a condition imposing an instantaneous propagation of any pressure disturbance

throughout the liquid, has permitted the transformation of the partial differential equation of motion, Equation (6), into an ordinary, first order differential equation, Equation (8). It will be shown later that the choice of similar assumptions regarding the propagation of pressure or sound waves and also the propagation of other mathematical quantities determines the degree of accuracy of analytic solutions which are frequently used in handling the partial differential equation of motion. It should be noted that the Equation (8) is a non-linear equation. Its solution was obtained by Rayleigh without actually using the equation by considering the physical problem and directly equating the available energy of the pressure differential to the kinetic energy of motion. Lamb,[16] in a formal, purely mathematical procedure, obtained the solution to this simple case for a constant pressure differential by using an integrating factor as follows. Equation (8) is equivalent to

$$d(U^2 R^3) = -\frac{2\left(P_\infty(R_o) - P_o(R_o)\right) R^2 dR}{\rho} \tag{9}$$

which, upon integrating between $U = 0$ at $R = R_o$ and any velocity U at R, becomes

$$U^2 = \frac{2}{3}\frac{\left(P_\infty(R_o) - P_o(R_o)\right)}{\rho}\left(\frac{R_o^3}{R^3} - 1\right) \tag{10}$$

and is identical to Rayleigh's result for the bubble wall velocity as a function of the bubble radius, with a constant pressure differential, $(p_\infty(R_o) - p_o(R_o))$.

Using the following normalization, where primed quantities shall henceforth denote dimensionless quantities,

$$U' = \frac{U}{\sqrt{\frac{(P_\infty(R_o) - P_o(R_o))}{\rho}}} \; ; \; t' = \frac{t}{R_o}\sqrt{\frac{P_\infty(R_o) - P_o(R_o)}{\rho}} \; ; \; R' = \frac{R}{R_o}$$

Equation (10) becomes

$$U'^2 = \frac{2}{3}\left(\frac{1}{R'^3} - 1\right) \tag{11}$$

Expressing R' in terms of t', using $dR'/dt' = U'$, Equation (11) gives

$$t' = \sqrt{\frac{3}{2}} \int_1^{R'} \left(\frac{R'^3}{1 - R'^3}\right)^{1/2} dR' \tag{12}$$

A solution to Equation (12) for complete collapse to $R' = 0$ was given by Rayleigh as the time for total collapse of a bubble in an incompressible liquid, collapsing under a constant pressure differential.

$$t' = 0.91468 \tag{13}$$

For intermediate values of R', a numerical solution in tabular form was presented by Knapp and Hollander.[57] It should be noted that the particular form of Equations (11) and (12) permits a single solution

of the normalized equations to give all possible information. There are no physical scaling factors involved. Equation (11) says that regardless of the initial bubble sizes they will have the same real velocity when they have collapsed to the same fraction of their original size, provided only that the ratio of pressure differential to liquid density is the same. However, the actual real time elapsed will be greater for larger bubbles. Scaling factors will appear, however, when other physical parameters such as surface tension and viscosity are considered.

C. Incompressible Liquid with Surface Tension and Viscosity

The inclusion of surface tension in the analysis changes the liquid pressure at the bubble wall so that it is no longer equal to the internal pressure. These pressures are related by

$$P(R) = P_o(R) - \frac{2\sigma}{R} \tag{14}$$

where σ = surface tension. Then Equation (8) for wall velocity becomes

$$2R^3 U \frac{dU}{dR} + 3R^2 U^2 = -\frac{2(P_\infty(R) - P_o(R))R^2}{\rho} - \frac{4\sigma R}{\rho} \tag{15}$$

After integrating in the same manner as before, the velocity is, for constant $(p_\infty(R_o) - p_o(R_o))$.

$$U^2 = \frac{2}{3}\frac{(P_\infty(R_o) - P_o(R_o))}{\rho}\left(\frac{R_o^3}{R^3} - 1\right) + \frac{2\sigma}{\rho R}\left(\frac{R_o^2}{R^2} - 1\right) \tag{16}$$

In normalized form Equation (16) becomes

$$U'^2 = \frac{2}{3}\left(\frac{1}{R'^3} - 1\right) + \frac{2\sigma'}{R'}\left(\frac{1}{R'^2} - 1\right) \tag{17}$$

where

$$\sigma' = \frac{\sigma}{R_o\left(P_\infty(R_o) - P_o(R_o)\right)}$$

In comparing Equation (17) with Equation (11), it is seen that the solution for velocity is now dependent upon a parameter σ', in the equation, so that for each value of the parameter there is a solution. The effect of surface tension on velocity is, as shown by Equation (17), that for a given radius R' the velocity is larger, and that the influence of surface tension is stronger as the radius gets smaller.

A second physical parameter which has a scaling effect on the motion of a collapsing bubble is the liquid viscosity. The inclusion of viscosity in the incompressible case has no effect on the solution of the continuity Equation (4). Further, as shown by Poritsky,[19] the equation of motion, Equation (5), for an incompressible irrotational flow as in a spherical collapse, is the same whether or not viscous effects are included. The effect of viscosity appears only in the boundary conditions at the bubble wall. Its influence causes the three principal stresses at any point in the liquid to be different, and this difference is taken into account at the liquid boundary. Instead of equating the pressures in the liquid and in the gas at the bubble wall, it is then necessary to equate only the

principal radial stresses. However, since the viscosity of the gas and/or vapor within the bubble is small in comparison to the liquid viscosity, it is assumed that the radial stress in the gas is the same as the gas pressure. Equation (14), when viscosity is included, is then

$$P(R) = p_o(R) - \frac{2\sigma}{R} + 2\mu \frac{\partial u}{\partial r} \tag{18}$$

where μ = liquid shear viscosity.

The partial derivative is obtained from Equation (3), at the bubble wall, and Equation (18) is then

$$P(R) = p_o(R) - \frac{2\sigma}{R} - \frac{4\mu U}{R} \tag{19}$$

Equation (19) is substituted into Equation (8), where $p_o(R)$ is replaced by $P(R)$, and the result equivalent to Equation (15) which contained only surface tension, is*

$$2R^3 U \frac{dU}{dR} = -2R^2 \left\{ \frac{3}{2} U^2 + \frac{(p_\infty(R) - p_o(R))}{\rho} + \frac{2\sigma}{R\rho} + \frac{4\mu U}{\rho R} \right\} \tag{20}$$

From Equation (19) or (20), it is seen that the viscosity effect during collapse when U is negative is such that the pressure at the bubble wall is increased, reducing the pressure differential causing collapse and therefore presumably reducing the wall velocity.

*If gas viscosity is also included, the last term becomes $\frac{4(\mu_{liq} + \mu_{gas})U}{\rho R}$. Hence if, as is usual, $\mu_{liq} \gg \mu_{gas}$, it is permissible to neglect the effects of gas viscosity.

For a variable pressure differential, $p_\infty(R) - p_o(R)$, Equation (20) is normalized by using the initial value of the pressure differential, $p_\infty(R_o) - p_o(R_o)$. If the normalized viscosity parameter is defined as

$$\mu' = \frac{4\mu}{R_o\sqrt{\rho\left(p_\infty(R_o) - p_o(R_o)\right)}}$$

Equation (20) becomes

$$2R'^3U'\frac{dU'}{dR'} = -2R'^2\left\{\frac{3}{2}U'^2 + \frac{\left[p_\infty(R') - p_o(R')\right]}{\left[p_\infty(R_o) - p_o(R_o)\right]} + \frac{2\sigma'}{R'} + \frac{U'\mu'}{R'}\right\} \qquad (21)$$

where all other appropriate terms are also normalized using the initial pressure differential. If the internal and external pressures were constant during collapse, the pressure term in Equation (21) would be unity, and the remaining terms the same as shown. Equation (20) differs from the previous Rayleigh Equation (8), or Equation (15) in that it contains two additional parameters. When both the viscosity and surface tension are included, the additional term containing viscosity has the velocity in it in such a way as to prevent a simple integration as performed on Equation (15). An attempt to integrate Equation (21) yields, for constant $p_\infty(R') - p_o(R')$,

$$U'^2 + \frac{2\mu'}{R'^3}\int_1^{R'} U'R'dR' = \frac{2}{3}\left(\frac{1}{R'^3} - 1\right) + \frac{2\sigma'}{R'}\left(\frac{1}{R'^2} - 1\right) \qquad (22)$$

Poritsky[19] and Shu[20] show that there is a limiting value of the normalized viscosity parameter which determines the bubble behavior. They reduce Equation (21) by substituting a new independent variable $\delta = R'/\mu'$ and, assuming $(p_\infty - p_o)$ is constant, obtain

$$\frac{dU'}{d\delta} = -\frac{1}{U'\delta}\left\{\frac{3}{2}U'^2 + 1 + \frac{2\sigma'}{\delta/\mu'} + \frac{U'}{\delta}\right\} \qquad (23)$$

When $\sigma' = 0$, Poritsky[19] shows a series of curves of U' vs δ obtained numerically, for several values of μ'. While the viscosity no longer appears in Equation (23) if the surface tension is neglected, it still affects the solution because it determines the initial boundary condition at $U = 0$ and $R' = 1$ or $\delta = 1/\mu'$. He concluded that if $\mu' > 0.46$ the bubble will require an infinite time to completely collapse. Shu[20] arrives at a similar result that the time is infinite if $\mu' > \mu'_o$ where $\mu'_o < \sqrt{6}$, $(\sqrt{6} = 2.449)$ and finite otherwise. If surface tension is included, both analyses show the collapse time is finite.

The viscosity need not be large for the normalized viscosity parameter to have its limiting value, in view of the definition of μ'. A very small initial bubble radius and/or a small pressure differential have the same effect of increasing μ'.

For a variable pressure differential, $p_\infty(R) - p_o(R)$ Equation (21) is valid, and is solved numerically here. This simple inclusion of a variable pressure either at infinity or within the bubble is possible because the liquid is incompressible, and any change in

these pressures is felt immediately throughout the liquid. It is noted that only the difference in pressure is important, so that a rise in internal bubble pressure has exactly the same dynamic effect on the collapse as a fall in the pressure at infinity. Of course in a real liquid and pressure rise within the bubble can be very much larger than the environmental liquid static pressure so the comparable effect of such a rise can be obtained only by lowering the pressure at infinity well below zero, thereby putting the liquid in tension. Real liquids are of course limited in this respect.

The effect of viscosity is to change the available collapse pressure differential by increasing the liquid pressure at the bubble wall. The pressure distribution in the liquid away from the bubble, for an incompressible liquid at any instant of time, is dependent only upon the instantaneous value of the bubble wall velocity and acceleration, and therefore only indirectly dependent upon the viscosity through the viscosity affect on these two variables. Equation (4) is substituted into Equation (6), the result is integrated between p(r) at r and p_∞ at $r=\infty$, and using dU/dt = UdU/dR, Equation (20) is substituted for dU/dR, giving

$$\frac{P(r)-P_\infty(r)}{\rho}=\left\{\frac{U^2R}{2r}-\frac{U^2R^4}{2r^4}-\frac{R}{r}\left[\frac{P_\infty(R)-P_v(R)}{\rho}+\frac{2\sigma}{\rho R}+\frac{4\mu U}{\rho R}\right]\right\} \qquad (24)$$

This is identical to Rayleigh's result if the last two terms are omitted and if his analytic solution for U is substituted. If the variables are normalized using the initial pressure differential as before, Equation (24) becomes

$$P'(r') = P'_{\infty}(R')\left(\frac{r'-1}{r'}\right) + \frac{U'^2}{2r'} - \frac{U'^2}{2r'^4} - \frac{1}{r'R'}\left\{2\sigma' + \mu' U'\right\} + \frac{P'_v(R')}{r'} \qquad (25)$$

where

$$P'(r') = \frac{P(r)}{P_{\infty}(R_o) - P_o(R_o)} \quad , \quad r' = \frac{r}{R}$$

Solutions for Equation (25) are given later for various pressure differentials and parameter values after the velocity is determined numerically from Equation (21).

D. Compressible, Viscous Liquid

The Navier-Stokes equation of motion, Equation (5), is used for the compressible case, and the solution presented here for a collapsing bubble follows that of Gilmore.[58,59] For spherically symmetric flow,

$$\text{curl}\,\vec{V} = 0$$

Using the vector identity[55]

$$\nabla^2\vec{V} = \text{grad}(\text{div}\,\vec{V}) - \text{curl}(\text{curl}\,\vec{V})$$

to eliminate the first term in the bracket in Equation (5),

$$\frac{D\vec{V}}{Dt} = -\frac{1}{\rho}\,\text{grad}\,P + \frac{4}{3}\frac{\mu}{\rho}\left[\text{grad}(\text{div}\,\vec{V})\right]$$

The continuity Equation (1) is then substituted into this equation, giving

$$\frac{D\vec{V}}{Dt} = -\frac{1}{\rho}\,\text{grad}\,P + \frac{4}{3}\frac{\mu}{\rho}\left[\text{grad}\left(-\frac{1}{\rho}\frac{D\rho}{Dt}\right)\right] \tag{26}$$

At this point, several assumptions have been made by Gilmore and by others who have used the same procedure. First, the viscous effect is assumed to be small, and second, the compressible effect is also assumed small so that the product of the two in the last term in Equation (26) can be neglected. Gilmore[58] points out that the change in viscosity with pressure in liquids is greater than the change in density with pressure so the neglected term can be shown to be smaller than those variable viscosity effects usually neglected in the Navier-Stokes equation. However, the effect of compressibility is still partially included through the continuity equation, and there is no mathematical inconsistency in this procedure since the compressibility term would have been dropped if the viscosity were simply assumed to be zero. Therefore, in spherical coordinates, the compressible equation of motion, Equation (26), becomes the same as Equation (6).

Another assumption is now made concerning the liquid: namely that it is barotropic, i.e., the density is a function only of pressure, so that

$$\frac{1}{\rho}\,\text{grad}\,P = \text{grad}\,\frac{P}{\rho}$$

Define a new quantity, which for now may be thought of as simply a new variable called enthalpy, and defined by

$$h(p) = \int_{p_\infty}^{p} \frac{dp}{\rho} \tag{27}$$

Then, from the preceding equation

$$\text{grad}\,\frac{p}{\rho} = \text{grad}\int_{p_\infty}^{p} \frac{dp}{\rho} = \text{grad}\; h(p)$$

Equation (26), in spherical coordinates is then

$$\frac{D\vec{V}}{Dt} = -\frac{\partial h}{\partial r} \tag{28}$$

Introduce now another new variable which is recognized as the sonic velocity, c ,

$$c^2 = \frac{dp}{d\rho} \tag{29}$$

From the definition of h ,

$$\frac{dh}{dp} = \frac{1}{\rho}$$

so that

$$\frac{D\rho}{Dt} = \frac{d\rho}{dh}\frac{Dh}{Dt} = \frac{Dh}{Dt}\left(\frac{d\rho}{dp}\right)\left(\frac{dp}{dh}\right) = \frac{Dh}{Dt}\,\frac{\rho}{c^2} \tag{30}$$

and the continuity Equation (1) becomes

$$-\frac{1}{c^2}\frac{Dh}{Dt} = \text{div}\,\vec{V} \tag{31}$$

There are now two partial differential equations, (28) and (31), in which there are three dependent variables, V, h, c, and two independent variables r and t. An appropriate equation of state for the liquid, giving pressure as a function of the density, is given later, so essentially c and h can be reduced to one variable, leaving two equations, with two dependent and two independent variables, which must be solved simultaneously.

There are various solutions to these equations in the literature and a discussion of some of the more important methods seems in order here. Flynn[60] presented an approximate analytic solution wherein he used a table of values of pressure and density instead of an explicit equation of state for the liquid. His solution was in terms of either the exponential integral or the confluent hypergeometric function, values of which he calculated and presented as curves. Mellen[61] computed the bubble wall velocity using Gilmore's method, and used this to get the pressure in the liquid at a fixed distance far from the point of collapse. He computed the propagation of the shock resulting from complete collapse of the empty bubble to zero radius. A later work[62] included the shock pressure as a function of distance, both with some experimental verification from spark induced cavitation bubbles of about one or two cm initial radius. Schneider[63] obtained a graphical solution to the compressible flow equations using the method of characteristics in a hand calculation. The bubble collapsed onto an imaginary rigid sphere, and the compressibility effect caused the bubble to rebound away from the sphere after collapse. Brand[64,65] presented

similar calculations to those of Schneider, but by finite difference computation of the characteristics on a computer rather than graphically. He also found the shock wave resulting after collapse onto a rigid sphere. Hickling and Plesset[66] present one of the most thorough solutions to the compressible equations, for bubbles collapsing and then rebounding from gas contained within, which was compressed adiabatically. The machine solution was taken up to the point where a shock wave formed on the rebound pressure wave. It is important to note that all the above authors considered compressible effects, but none considered the possible viscous effects. The present solution will include both.

The above Equations (28) and (31) must be solved simultaneously, or a method must be obtained to eliminate one of the independent variables. There are various other acoustic and quasi-acoustic approximations to account for a finite instead of infinite velocity of propagation of waves. The Kirkwood-Bethe[67,68] assumption is based on experiments with underwater explosions, and is the one used here and by Gilmore. It is assumed that the quantity or characteristic $r(h + u^2/2)$ is propagated outward in the liquid with characteristic velocity $(c + u)$ where c is the local sonic velocity. Therefore, the relation between r and t can be expressed by

$$\frac{\partial}{\partial t}\left[r\left(h+\frac{u^2}{2}\right)\right] + (c+u)\frac{\partial}{\partial r}\left[r\left(h+\frac{u^2}{2}\right)\right] = 0 \qquad (32)$$

and one of these variables may be eliminated.

Since the convective derivative in spherical coordinates is

$$\frac{D}{Dt} = \frac{\partial}{\partial t} + u\frac{\partial}{\partial r} \tag{33}$$

Equation (32) becomes

$$\frac{D}{Dt}\left[r\left(h+\frac{u^2}{2}\right)\right] = -c\frac{\partial}{\partial r}\left[r\left(h+\frac{u^2}{2}\right)\right] \tag{34}$$

which, when expanded, yields

$$r\frac{Dh}{Dt} + ru\frac{Du}{Dt} + (c+u)\left(h+\frac{u^2}{2}\right) + rc\frac{\partial h}{\partial r} + rcu\frac{\partial u}{\partial r} = 0 \tag{35}$$

Equation (35) is then merely the Kirkwood-Bethe assumption in appropriate form in spherical coordinates. The two partial differential Equations (28) and (31) are substituted into Equation (35) and the derivatives with respect to r are eliminated. Since D/Dt is the derivative at a particular particle of liquid, and since a point on the bubble wall is such a particle, the resulting equation will immediately describe the motion of the particles on the bubble wall. Letting capital letters represent the variables at the wall, and using the relation $U = dR/dt$, Equation (35) becomes

$$RU\frac{dU}{dR}\left(1-\frac{U}{C}\right) + \frac{3}{2}U^2\left(1-\frac{U}{3C}\right) = H\left(1+\frac{U}{C}\right) + \frac{RU}{C}\frac{dH}{dR}\left(1-\frac{U}{C}\right) \tag{36}$$

So far in Gilmore's method, an equation of state for the liquid has been assumed but has not been explicitly stated. It will be assumed

that viscous dissipation which occurs in the liquid at the bubble wall, as was also the case for the incompressible analysis by Poritsky, does not affect the liquid properties such as temperature or density. Any heat generated by viscous effects will be assumed to be lost from the system, so no heat conduction effects need be considered in the liquid. The equation of state assumed for approximately isentropic compression in many liquids is[58]

$$\left(\frac{p+B}{p_r+B}\right) = \left(\frac{\rho}{\rho_r}\right)^n \tag{37}$$

where p_r and ρ_r are any reference pressure and density.

$B \cong 3000$ atm.
$n \cong 7$
} are constants for water.

Using (37), the sonic velocity is calculated from Equation (29)

$$c^2 = \frac{dp}{d\rho} = \frac{n(p+B)}{\rho_r}\left(\frac{p+B}{p_r+B}\right)^{-1/n} = \frac{n(p+B)}{\rho} \tag{38}$$

and the enthalpy h from Equation (27)

$$h = \frac{n(p_\infty+B)}{(n-1)\rho_\infty}\left[\left(\frac{p+B}{p_\infty+B}\right)^{\frac{n-1}{n}} - 1\right] \tag{39}$$

Therefore, Equation (36) can be formally expressed in terms of the dependent variable U, the independent variable R, and the boundary condition for the pressure, $P(R)$, at the bubble wall.

The boundary condition for pressure far from the bubble, p_∞ is assumed constant during collapse since the Kirkwood-Bethe

assumption, Equation (32), provides for only outward moving characteristics and a varying p_∞ would cause inward moving waves in the physical situation. However, comparison of the compressible and incompressible solutions shows little difference between the two during the early portions of collapse which consumes most of the total collapse time. The reason is that since $c \gg u$ throughout the liquid for this period, a finite propagation velocity is still relatively so large that the liquid behaves approximately as an incompressible liquid. Therefore, in spite of the solution by means of the Kirkwood-Bethe assumption, a variable pressure at infinity may be imposed for about the initial three-fourths of the change in radius without any numerical inconsistency.

The boundary condition at the bubble wall is introduced now and this introduces the viscosity, surface tension, and the pressure within the bubble. Equation (18) for the incompressible case, becomes as follows for a compressible liquid:

$$P(R) = P_o(R) - \frac{2\sigma}{R} - \frac{4\mu U}{R} - \frac{4\mu U}{3c^2}\frac{dH}{dR} \qquad (40)$$

According to Gilmore, the last term is of the same order of significance as the term for the product of the viscosity and compressibility which was dropped from the Navier-Stokes equation and is therefore appropriately neglected here. The result for the liquid pressure is substituted into Equation (38) and (39) for C^2 and H at the bubble wall, and they in turn are substituted into Equation (36) for the bubble wall velocity as a function of radius. These substitutions are made during the numerical solution of Equation (36) on a computer and are not made explicitly here. Appendix A gives the detailed procedure.

The internal pressure $p_o(R)$ is as yet unspecified, and can be assumed to be any function of R. The actual function may accomodate an adiabatic compression of an initial quantity of gas in the bubble or some combination of isothermal and adiabatic compression, or anything which can be specified in terms of R. This function will be chosen along with the pressure p_∞ to correspond approximately to the conditions for a bubble in the experimental venturi.

The velocity and pressure distribution throughout the liquid surrounding the collapsing bubble at any instant of time is found by using the Kirkwood-Bethe hypothesis. By definition there is a quantity z, where

$$z(r,t) = r\left(h + \frac{u^2}{2}\right) \tag{41}$$

which is a constant along a path or "characteristic" traced by a point moving with velocity $(c + u)$. In otherwords, along such a path in the $r - t$ plane the time rate of change of any variable is given by

$$\left(\frac{d}{dt}\right)_c = \frac{\partial}{\partial t} + \frac{\partial}{\partial r}\left(\frac{dr}{dt}\right) = \frac{\partial}{\partial t} + (c+u)\frac{\partial}{\partial r} \tag{42}$$

where the subscript c signifies the derivative along a characteristic. The value of the quantity $z(r,t)$ is known as a function of radius and time for a particular particle of fluid, namely one on the bubble wall. Therefore, start with the value of $z(r,t)$ on the bubble wall at some instant of time, and trace a path through the liquid such that Equation (42) is satisfied, and such that $z(r,t)$ remains constant. To do this,

expand the momentum Equation (28) and the continuity Equation (31) and add the two together, giving

$$\left[\frac{\partial u}{\partial t} + (c+u)\frac{\partial u}{\partial r}\right] + \frac{1}{c}\left[\frac{\partial h}{\partial t} + (c+u)\frac{\partial h}{\partial r}\right] + \frac{2uc}{r} = 0 \qquad (43)$$

Using Equation (42), Equation (43) becomes

$$\left(\frac{du}{dt}\right)_c + \frac{2cu}{r} = -\frac{1}{c}\left(\frac{dh}{dt}\right)_c \qquad (44)$$

From Equation (41)

$$h = \frac{z}{r} - \frac{u^2}{2} \qquad (45)$$

where z is a constant in the derivative in Equation (44), into which h is substituted. The result is

$$\left(\frac{du}{dt}\right)_c = \left[\frac{z}{r^2} + \frac{zu}{cr^2} - \frac{2cu}{r}\right]\frac{c}{(c-u)} \qquad (46)$$

The relation between radius and time along a characteristic path is given by

$$\left(\frac{dr}{dt}\right)_c = (c+u) \qquad (47)$$

Therefore, there are two simultaneous ordinary differential equations with u and r as the dependent variables and t as the independent variable, and related to the bubble wall motion through the constant

parameter z which, along with the initial conditions on u , t , and r , is obtained from the instantaneous values at the bubble wall.

Once u , and r are known for a given z , h is obtained from Equation (45) and then pressure is obtained from Equation (39). The result is

$$P(r,t)_c = (P_\infty + B)\left[\left(\frac{z}{r} - \frac{u^2}{2}\right)\left(\frac{n-1}{n}\frac{\rho_\infty}{(P_\infty+B)}\right) + 1\right]^{\frac{n}{n-1}} - B \qquad (48)$$

The independent variable was chosen as t rather than r , as in the bubble wall solution, because it facilitates the numerical procedure for solution. If r were used, and if the bubble wall velocity were greater than the local sonic velocity, then although the characteristic would move away from the bubble wall at first it actually would move inward, and then outward only when the local sonic velocity exceeded the particle velocity. In a numerical solution the increment dr in radius would have to be changed from negative to positive, while if time is used, the increment is of course always positive.

E. Surface Tension Effects in Bubble Collapse

It is assumed throughout this analysis that the surface tension of the liquid in which the bubble is collapsing is constant during the collapse. It is, however, well-known that surface tension is a function of liquid temperature and also of liquid pressure. Furthermore, there is evidence that it is a function of very small quantities of impurities

present at the liquid interface. A discussion of some of the real properties involved is then in order here in order to appreciate the possible effects, but no attempt will be made to analytically introduce these properties into the theoretical presentation of bubble behavior.

Burdon[69] has extensively discussed the properties of liquid interfaces and the surface energy. He considers the absorption of impurities at liquid surfaces and the requirements for equilibrium to exist. The molecules in the layer at the surface of a pure liquid possess energy by virtue of having been placed on the surface, where there is an unequal attraction with surrounding molecules because the surface molecules do not have liquid attractive forces on one side. When impurities are present, they might be in the form of a monomolecular layer of some fatty substance as on water of a variation in the concentration of impurity molecules within the liquid and on the surface.

Fox and Herzfeld[70] have considered such an organic skin as a reason for micro-bubble persistence in liquids. The effect of impurities either on the surface or in the liquid is almost always to lower the surface tension of a pure liquid. Burdon discusses the fact that there is a time lag after formation of a new surface before the surface tension reaches an equilibrium value. The reasons for the time lag are not clear, since the lag is of the order of 10^6 x the computed time for diffusion to the surface. A surface, well-protected from contamination, may continue to fall in surface tension for hours after the surface is formed. The surface tension of mercury is especially variable when minute quantities of impurities are present. Burdon indicates that

probably Kemball's[71] value for the surface tension of mercury in vacuum of 485 dynes/cm at 20°C is the most nearly correct, but values are reported of from 430 to 515 dynes/cm with experimental accuracy of 1/4 of 1 percent. On exposure to air, the decrease varies from 40 to 50 dynes/cm/minute to a decrease as little as 5 dynes/cm/24 hours. Therefore, we can conclude that the speed of formation of the bubble in the venturi, and the constituents of the original microbubble could have some influence on the effective value of the surface tension at the bubble interface.

Probably the most important consideration with regard to surface tension and bubble collapse is that at the critical pressure and temperature of a pure liquid the surface tension is zero. As shown later the pressures within a bubble can easily reach the critical pressure, and the temperature is also predicted to rise.

Nowak,[72] in developing an equation of state for water near the critical point discusses the laws which must be satisfied at the critical point. One of these is that the latent heat of vaporization will become zero. In discussing the stability of bubbles during collapse, Plesset[23] mentions this disappearance of the difference between liquid and vapor phase when the vapor in a bubble is rapidly compressed. He uses this argument together with his derived instability for collapsing bubbles to explain why a bubble may not reopen, but instead will fragment. This is reasonable if one considers a local region of very high-pressure compressed liquid, and the fact that since the latent heat and surface tension are zero, no additional energy is required to form

new surfaces in such a liquid when the region suddenly expands. In the theoretical analysis it is assumed that the surface tension effect increases the pressure of the bubble contents as the radius becomes very small, while in real situations where the pressure approaches the critical point the opposite may occur. The effect becomes less at high pressure and the lack of an interface promotes greater instabilities and deviation from spherical collapse. It is shown, however, that for rapidly collapsing bubbles the relative effect of a constant value of surface tension is small in the theoretical analysis, so the neglect of its variation with pressure will not of itself cause the analysis to deviate greatly from the physical situation.

F. Viscosity Effects in Bubble Collapse

Some of the possible effects of viscosity on the motion of the bubble wall during collapse will be discussed here, and as in the case of surface tension, the results will not be explicitly used in the theoretical analysis, but rather will merely help to understand and interpret the probable degree of validity and application of that analysis. Considered here are the effects of viscosity, other than as considered in the numerical analysis, on the assumed spherically symmetric flow of liquid near a collapsing bubble. There are also other macroscopic effects which involve the effective viscosity of a mixture of water and bubbles as occurs in a cavitating venturi. The hydrodynamic behavior of such a mixture of bubbles in water will differ from that of pure water because of both the increased compressibility of such a mixture

and the change in the effective dilational viscosity and in the effective shear viscosity of the mixture. Equations for calculating the effective viscosity of dispersions of solid particles and of liquid particles dispersed and maintained by surface tension have been discussed by Oldroyd[73] for very low shear rates. No analysis of the overall cavitating venturi flow properties will be attempted here since single bubbles are the main concern, and the analysis would not obviously contribute to this.

The first consideration is that of the effect of pressure on the usual shear viscosity of a liquid. Pressures in the liquid near a collapsing bubble are high, and therefore if pressure affects shear viscosity causing it to vary from the assumed constant value, then the effect will be apparent when the bubble is small and the velocity high. It is the bubble behavior in this region of collapse which is most important to the study of the damage caused by cavitation bubbles and on possible correlations of damage and fluid properties, so such consideration of viscosity is appropriate. Bridgman[74] has investigated the shear viscosity of many pure liquids at pressures up to 10,650 atm for low shear rates. For water, relative to the value for water at 0.9678 atm and 0°C, the viscosity at 0.9678 atm and 30°C and 75°C is respectively 0.488 and 0.222. At 5800 atm, the viscosity at 0°, 30°, 75°C is 1.347, 0.786, and 0.367. At 10,650 atm and 30°C, the relative viscosity is 1.126. Water has a peculiar behavior in that for temperatures below 30°C, the viscosity decreases with increasing pressure for pressures up to about 1000 atm, and then increases. For higher temperatures it increases with

increasing pressure for all pressures above one atmosphere. Therefore, the shear viscosity in the vicinity of a cavitation bubble in water at 30°C can increase by the ratio 1.126/0.488 = 2.3 and possibly even more. Since the viscosity appeared analytically to have a retarding effect on the bubble collapse (although later numerical results qualify this statement), the assumption of a constant viscosity with respect to pressure is probably a conservative one when seeking to show that collapsing bubbles can cause damage to adjacent solids. However, when considering the possible temperature rise in and near a bubble, the variation of viscosity with temperature may counteract the change with pressure. The viscosity of water decreases by about a factor of two for a temperature rise from 30°C to 75°C over the entire pressure range considered by Bridgman. In conclusion then, a detailed consideration of the variation in shear viscosity would be difficult to apply to the calculations of bubble wall velocity and is not warranted here, since the variation with pressure and temperature tend to cancel each other for collapsing cavitation bubbles.

The variation in viscosity of the water in the venturi with dissolved air was considered since the experimental system is operated with tap water which initially is essentially saturated with air. Deaeration equipment on the system can reduce the air content to about 30 percent of the saturation value. Suciu, Zoss and Sibbitt[75] investigated the solubility of nitrogen in water for temperatures to 700°F and partial gas pressures to 5000 psia. A shallow minimum in the curve of solubility vs temperature was found for all partial gas pressures, at just below

200°F; then the solubility increased without limit as the critical temperature of water was approached. At a constant temperature of 100°F the solubility increased from about 0.1 cc nitrogen per gram of water (STP) when the partial gas pressure was 100 psia, to about 30.0 cc gas/gm water at 3000 psia (STP). In other words if the water in the venturi is saturated with air at about atmospheric pressure and if the air solubility behaves like the nitrogen solubility, then the water in the high pressure region surrounding a collapsing bubble is highly under saturated in the local high pressure region. It then remains to present information on the viscosity of air-saturated water at high pressures. Unfortunately no such data were found at high pressure, but there are data reported for atmospheric pressure.

Caw and Wylie[76] reported the viscosity of air-saturated water relative to that of air-free water. They found that the effect of air on the kinematic viscosity of water at one atmosphere pressure does not exceed 13 parts in 10^5, and further, that the effect of the pressure of one atmosphere of air over the water did not change the viscosity by more than a few parts in 10^5. The results apply for temperatures of 20° to 30°C. No mention has been made of the possible diffusion of gas in the vicinity of the bubble, due to gas concentration gradients or to pressure gradients, because the very short times involved during the collapse tend to negate such contributions. Therefore, even though the effect of dissolved gas on the dynamics of the collapsing bubble system is uncertain, it probably is less important than some of the other assumptions which are made, and will, therefore, be neglected here.

The viscosity term appearing in the usual Navier-Stokes equation of motion has certain inherent limitations in its applicability to real hydrodynamic situations. In the derivation of the viscous equation of motion according to Lamb,[77] a mean pressure p is defined as the arithmetic mean of three mutually perpendicular instantaneous stresses acting on a fluid element, but this definition has certain implications as will be shown. The pressures in the three principal directions are related to the fluid element deformation according to Stokes by a general linear relationship, which for the X direction in rectangular coordinates is, as expressed by Tisza[78]

$$p_{xx} = p_s - 2\mu \frac{\partial u}{\partial x} - \mu' \operatorname{div} \vec{V} \tag{49}$$

where $\vec{V}$ is the vector velocity and u its x component, and similar expressions apply for the Y and Z directions. The two quantities μ and μ' are here simply assumed constants of proportionality between stress and deformation, and p_s is the hydrostatic pressure. For a static fluid then, the three component pressures are all equal to each other and to the usual hydrostatic pressure. If, for a fluid in motion, the mean pressure p is used in describing the fluid behavior, then Equation (49) gives

$$p = \frac{1}{3}(p_{xx} + p_{yy} + p_{zz}) = p_s - \left(\frac{2}{3}\mu + \mu'\right) \operatorname{div} \vec{V} \tag{50}$$

If k is defined by

$$\left(\frac{2}{3}\mu + \mu'\right) = k \tag{51}$$

and the continuity equation is used, Equation (50) becomes

$$p = p_s + \frac{k}{\rho}\frac{d\rho}{dt} \tag{52}$$

Therefore, if the fluid behavior is given by Equation (49) and if also the mean pressure is defined as in Equation (50) then the pressure is dependent upon the time rate of change of density as shown in Equation (52). Stokes, in a quotation given by Tisza,[78] indicated that the quantity k should be zero if in a uniform dilation the pressure is to depend only on the instantaneous value of density and temperature. It is a usual assumption of hydrodynamics and the Navier-Stokes equation of motion to make $k = 0$. Stokes justified this by saying that in most fluid-flow problems the density is nearly constant or at least is changing slowly with time. If this assumption is not made, then the Navier-Stokes equation becomes the following, as given by Liebermann,[79] in the absence of body forces,

$$\frac{D\vec{V}}{Dt} = -\frac{1}{\rho}\,\mathrm{grad}\,p + \frac{\mu}{\rho}\nabla^2\vec{V} + \frac{(\mu+\mu')}{\rho}\,\mathrm{grad}(\mathrm{div}\,\vec{V}) \tag{53}$$

the constant μ is the usual shear viscosity, and μ' is called the dilational or compression viscosity. For an ideal monatomic gas it can be shown[86] that k is exactly zero, so that $\mu' = -2/3\,\mu$.

The justification for $k = 0$ given by Stokes does not apply in many situations where either the pressure change is sufficient to significantly change the fluid density, as in the following numerical results for cavitation bubbles, or the pressure changes very rapidly

with time as in the ultrasonic studies of energy absorption in liquids or in any case involving shock waves in fluids. Karin and Rosenhead[80] in a review of the quantity μ' or k, which is frequently called the second coefficient of viscosity, discuss the importance of including μ' in determining energy absorption of waves in fluids. They point out that in all experiments to measure absorption in gases or liquids since the first in 1898, the experimental values of absorbed energy were larger than the values calculated, with the exceptions of mercury and liquid argon, on the basis of Stokes coefficient

$$\alpha = \frac{2\omega^2\mu}{3\rho C_o^2} \tag{54}$$

where C_o is the sonic velocity and α is defined by

$$J_x = J_o \; e^{-2\alpha x} \tag{55}$$

and J_x is the intensity of a plane sound wave after traveling a distance X. Equation (54) shows that if the density is relatively high, as it is for liquids as compared to gases, then the absorption will be significantly measurable only at very high frequencies. At high frequencies however, or high rate of change of density, the second viscosity coefficient becomes important, and therefore Equation (54) does not hold. Liebermann[79] gives as an approximation for the absorption coefficient

$$\alpha = \frac{\omega^2(2\mu+\mu')}{2\rho C_o^3} \tag{56}$$

Using a method proposed by Eckart,[81] Liebermann measured the ratio of the two viscosities, μ'/μ, for twelve liquids, mostly at a frequency of five megacycles. The ratio was positive for all liquids, instead of $-2/3$ as it would be from Equation (51) if k were set equal to zero. He concluded that it was definitely necessary to include the dilational viscosity, and that when it was included, Stokes absorption theory agreed well with the experimental results.

For at least one liquid the ratio of viscosities was a function of frequency, with the ratio apparently increasing with decreasing frequency. Liebermann explained this by including a relaxation effect in the dilational viscosity. The relaxation time for shear viscosity is usually assumed to be the mean free travel time of the molecules, or on the order of 10^{-12} second, and is thus not significant at megacycle frequencies. When appropriate correction was made for the dilational relaxation, the results gave a dilational relaxation time about 2×10^{-7} second for the liquid ethyl formate. Karin and Rosenhead[80] discuss some of the proposed molecular mechanisms for dilational relaxation, and give values of μ' for water at 17 megacycles of 0.052 poise at 4°C and 0.026 poise at 20°C. Libermann gave the value of μ'/μ for water at five megacycles as 2.4, independent of temperature from 4°C to 25°C. Litovitz[82] further discussed the theory involved in the molecular structure of compressed liquids, and has separated the contribution to compressibility into the relaxation effect due to structural relaxation and the effect due to so called solid-like compression of the liquid lattice. He quotes a ratio for the relaxational

compressibility to the total adiabatic compressibility of water as 0.61. Litovitz also mentions that liquids exhibit shear rigidity when sheared at high rates, with a shear relaxation time comparable to the structural relaxation time.

The question now occurs as to what significance these effects may have with respect to cavitation bubbles. So little comprehensive data is available that at most it can only be estimated whether or not such effects are important, without attempting for the present to quantify them. As a typical example, consider the result for a cavitation bubble collapsing from an initial radius of 50 mils in compressible water at a static pressure of one atmosphere, and containing gas which is compressed adiabatically from an initial pressure of 1.0×10^{-3} atmosphere with $\gamma = 1.3$. As will be shown later, the maximum wall velocity is slightly less than the sonic velocity in water at one atmosphere. Taking the ratio of wall velocity to instantaneous bubble radius to obtain an appropriate frequency, the frequency is about 7×10^{7} sec^{-1}. The pressure in the liquid at the bubble wall is 1.26×10^{4} atmospheres giving a liquid density 1.27 times larger than at one atmosphere and the total time elapsed is 1.1×10^{-4} seconds. Therefore, the combination of a large change in density in a very short elapsed time suggests that the dilational viscosity effects may be of importance in collapsing cavitation bubbles. As the bubble wall accelerates inward the appropriate frequency becomes very large, and it is conceivable that dilational and shear relaxational effects might also become important in some liquids. The possible magnitude of the

compressibility term omitted from the Navier-Stokes equation in the numerical solution will be considered later. If the second viscosity effect were included there also, then the magnitude of the last term would be from 3.4 times as large for water to several hundred times as large for carbon disulphide when the time rate of compression is high.(79)

In view of the magnitude of these relaxational effects and the definite possibility that such effects can occur in cavitation bubbles, some questions arise concerning the liquid behavior. For example when a liquid undergoes an extremely high shear or compression rate as in the vicinity of a small radius bubble during collapse, and the liquid exhibits relaxation, by what mechanism does the liquid relaxation occur? The molecules of liquid could undergo rotation, or transfer from one so called lattice site to another with an accompanying release of energy. It is conceivable that this energy is emitted as discrete quanta with wavelengths in the visible light spectrum, and that this be a mechanism for sonoluminescence. It is interesting to note that the second viscosity effect for carbon disulphide is very large, and also the sonoluminesence from carbon disulphide in water is large when compared to water alone. However, other liquids having high second viscosity ratios do not have extremely high sonoluminescent intensity. A detailed survey of the molecular behavior of liquids and liquid mixtures, including the frequency dependence of the relaxation effects is of course not warranted here, but its desirability is certainly suggested by the above analysis.

III. RESULTS OF NUMERICAL ANALYSIS

A. Behavior of Characteristic Curves

The variables at the bubble wall are evaluated independently of the liquid behavior away from the bubble wall. This method is possible because of the Kirkwood-Bethe assumption on propagation of the characteristic constant quantity $r(h + u^2/2)$ at known velocity $(c + u)$. If this condition were not analytically imposed on the equations for motion of the bubble wall, then the motion of the entire liquid field and the wall would have to be considered at the same time in the numerical analysis. As it is, the values at selected increments of bubble radius are computed first and used as initial conditions to start each characteristic curve. Once the initial values of radius, velocity, and pressure are known, the characteristic path is determined completely independently of all other liquid or bubble behavior. The relation of one characteristic curve to all the others is made through the variables time and location along a characteristic path. Consider the plane of liquid radius vs time. The bubble wall is represented by a single curve in this plane, and for radii less than the bubble radius at a given instant of time, there are no characteristic curves defined -- the curve for the bubble wall is the boundary of the region in the entire $r - t$ plane in which the characteristic curves exist. Each point in the region has a value of the quantity $r(h + u^2/2)$, and only one value can exist at any liquid particle position r at a given time t. The path of those points for which this quantity is a constant is the characteristic path, and all such paths originate on the bubble wall.

In Figure 1 the bubble wall (for parameters of a reference bubble used throughout this chapter) is represented by the curve through the circled points, which merely indicate the origins of each of the characteristic paths which extend into the liquid. It is important to note that as the bubble becomes smaller, the change in time both between the points of origin of the paths and along the path becomes very small. It is essential that the paths be properly located in time so that there is no incorrect situation caused by numerical inaccuracy where two characteristic curves cross. This situation would represent the fact that two different values of $r(h + u^2/2)$ exist at the same liquid particle at the same instant of time and is of course physically impossible. Considerable care is required to retain sufficient numerical accuracy in the normalized time to prevent such incorrect overlap. The numerical procedures involved in this are discussed further in Appendix III. However, since each path can be followed out as far as desired without reference to what happens at the bubble wall after it leaves, it is conceivable that a path originating at a later time overtakes a preceding path. Such a possibility has been indicated by Fitzpatrick and Strasberg[84] who indicate that this situation represents the formation of a shock in the liquid, which forms after the bubble wall has been stopped either by the common, but artificial, assumption of a small concentric rigid sphere or by assuming a sudden pressure rise in the gas contained within the bubble. No overlap of characteristics was observed for the range of parameters chosen here during the collapse of the bubble. The propagation of a pressure pulse

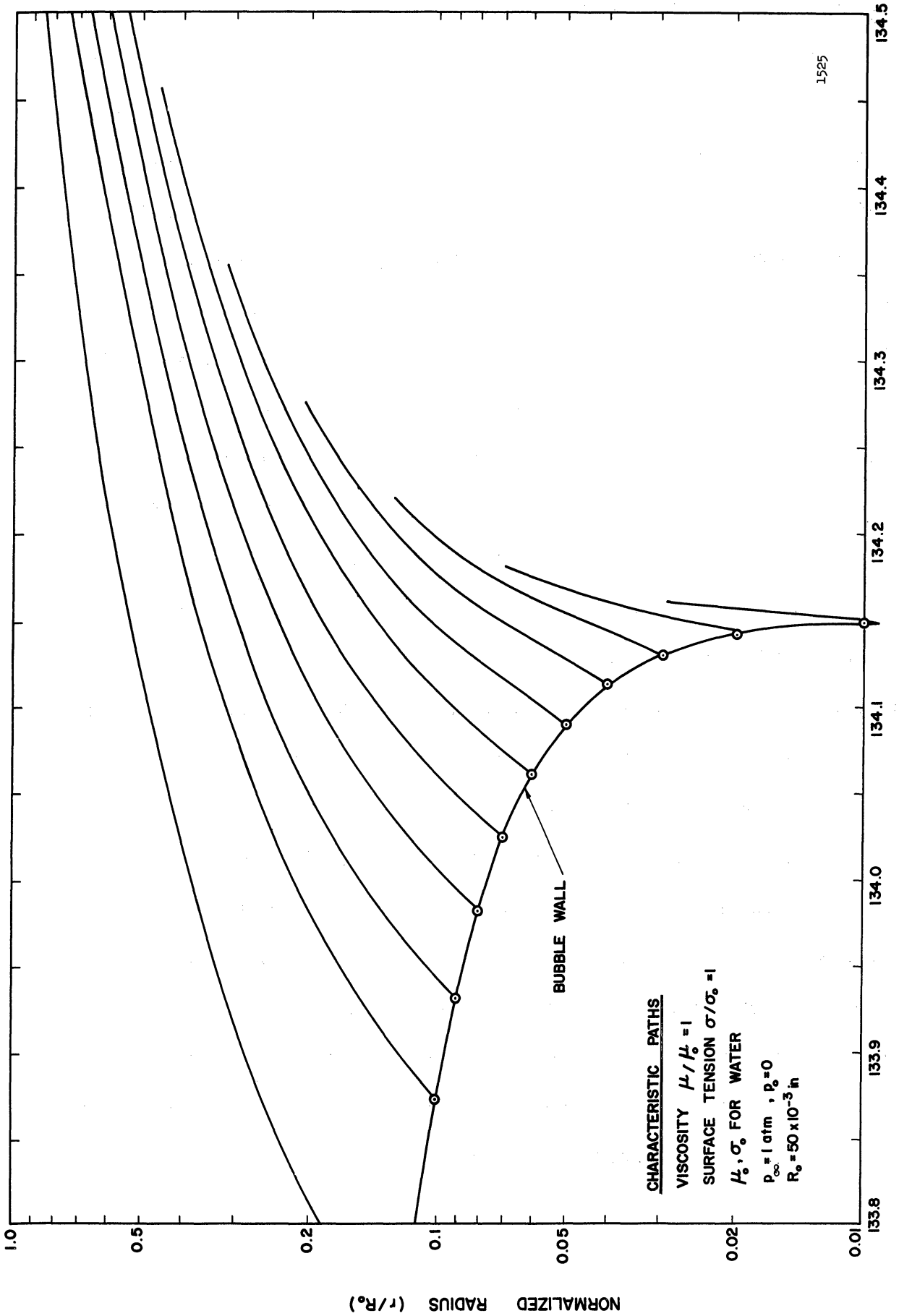

Figure 1. Location of Characteristic Paths vs Normalized Time for Normalized Bubble Radii Down to 0.01 for Reference Bubble Parameters.

or shock outward into the liquid subsequent to the arrest of the bubble wall motion is considered later.

Figures 1, 2, 3, 4, are plots of the characteristic paths for succusively smaller bubble radii. Each succeeding figure has been plotted on an expanded time abscissa but all with the same time normalization and referred to the same zero point at the start of bubble collapse. Figure 2 is expanded by a factor of 250 over Figure 1, 3 by a factor 20 over Figure 2, and 4 by a factor 50 over 3, so that if Figure 1 were plotted on the same scale as Figure 4, it would have an abscissa 250,000 times longer. Such a portrayal demonstrates the inherent difficulties in the calculations, especially when interpolation between the curves is necessary to obtain the variables for a given fixed value of time.

The slope of those curves which are marked with circles is the bubble wall velocity $dR'/dT' = U'$. The slope of the characteristic paths is $(dr'/dt')_c = (u' + c')$, the velocity of propagation of the characteristic. Since the liquid particle velocity, u , is always negative for collapse, the quantity $(u + c)$ becomes zero when the Mach number $|u|/c$, becomes equal to 1.0. This occurs in Figure 1 for a radius of 0.02, but the horizontal slope is not visible on the scale of the figure. For smaller bubble radii when $|u|/c > 1$, the slope of the characteristic at the bubble goes negative as seen in Figures 2 through 4. A negative slope represents a negative propagation velocity as viewed from a fixed frame of reference so that even though the characteristic moves away from the bubble wall, it actually moves inward toward $r = 0$. This continues until the pressure along the characteristic

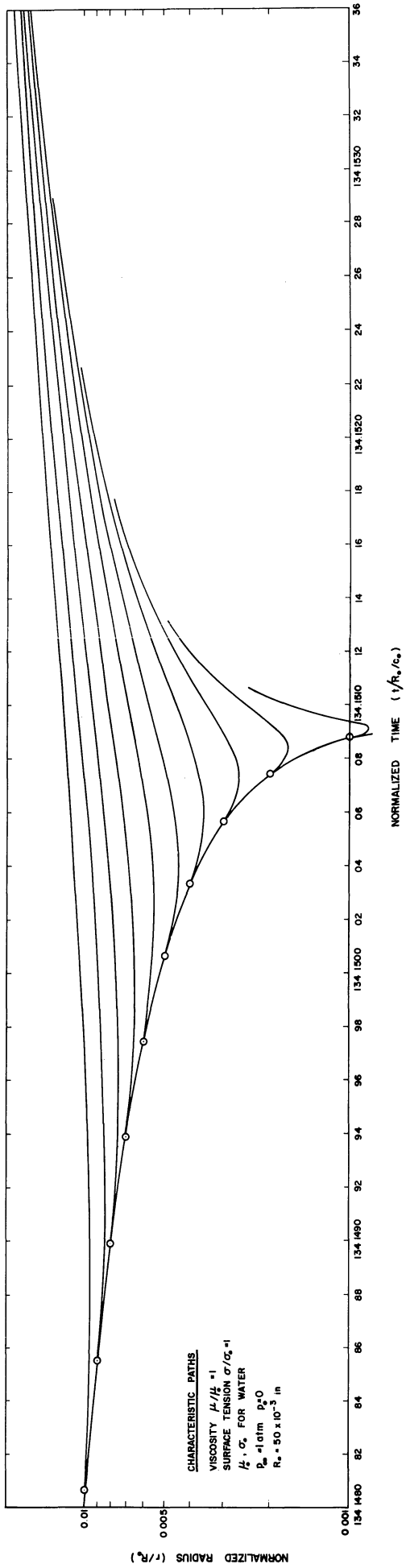

Figure 2. Location of Characteristic Paths vs Normalized Time for Normalized Bubble Radii from 0.01 to 0.001 for Reference Bubble Parameters.

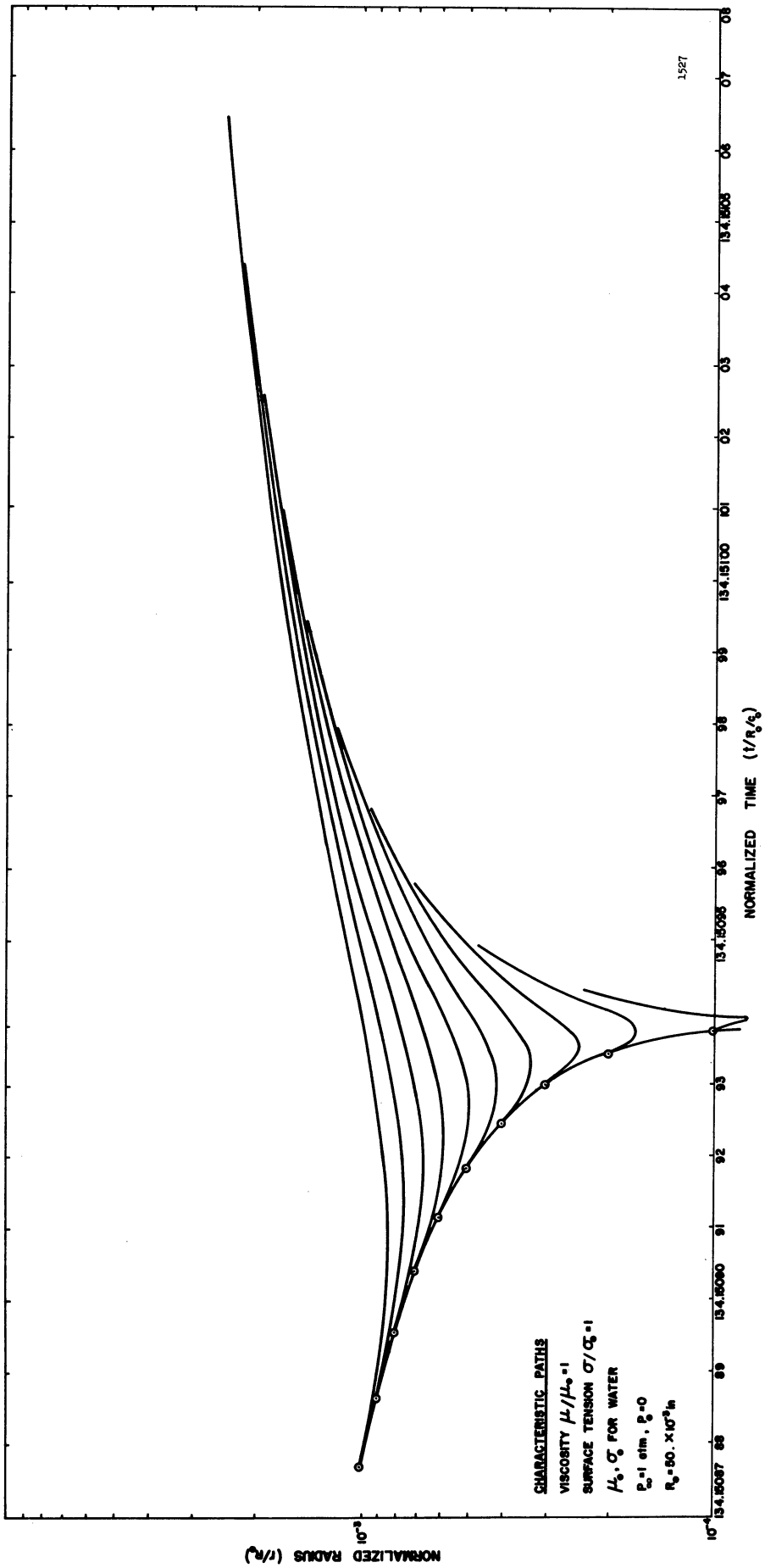

Figure 3. Location of Characteristic Paths vs Normalized Time for Normalized Bubble Radii from 10^{-3} to 10^{-4} for Reference Bubble Parameters.

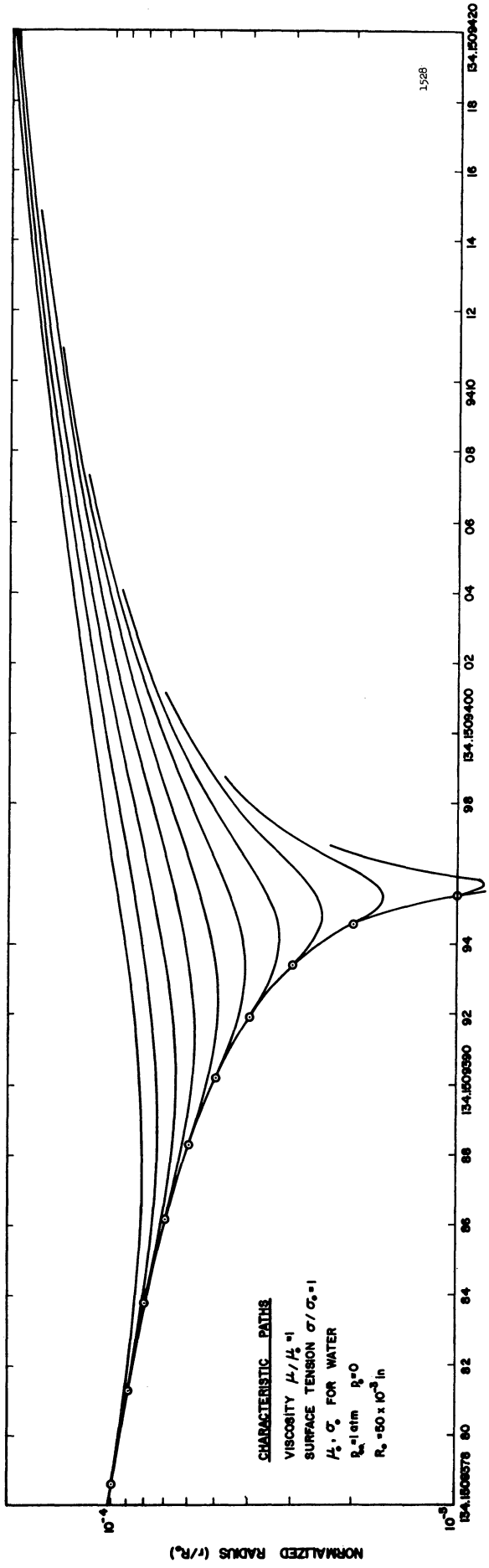

Figure 4. Location of Characteristic Paths vs Normalized Time for Normalized Bubble Radii from 10^{-4} to 10^{-5} for Reference Bubble Parameters.

rises enough so that the sonic velocity becomes large, and therefore the Mach number decreases even if there were no decrease in velocity. Also, the pressure rise, and therefore also the rise in h, near the bubble wall is very rapid so that for the quantity $r(h + u^2/2)$ to remain constant when h is increasing, the velocity u must decrease rapidly. The result is that the characteristic moves inward for a distance of only about two tenths of the bubble radius, then reverses and moves outward. This rapid reverse in direction was one of the most difficult properties of the solution to evaluate numerically with the excellent accuracy desired as shown by the curves.

Figure 5 shows the liquid particle velocity and Mach number along several of the characteristic paths shown in Figures 1 through 4. The solid lines are normalized velocity and the dotted lines are Mach number at the same radial position. It is seen that for normalized bubble radii less than about 10^{-3}, and for the conditions and parameters listed which were taken as a reference set, the absolute value of the liquid velocity along a characteristic path increases as the radial position decreases, then the absolute velocity decreases with the characteristic still moving inward and finally the characteristic moves outward and the absolute velocity very rapidly approaches zero. The Mach number at the bubble wall is considerably less than the normalized velocity for small bubble radii because the pressure and therefore sonic velocity rise rapidly as the bubble collapses. A sharp pressure peak occurs along the characteristic path near the bubble so that even though the absolute normalized velocity increases, the Mach number starts

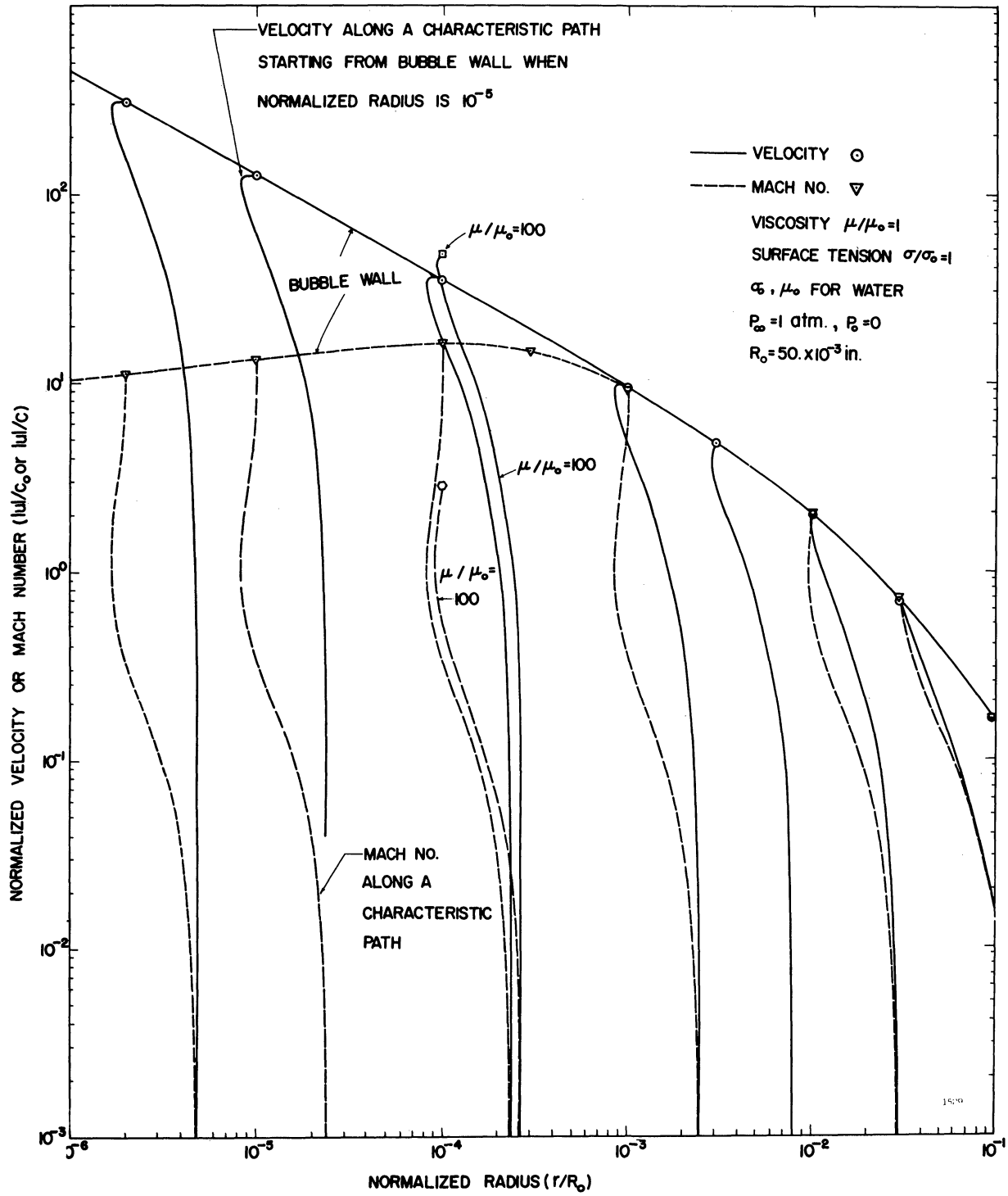

Figure 5. Liquid Velocity and Mach Number Along Characteristic Paths vs Normalized Radius for Reference Bubble Parameters and Including High Viscosity Curve.

decreasing from the bubble wall and continues to drop sharply along the path. At the point where the characteristic curve for Mach number reaches a minimum radius, the quantity (u + c) is zero and the Mach number should be exactly equal to one since the outward propagation with velocity c is countered exactly by the inward propagation of velocity (-u) at this time. All the characteristics are consistent in this respect as evidenced by the fact that the minimum radius on all the Mach number curves occurs at Mach number = 1.0 in Figure 5.

The physical meaning of the characteristic curves is sometimes difficult to appreciate. It is more desirable to have the equivalent of an instantaneous picture showing the variables as a function of liquid radius. The method of interpolation along each characteristic to find the variables at a fixed time is given in Appendix III and the results are discussed in the following.

B. Pressure and Velocity Fields in the Liquid During Bubble Collapse

The curves in Figures 1 through 5 are replotted in Figure 6 in terms of Mach number and normalized velocity vs normalized liquid radius at several selected fixed instants of time. The identified points represent values at the bubble wall and the curves then represent the velocity of the liquid when the bubble has collapsed to that radius. Again, the solid lines are normalized particle velocity and the dotted lines are Mach number. In addition to the previous reference values of the parameters, curves are shown for an increase in the liquid viscosity to 100 times that of water. The most important observation from these curves is that the bubble wall normalized velocity for normalized bubble

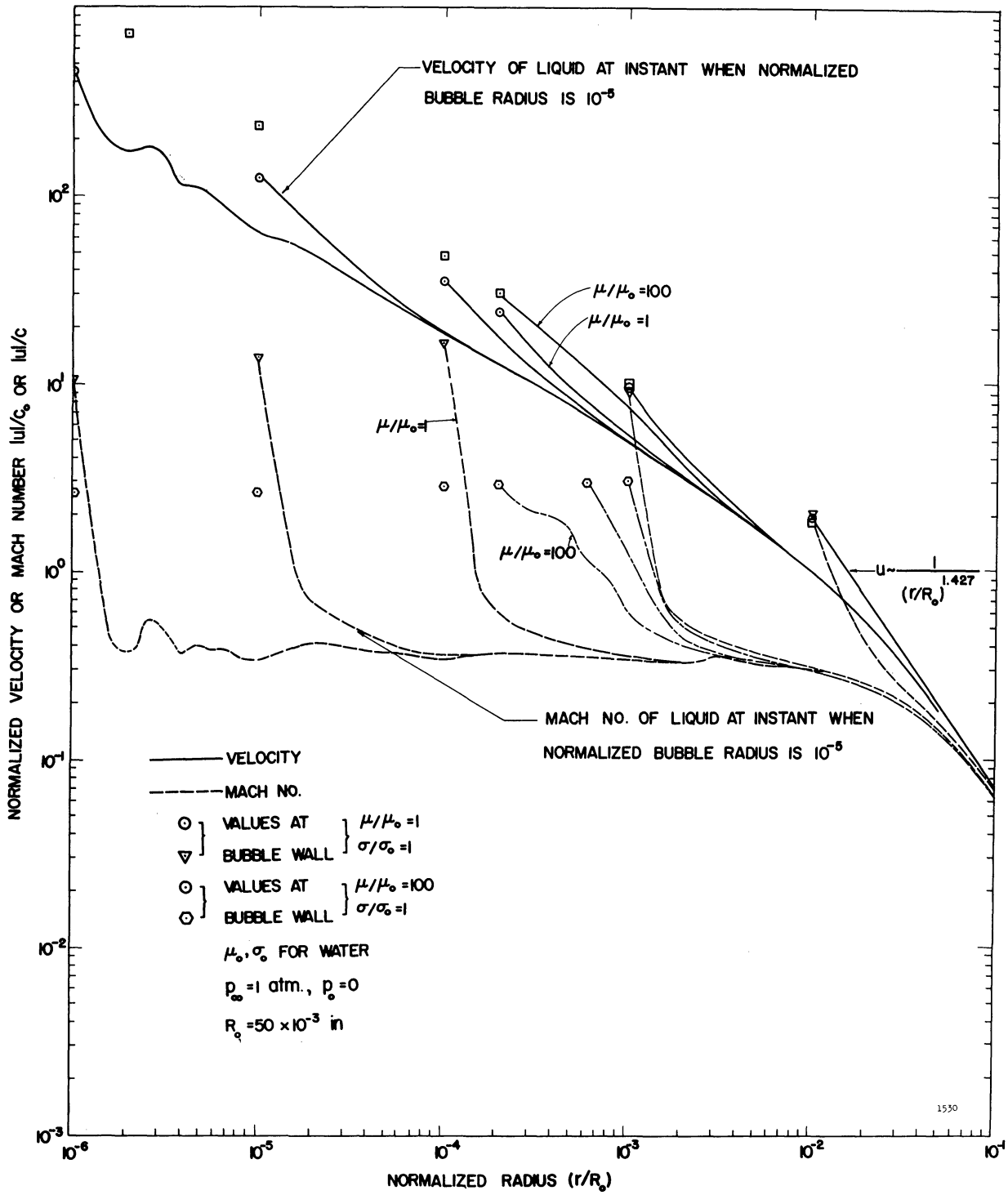

Figure 6. Velocity and Mach Number at Constant Times vs Normalized Radius, for Reference Bubble Parameters and Including Curves at High Viscosity.

radii less than 1×10^{-3} increases when the viscosity is increased. This same behavior is observed for viscosities from 2 to at least 500 times the viscosity of water, other parameters remaining the same. A more extensive discussion of the effect of variation of parameters on only the bubble wall variables will follow. It is noted that while the actual wall velocity increases with increased viscosity, the wall Mach number decreases because the liquid pressure at the wall is increased, for a given bubble radius, when the viscosity is increased, thereby increasing the sonic velocity.

For values of bubble radius less than 10^{-5}, Figure 6 shows considerable variation in the velocity curve. This is attributed to the interpolation method for finding values of the velocity at constant times by selecting points from many characteristic curves. For such very small bubble radii, the time increments are too small to retain sufficient numerical accuracy. However, the method of computation is such that the characteristics leaving the wall at earlier times are still well defined, and are not affected by later leaving characteristics, so the solutions are valid for all greater bubble radii. The fact that the curves at constant times are smooth for all larger bubble radii indicates a valid method of interpolation. The curves for the behavior only at the bubble wall are not in any way affected by the behavior of the numerical solution on the characteristics because the two are analytically distinct.

In considering the curves for velocity for $\mu = 1$, it is seen that the slope du/dr at the bubble wall appears to decrease with

decreasing bubble radius, but this appearance is because of the log coordinates. The numerical value of du/dr actually increases drastically as radius decreases, thereby increasing the viscous pressure term at the bubble wall. It is seen however, that for the same value of bubble radius when the bubble radius is less than about 1×10^{-3}, the slope du/dr is less in the liquid at the wall when the viscosity is larger. From Equation (18), the contribution to the pressure in the liquid at the wall due to viscous stresses is given by $2\mu\partial u/\partial r$, which for the incompressible liquid at the bubble wall is simply $-r\mu U/R$. When the incompressible solution is used, an increase in viscosity causes a decrease in bubble wall velocity as expected. However, in the compressible case, the contribution to the pressure at the wall from viscous effects is given by Equation (40) as $-4\mu U/R - (4\mu U/3C^2)(dH/dR)$, but the last term here has been neglected in the numerical solution. It will be shown in the present calculations that the wall pressure (and therefore also the enthalpy, H) increases more rapidly with decreasing bubble radius when the viscosity is increased. Therefore, the term containing dH/dR increases and the net effect of the entire term above, which was neglected, would be to tend to counteract the effect of the viscous term which was included. Unfortunately, no analytical presentation has been obtained which could definitely show that an increase in viscosity would or would not have the effect observed on an analytic model which included both terms, even though a possible reason has been given above, so that the validity of the numerical results of a viscosity increase in describing the behavior in a real physical situation remains in doubt.

Consider now the variation in velocity at a fixed point in the liquid starting from the instant when the bubble wall passes that point. For example, when the bubble wall passes $r' = 1 \times 10^{-2}$, the normalized liquid velocity is 1.95. By the time the bubble wall has reached 1×10^{-3}, the velocity at $r' = 1 \times 10^{-2}$ has dropped to 1.02 and remains at essentially that value as the bubble continues to collapse. Similar behavior occurs at other points in the liquid, but the ultimate constant velocity at each point is different. For values of normalized radius greater than about 1×10^{-2}, there is little difference in this ultimate velocity for an increase in viscosity as shown.

The variation of Mach number near the bubble wall is different from that of velocity. At any instant of time after the normalized bubble radius is less than about 0.5 there is a large pressure peak near the bubble wall. Therefore, the sonic velocity within the pressure peak is very large and the Mach number accordingly small. The plot of Mach number vs liquid radius then shows an extremely rapid drop near the bubble wall as seen in Figure 6. The Mach number then remains essentially constant throughout the liquid out to a normalized radius of about 1×10^{-2}, where it then drops in about the same manner as the liquid velocity, with increasing radius. At a fixed point in the liquid, the Mach number drops rapidly from the value at the bubble wall after the wall passes and then remains constant as the bubble continues to collapse, in a manner similar to the velocity. However, the Mach number is different from velocity in that for all points in the liquid at radii less than about 1×10^{-2} the Mach number drops to about the same value

after the bubble wall passes, namely 0.35. In interpreting such behavior in the liquid it should be recalled that the plot of Figure 6 is on log coordinates so that the distance being considered is less than 10^{-2} of the original bubble radius or a distance less than 5×10^{-4} inches for the reference bubble under consideration, where the Mach number remains constant.

The velocity in the liquid at a fixed time varies, as indicated in Figure 6 to approximately $1/(r')^{1.4}$. The bubble wall velocity in an incompressible liquid varies as $1/(R')^{1.5}$ (Figure 11) and the velocity in the liquid at a fixed time varies according to Equation 4 as $1/(r')^{2}$. The bubble wall velocity for the reference parameters in compressible liquid, for bubble radii less than about 10^{-3} varies as $1/(R')^{.55}$. An approximate, inviscid, analytic result of Gilmore[58] for compressible liquid gave $1/(R')^{.5}$. Hickling and Plesset[66] reported the wall velocity to vary as $1/(R')^{.785}$ for the empty bubble in inviscid liquid. Therefore, the effect of viscosity in water for an incompressible analysis does not significantly change the bubble wall velocity as a function of bubble radius. For the compressible case, the bubble wall is definitely slowed down by the effects of compressibility.

Figure 7 is a plot of liquid pressure vs radius for several bubble radii, and for several liquid viscosities. When the viscosity is one times that of water, it is seen that the pressure at the bubble wall is relatively low, but rises extremely rapidly by almost three decades at a distance into the liquid of somewhat less than twice the bubble

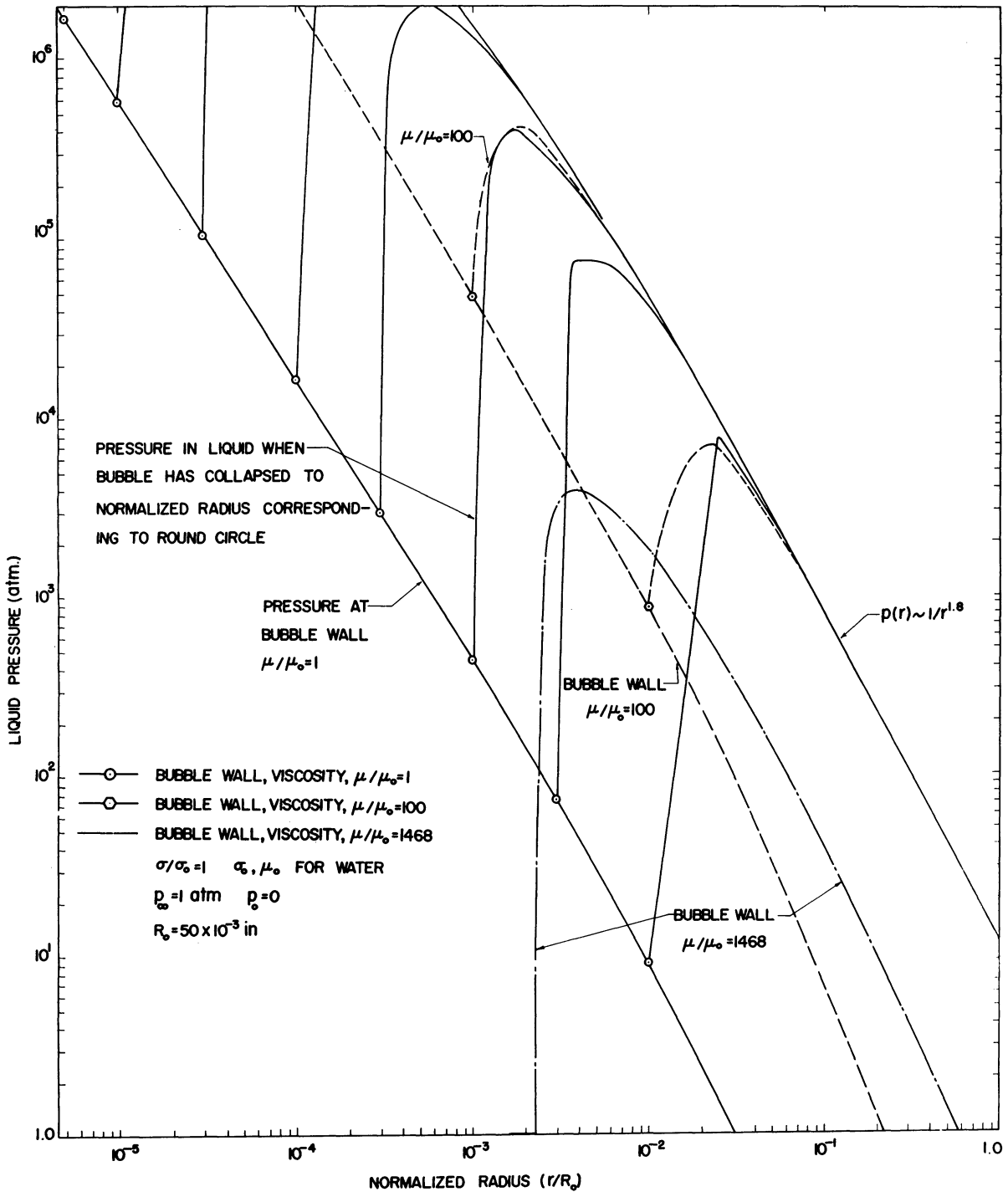

Figure 7. Liquid Pressure at the Bubble Wall and in the Adjacent Liquid for Two Viscosities and at the Bubble Wall for Limiting Viscosity vs Normalized Radius.

radius. The pressure in the liquid at a fixed point rises as the bubble wall passes, then remains at a constant high value as the collapse proceeds. The pressure varies with r', as indicated on Figure 7, as $1/(r')^{1.8}$. When the liquid viscosity is increased to 100 times that of water, the pressure at the wall increases faster with respect to bubble radius. The peak pressure near the wall, however, is about the same as that for the smaller viscosity, and the constant pressure at a fixed radius in the liquid after the wall has passed is also the same. Therefore, when considered with the results for velocity and Mach number, an increase in viscosity has little effect on the liquid behavior other than at or very near the bubble wall.

Poritsky[19] defined a viscosity parameter in his analysis for incompressible liquids according to

$$\mu' = \frac{4\mu}{R_o\sqrt{\rho(p_\infty - p_o)}}$$

and indicated that when $\mu' > 0.46$, the bubble would not collapse with infinite velocity, but would slow down and take infinite time to collapse. He further stated that if surface tension were also included the bubble would always collapse in a finite time. Using the parameters of Figure 7, the limiting viscosity would be 1468 times as large as that for water. The pressure, only at the bubble wall, for this case is also plotted in Figure 7, where surface tension is included. It is seen that the wall pressure is above that for both other curves down to a normalized bubble

radius of about 4×10^{-3}, at which point the wall pressure drops sharply to exactly 1.00 and remains there as the bubble continues collapsing. The normalized wall velocity at this point is about -5×10^{-5}, which is equivalent to three inches per second, or the wall has essentially stopped. The normalized viscosity parameter can be increased by decreasing the initial bubble radius, the liquid density, or the pressure differential causing collapse as well as by increasing viscosity. It is of interest to note that the bubble wall slows down and nearly stops even though surface tension is included (Poritsky's results for an incompressible liquid showed a continued collapse in this case). Also, the numerical solution for an incompressible liquid including surface tension indicates a sudden slowing down of the bubble wall when $\mu' = 0.46$.

As a check on the numerical accuracy of the incompressible solution, which is the same method as that used for the compressible case, results were obtained for a Rayleigh bubble in inviscid water without surface tension, and compared with the exact analytical result for complete collapse of an empty bubble. The computed collapse time was less than the analytic time by only 0.082 percent when the bubble radius was taken down to the point when the computed time for that program no longer changed within the numerical significance used. This result is considered indicative of the appropriateness of the Runge-Kutta type numerical solution for this type of problem, where many increments are made in the independent variable, i.e., bubble radius. At a normalized bubble radius of 1×10^{-6}, the computed normalized

velocity is -8.16×10^{11} which is only 0.033 percent lower than the exact analytic result given by Equation (11), and this after a thousand or more computed steps in the bubble radius. A detailed numerical analysis of the non-linear incompressible or compressible equations as programmed on the computer to enable one to say with certainty whether it is the numerical procedure which caused a difference with other published analyses is extremely difficult. Hence the other alternative of comparison with an exact solution was used. This comparison indicated no evidence of a numerical inconsistency in the results, and yet as will be explained later the results appear to differ slightly with other analyses. No explanation is available at this time.

C. Bubble Collapse with Adiabatic Internal Gas Compression

Figures 8 through 10 show the collapse behavior of a bubble with the same set of parameters as before with the exception that the internal gas pressure is not zero, but varies from an initial value of 1×10^{-3} atmospheres in proportion to $(1/R'^3)^{1.3}$. In Figure 8, the dashed line represents the bubble wall velocity and the solid lines the velocity of the liquid away from the bubble wall at various times. It is seen that the wall motion is abruptly stopped when there is internal gas in the bubble. The wall velocity decreases much more rapidly at first than the nearby liquid velocity. This behavior is attributed to the compressibility of the liquid and the finite velocity of propagation of a disturbance, in this case the pressure rise at the bubble wall. As a result, the velocity gradient in the liquid at the bubble wall changes

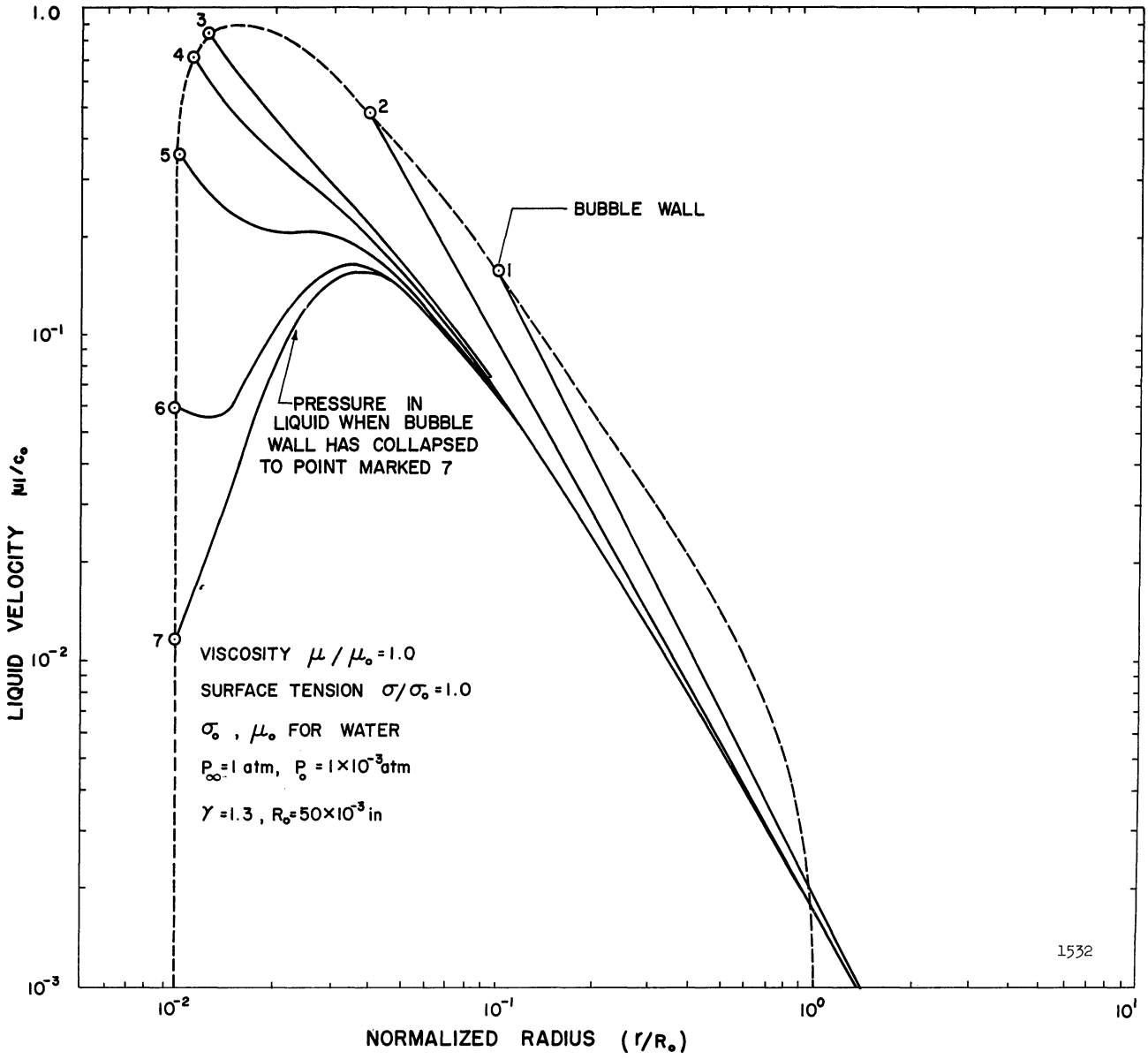

Figure 8. Liquid Velocity vs Normalized Radius for Bubble Containing Gas.

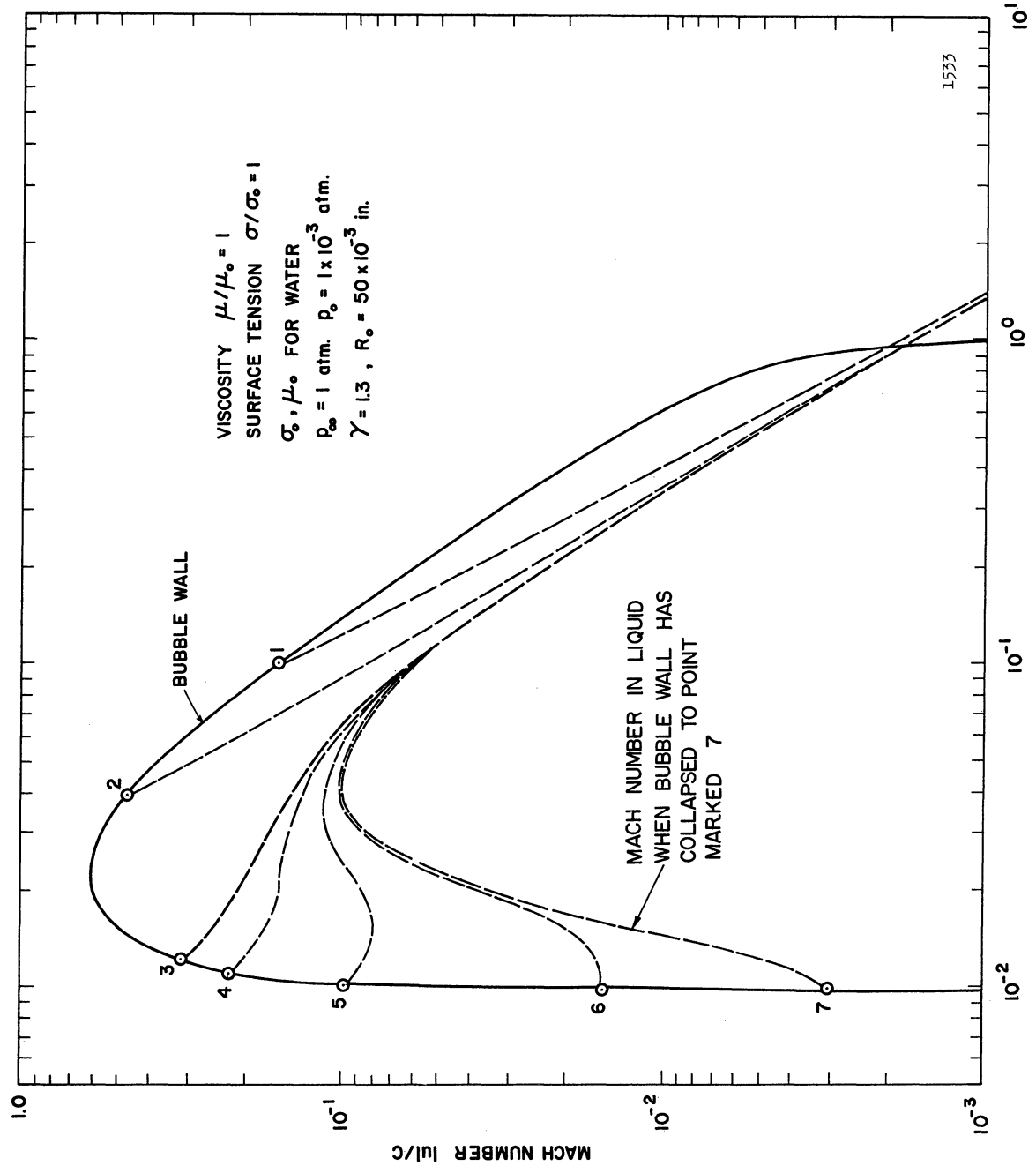

Figure 9. Mach Number vs Normalized Radius for Bubble Containing Gas.

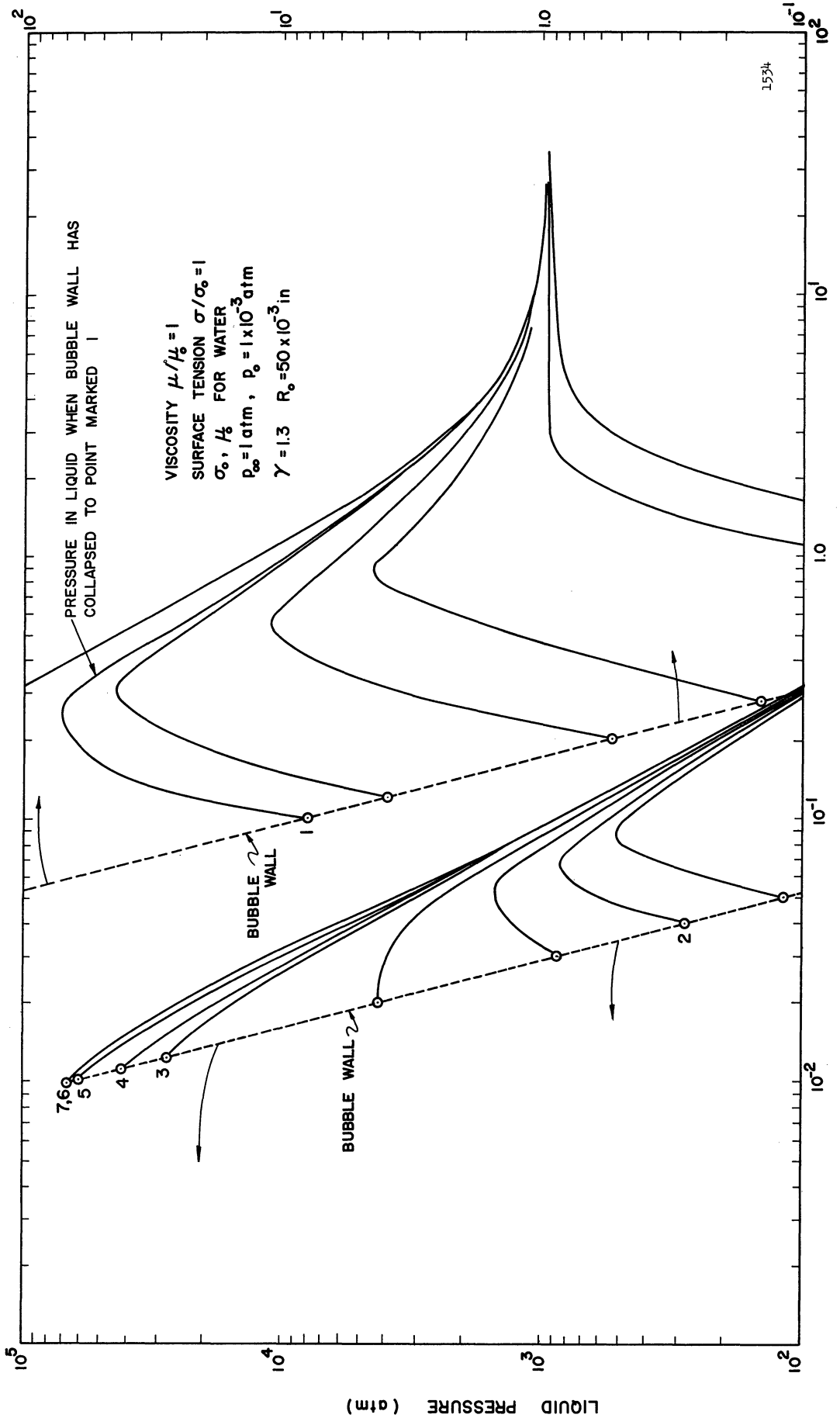

Figure 10. Liquid Pressure vs Normalized Radius for Bubble Containing Gas.

sign. The numbered circles on the bubble wall curve represent selected values of time so that the velocity curves can be compared with the Mach number and pressure curves at the same instant.

Figure 9 is a plot of the Mach number vs liquid radius. The maximum value of Mach number occurs at a normalized bubble radius of 2.3×10^{-2}, whereas the maximum wall velocity did not occur until the bubble wall radius was 1.6×10^{-2}. The Mach number on the curve numbered five has a minimum near the wall, and a maximum farther away from the wall. These results compare with those of Hickling and Plesset[66] who used a different numerical method from the Kirkwood-Bethe assumption of propagation used here, and who neglected both surface tension and viscosity effects. Actually, surface tension and viscosity for the particular values of parameters used here do not affect the general bubble behavior significantly, but as shown before, at least viscosity can have a significant effect within a realistic range of parameters. The Mach number and the velocity at a radius equal to the initial bubble radius rise as the bubble starts to collapse, and then fall to constant values as the collapse proceeds. The approximately constant values at $r/R_o = 1.0$ after the bubble radius is less than 0.1 is less than about 10 ft/sec.

The corresponding numbered curves of liquid pressure vs radius are shown in Figure 10, along with some additional curves at other times. The pressure gradient at the bubble wall becomes zero at the same time that the bubble wall reaches its maximum velocity. This is of course entirely consistent with the equation of motion, Equation (28),

which was used in the analysis. The behavior of the liquid after the velocity goes to zero at the wall and then becomes positive is that of the familiar bubble rebound, and will be considered in more detail later. During the collapse, the pressure in the liquid at a fixed radius rises rapidly as the bubble wall passes, and then remains relatively constant, or at least rises less in proportion to the bubble wall motion. Recall however, that time is not proportional to bubble radius. At a bubble radius of 1×10^{-2} the normalized time is 134.00119, and at the final minimum radius of 9.8×10^{-3} time is only 134.29303. The maximum liquid pressure at a radius equal to the initial bubble radius is 12 atmospheres, and at a radius 10 times the initial radius the maximum liquid pressure during collapse is only 1.1 atmospheres, or 10 percent above the initial liquid pressure.

D. Bubble Wall Velocity with Various Parameters

The velocity and Mach number at the bubble wall for various liquid parameters are plotted in Figure 11. Consider first the three curves for values of viscosity equal to zero, one, and one hundred times that of water. All other parameters have the reference values indicated unless otherwise specified on the separate curves. For normalized radii less than 10^{-3}, the velocity is increased with viscosity, as noted previously in discussing the velocity in the liquid away from the bubble wall. For larger radii, the opposite behavior exists. This tends to confirm the previously stated reason for the anomoly, namely that it is caused by the neglect of the term proportional to the rate of

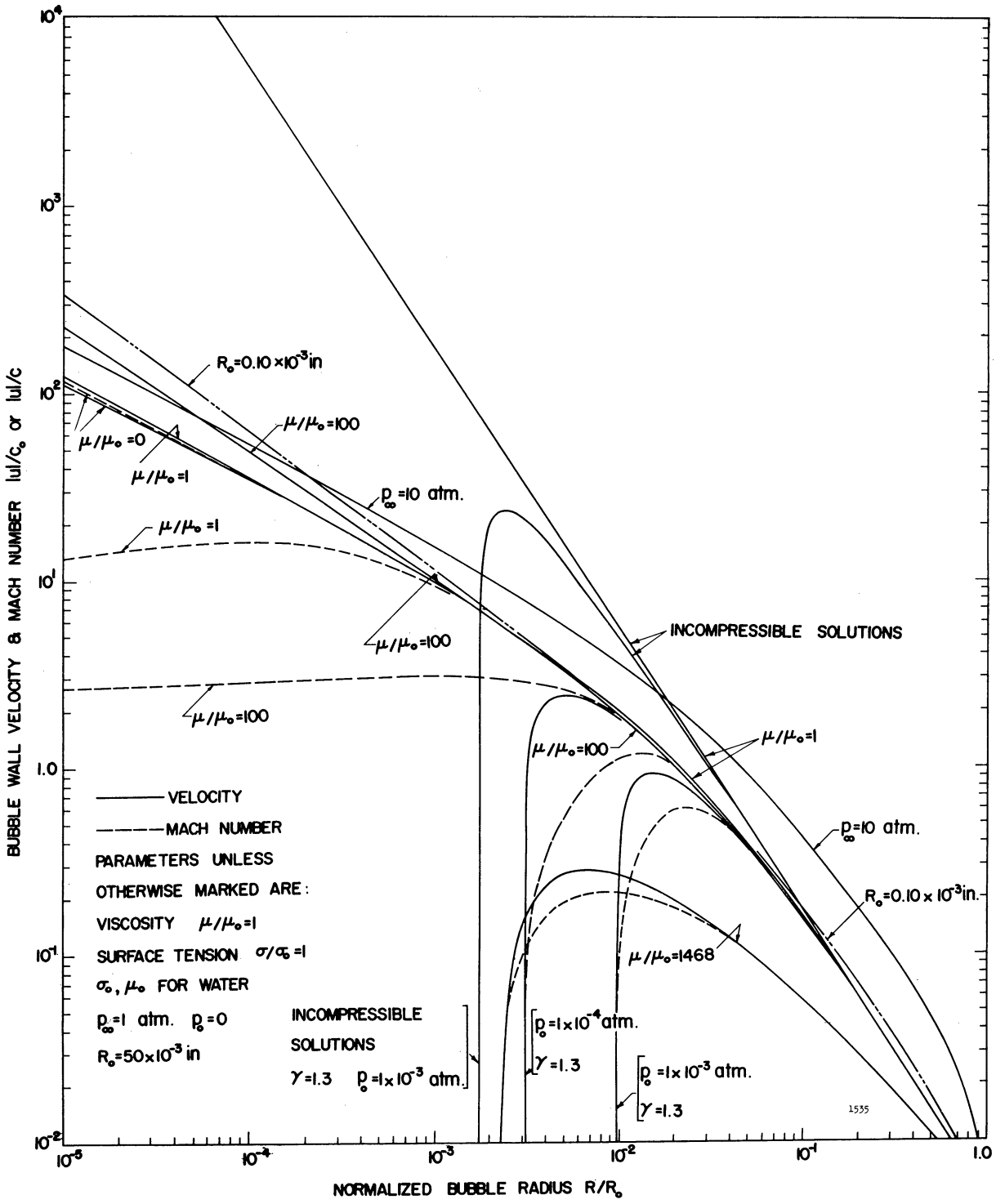

Figure 11. Bubble Wall Velocity and Mach Number vs Normalized Bubble Radius for Reference Bubble Parameters Except Where Noted Otherwise on Individual Curves.

change of enthalpy, H, at the bubble wall. The rate of change of H would be large only when both the velocity is large and the radius is small enough to cause the wall pressure to be large. The Mach number is seen to behave exactly opposite from the velocity - decreasing at a given bubble radius with an increase in liquid viscosity.

When the viscosity is increased to the limiting value stated by Poritsky[19], the wall velocity decreases in a manner very similar to the sudden decrease caused by the presence of gas within the bubble. It is apparent that there is a cut-off point in viscosity somewhere between $\mu = 100$ and $\mu = 1468$ times that of water. The limiting number 1468 would change of course if R_o, ρ, or $(p_\infty - p_o)$ were to change.

The incompressible solution gives a velocity at the bubble wall which is 17 times larger than the compressible solution at $R' = 1 \times 10^{-3}$. Similarly, when a gas is included, the incompressible liquid collapses to a radius which is 0.18 of the minimum radius for the compressible liquid, when the internal gas pressure varies in the same manner with bubble radius. If the initial internal gas pressure is decreased, the bubble collapses farther and attains a greater wall velocity. A decrease from 1×10^{-3} atm to 1×10^{-4} atm causes the maximum wall velocity to increase by a factor of 2.6.

A decrease in the initial bubble radius, R_o, has a similar scale effect as an increase in both the viscosity and surface tension. Figure 11 includes the wall velocity for $R = 0.10$ mils. The curve indicates slightly higher velocities for normalized radii to 1×10^{-2} where it meets the standard curve for $R_o = 50$ mils, then the velocity

for $R_o = 0.10$ mils increases more rapidly than the standard curve as the radius continues to decrease. An increase only in the surface tension, up to six times that of water, causes a very slight increase in wall velocity which cannot be distinguished when plotted on Figure 11.

An increase in the liquid pressure causing bubble collapse, from 1 to 10 atmospheres, causes a proportionately greater velocity increase at the start of bubble collapse than after the bubble is very small. At $R' = 0.6$ it increases the wall velocity by a factor of 3.2, and at $R' = 1 \times 10^{-5}$ the wall velocity increases by a factor 1.48.

E. Pressure Pulse from Rebounding Bubble

It has been shown by Hickling and Plesset[66] that the peak pressure from a gas bubble rebounding in a compressible liquid is attenuated in proportion to $1/r$. Two cases from the present numerical analysis are included here for gas pressure within the bubble for both compressible and incompressible liquids, and are summarized in the following table.

BUBBLE COLLAPSE WITH INTERNAL GAS

$R_o = 50 \times 10^{-3}$ in, σ, μ for water; $p_\infty = 1$ atm $p_i(R') = p_o(R'^3)^{-1.3}$

Compressible	Incompressible
$p_o = 1 \times 10^{-3}$ atm	$p_o = 1 \times 10^{-3}$ atm
$P_{max} = 6.77 \times 10^{4}$ atm	$P_{max} = 5.51 \times 10^{7}$ atm
$R'_{min} = 9.82 \times 10^{-3}$	$R_{min} = 1.76 \times 10^{-3}$
$p_o = 1 \times 10^{-4}$ atm	$p_o = 1 \times 10^{-4}$ atm
$P_{max} = 5.82 \times 10^{5}$ atm	$P_{max} = 1.170 \times 10^{11}$ atm
$R'_{min} = 3.13 \times 10^{-3}$	$R'_{min} = 1.369 \times 10^{-4}$

The peak pressure on the rebounding pulse from the indicated radii is shown in Figure 12 for the two compressible cases. The incompressible results have been omitted as they are so much different and are not really applicable. The initial bubble radius is significant in two respects. First, the magnitude of R_o has a scaling effect on the results, through the viscosity and surface tension parameters, which can be important especially for small bubbles. Second, the pressures have previously been plotted vs normalized radius, but the actual distance a pressure peak will travel will be greater if the initial bubble radius is larger. This is of particular importance in estimating the pressure applied to adjacent solid surfaces in regard to cavitation damage. However, because of the scaling effects, each initial size bubble requires a separate computer solution, unless an appropriate scaling law can be established.

A comparison was made between the total energy available and the energy used to compress the gas within the bubble according to the known pressure variation. The available energy is given by

$$\int_{R_{min}}^{R_o} P_\infty (4\pi R^2) dR + \int_{R_{min}}^{R_o} \frac{2\sigma}{R} (4\pi R^2) dR =$$

$$4\pi\sigma R_o^2 \left(R'^2_{min} - 1\right) + \frac{4}{3}\pi R_o^3 \left(R'^3_{min} - 1\right)$$

where $R'_{min} = R_{min}/R_o$ and R_{min} is the minimum radius when the gas

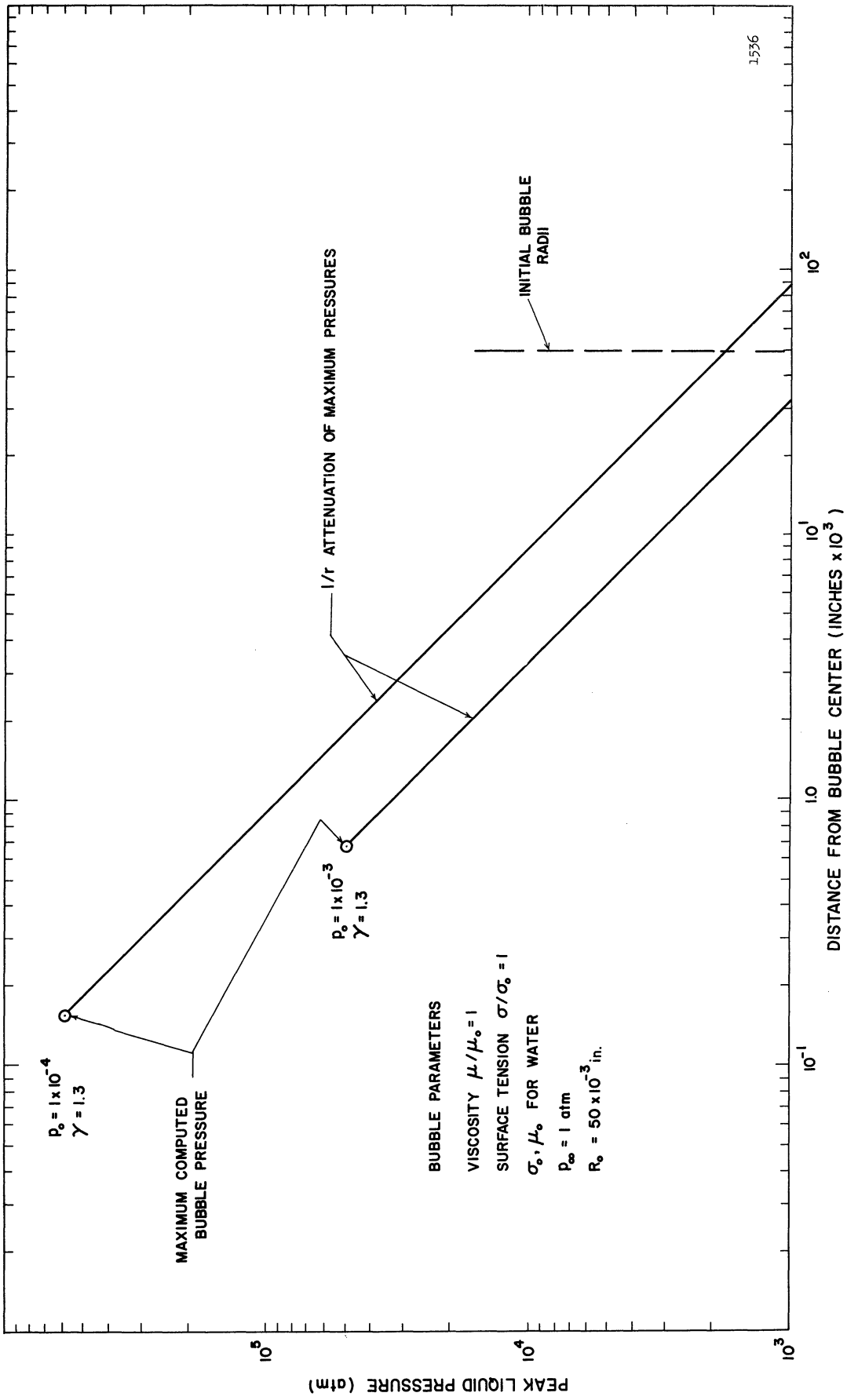

Figure 12. Peak Liquid Pressure on Rebounding Pressure Wave vs Distance from Bubble Center, Assuming 1/r Attenuation.

has stopped the bubble, obtained from the computer solution. The energy used to compress the gas is

$$\int_{R_{min}}^{R_o} p_i \, dV = \int_{R_{min}}^{R_o} p_o \left(\frac{R_o^3}{R^3}\right)^{1.3} (4\pi R^2) dR = \frac{4\pi p_o R_o^3}{0.9} \left[R_{min}^{0.9} - \frac{1}{R_{min}^{0.9}} \right]$$

The difference in the two energy quantities is the viscous dissipation in the incompressible case. In the compressible case the difference represents the viscous dissipation plus the kinetic and pressure energy in the liquid. As shown in Figure 8, the bubble wall velocity becomes zero before the liquid velocities farther from the bubble so that there is still kinetic energy.

For the bubble in the table, when $p_o = 1 \times 10^{-4}$, the total available energy is 6.51×10^{-4} ft - lbf for essentially all the minimum radii shown since the energy is proportional to the difference of the cubes of the maximum and minimum radii. The energy to compress the gas in the incompressible liquid, when $p_o = 1 \times 10^{-4}$ atm, is 6.40×10^{-4} ft - lbf, indicating that 1.69 percent of the initial energy is lost to viscous effects at the bubble wall. In the compressible liquid the available energy is the same when $p_o = 1 \times 10^{-4}$ atm, but the energy to compress the gas is only 0.383×10^{-4} ft - lbf since the minimum radius is 22 times larger. Therefore, at the minimum radius, 94 percent of the bubble collapse energy exists as liquid potential and kinetic energy, or has been degraded through viscous effects. When the initial gas pressure is increased to 10^{-3} atm, the lost portion in the

incompressible liquid remains the same at 1.69 percent. The portion in the compressible liquid is reduced to 79 percent.

The viscous dissipation per unit time in the incompressible liquid is given by[19]

$$\int_R^\infty 12\mu \frac{u^2}{r^2} (4\pi r^2)\, dr = 16\pi\mu U^2 R$$

Note that this is given as energy dissipated per unit time at a given bubble radius and wall velocity. The total energy dissipated during the collapse can only be obtained by numerical integration because the velocity, U, is not known as a function of radius, R. However, we can obtain the instantaneous dissipation rate at the maximum wall velocity. For example, when $p_o = 1 \times 10^{-4}$, and $R' = 1.83 \times 10^{-4}$,

Maximum Viscous Energy Dissipation Rate for Bubble in Incompressible Liquid.

$= 2.19 \times 10^4$ ft-lbf/sec

$= 39.8$ Horsepower

$= 29.7$ Kilowatts

It must be remembered that such rates apply only for time durations of fractions of micro-seconds. The instantaneous dissipation rate is not available for the compressible liquid, since it would require a numerical integration of liquid velocity throughout the liquid.

In conclusion then, the magnitude of the maximum pressure in the bubble when it contains gas cannot be simply obtained by an energy

balance since the compressibility effects in the liquid and the initial gas pressure strongly affect relative distribution of the available energy in the bubble gas and in the liquid. If the proportion of available energy which went into compressing the gas were approximately a constant as was the case for the incompressible solution over the range taken, then for a given initial gas pressure within the bubble the maximum internal pressure and minimum bubble radius could be easily calculated. Assuming a $1/r$ peak pressure attenuation, the pressures at various distances from various size bubbles could be determined.

No mention has yet been made here of the detailed shape of the shock front which forms in the liquid. Benjamin[85] states that a shock will form when the peak pressure is above about 2000 atm. Hickling and Plesset[66] set a lower limit of about 1000 atm for the wave to steepen into a shock. To calculate the shape of the shock front requires a detailed analysis which includes energy dissipation in the liquid. Such a procedure is beyond the immediate scope of this work. However, since the time rate of loading by the shock on a solid boundary can be significant in determining the material behavior, such a detailed analysis might seem appropriate. For the present, it can be said that the magnitude of the pressures near a rebounding bubble is sufficient to cause material damage (Figure 12), but that the pressures during collapse, assuming that the bubble collapse center is stationary, apparantly are not. Of course, potential flow analyses[33] show that a collapsing bubble will actually migrate toward an adjacent solid, so that

during the collapse, surfaces could be closer to the collapse center than the initial bubble radius and hence damaging pressures could impinge on such surfaces. A useful extension of the present work would be an examination of the possibility of a sufficiently rapid center motion to occur.

IV. EXPERIMENTAL EQUIPMENT AND RESULTS

A. Water Damage Facility

The investigations of cavitation in the Nuclear Engineering Department of the University of Michigan have been described by Hammitt.[83] One of the facilities for investigating the damage mechanisms of cavitating water flow in a venturi was also used for this work. A centrifugal pump with a variable speed drive provides water flow to a high pressure tank. There are four outlets from this tank to four experimental loops, so that from one to four loops may be operated at once. The loops return to a low pressure tank, and then to the pump inlet, thereby completing the flow path. A surge tank is connected to the low pressure tank, and the gas pressure over the water in the surge tank determines the loop reference pressure. A schematic of the loop is shown in Figure 13 with the cylindrical damage test venturis in place. For the observations of bubbles reported herein, three of the loops were blanked-off at the high and low pressure tanks, and the fourth loop assembled with a two-dimensional plexiglas venturi.

There are three possible flow variables for a constant condition of incipient (first visible) cavitation in the venturi. The flow-rate is determined by pump speed, since there are no valves in the main loop flow, and monitored by an orifice and differential manometer in the return leg of the loop. Once the flow-rate is set, the pressure on the surge tank is set for the desired extent of cavitation in the venturi, which was always the minimum condition necessary for good photographs.

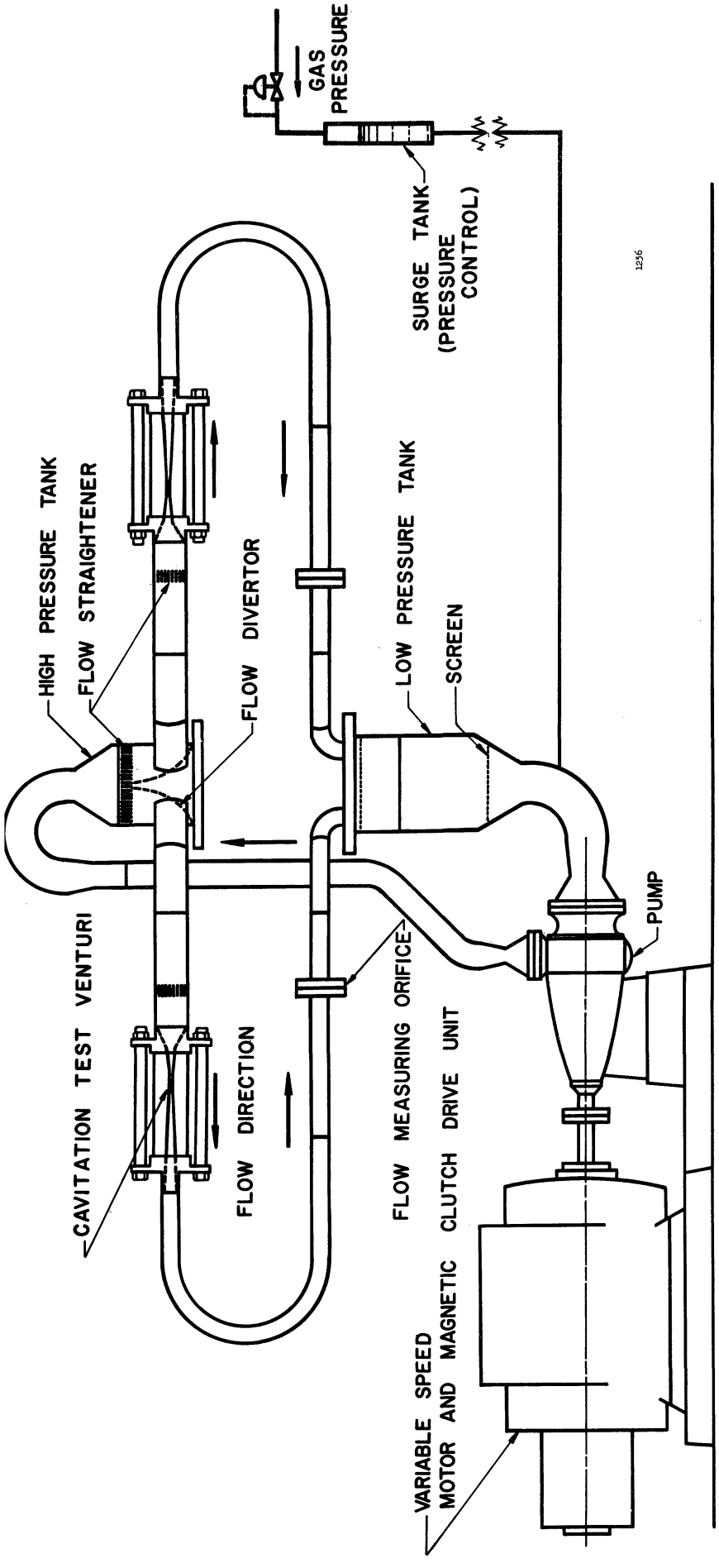

Figure 13. Overall Water Loop Schematic.

The second variable is air content of the water. Deaeration is accomplished by spraying a bypass flow from the main loop into a tank held under vacuum. The third variable is temperature. For a given flow-rate, the minimum temperature is determined by the flow of tap water in the cooling coils within the low pressure tank. The maximum attainable temperature is determined by the pump-work input and therefore by pump speed, assuming minimum cooling of the loop.

B. Two-Dimensional Plexiglas Venturi

The design of the experimental venturi was dictated by several requirements. First, it was necessary to provide a cavitating flow in a known pressure environment. Second, it was necessary to have a transparent venturi in order to photograph the flow. The cross-sectional flow area of the venturi is rectangular at every axial position, with the long edge of the rectangle constant at three inches. The nozzle tapers at a six degree included angle to a constant area throat about three inches long, and is followed by the diffuser portion having the same taper as the nozzle. The venturi flow area is then symmetrical about the throat, except that the diffuser portion is longer. Adjustments are provided so that the throat opening can be varied from 1/8" x 3" to 7/8" x 3". After initial runs and photography, pressure taps were put into one of the two tapered plexiglas pieces as shown in Figure 14.

The assembly and appearance of the venturi are shown in Figures 15 to 19. Figure 16 shows the two tapered sections and one of the flat plexiglas plates removed to show the flow area. The four plexiglas pieces are pinned together and inserted into the cast aluminum end pieces. A

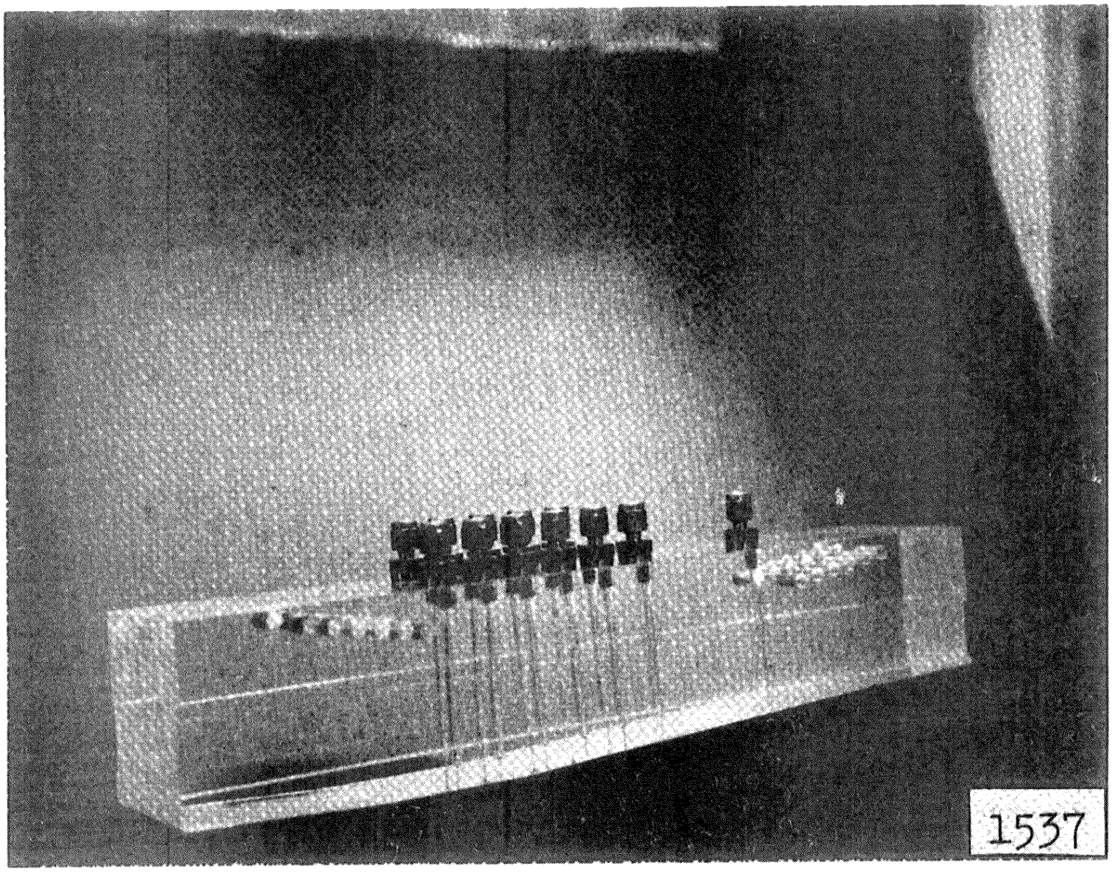

Figure 14. One of the Two Tapered Plexiglas Sections of the Venturi After Pressure Taps had been Installed in it.

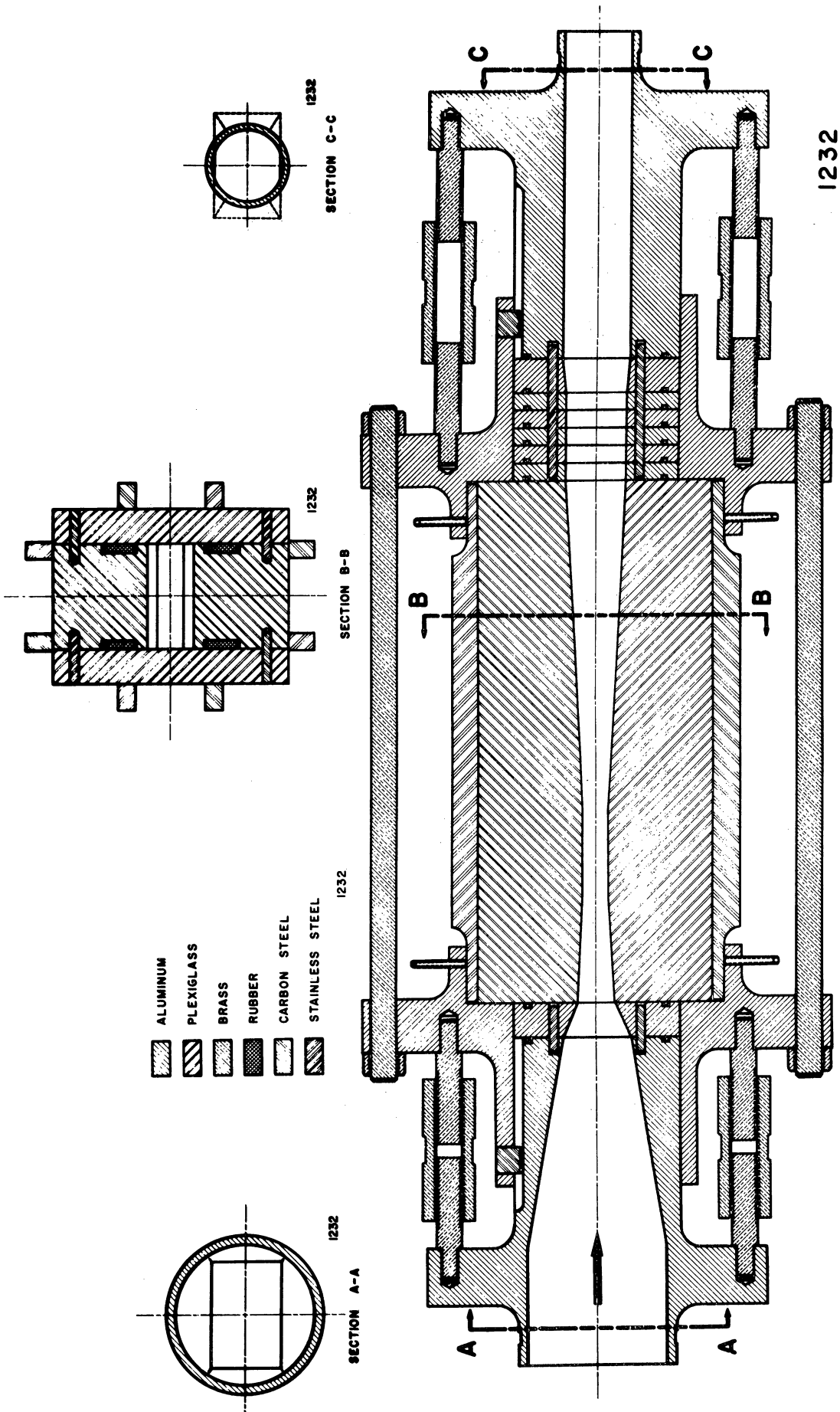

Figure 15. Schematic of Two Dimensional Venturi.

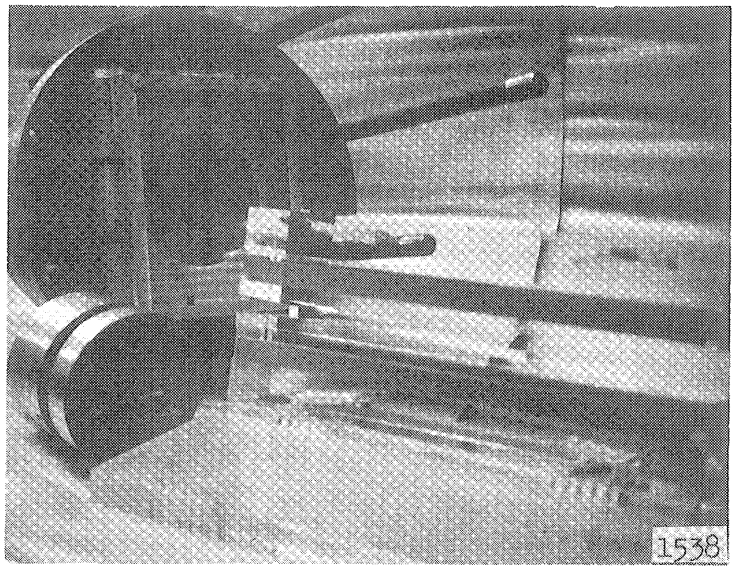

Figure 16. Assembly of Venturi Showing End Pieces.

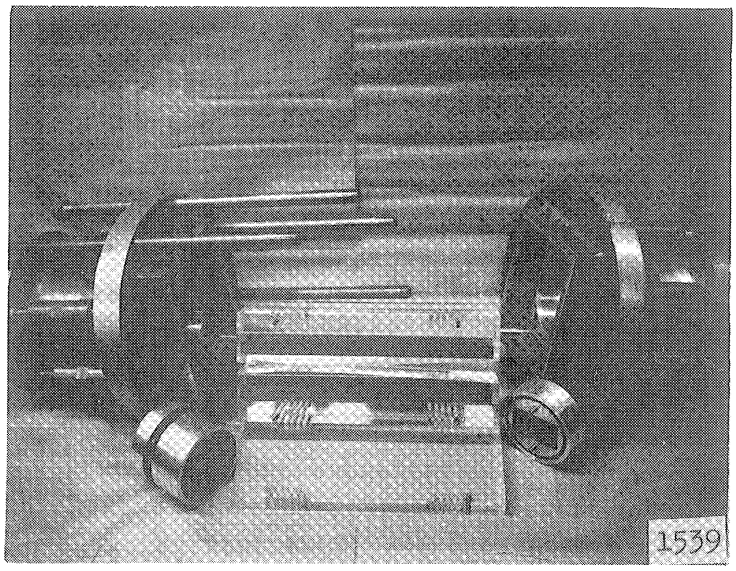

Figure 17. Assembly of Venturi Showing Axial Bars Partially Inserted and Showing Spacer Discs for Both Ends.

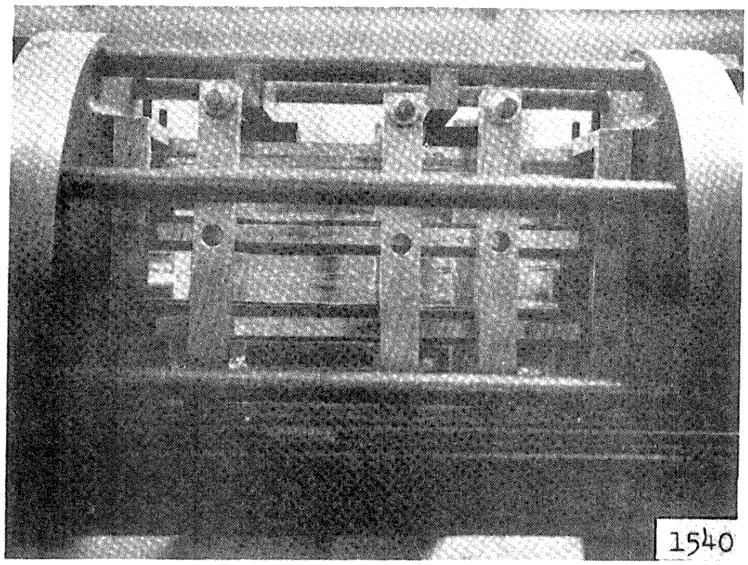

Figure 18. Venturi Assembled Showing Bars and Clamps on Plexiglas Faces.

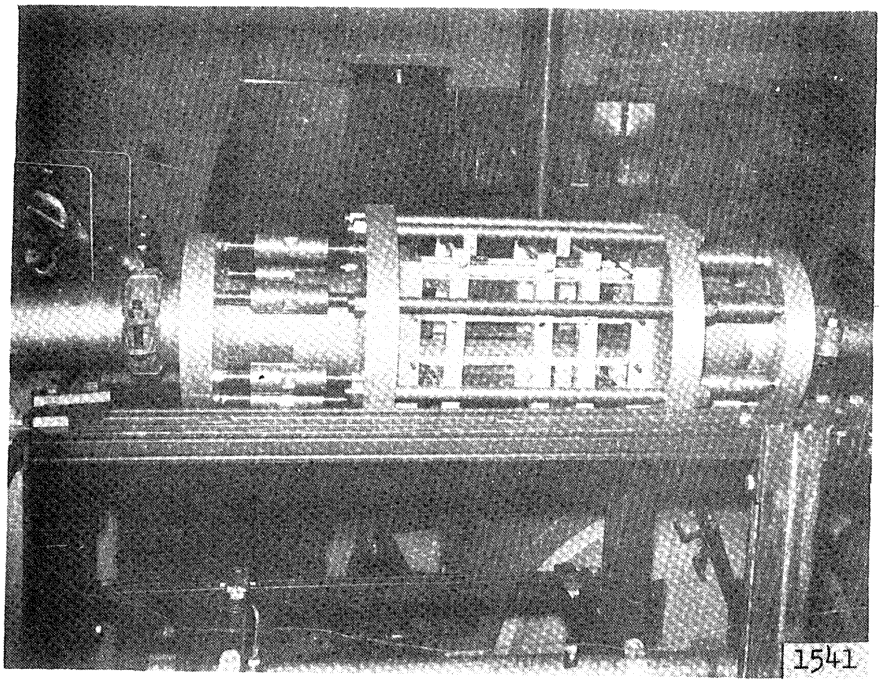

Figure 19. Assembled Venturi in Loop.

smooth entrance to the rectangular venturi from the round four inch pipe of the loop is provided by a cast aluminum piece, and the variation in throat size is accomodated by a series of aluminum discs with tapered rectangular openings as shown in Figure 16. One disc is removed, and another placed at the other end of the plexiglas to maintain constant overall length, for each 1/8 inch increase in throat size. The large aluminum end pieces are held axially by eight round threaded bars shown partially inserted in Figure 17. Two square steel bars run axially on each of the four sides of the plexiglas and are held by a series of clamps as shown in Figure 18. The entire assembly is connected into the loop with standard pipe couplings as shown in Figure 19. The entire water facility with three damage test venturis in place and connected, and with the two-dimensional venturi in place but not connected is shown in Figure 20.

C. High Speed Photography and Pressure Profiles

High speed motion pictures were taken of the cavitating flow in the venturi to observe the growth and collapse of individual cavitation bubbles. A Fastax camera was used at about 7700 frames per second. The camera was synchronized with a high-speed short-duration strobe-light which provided exposure times of about one microsecond per frame. The venturi was arranged so that the constant three inch dimension was vertical as shown schematically in Figure 21. Light was from behind and passed through a diffuser. At the time of some of the high speed photographs, there were no pressure taps in the venturi.

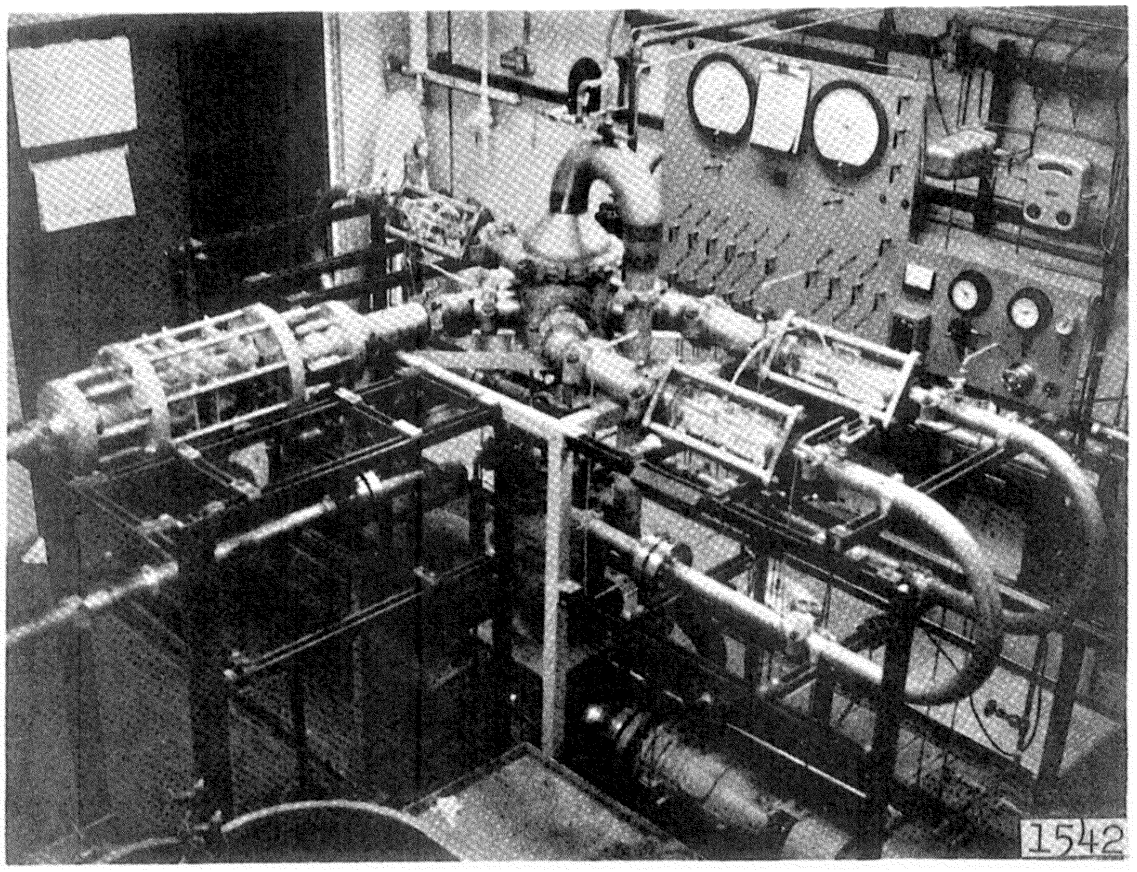

Figure 20. Water Cavitation Facility with Three Damage Venturis and the Two Dimensional Venturi.

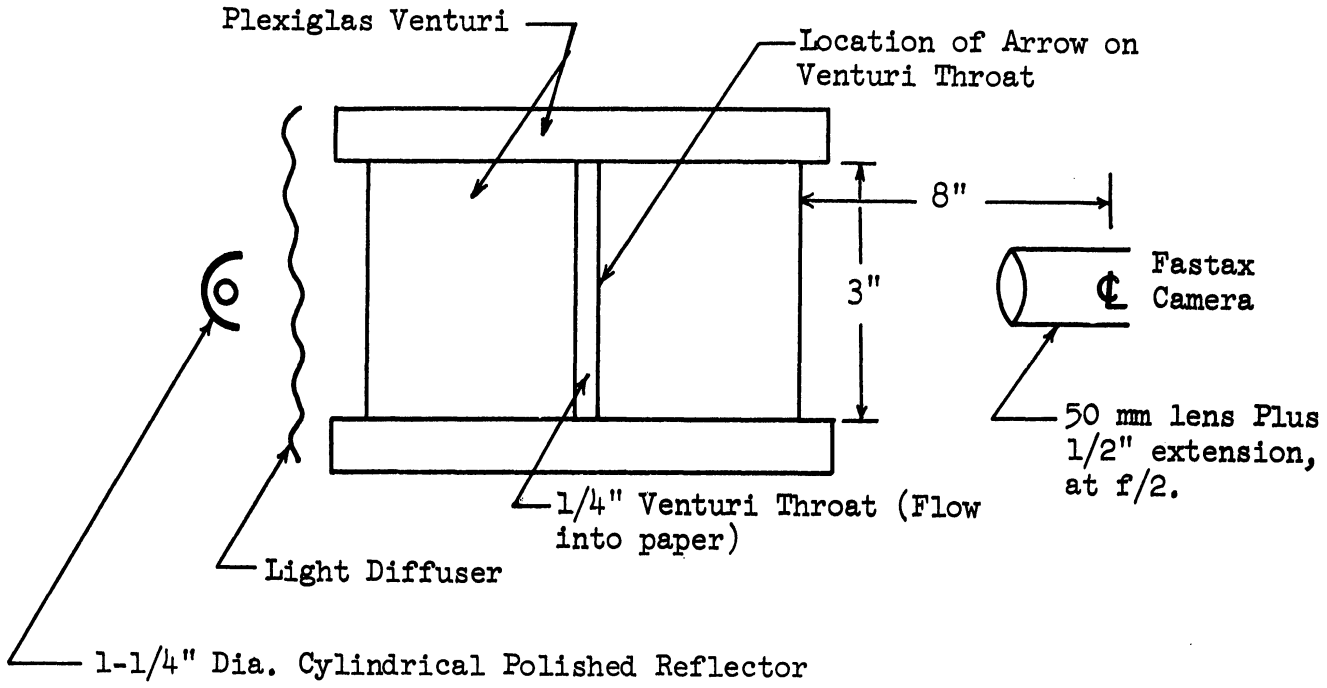

Arrangement for High Speed Photography

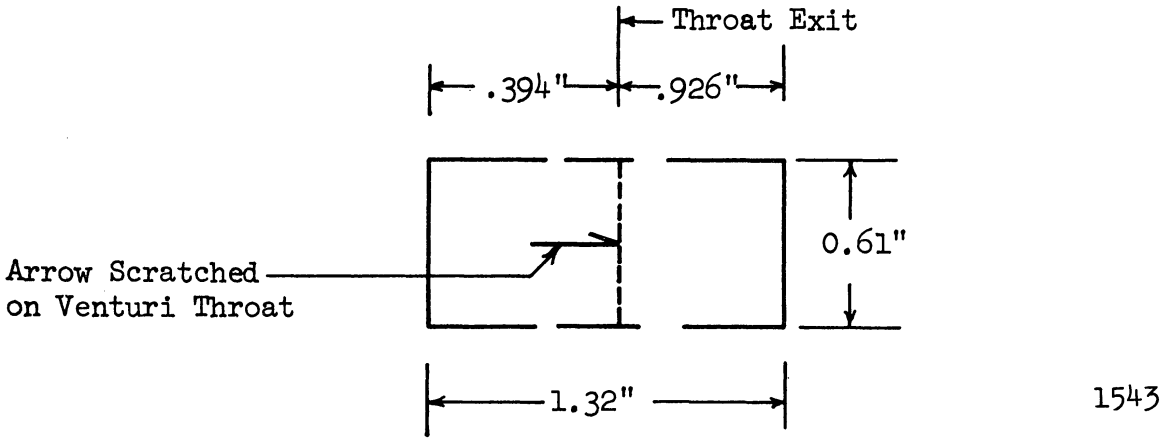

Field of View with Above Arrangement

Figure 21. Schematic Arrangement of Venturi, Camera, and Strobe Light, and Field of View Photographed.

An arrow was scratched very lightly on the inner front surface of the venturi throat to use as a scale dimension in the analysis of the photographs. The point of the arrow is at the throat exist and it points in the direction of flow as shown in Figure 21. The actual field of view for that film which was examined in greatest detail was 0.61 inches high by 1.32 inches long, making the film image about one third true size.

Pressure taps were placed at twelve locations on one of the tapered plexiglas pieces of the venturi as shown in Figure 22. Pressure profiles were taken at twelve flow conditions. Simultaneously with the pressure profiles, still pictures were taken of the flow. A 4" x 5" press camera with the bellows fully extended was used, giving about a one to one image on high speed Polaroid sheet film. The light source, from above the venturi, was a single flash from a small commercial strobe light with a duration of three microseconds. The slow decay in the intensity of the light output from this strobe is evident in the streaks of light from the bubble highlights trailing downstream as the bubble moves.

In all the photography and pressure profiles it was difficult to obtain a perfectly steady cavitation field. The intermittant appearance and disappearance of the cavitation was caused in part by surges in the pump speed resulting from difficulties with the variable speed drive, and in part by the phenomenon itself. The still photographs represent the appearance at only one instant of time as an appropriate average. A much more steady cavitation field occurs with extensive cavitation, but it is then impossible to photograph individual bubbles collapsing.

2-D Venturi Pressure Taps

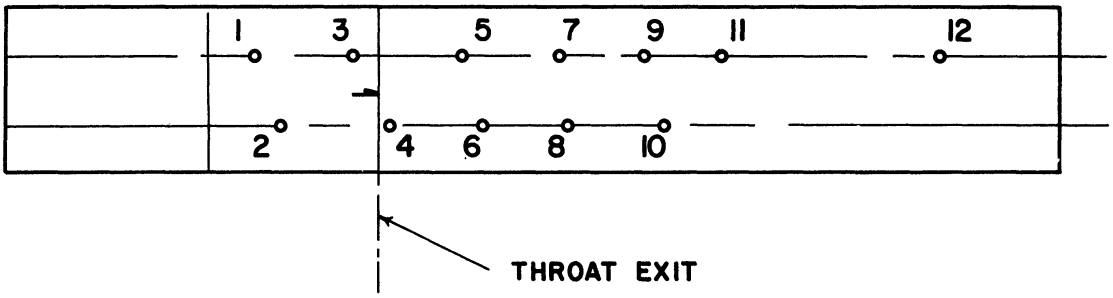

TAP #	DIST. FROM THROAT EXIT (in.)
1	− 1.030
2	− 0.654
3	− 0.275
4	+ 0.035
5	0.568
6	0.942
7	1.321
8	1.689
9	2.062
10	2.439
11	2.814
12	5.060

ARROW SIZE

1544

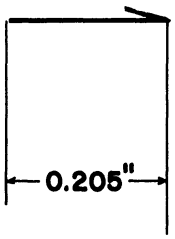

Figure 22. Locations of Pressure Taps in Venturi.

High speed photographs were taken at two throat openings, 1/8 inch and 1/4 inch, at the minimum velocity for which cavitation occurred.* Two sequences of frames with the 1/8 inch throat are shown in Figures 23 and 24. It is seen that the circular images are definitely not spherical since the diameter of the circle is greater than the dimension of the throat opening. The comet-like tail on the circular voids is typical of the appearance of spherical bubbles when they touch the venturi wall. The peculiar wave-like appearance of the steady void in Figure 23 is of interest but is unexplained. The sequence in Figure 24 shows individual bubbles distorting and combining with the stationary mass of void, but the individual bubbles appear to remain distinct as separate cells in the mass. This particular combination of transverse bubble velocity and bubble growth rate evidenced in this film is such that the bubbles grow too large to remain spherical with the 1/8 inch throat. At a higher throat velocity the bubbles would have less time to grow in the low pressure throat region. Photographs of about 200 ft/sec showed much too extensive a cavitation field to observe individual bubbles. Attempts to lessen the cavitation by either increasing the loop pressure or by decreasing the flow rate resulted in a complete dissappearance of cavitation, i.e., a fine enough adjustment of the operating point did not prove possible.

*The pipe-gasketing system used is not suitable for vacuum operation, so that minimum cavitating velocity is fixed by the requirement of maintaining positive gage pressures throughout the loop.

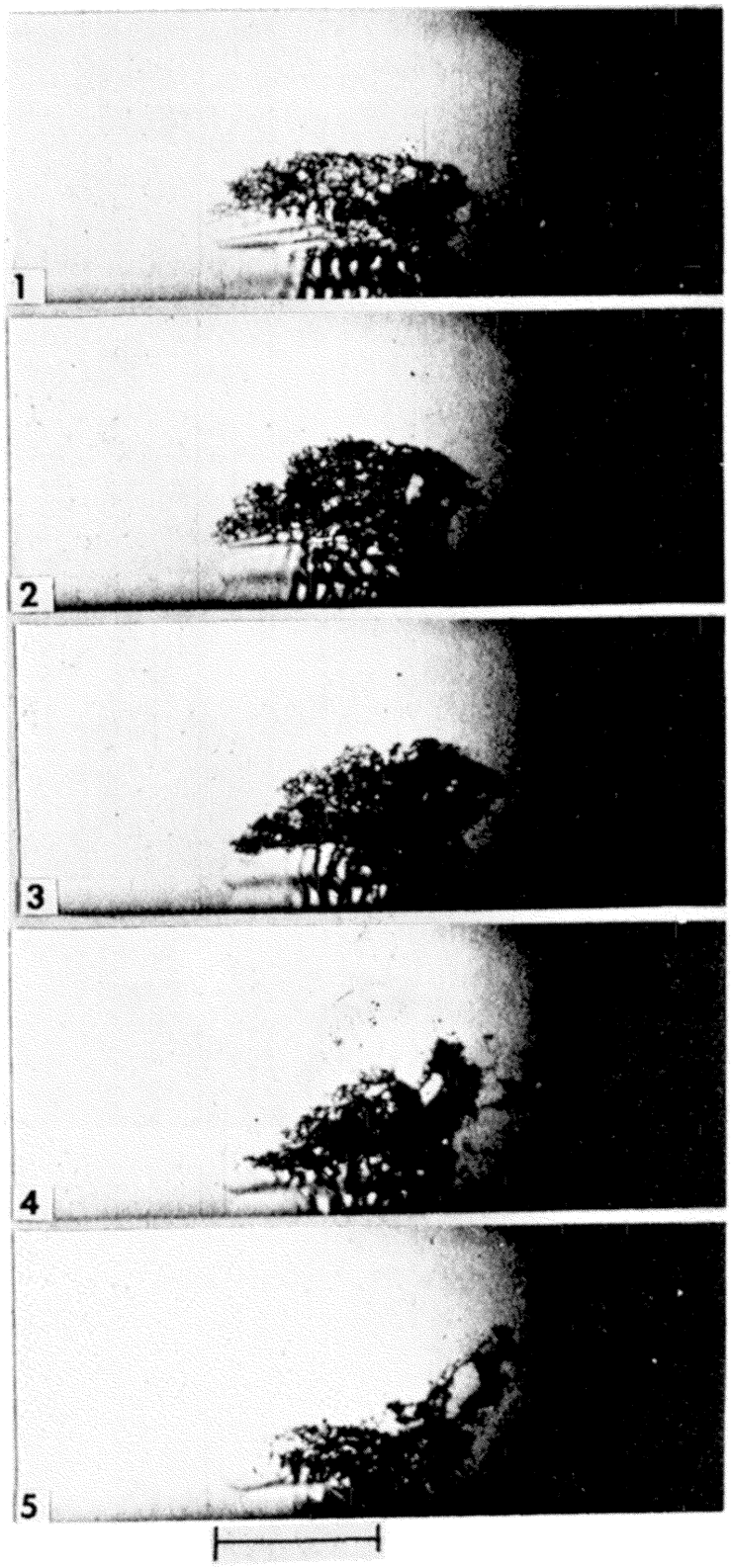

Figure 23. High Speed Photographs, 1/8 inch Venturi Throat, Velocity 75.4 ft/sec, Air Content 1.64 vol. %, 177 Microseconds per Frame, Scale Length 0.25 in. (Reel A)

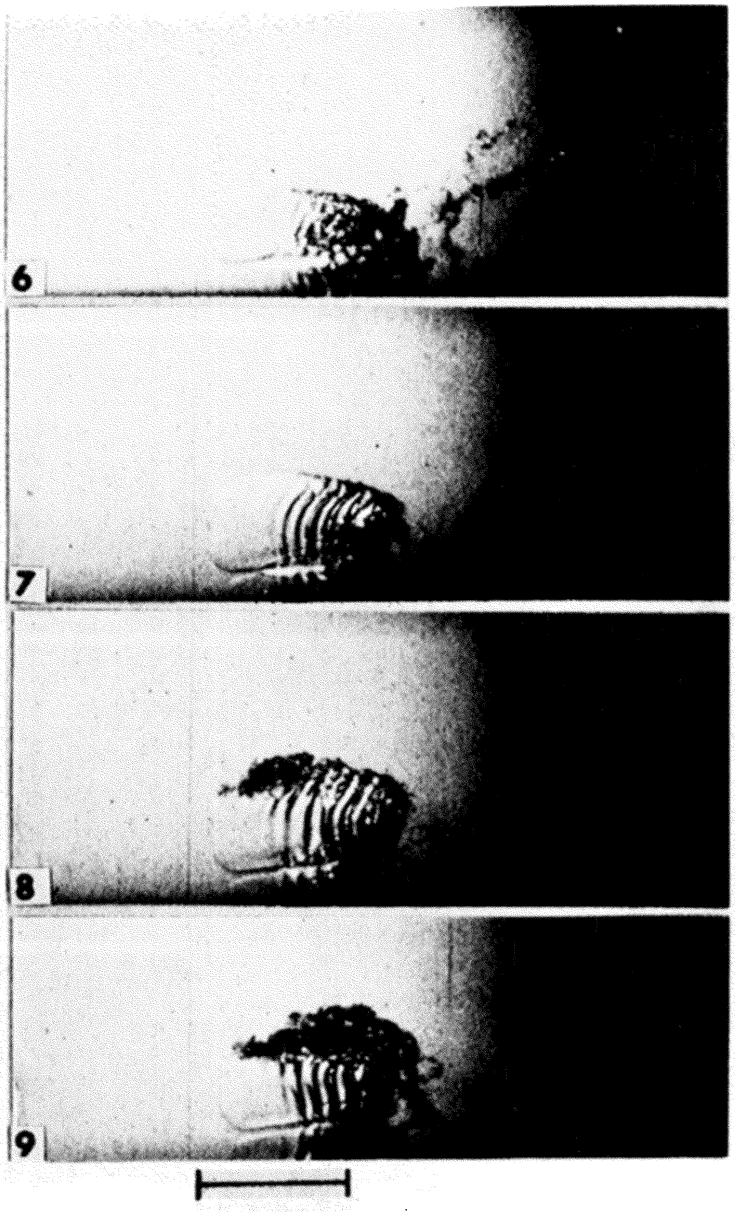

Figure 23. (Continued)

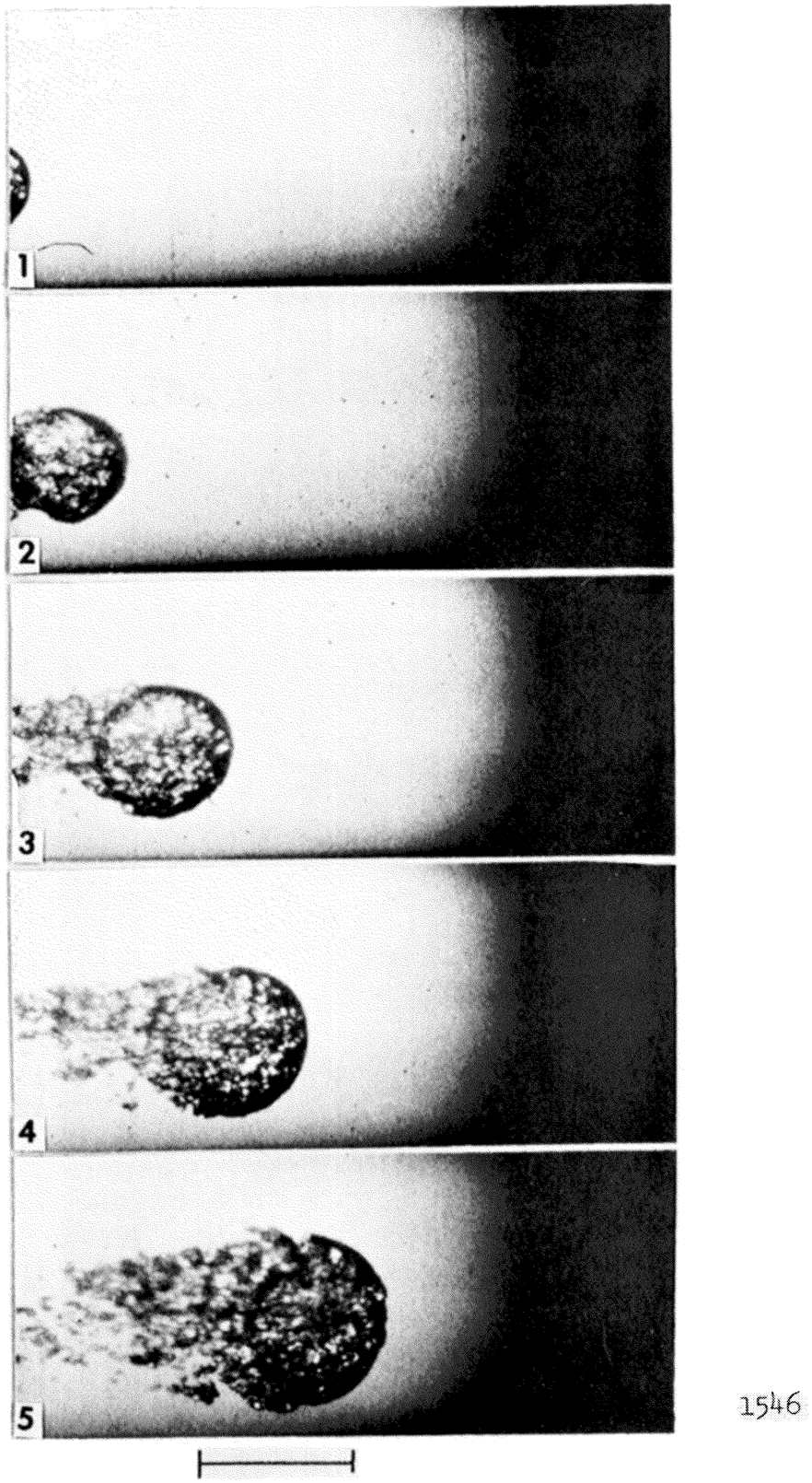

Figure 24. High Speed Photographs, 1/8 inch Venturi Throat, Velocity 75.4 ft/sec, Air Content 1.64 vol. %, 137 Microseconds per Frame, Scale Length 0.25 in. (Reel A)

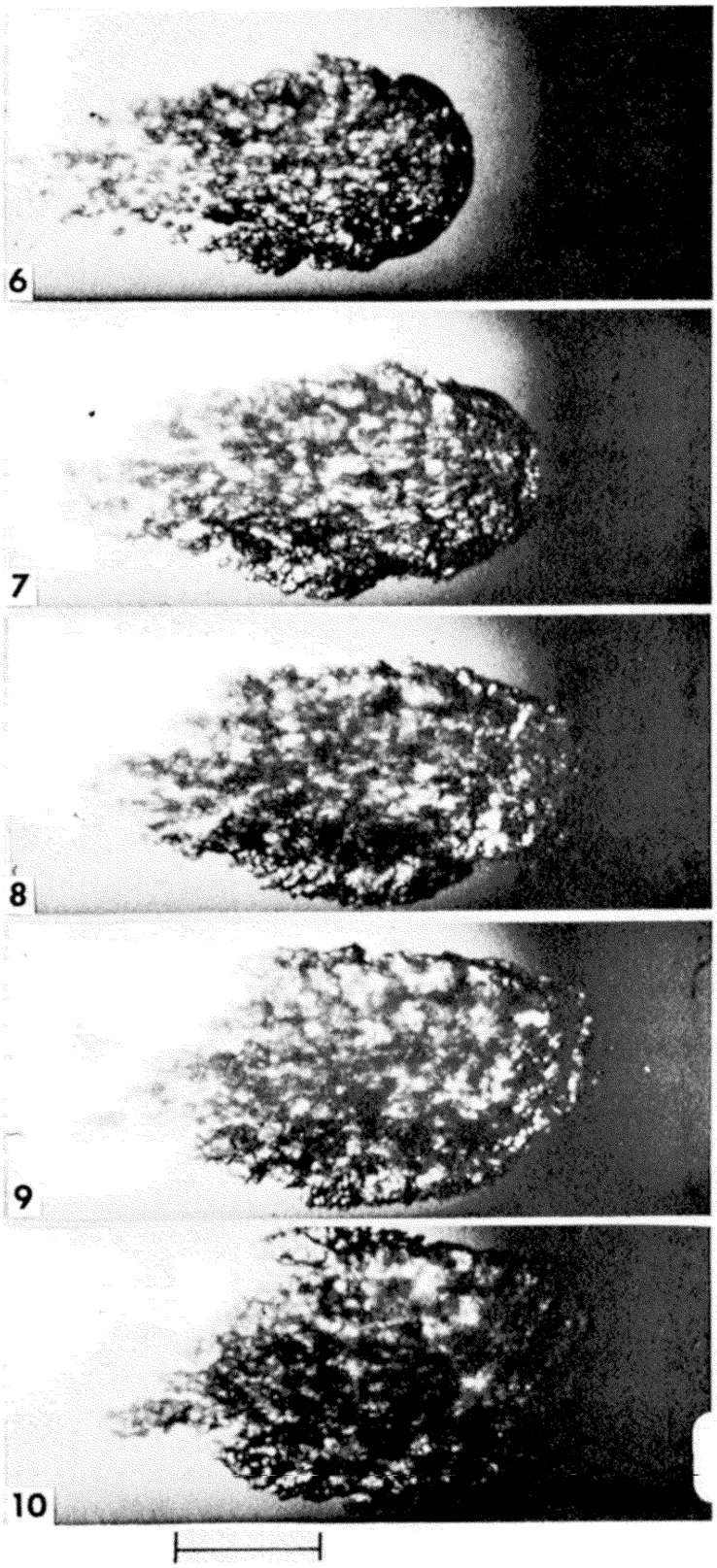

Figure 24. (Continued)

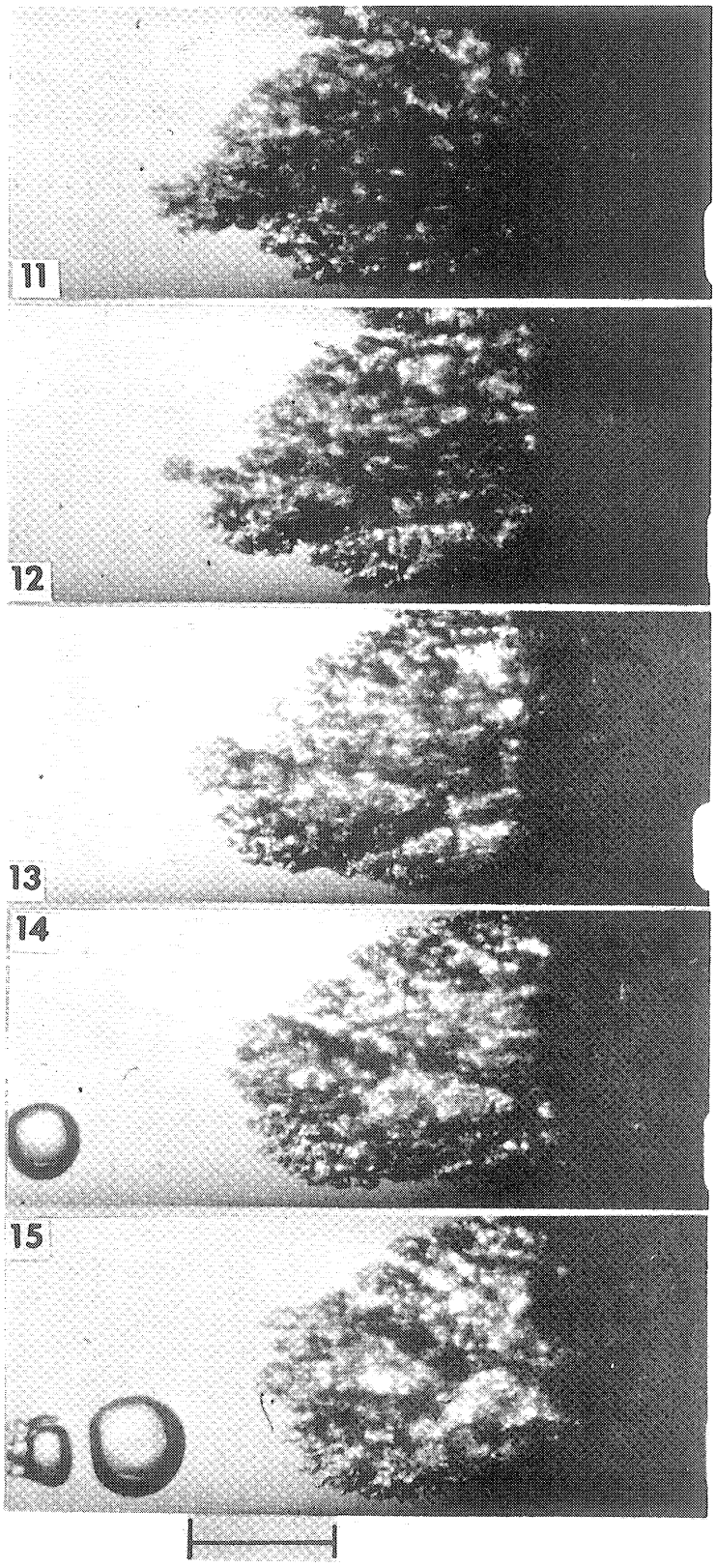

Figure 24. (Continued)

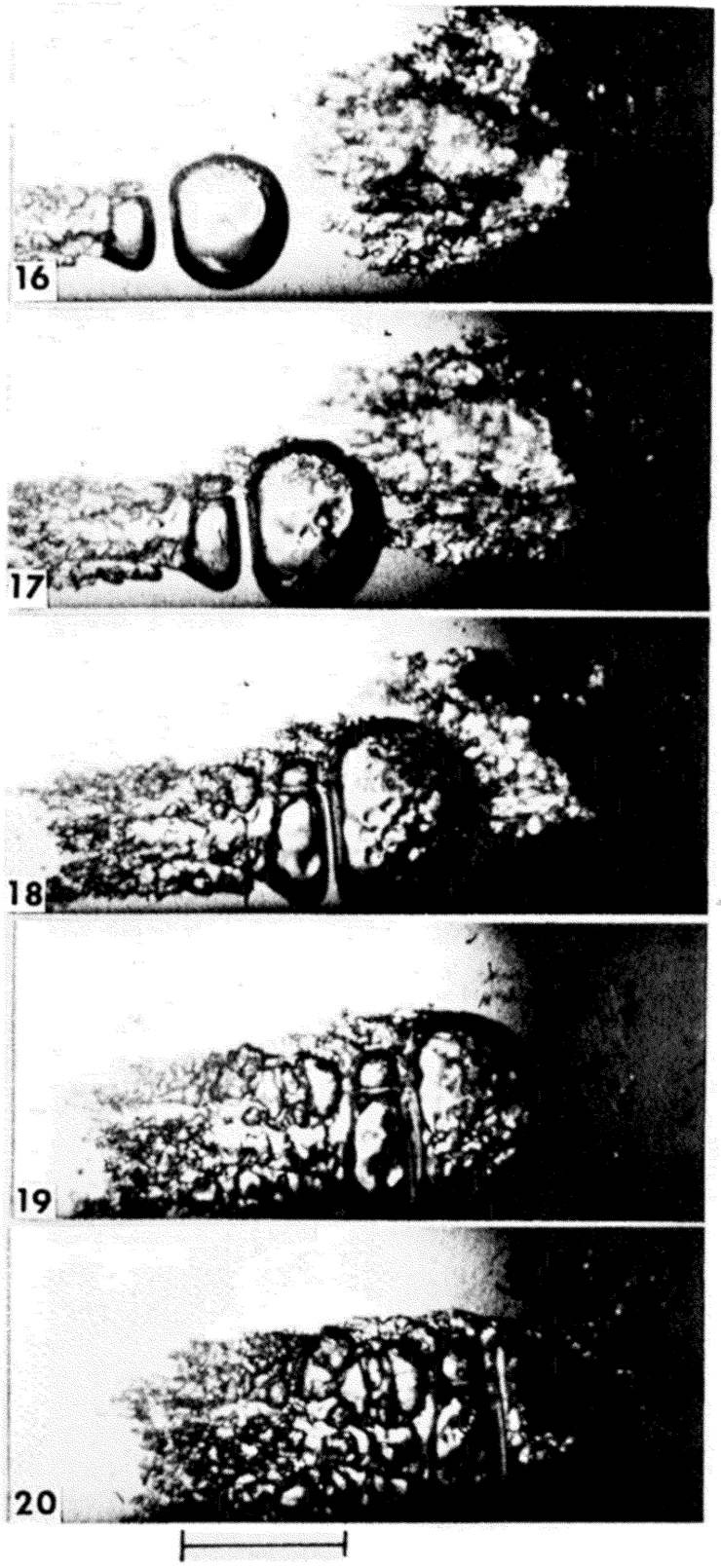

Figure 24. (Continued)

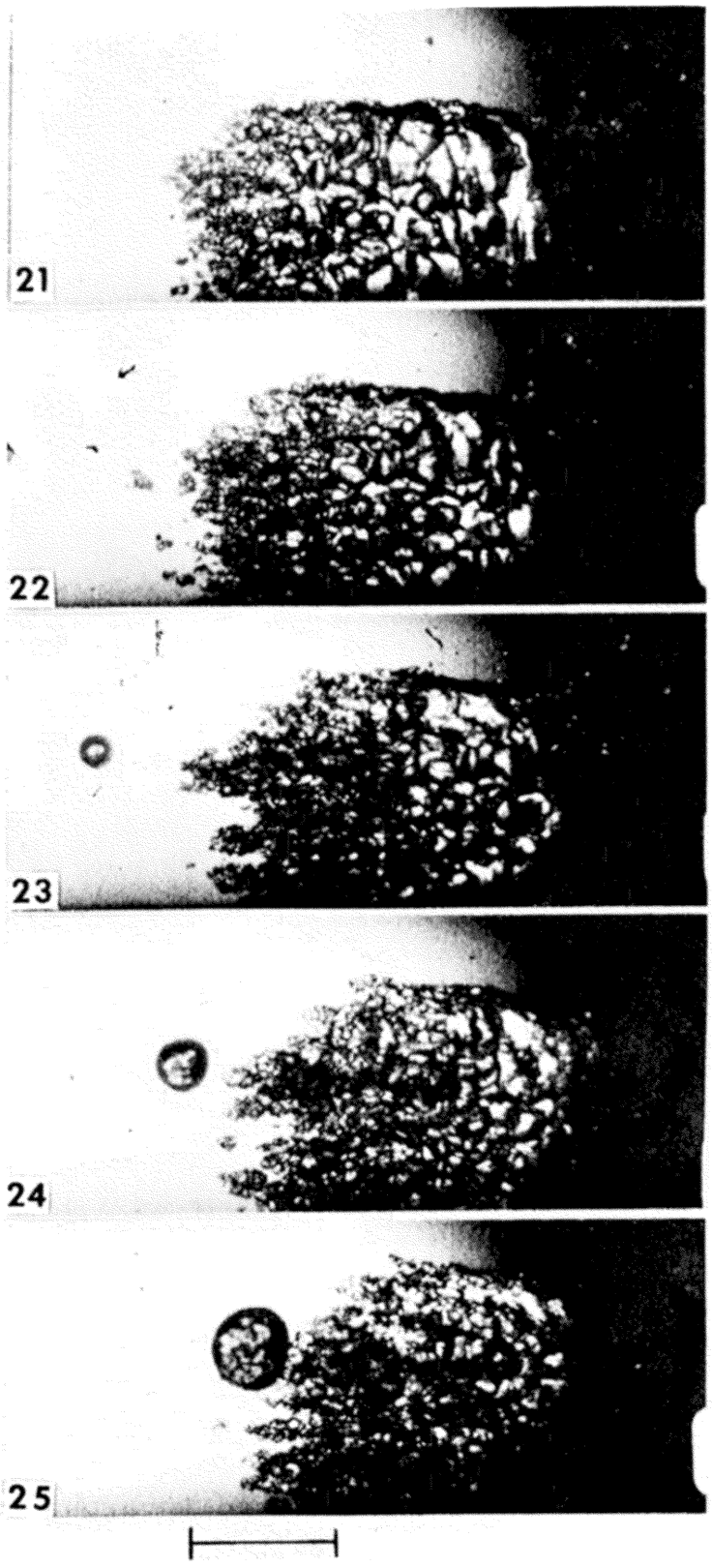

Figure 24. (Continued)

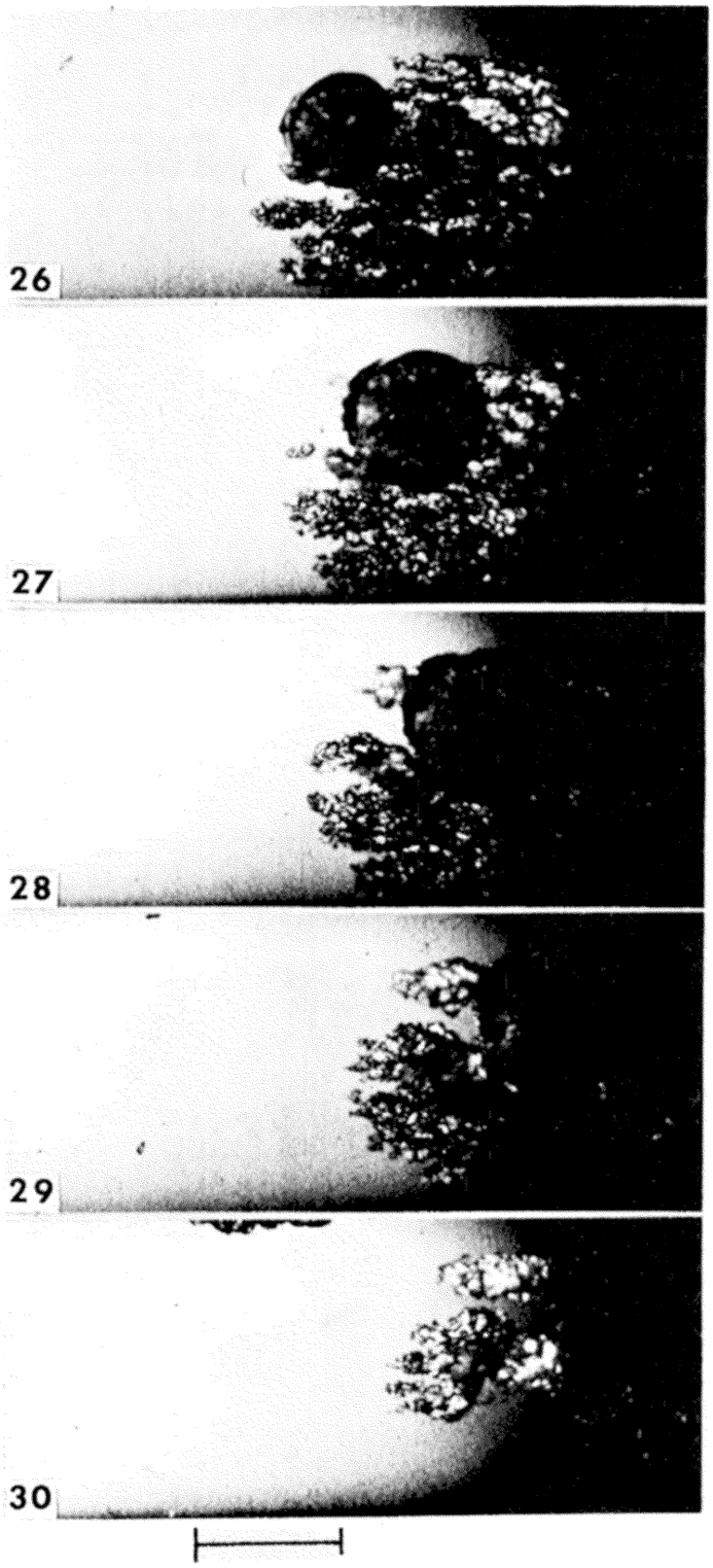

Figure 24. (Continued)

The venturi throat opening was then increased from 1/8 inch to 1/4 inch and high speed photographs were taken at a velocity of 74.6 ft/sec. The results are shown in three sequences in Figures 25 to 27. There are many perfectly spherical and separate bubbles visible,* all of which flatten in the direction of flow as they collapse. The non-symmetric collapse is caused by the sudden pressure rise in the venturi diffuser. Collapsing bubbles in Figure 27 appear to have a shape similar to that of bubbles rising in a gravitational field, the sudden deceleration being equivalent to a field acting in the downstream direction causing bubbles to tend to move upstream. Figure 25 shows an apparent rebounding bubble. Figure 26 shows the typical behavior of two bubbles, one of which is close behind the other. In all such cases observed they join together before collapsing. Bubbles which are close together in the direction transverse to the flow always move parallel to each other, and collapse separately and never appear to influence each other. A good example of a non-symmetric collapse is shown in Figure 27. The spherical bubble flattens on the downstream side, and the flat side then appears to move into the bubble creating a torus shaped void. These pictures are believed unique in showing the collapsing behavior of cavitation bubbles in a high pressure gradient. A total of 597 bubble images were analyzed from this film. All the bubbles on the film which were perfectly spherical, did not strike the wall, and were greater than about 15 mils diameter maximum size were included.

* It is obvious from these observations that the bubble size spectrum does not scale directly with throat opening, if the throat length is maintained constant. No information is available in this regard if throat length is scaled with opening.

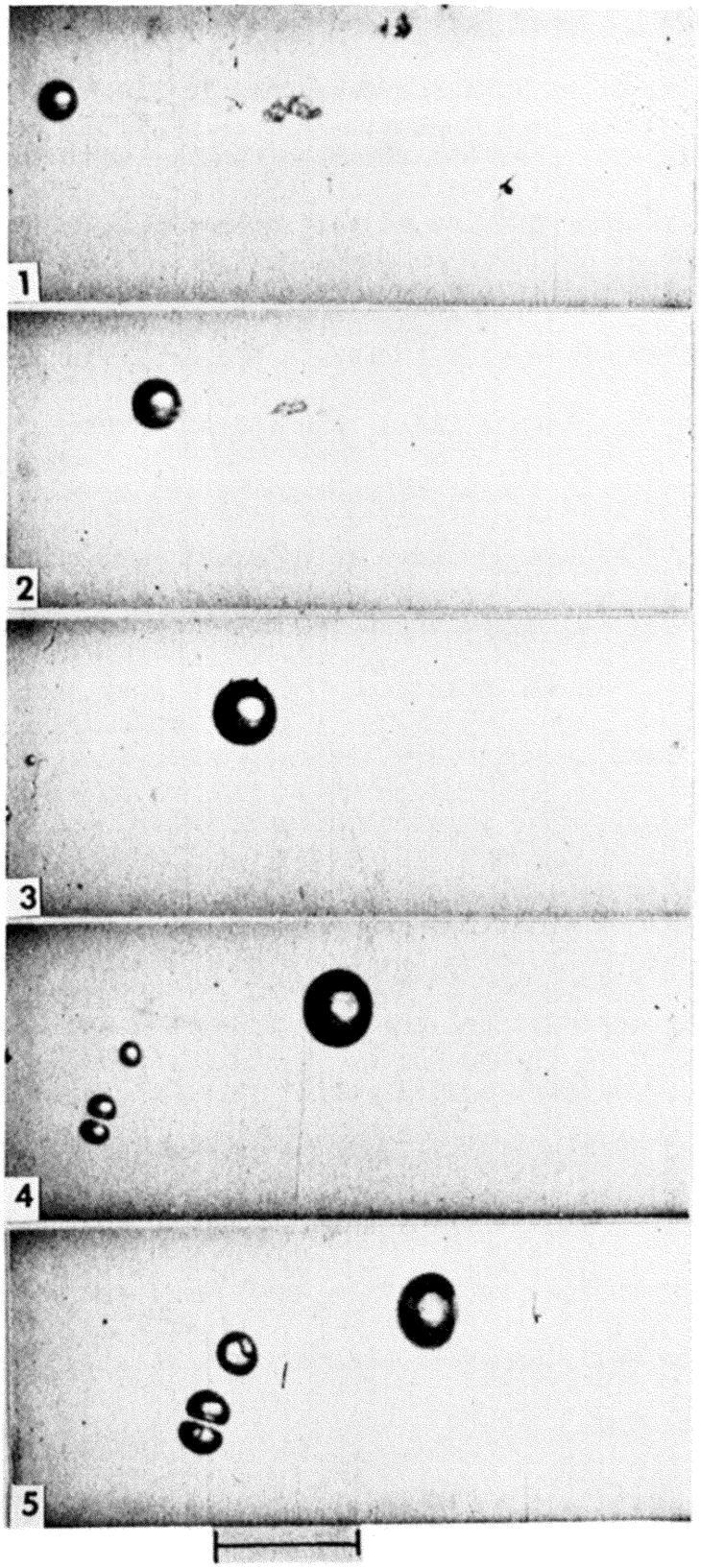

Figure 25. High Speed Photographs, 1/4 inch Venturi Throat, Velocity 74.6 ft/sec, Air Content 2.35 vol. %, 157 Microseconds per Frame, Scale Length 0.25 in. (Reel D)

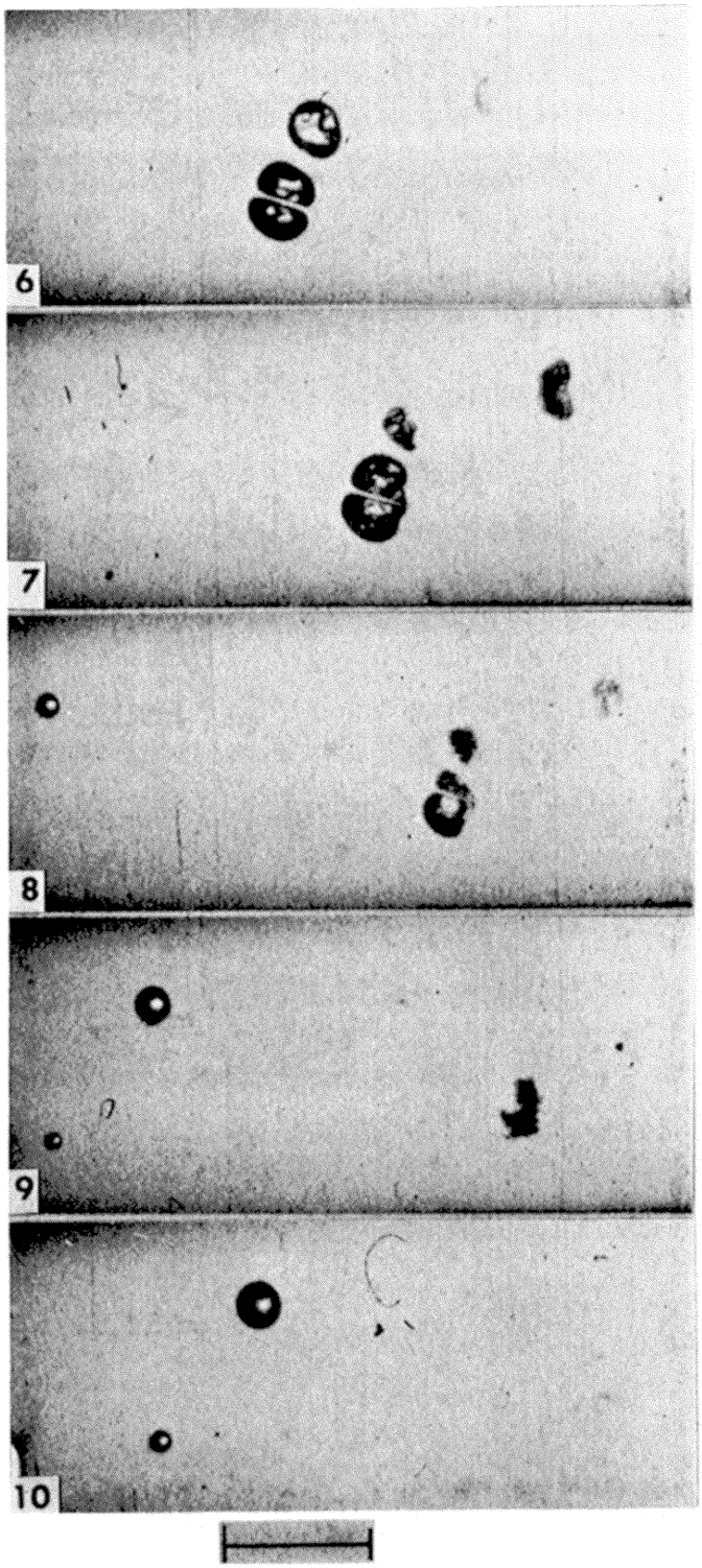

Figure 25. (Continued)

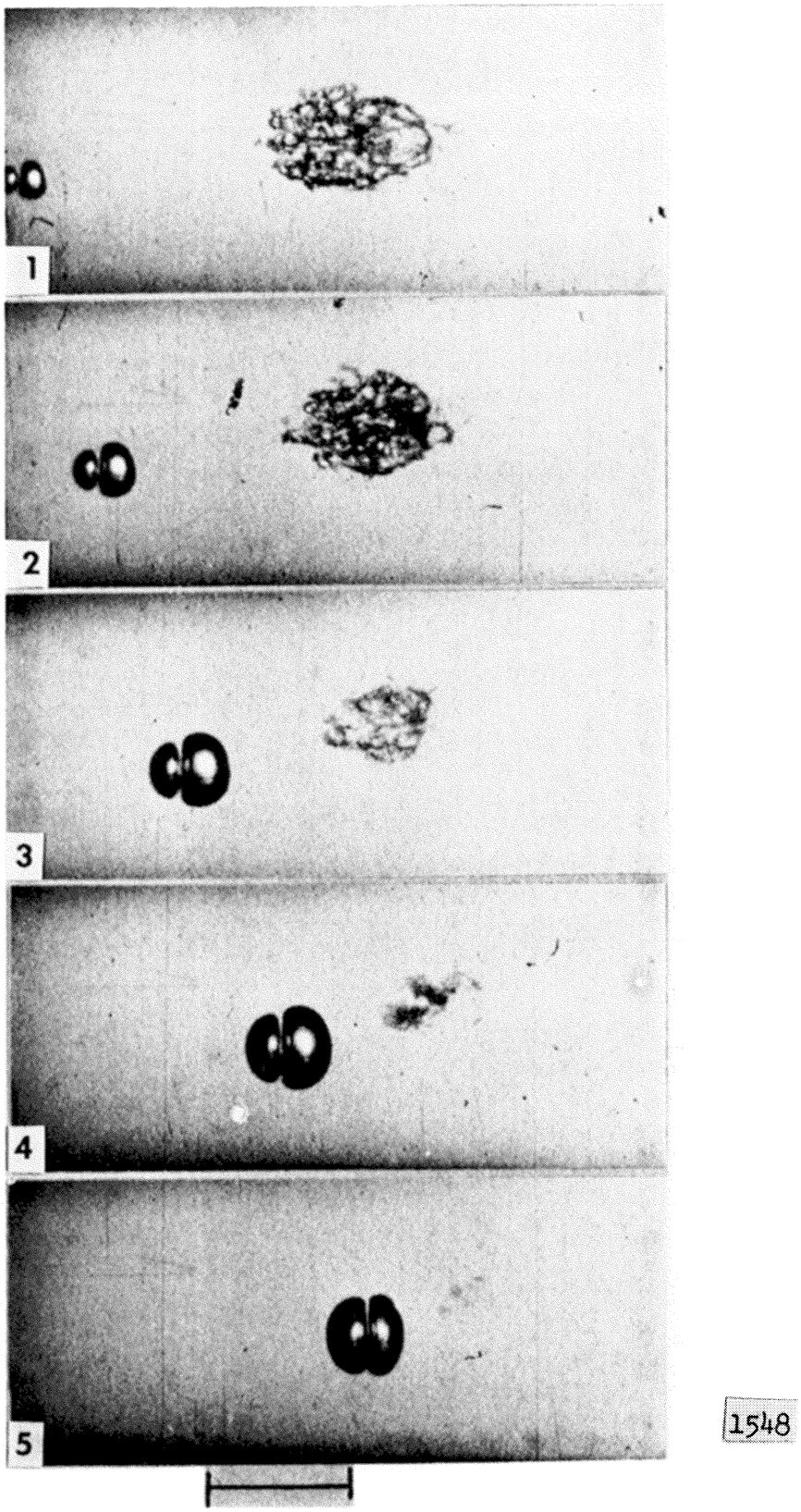

Figure 26. High Speed Photographs, 1/4 inch Venturi Throat, Velocity 74.6 ft/sec, Air Content 2.35 vol. %, 150 Microseconds per Frame, Scale Length 0.25 in. (Reel D)

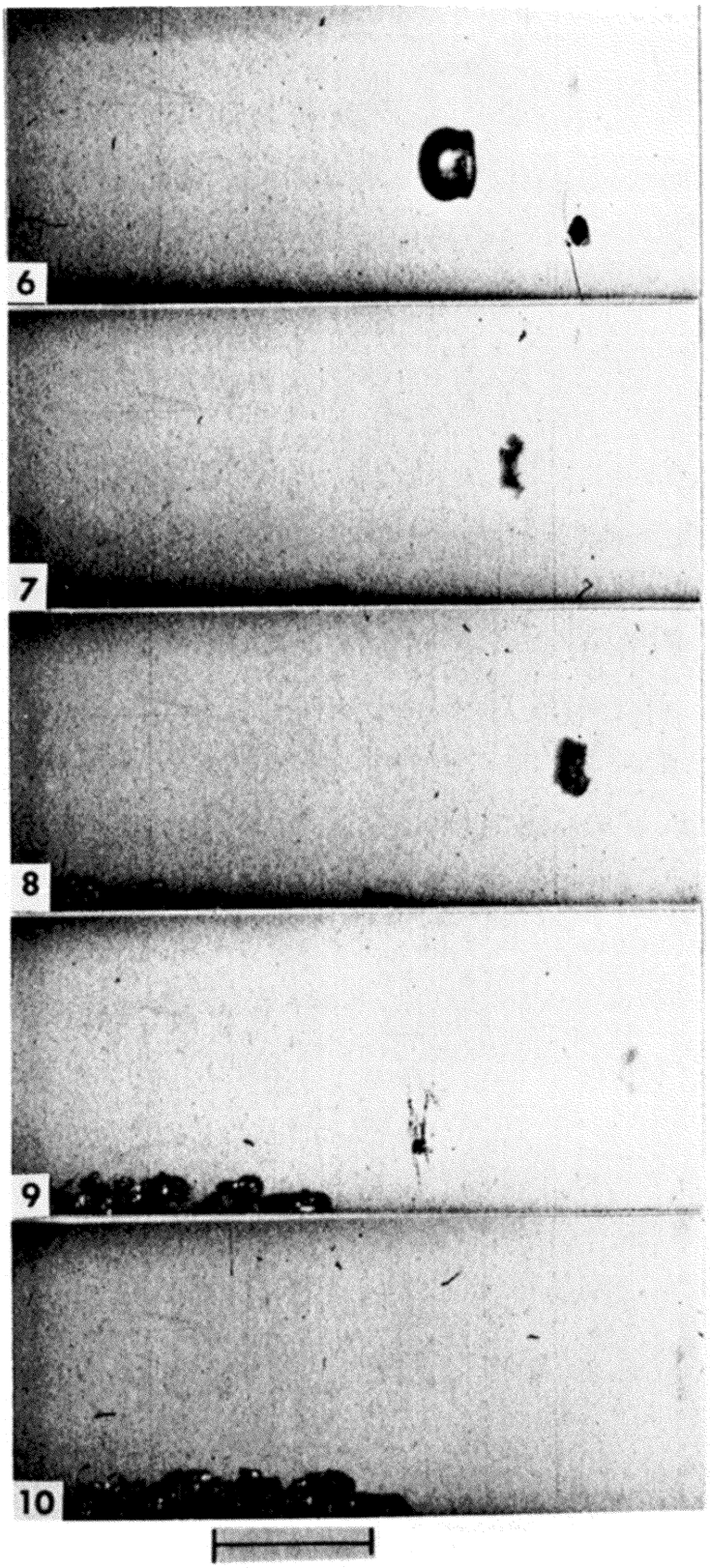

Figure 26. (Continued)

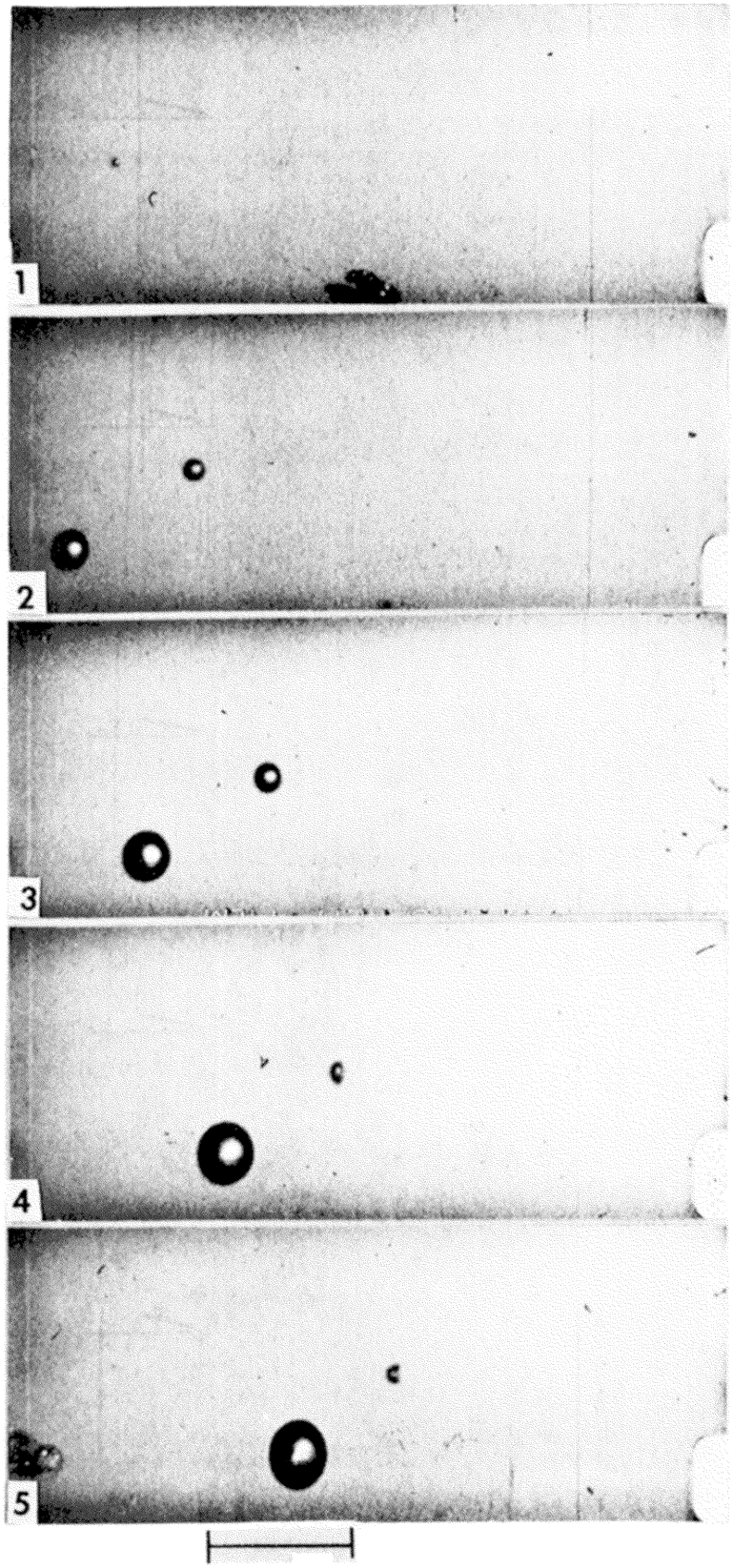

Figure 27. High Speed Photographs, 1/4 inch Venturi Throat, Velocity 74.6 ft/sec, Air Content 2.35 vol. %, 132 Microseconds per Frame, Scale Length 0.25 in. (Reel D)

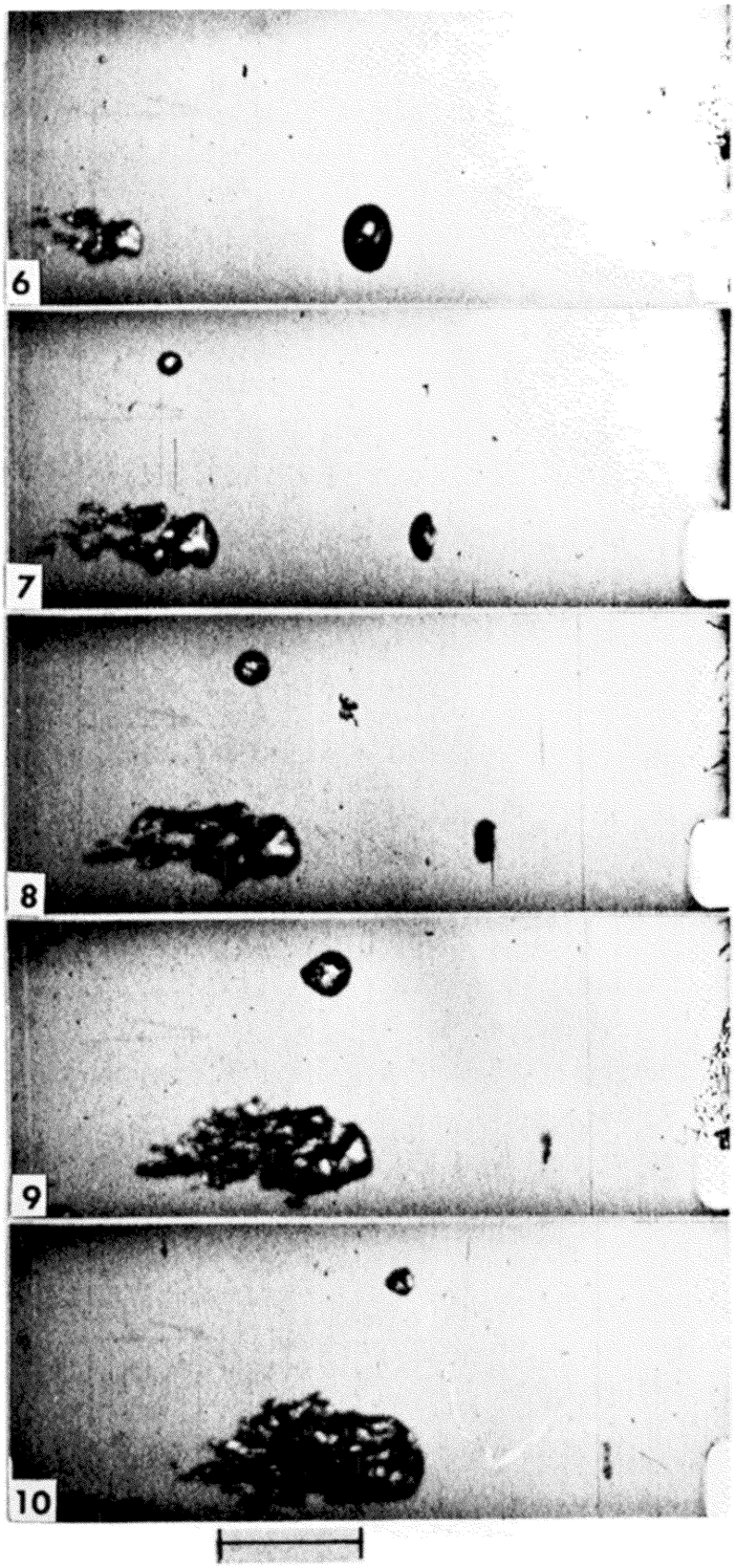

Figure 27. (Continued)

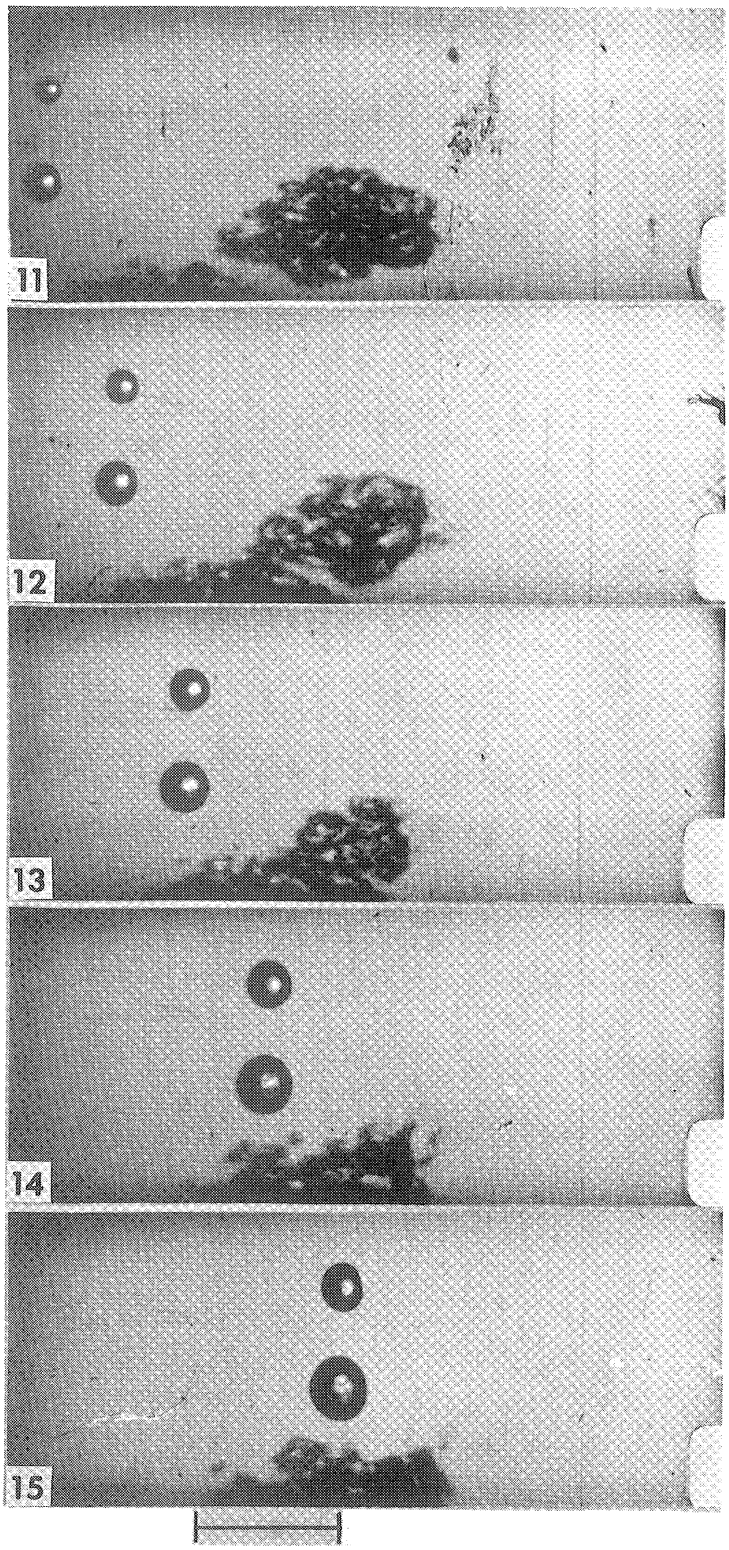

Figure 27. (Continued)

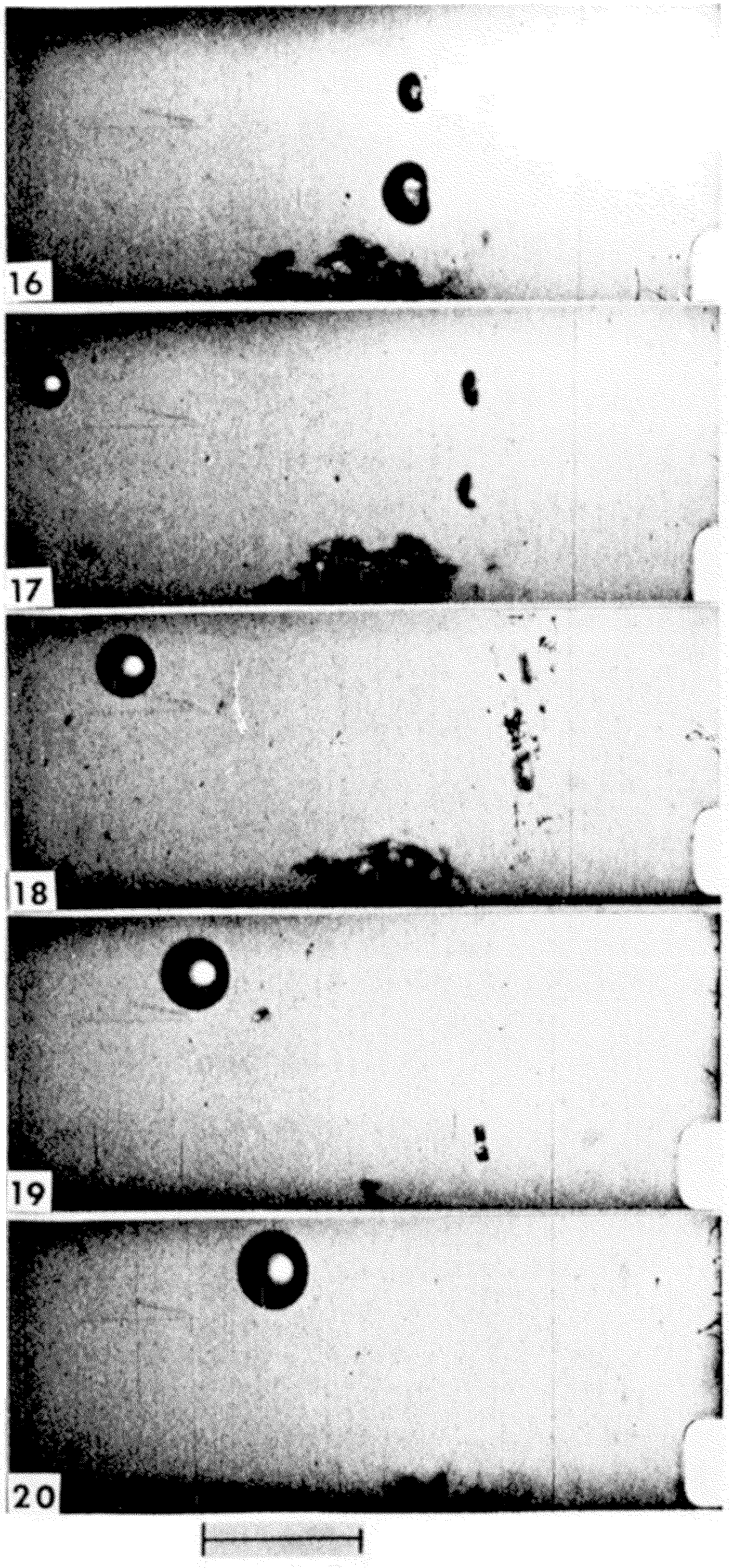

Figure 27. (Continued)

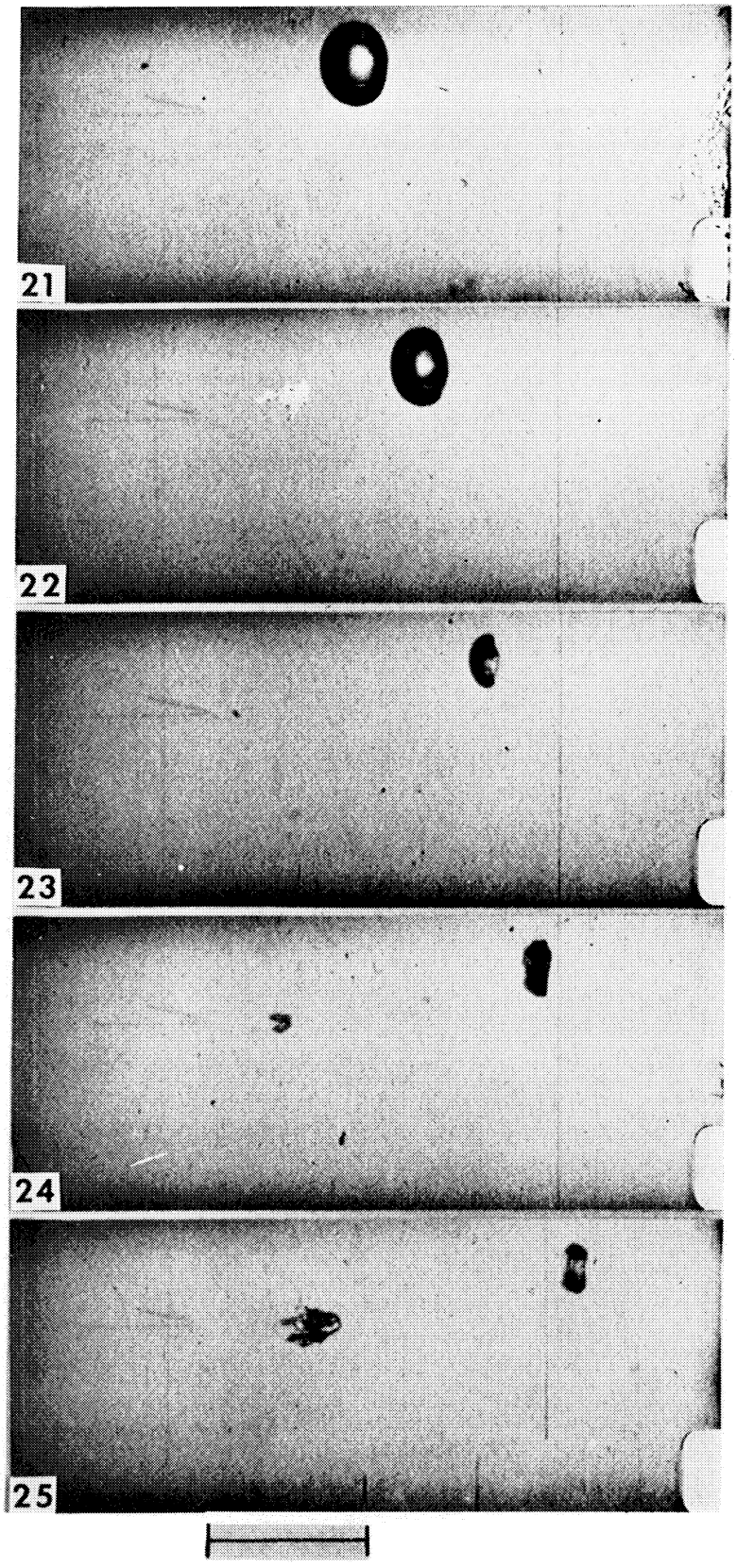

Figure 27. (Continued)

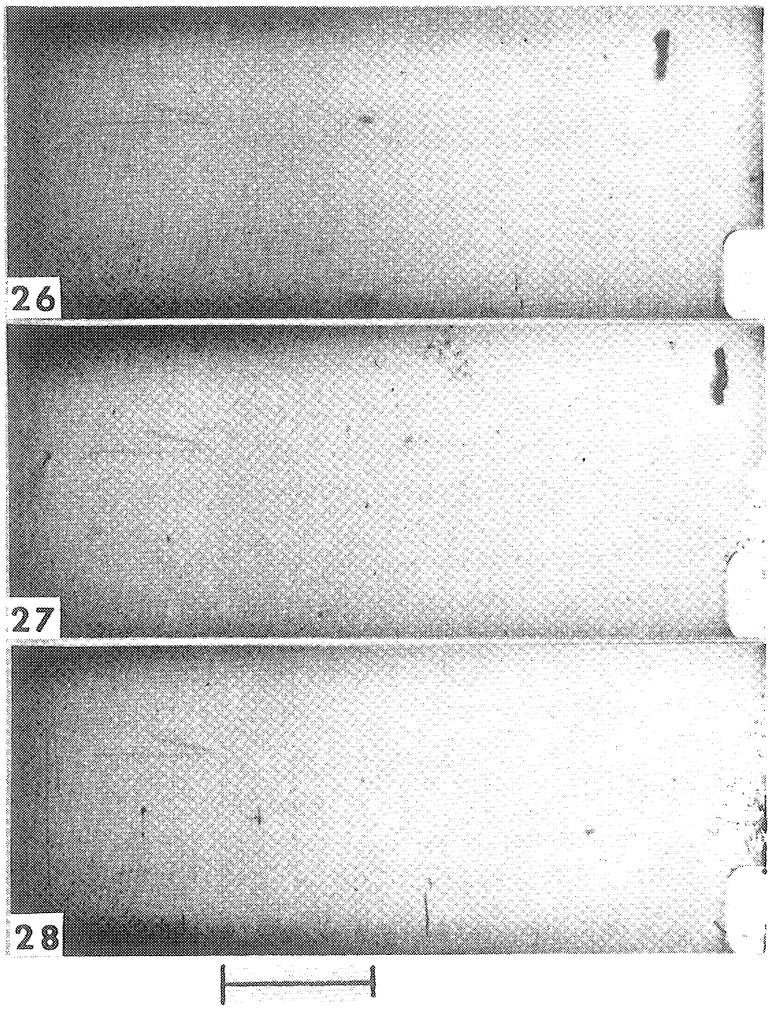

Figure 27. (Continued)

The first step in analyzing the motion pictures was to determine the framing rate. Timing marks on the edge of the film occur every 1/120 seconds, and the film manufacturer places footage marks also along the edge of the film. A one hundred foot roll of film accelerates through the camera so that the framing rate changes continuously. Therefore, a curve of microseconds per frame vs film footage was plotted (Figure 28) and the location on the film of each bubble is noted by the footage number.

The film was analyzed in a standard microfilm viewer, giving an image magnification as determined by the scale arrow marked on the inner venturi surface of about 6.6 x real size. Four pieces of information were obtained for each spherical bubble image -- the film foot number to obtain framing rate, the axial distance from the venturi throat exit measured positive downstream and negative upstream, and the bubble vertical and axial dimensions if it collapsed non-symmetrically, otherwise just the spherical diameter. Time was then determined with an arbitrary zero being assumed when the bubble axial position was at the throat exit. Therefore, time is negative if the bubble is upstream, and positive if downstream from the exit. Since the bubbles do not appear exactly at the throat exit point in one of the frames, the position for zero time was linearly interpolated between the two frames. If all bubble translational velocities are the same, then all 597 observations should fall closely on a single curve of time from throat exit vs distance from throat exit. Figure 29 is such a plot, and included is a curve of time vs position of a liquid particle based on the measured flow rate and flow area assuming zero void.

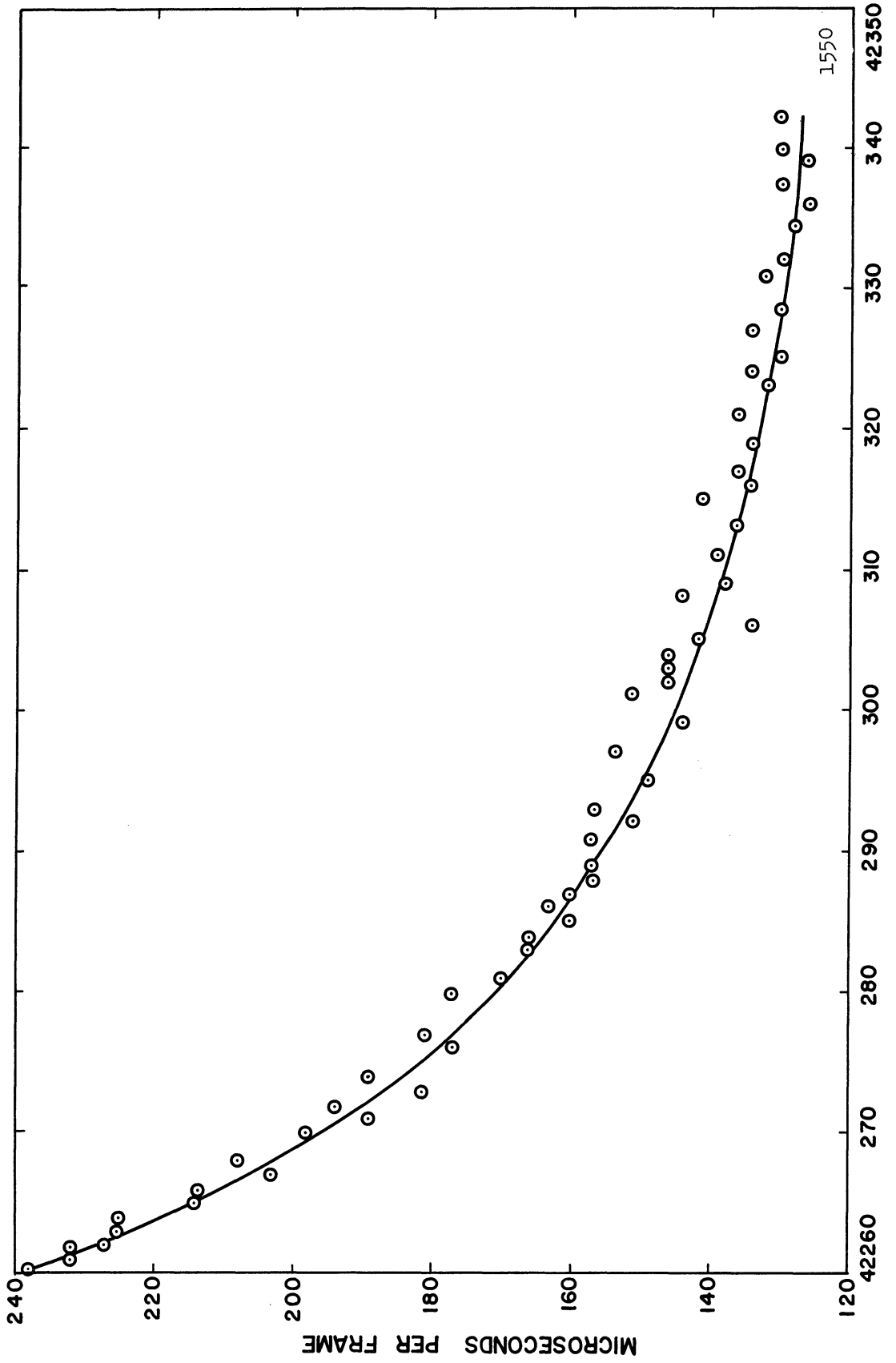

Figure 28. Framing Speed of Film vs Film Footage (the footage numbers are as marked on the film by the manufacturer). (Reel D)

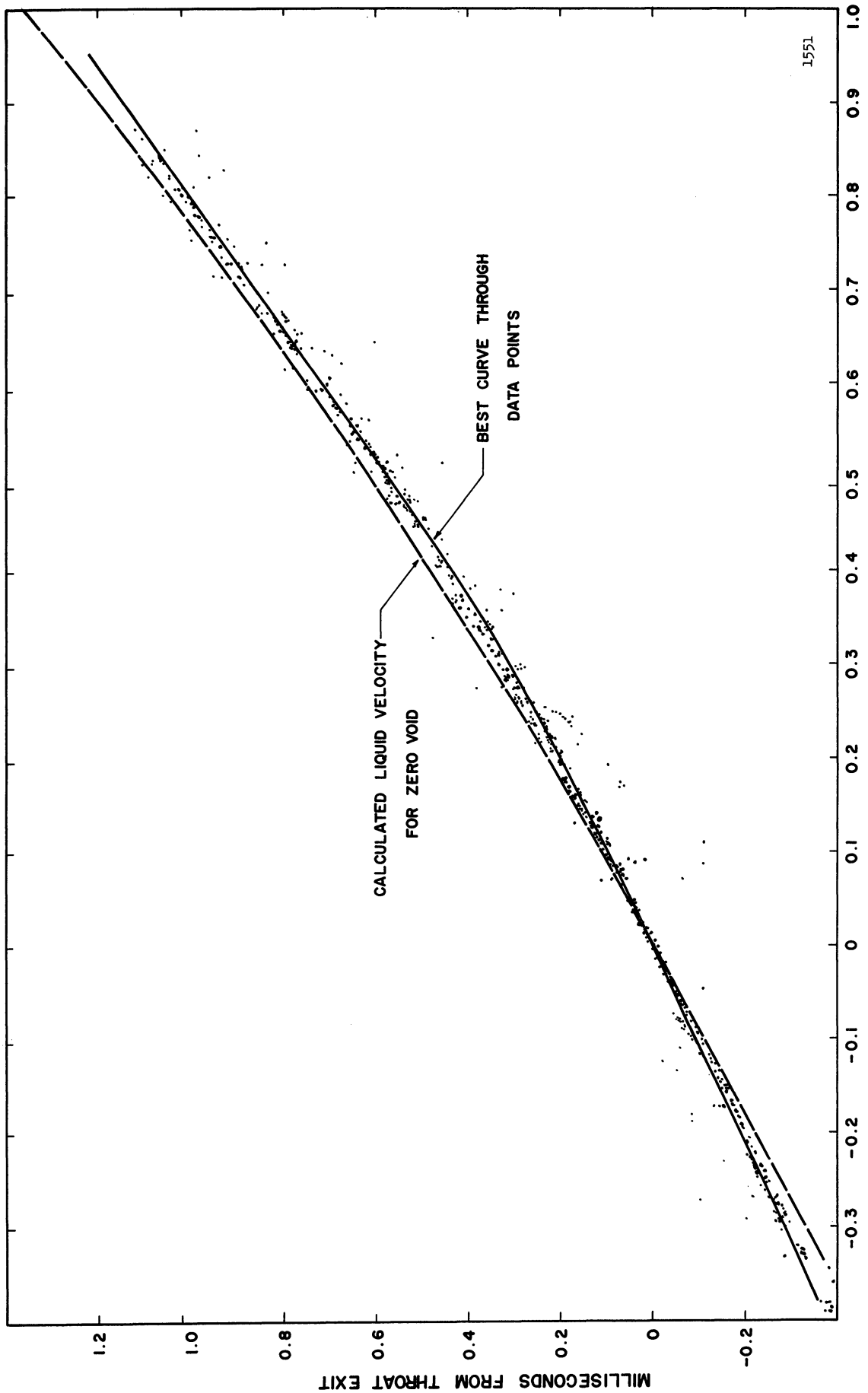

Figure 29. Time vs Position of Bubble with the Time and Position Arbitrarily Assumed to be Zero at the Throat Exit, also Liquid Velocity Assuming Zero Void. (Reel D)

The actual liquid velocity may be larger than calculated if the void content is large. For the limited field of view of the photographs, 360 frames were analyzed and the total void content measured. Both spherical and nonspherical voids were measured, and the thickness of the nonspherical voids along the line of sight estimated from still photographs taken at 90° to the motion pictures. Most of the void volume consisted of irregular shaped masses which occurred mostly downstream of the throat exit, and remained relatively stationary. Expressed as a percent of the volume in the diffuser only, and within the field of view, the time-averaged void content was about 0.2 percent. However, as seen in Figure 30 where the void content is plotted vs frame number, the void varies considerably in time. The maximum void observed in any one frame was 4.1 percent. Of the total volume of void observed in 360 frames, 28 percent was individual bubbles which grew spherically and 72 percent was irregular masses.

Since the time average void content is very low, the actual liquid velocity is very nearly equal to the calculated velocity based on zero void content. From Figure 29, the bubble translational velocity in the throat and for about 0.2 inch into the diffuser is 87 ft/sec. The liquid velocity in the throat is 74.6 ft/sec. Therefore, the bubble slip ratio of bubble velocity to liquid velocity is 1.17 in the throat, and decreases to 1.0 in the diffuser. This is as expected since in an accelerating flow in a falling pressure gradient the bubbles are accelerated faster than the liquid because of their lower density.

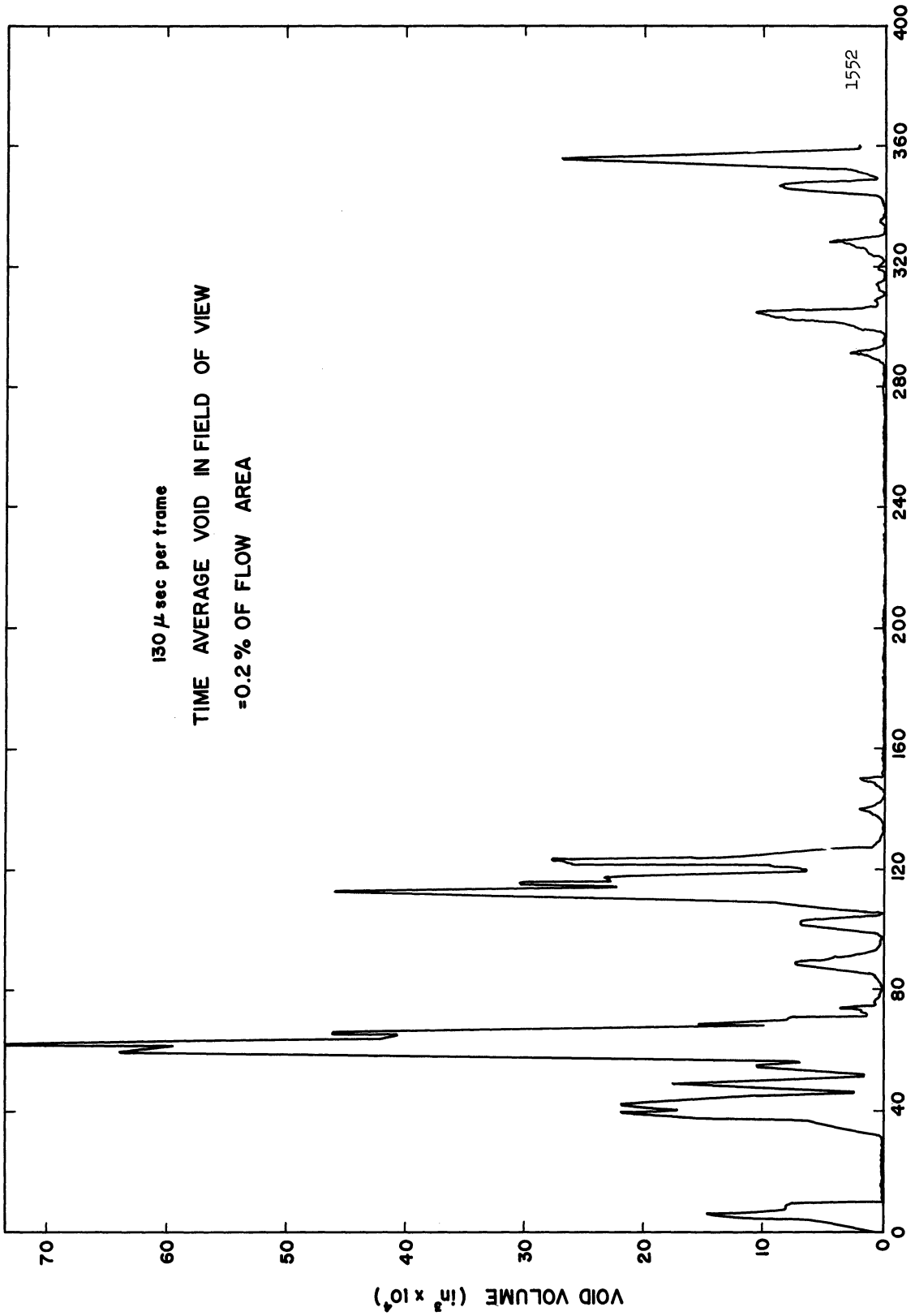

Figure 30. Total Void Content in the Field of View vs Arbitrary Frame Number. (Reel D)

The normalized bubble radius R/R_{max} from the high speed photographs was calculated as a function of time based on the first observed maximum on the film. Since some bubbles had the same maximum size in two frames the first frame was taken as the zero time reference. An equivalent bubble radius was defined for that portion of the collapse where the bubbles became non-spherical. The volume was assumed to be equivalent to an ellipsoid,

$$\text{Volume} = \frac{4}{3}\pi\frac{A}{2}\frac{B}{2}\frac{C}{2}$$

where A, B, and C are the axes. For the observed bubbles, it was assumed that the vertical ellipsoid axis was the same length as the axis in the line of sight, or in other words the bubbles were axially symmetric. The third axis was taken as the maximum dimension of the bubbles in the direction of flow. If A is the vertical measured length and B the axial length, then a sphere having the same volume as that calculated for an ellipsoid from the above formula would have a radius of

$$R = \frac{1}{2}(A^2B)^{1/3}$$

The equivalent spherical radius and the normalized radius was calculated for each of the 73 bubbles analyzed. The average maximum radius, R_o, was 36.5×10^{-3} inch, and the maximum and minimum values of R_o for bubbles which were tabulated were 68.3×10^{-3} and 19.6×10^{-3} inch respectively.

Figure 31 is a plot of the normalized bubble radius vs distance from the venturi throat exit. The curve drawn on this figure was used along with the axial pressure profile to obtain the venturi pressure vs

observed bubble radius. Since all bubbles are normalized to their individual maximum sizes, each of the 73 bubbles is represented by a point at a normalized radius of 1.0. It is seen that the average venturi location of the maximum size of the bubbles is about 0.15 inch downstream from the throat exit. There is a quite extensive spread of the points along the horizontal axis, indicating either that the pressure profile in the venturi does not strongly govern the actual growth and collapse region, or that, as is known to be the case, there is considerable oscillation in the cavitation field and in the static pressures.

It was thought that a plot of normalized radius vs time measured from the maximum bubble size for each bubble might help to eliminate the scatter of Figure 31 if it were true that the static pressure gradient did not completely govern the collapse region. Figure 32 is a plot of the normalized bubble radii vs time from the first observed bubble maximum size. It is seen that there is still considerable spread in the data. However, the bubble collapse can be definitely seen to slow down at normalized radii of 0.5 to 0.6. This may indicate that inertia of the liquid is not the only factor involved in the collapse, and perhaps that based on numerical results, one can say that there is a considerably faster internal pressure rise than that predicted for a small amount of gas under adiabatic or isothermal compression. An alternative explanation is that departure from ideal spherical symmetry results in a slower collapse. Note that the growth curves are considerably steeper in the low R/R_o range than the collapse curves.

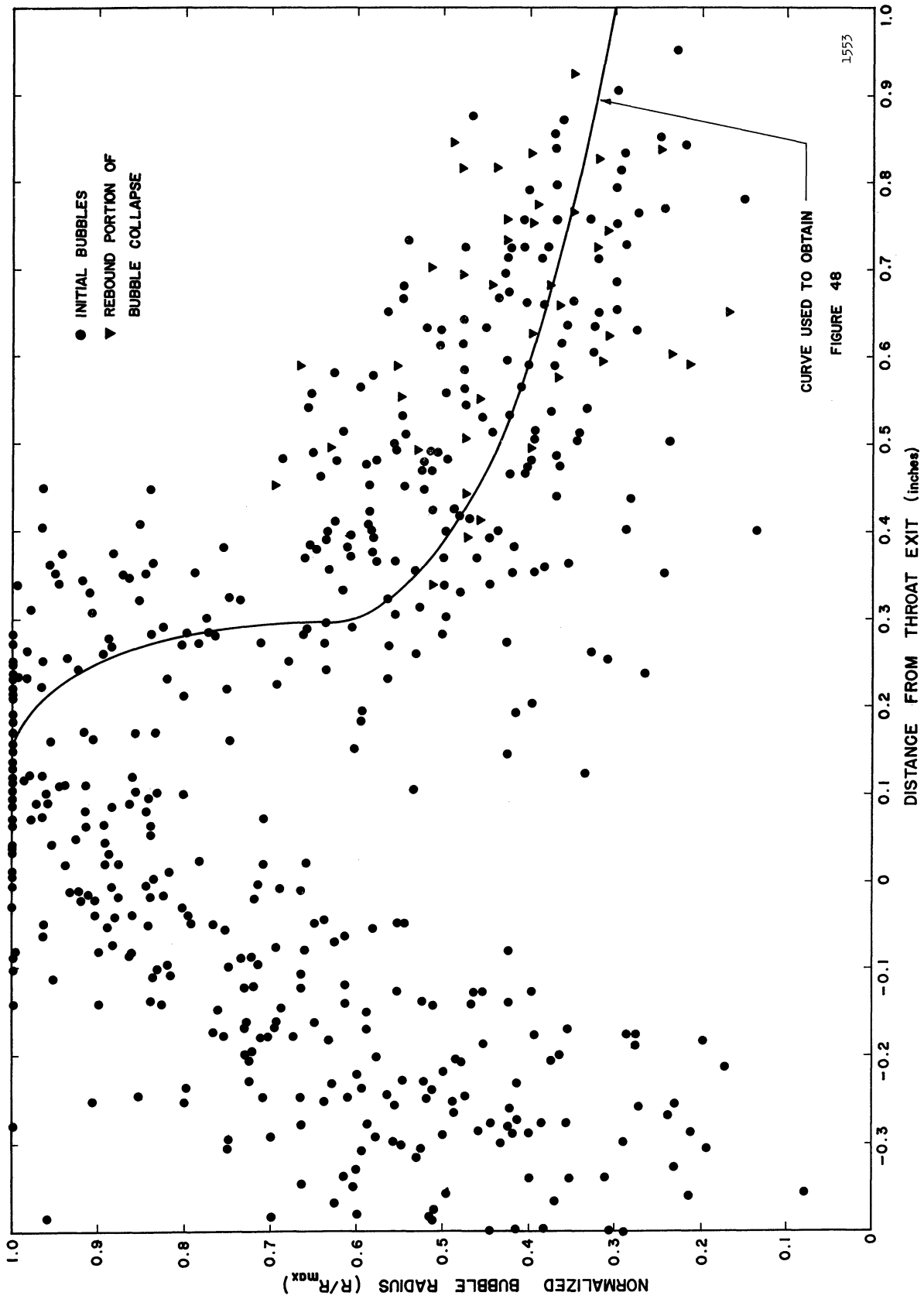

Figure 31. Normalized Observed Bubble Radius vs Distance from Throat Exit, 73 Bubbles. (Reel D)

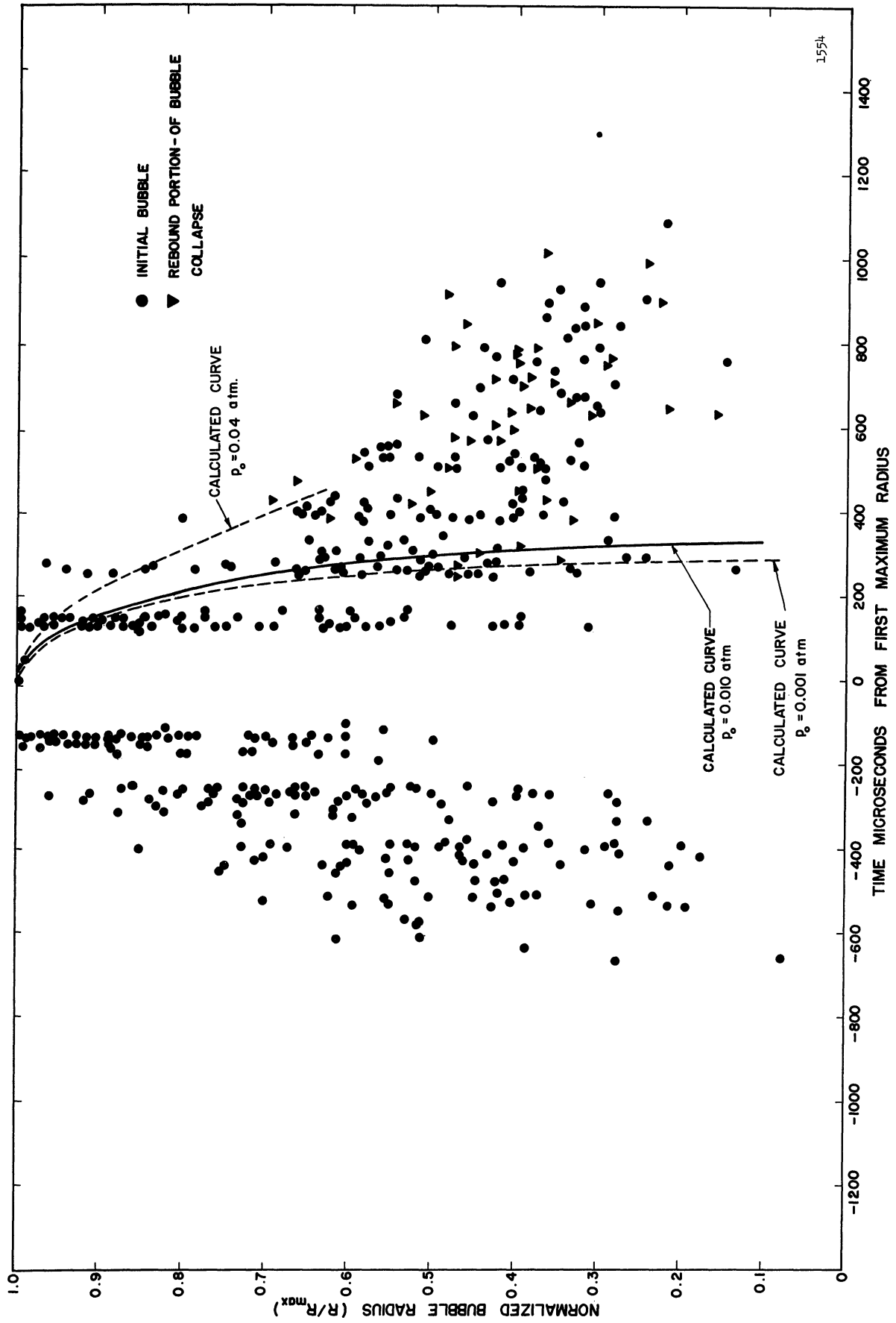

Figure 32. Normalized Observed Bubble Radius vs Time from the First Observed Maximum Radius, 73 Bubbles. (Reel D)

A plot of the data with a time normalization similar to that used in the theoretical analysis requires the pressure differential between the liquid far from the bubble and the internal pressure. The internal pressure can be assumed equal to saturated vapor pressure at the liquid temperature as a first try, and the external pressure for each bubble location is obtained from the measured pressure profile. Therefore, the experimental profiles will be considered next.

Figure 22 shows the locations of the twelve pressure taps in the venturi. The first set of pressure profiles was obtained for six flow conditions in the venturi. The minimum velocity was determined by the minimum surge tank pressure which, as previously indicated, must be a positive gauge pressure. The flow rate was then adjusted until just sufficient cavitation was visible to obtain pictures of individual bubbles. The nominal venturi throat velocity was about 80 ft/sec. The maximum velocity was determined by the maximum range of the calibrated orifice used for measuring flow rate (about 280 gallons per min). The gas pressure in the surge tank was adjusted for the same appearance of cavitation, resulting in a nominal maximum throat velocity of 120 ft/sec. At each of the velocities, profiles were obtained with air saturated tap water (at STP) and with about 50 percent of saturation (STP) at temperatures between about 70°F and 80°F. Then the loop cooling was turned off and hot, deaerated profiles were obtained at 113°F for the lower velocity and 133°F for the higher velocity. A normalized suppression pressure was calculated, defined as pressure above vapor pressure divided

by the liquid kinetic pressure in the venturi throat, i.e., "cavitation number". The results are shown in Figures 33 and 34. In all the curves except those for the high temperature, the upper row of pressure taps gives a higher pressure than the lower row, in the vicinity of the venturi throat. It was thought that this might have resulted from a slight difference in the 1/4 inch throat opening across the three inch width of the flow area. For example, a change in the throat size from 0.250 x 3.0" to 0.240" x 3.0" causes an 8.6 percent increase in the kinetic pressure at the same flow rate. Unfortunately, no zero cavitation, i.e., single-phase flow, pressure profiles were included in the first runs so it could not be determined whether the cavitation cloud caused the non-symmetric behavior or whether other effects as the possible slight differences in flow area dimensions due perhaps to the clamping arrangement on the plexiglas venturi, etc., caused them.

Another set of pressure profiles were obtained after the venturi had been dissassembled and then reassembled with a slightly different clamping arrangement. The same flow conditions were used, with some additions at each flow rate and temperature. The normalized pressure profiles are shown in Figures 35 to 37. Each curve represents average values of the normalized pressures of from two to five runs. Two additional cavitation conditions were used: zero cavitation, plotted with an arbitrarily selected minimum normalized pressure, and visible initiation, corresponding to the first visible trail of tiny bubbles from the two taps closest to the throat exit. In each of these profiles, all

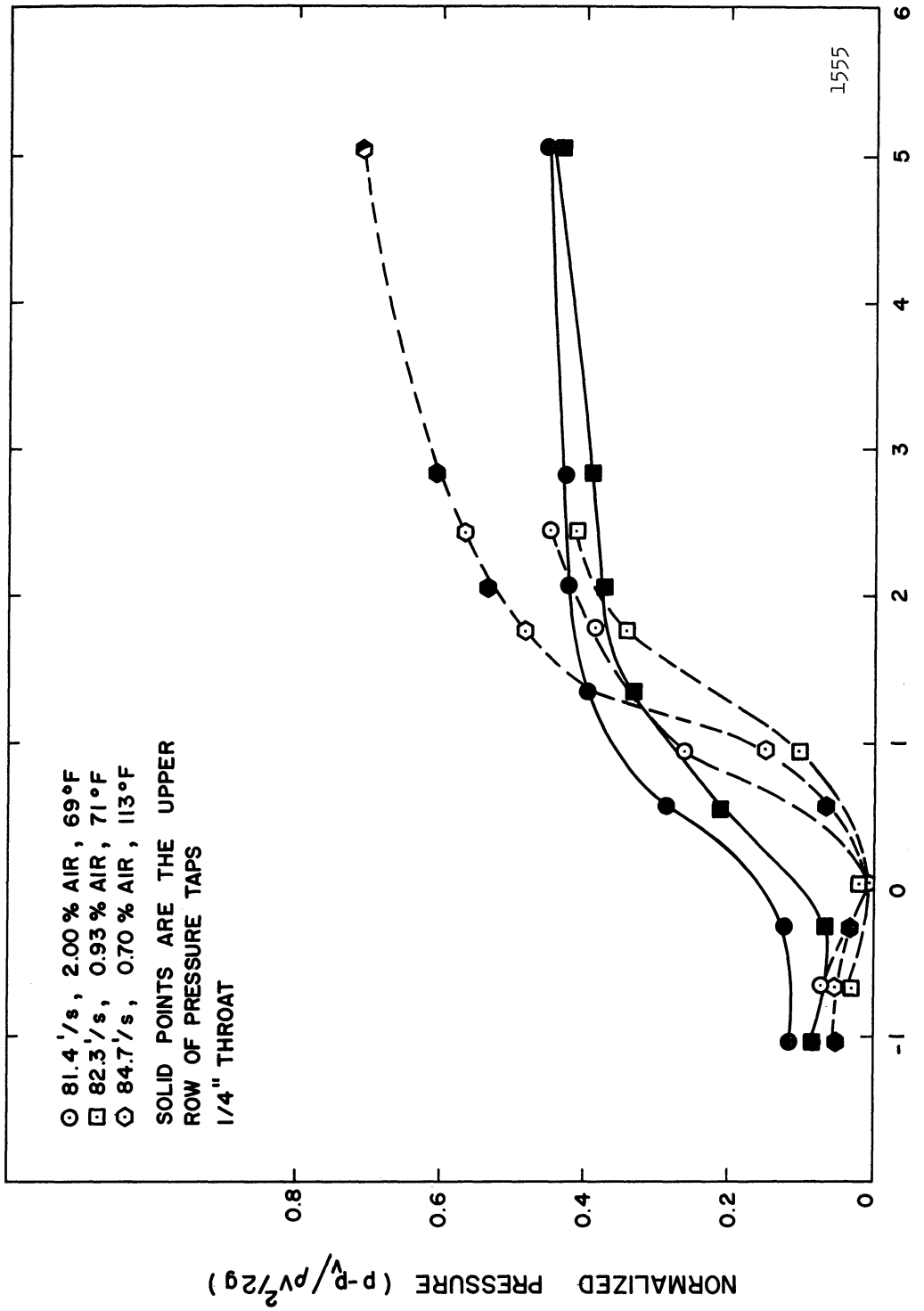

Figure 33. Normalized Pressure vs Distance from Throat Exit. (Low velocity) Curves Show Transverse Pressure Gradients May have Occurred. Cavitation to 0.75 in.

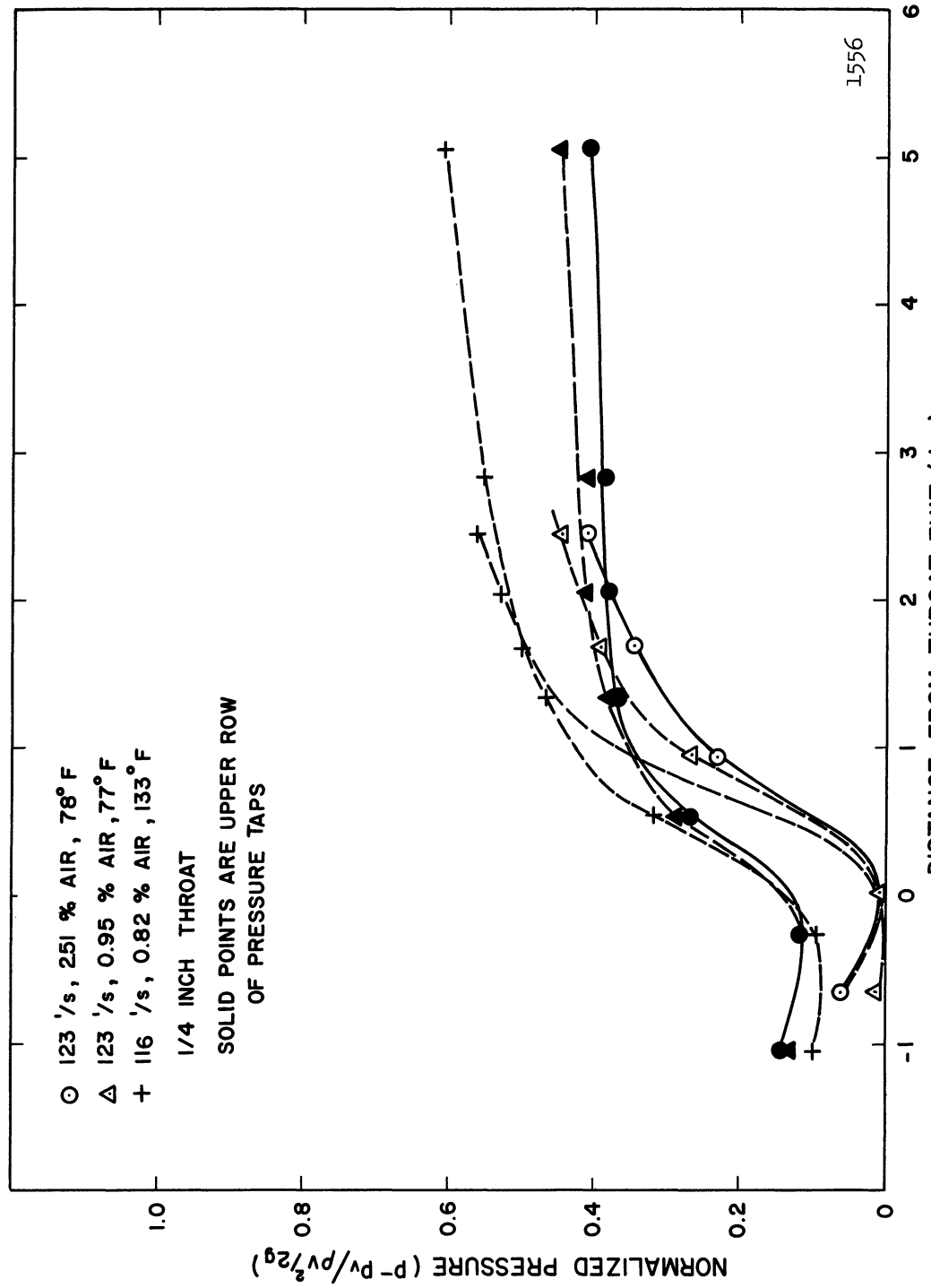

Figure 34. Normalized Pressure vs Distance from Throat Exit (high velocity). Curves Show Transverse Pressure Gradients May have Occurred. Cavitation to 0.75 in.

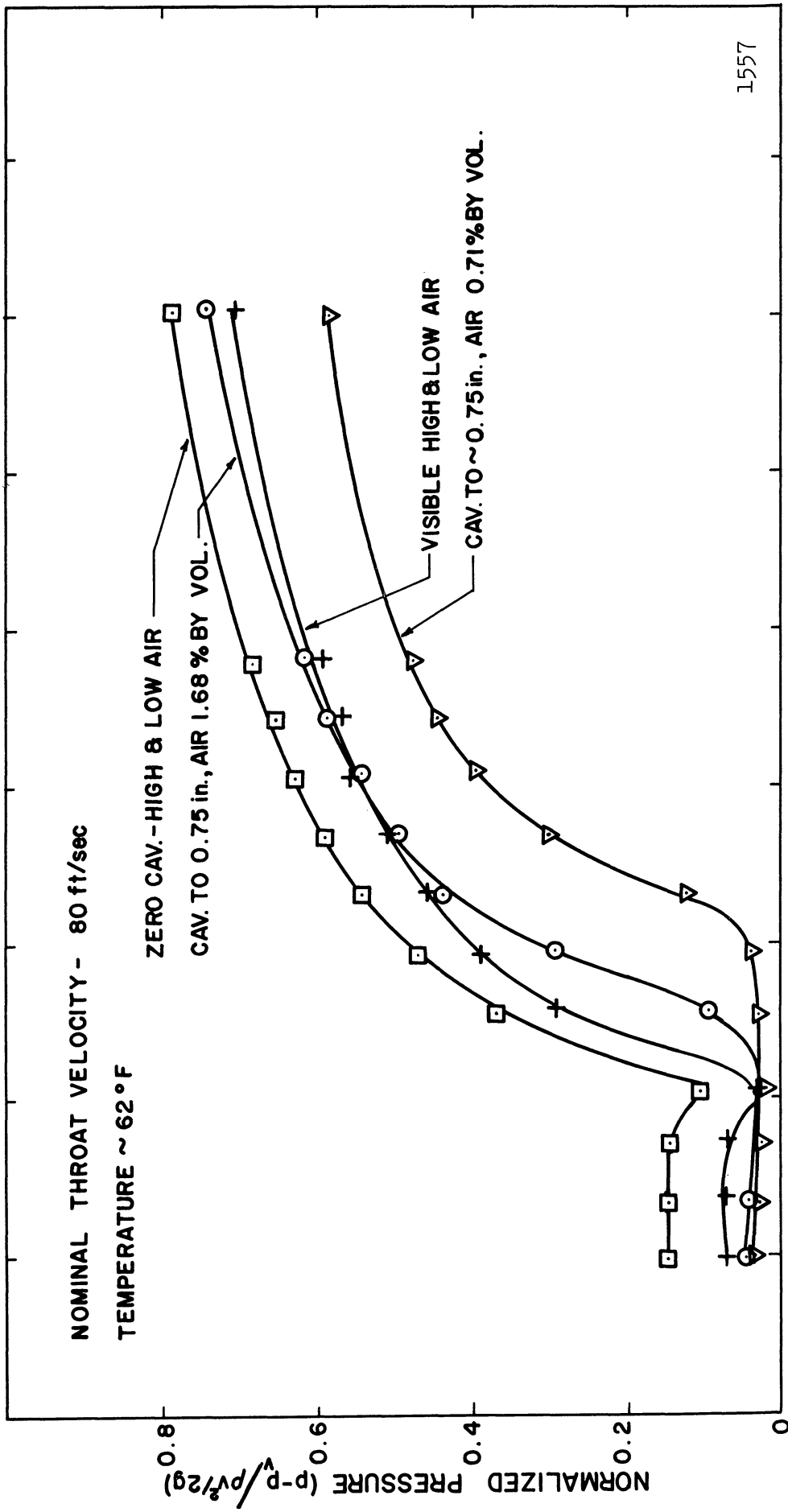

Figure 35. Normalized Pressure vs Distance from Throat Exit (low velocity).

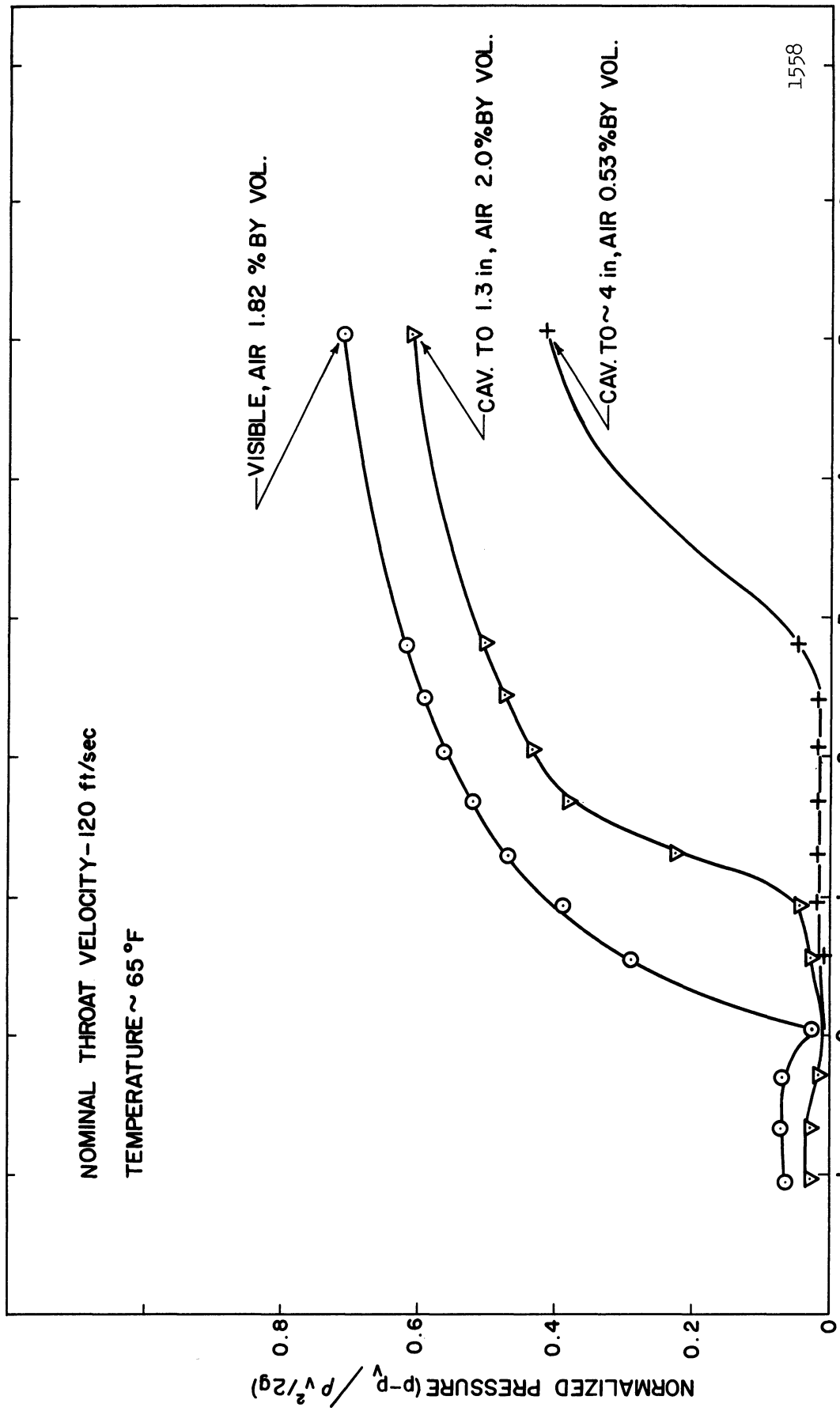

Figure 36. Normalized Pressure vs Distance from Throat Exit (high velocity).

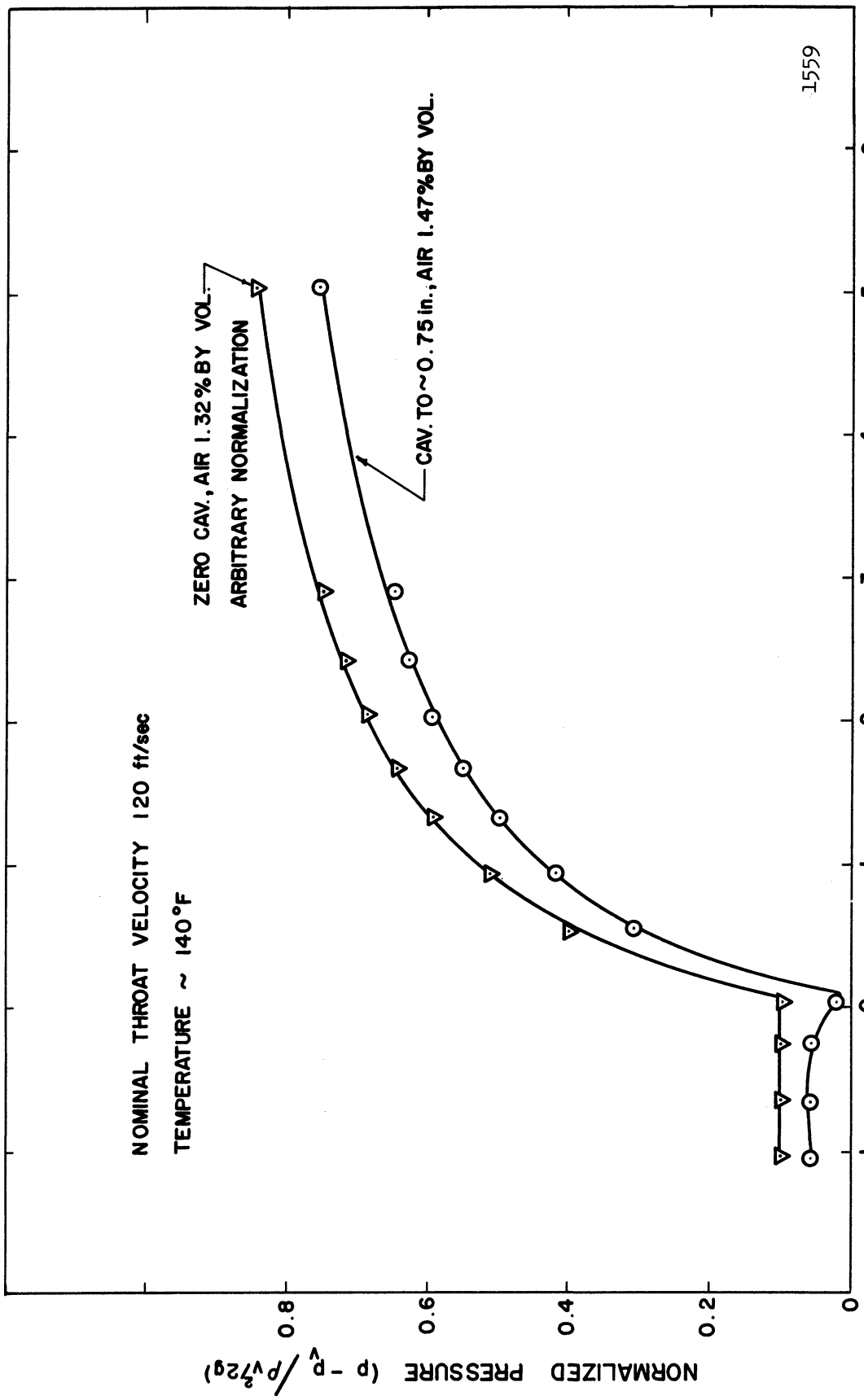

Figure 37. Normalized Pressure vs Distance from Throat Exit. (High temperature, high velocity)

points fall on the same smooth curve, so it is quite probable that the method of clamping the venturi can be important in maintaining uniform flow and pressure across the venturi width. In all further analyses, the second set of curves is used.

There was no significant variation in the appearance of the cavitation between the first and second set of curves. Still pictures, which were taken at the same time that the first set in Figures 33 and 34 were obtained, are shown in Figures 38 to 45. The arrow which was scratched on the inside flow surface is clearly visible in most of the photos. It is 0.205 inch long, and the tip of the arrow is at the throat exit and points in the direction of flow. For most flow conditions, the scratched arrow does not seem to act as a nucleating center for cavitation. Both those instances, shown in Figures 40 and 44, where the scratch does initiate a cavitation cloud are for high temperature water.

The high speed photography was obtained with a cavitation condition similar to the photograph in Figure 38 and to the normalized pressure curve in Figure 35 marked "Cavitation to 0.75". It is seen in Figure 35 that there is a significant difference in the pressures near the throat exit for different cavitation conditions. The normalized pressures for slightly different flow velocities is of course the best means of plotting the data, but it is necessary to have the actual pressure in the venturi to normalize the data on bubble radius obtained from the high speed photographs. The actual flow rates and absolute pressures for the curves in Figure 35 were well controlled, so that the average

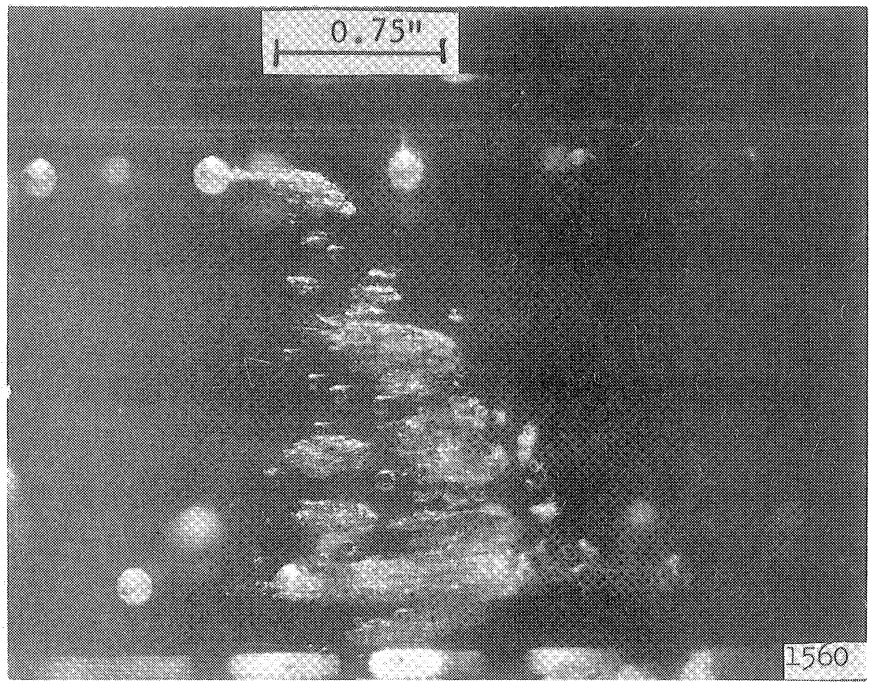

Figure 38. Still Photograph, 3μsec Exposure, 81.4 ft/sec, 2.05% Air Content by Volume, 68.8°F. Arrow is 0.205" Long and Tip is at Throat Exit.

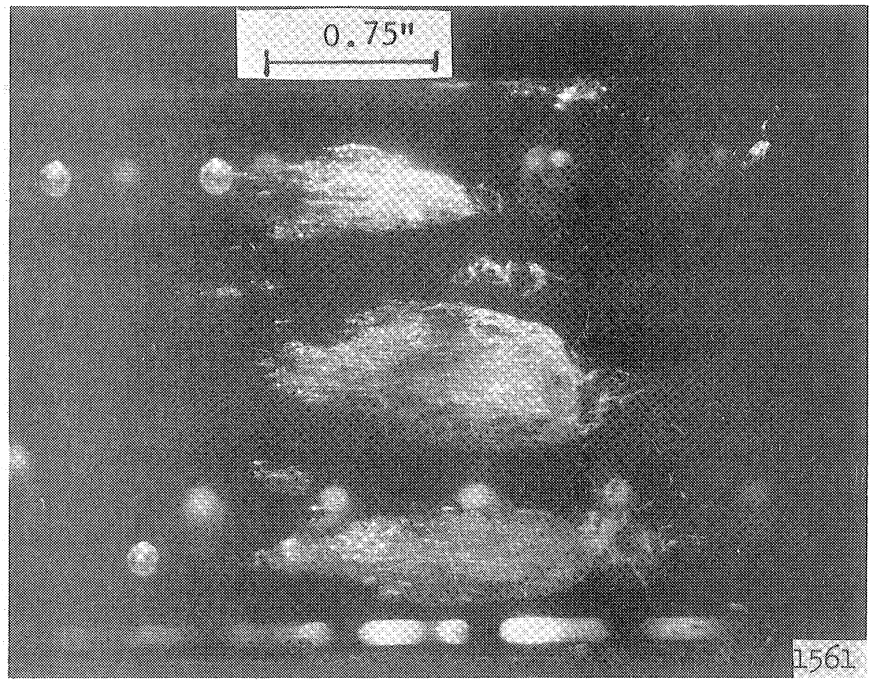

Figure 39. Still Photograph, 3μsec Exposure, 82.3 ft/sec, 0.93% Air Content by Volume, 70.5°F. Arrow is 0.205" Long and Tip is at Throat Exit.

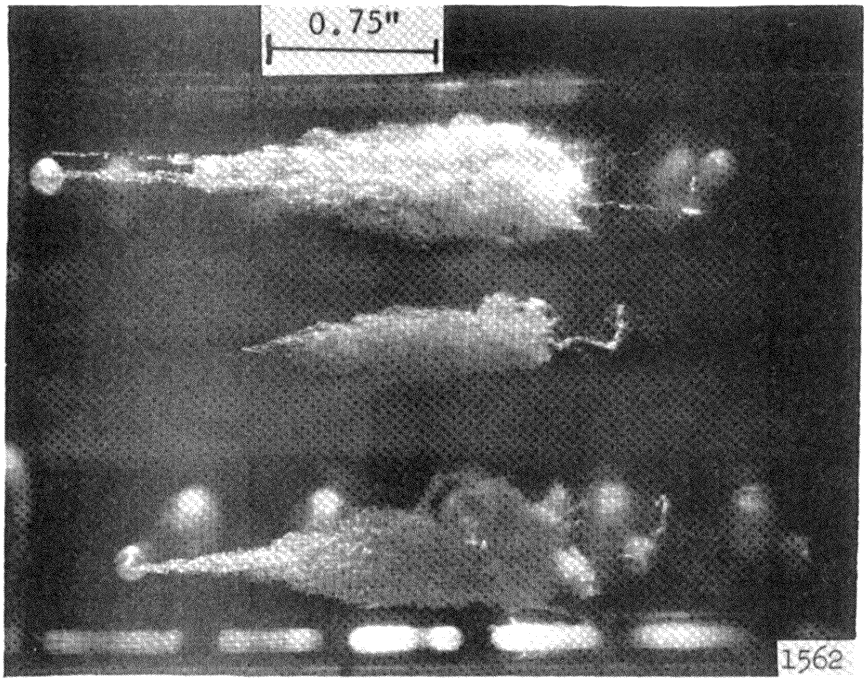

Figure 40. Still Photograph, 3μsec Exposure, 83.3 ft/sec, 0.699% Air Content by Volume, 112°F. Arrow is 0.205" Long and Tip is at Throat Exit.

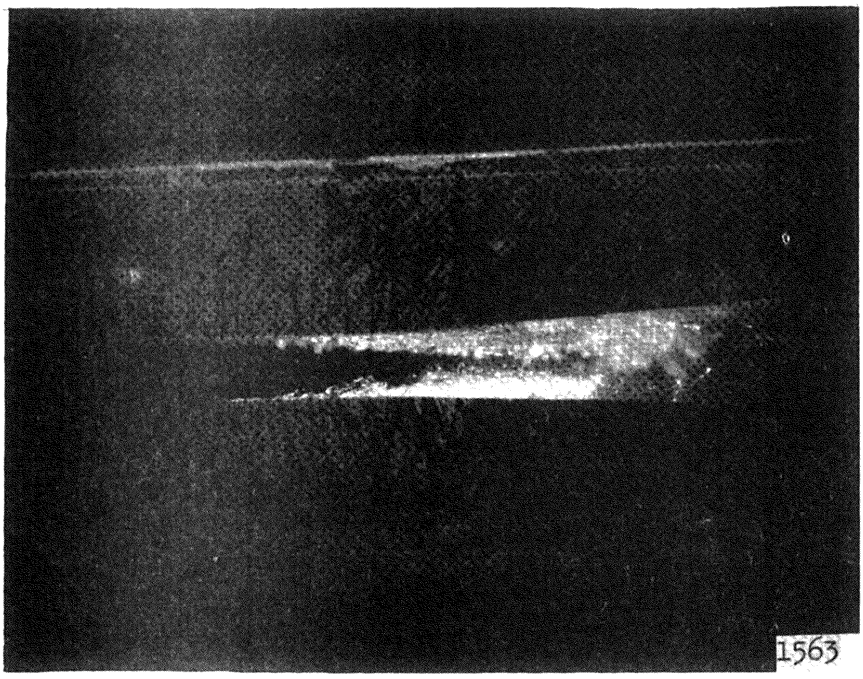

Figure 41. Still Photograph, 1.2μsec Exposure, 80.5 ft/sec, Low Air Content, ~70°F. Venturi is Rotated so the Pressure Taps are on the Top Half, and Flow is Left to Right.

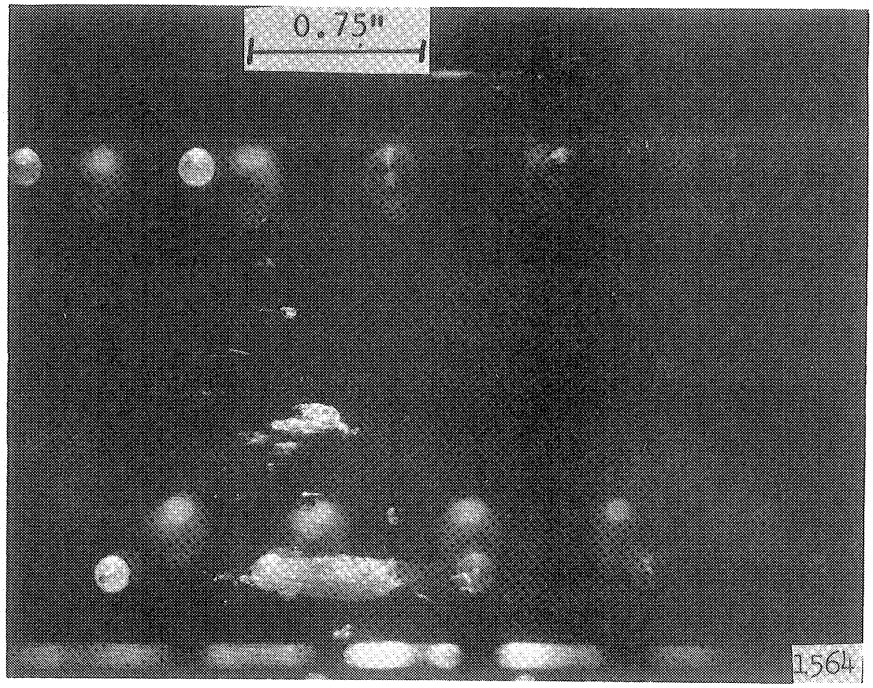

Figure 42. Still Photograph, 3μsec Exposure, 123 ft/sec, 2.51% Air Content by Volume, 78.4°F. Arrow is 0.205" Long and Tip is at Throat Exit.

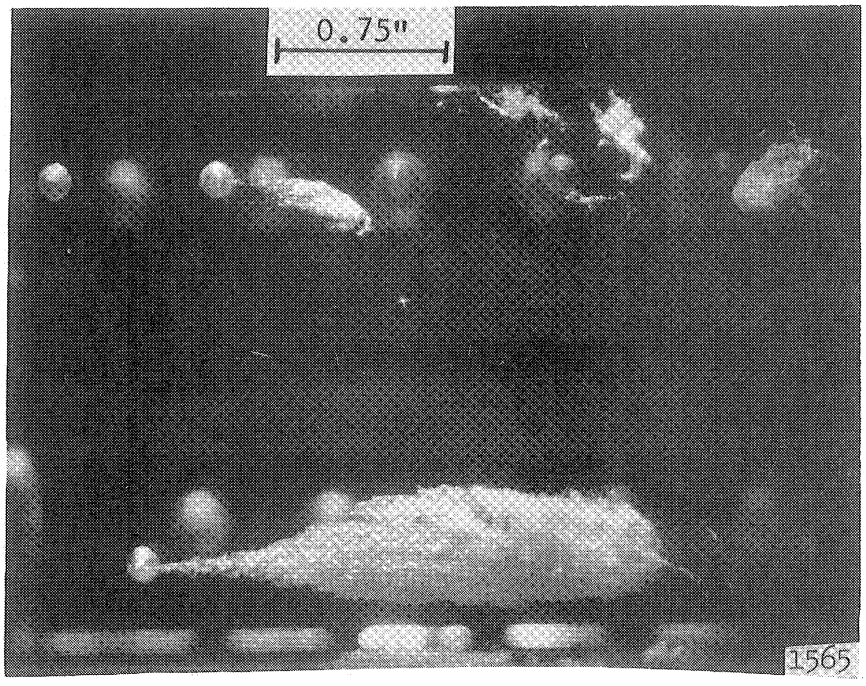

Figure 43. Still Photograph, 3μsec Exposure, 120 ft/sec, 0.95% Air Content by Volume, 77.0°F. Arrow is 0.205" Long and Tip is at Throat Exit.

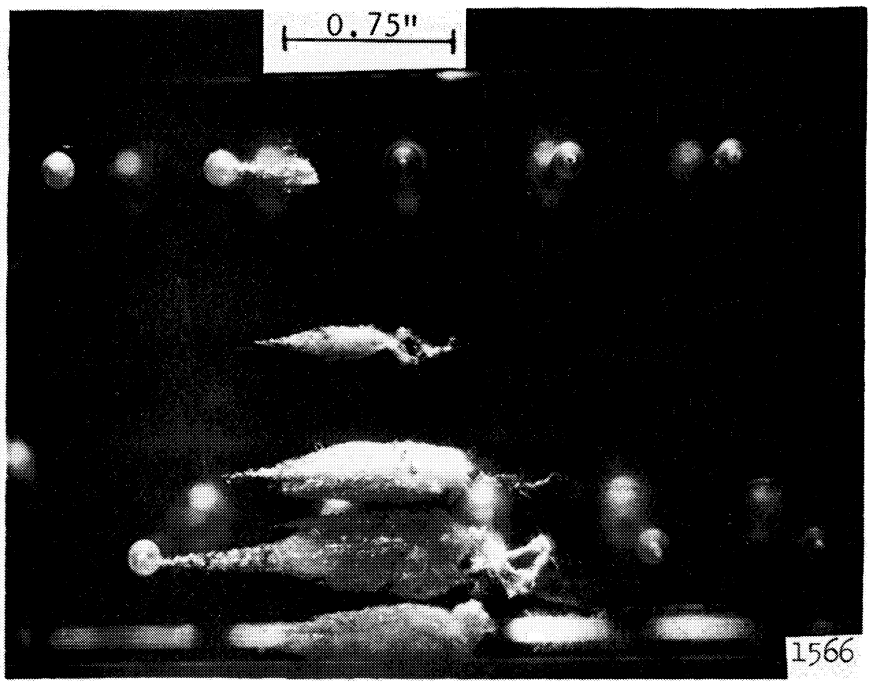

Figure 44. Still Photograph, 3μsec Exposure, 116. ft/sec, 0.82% Air Content by Volume, 136°F. Arrow is 0.205" Long and Tip is at Throat Exit.

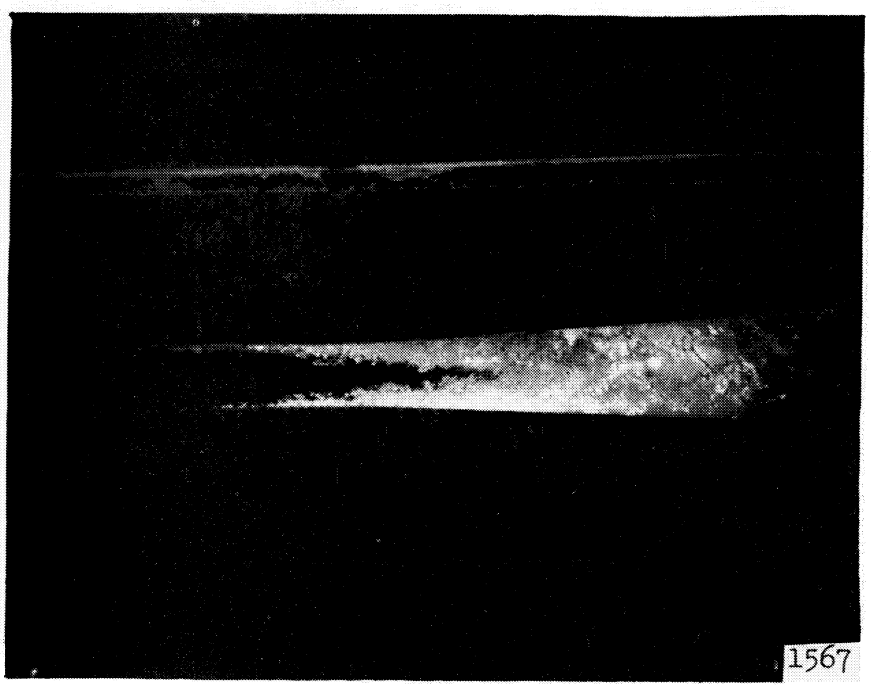

Figure 45. Still Photograph, 1.2μsec Exposure, 115. ft/sec, Low Air Content, ~78°F. Venturi is Rotated so the Pressure Taps are on the Top Half, and Flow is Left to Right.

values of the pressures above vapor pressure, $(p - p_v)$, for several different runs were appropriate values to use for comparison to the bubble photographs. Figure 46 is a plot of the average unnormalized pressures for visible initiation and for cavitation to 0.75 inch. These curves are at the same flow rate, the only difference in the loop settings being an increase in the surge tank pressure by an average of 2.7 psi. At 0.5 inch from the throat exit the pressure rises by 9.0 psi. Therefore, a very slight change in cavitation condition, even considerably less than that of the two curves in Figure 46, can have a very significant effect on the pressures near the throat exit. It is in this region where the photographs were taken. The field of view extended (from the throat exit) 0.926 inch downstream and 0.394 inch upstream. The location of the bubbles within this field can be accurately measured, as shown by the very smooth curve with small scatter in Figure 39. However, a small oscillation in the cavitation field, which is common, means a slight shift of the location of the sharp pressure rise and a large change in the local pressure.

The pressure differential, $(p - p_v)$, is used in a normalized time, t', according to

$$t' = \frac{t}{R_o}\sqrt{\frac{p - p_v}{\rho}}$$

In the incompressible numerical solution for collapse, a similar normalization was used except that the initial value of the quantity $(p - p_v)$

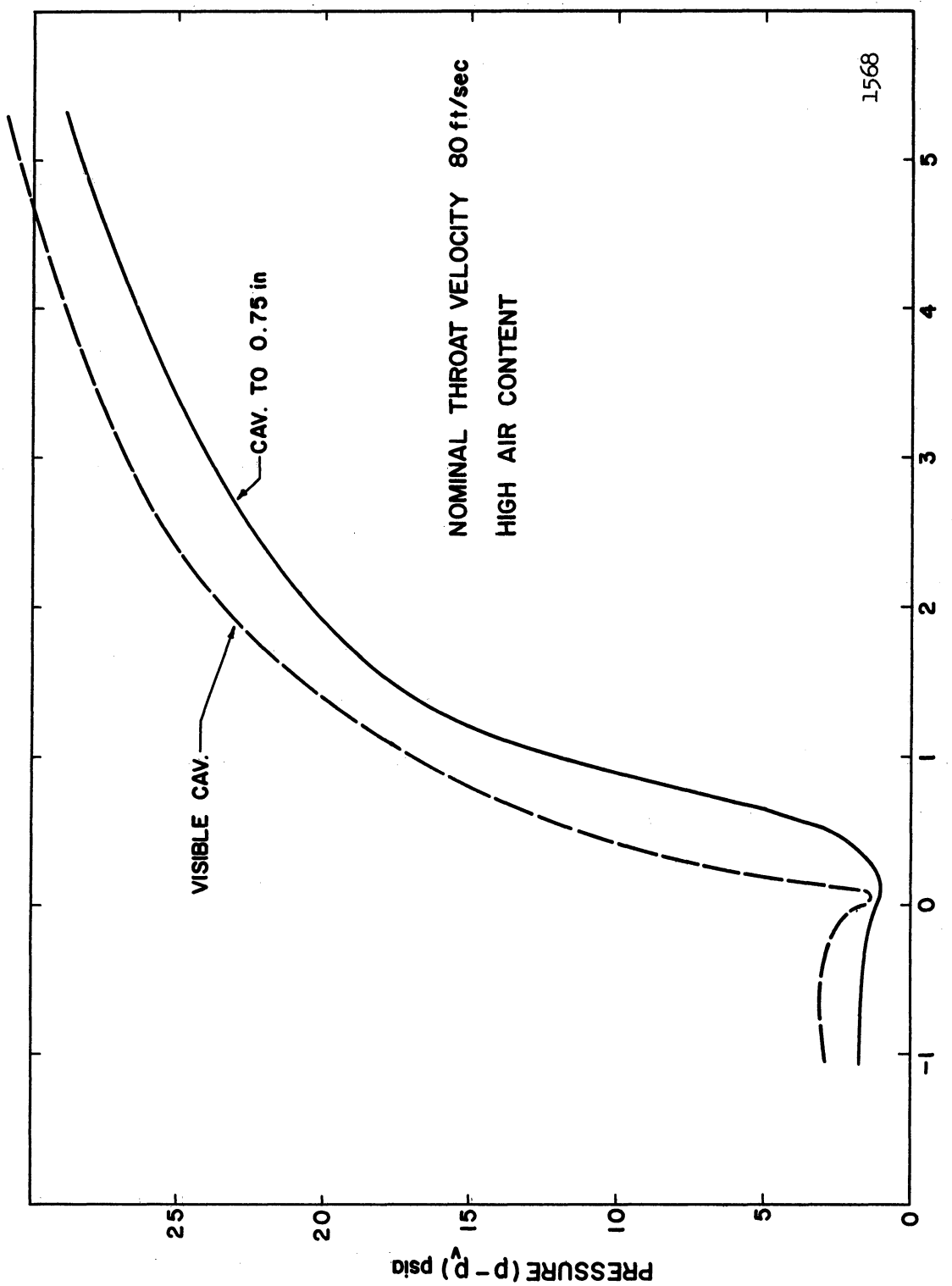

Figure 46. Pressure Above Vapor Pressure vs Distance from Throat Exit.

was used instead of the instantaneous value which will be used here. For a given bubble, the local pressure at the known venturi location is obtained from Figure 46, and the time is measured from the film frame with the first maximum bubble size. The normalized time was thus obtained for ten bubbles, arbitrarily selected from the 73 observed, for the curve "Cavitation to 0.75", and plotted with normalized radius in Figure 47. A comparison to Figure 32 indicates somewhat less scatter when the normalized time is used.

D. Comparison of Theoretical and Experimental Collapse Curves

It is desired to obtain a plot of normalized bubble radius vs time for the average observed bubble in order to be able to make a comparison with a calculated curve. The calculated curve, however, should be obtained from the same variation of external liquid pressure as a function of bubble radius. Accordingly, a best curve was drawn through the points of Figure 31 for normalized bubble radius vs distance from throat exit. At a given bubble radius, the distance from the throat exit was obtained and used to get the pressure from the pressure profile in Figure 35 for cavitation to 0.75 inch for high air content. A plot of normalized bubble radius vs bubble environmental pressure was obtained as shown in Figure 48. A curve was approximately fitted to the experimental curve resulting in the following equation

$$P - P_v = \frac{0.04}{R' - 0.25} + 0.02$$

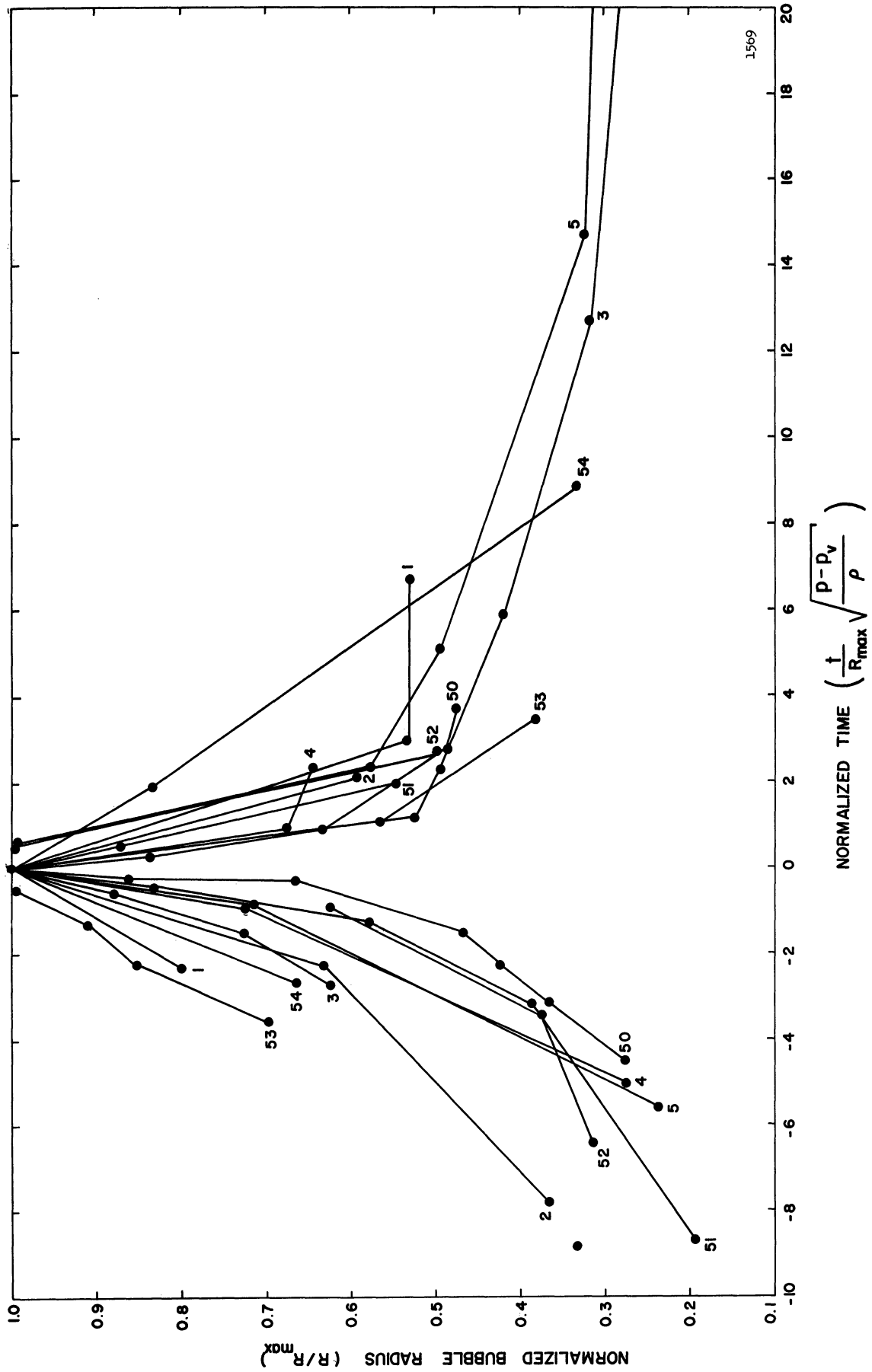

Figure 47. Normalized Bubble Radius vs Normalized Time for Ten Bubbles. Numbers on Curves are to Identify Bubbles.

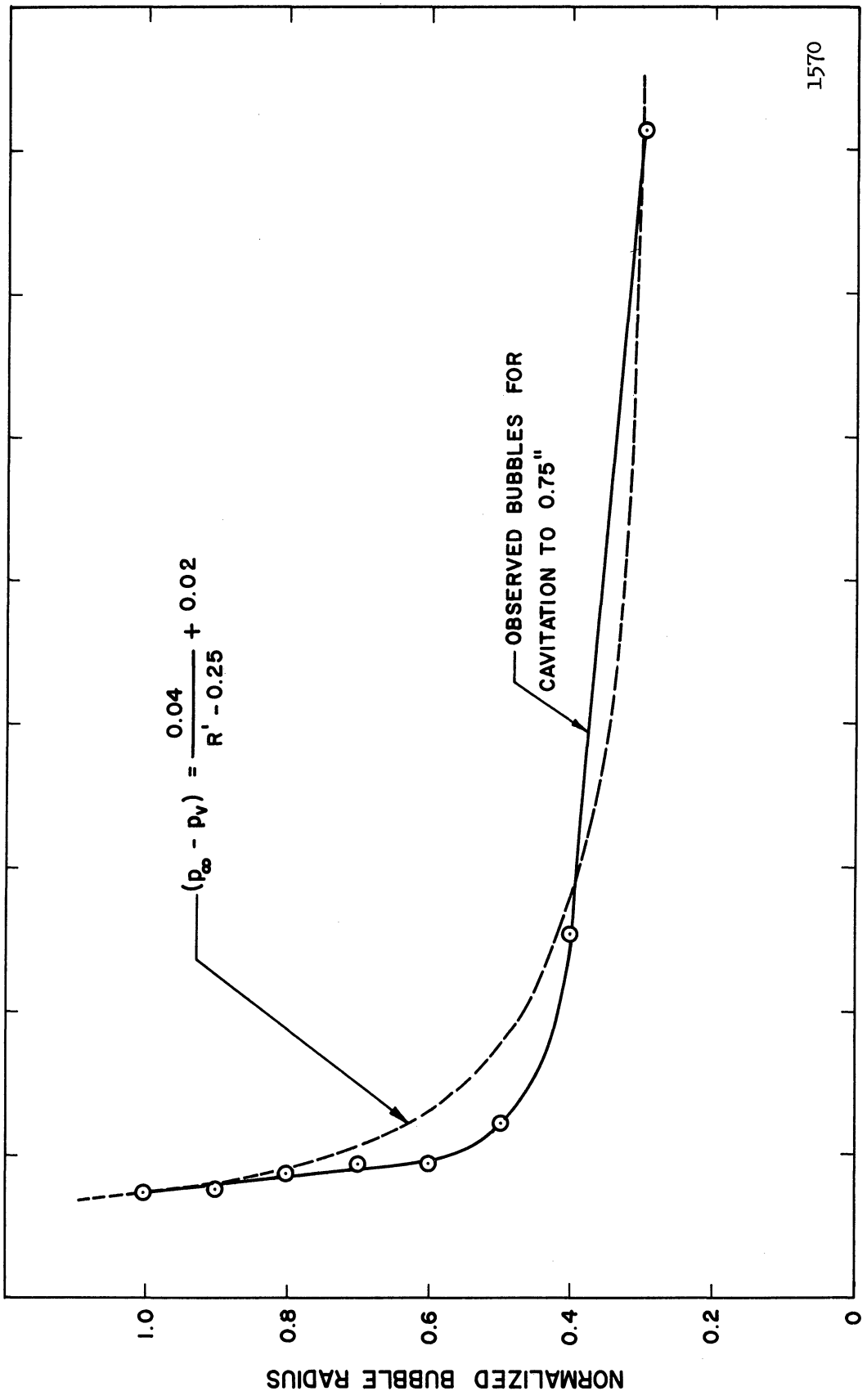

Figure 48. Normalized Bubble Radius vs Bubble Environmental Pressure for Observed Bubbles and Pressure Profile for Cavitation to .75 in.

where $(p - p_v)$ is measured in atmospheres; $R' \geq 0.3$. This equation was used as an external function in the incompressible solution to give the pressure, above a constant vapor pressure in the bubble, in the liquid far from the bubble during collapse. The initial pressure is 0.0733 atm. The internal gas pressure was assumed to be 0.010 atm initially and assumed proportional to $(1/R'^3)^{1.3}$. Other parameters were those of water, and the maximum radius was the average maximum observed, i.e., 36.5×10^{-3} in. The collapse curve obtained is shown in Figure 32. The curve compares with the experimental points to a normalized bubble radius of 0.5. Thereafter, the calculated collapse stops abruptly at $R' = 0.164$ because of the rise of internal gas pressure, whereas the experimental points indicate a gradual slowing down of the bubble wall velocity. The maximum calculated wall velocity was 48.2 ft/sec, near the final radius. The maximum experimental wall velocity was between 12 and 20 ft/sec, and occurred nearer the beginning of collapse. The assumption of an adiabatic gas compression inside the bubble is of course not justified in this case. A low initial internal pressure is necessary, but a more rapid pressure rise with decreasing bubble radius is needed. Perhaps the observed behavior is indicative of a substantial departure from thermal equilibrium in that the vapor within the bubble begins to behave as a perfect gas at that portion of the curve where the departure from the analytical prediction is observed. If so, this condition is reached earlier than predicted by previous investigations.[23]

The appearance of the collapse curve is similar to the theoretical collapse curves of Florschuetz and Chao.[45] Their curves follow

the pure inertia-controlled collapse curves, then the collapse slows down, or even rebounds depending on the thermal effects. Several rebounding bubbles are included in Figures 31 and 32, and also the general behavior of the time-normalized curve in Figure 47 is the same shape as the theoretical curves for a combined influence of inertia and heat transfer as considered by Florschuetz and Chao. They define several normalized parameters which they use to determine whether inertia or heat transfer or a combination of both effects is the predominant collapse mechanism. The parameters used were:

$$\text{Ja} = \text{Jakob number} = \frac{\rho C_p (T_{sat} - T_{liq})}{\rho_v L}$$

$$C = \frac{R_o^2 (P_{liq} - P_v)}{\rho \chi^2}$$

The usual thermodynamic parameter appearing in cavitation literature[92] is defined as

$$B_{cav} = \frac{\rho C_p}{\rho_v L}\left(\frac{\Delta T}{\Delta H}\right) = \frac{\rho C_p}{\rho_v L}\left(\frac{\Delta T}{\Delta P}\right)\rho$$

which has dimensions of 1/ft because of the term ΔH, representing liquid head. This is obviously closely related to the Jakob number.

Several corrections were applied to the parameters by Florschuetz and Chao[45] to take account of the non-linear variation in vapor pressure with temperature and to define a suitable average vapor density.

Using only the quantities above, the parameter $B_{sat} = Ja^2/\sqrt{C}$ was defined, and corrections to this value of B resulted in a quantity, B_{eff}, such that B_{eff} is always larger than B_{sat}. For values of $B_{eff} > 10.$, they concluded that liquid inertia control is assured. The value of B_{sat} for the venturi in the present investigation was calculated using the average pressure from Figure 46 at the location where the bubble collapsed most rapidly as determined from Figure 31 -- namely 0.25 to 0.35 inch downstream of the throat exit. The value of B_{sat} thus calculated was 28.9, and if appropriate corrections are made to obtain B_{eff} it would be even larger. Therefore, using the criteria of Florschuetz and Chao,[45] the bubble collapse in the venturi should be completely controlled by liquid inertia, whereas the curve appears similar to those theoretical curves presented for the case which includes heat transfer effects.

The presence of gas in the bubbles is not accounted for by the above analysis, and Florschuetz and Chao analytically estimate the effects of gas for only the case of purely heat transfer controlled collapse. It is possible, then, that their analysis is appropriate if there were no gas present. In the detailed photographic analysis herein, the water was about saturated with air at one atmosphere, so there could well have been significant quantities of air inside the bubbles although there is no direct measurement possible. However, similar films with water containing the minimum attainable level of air for the equipment used, namely 0.77 percent by volume at loop temperature and 1 atm (i.e., 39 percent

of saturation at 1 atm or 9.3 ppm by weight) also indicated identical bubble behavior in regard to shape of bubbles and rebounding bubbles. The fact that the reduction of dissolved gas by more than 1/2 did not prevent the occurrance of bubble rebound* suggests that there may not be a significant amount of gas diffusion into the bubbles during bubble growth, even for saturated liquid. Treaster,[54] in an investigation of cavitation hysteresis, presented an analysis by Parkin and Kermeen[93] to calculate the bubble growth times due to gas diffusion. The analysis includes the effect of a relative velocity between bubble and liquid which would tend to increase the growth rate by diffusion because the gas concentration gradient near the bubble surface is constantly maintained large. The relative bubble-liquid velocity in the venturi throat and slightly downstream was 12.4 ft/sec as obtained from Figure 29. Both the largest and smallest values of the observed bubbles when at their maximum sizes were used, and the pressure surrounding the bubble was taken as the average at the first four pressure taps in the venturi for the same conditions as in the high speed film. The largest bubble actually grew from 18.9 to 68.3 mils in 660 μsec and the analytically predicted growth time based on diffusion was 4.2 μsec. The smallest bubble grew from 5.3 to 19.6 mils in 405 μsec and the analytic growth time was 0.65 μsec. Thus the observed growth times were from 150 to over 600 times longer than the theoretical. Treaster[54] also presented another analysis

*It has been suggested in the past that rebound would only occur in liquids with high gas content. This is not borne out by the present observations over a relatively narrow range of gas content.

ignoring both velocity transport and liquid inertia, and the growth times were considerably longer. One may conclude that the diffusion of gas into the bubble during growth is probably significant, but the actual quantity of gas is difficult to determine because of the flow situation. It must be noted that the minimum measured pressure in the venturi was always above the liquid vapor pressure by the order of one psi or more, and yet cavitation occurred. The analysis just mentioned, by Treaster, indicated bubbles would grow by gas diffusion in such circumstances. Also, cavitation at the pressure taps, and local liquid turbulence mean that the measured value of pressure at the venturi wall may be well above the minimum local and instantaneous liquid pressure.

V. CONCLUSIONS

A. Viscosity

The predominant effect of shear viscosity is to increase the liquid pressure at the bubble wall during collapse. The magnitude of the pressure rise and the rapid change in density with respect to time suggests that the usual Navier-Stokes equation may not be completely satisfactory. That is, Stokes' assumption that stress is independent of the time rate of change of density may not be appropriate.

Moderate increases in viscosity from a reference value for water do not appreciably slow the bubble collapse. The bubble wall velocity in the incompressible analysis decreases as viscosity is increased. In the compressible analysis, moderate viscosity increases cause higher bubble wall velocities for small bubble radii, probably because of terms neglected in the compressible analysis for the pressure at the bubble wall. However, in both compressible and incompressible analysis, the large limiting viscosity defined by Poritsky[19] does cause the bubble collapse to abruptly slow down, and the complete collapse time to become large, although it can not be verified conclusively numerically whether or not the time is actually infinitely large as stated by Poritsky.

Calculation of the instantaneous viscous energy dissipation rate for a typical bubble collapsing in an incompressible liquid gives a rate of the order of 40 horsepower, indicating that local effects such as heating can become significant.

Very high time rates of density change in the liquid near a collapsing bubble, and high viscous shear stresses occur. A brief review of some of the relaxational phenomenon in liquids indicates that relaxation effects may exist for such collapsing bubbles. The possibility that such effects are in part responsible for the phenomenon of sonoluminescence is proposed.

Inclusion of the liquid viscosity and surface tension introduces two scaling parameters into the equations of motion. The Rayleigh type normalization and solution of the bubble dynamics equations is therefore not generally appropriate, since a solution is necessary for each set of these two parameters.

B. Surface Tension

The effect of surface tension is most important at small initial bubble radii. Usually the effect is small when the bubble has started collapsing because other effects such as liquid inertia and pressure at the wall (induced by viscosity) predominate even as very small radii are attained.

C. Compressibility

The proportion of the energy available for collapse which goes into compression of the liquid appears to be considerably more than the viscous dissipation. Consequently, the collapse rate for a compressible liquid is considerably less than that for an incompressible liquid since less available energy appears as kinetic energy.

D. Damage Mechanisms

There is no shock formation* observed during the bubble collapse. The pressure in the liquid at a distance equal to the initial bubble radius does not apparently change enough to cause the observed damage nor even change extremely rapidly during collapse. However, the rebound of the bubble which contains a compressed gas forms a shock which, according to Hickling and Plesset,[66] can cause damage to solids at distances equal to the initial bubble radius. This suggests that bubble migration during collapse may be required to place the bubble center close to a surface so that either the pressures generated during collapse can be damaging or the rebound shock, which originates from the final collapse region of compressed liquid and/or gas, will not be too greatly attenuated. The maximum final bubble pressure, and therefore maximum outward moving pressure amplitude, depends on the initial amount of gas and/or vapor in the bubble. Less gas permits the bubble to collapse farther and the resultant pressure to be higher.

E. Experimental

Photographic observation of bubbles in water in a cavitating venturi gave collapse rates comparable to those analytically predicted, down to about one-half of the initial bubble radius. Thereafter the experimental bubbles slowed down and some rebounded. Reduction of the dissolved gas from about saturation to about 30 percent of saturation did not eliminate the rebounding of the bubbles observed experimentally. The rebounded bubbles appear to have roughened surfaces so that it is

*i.e., a condition where later pressure characteristics overtake those starting earlier.

difficult to know whether or not single bubbles or a multiplicity of smaller bubbles is actually observed. The pressure rise in the venturi diffuser was of the order of one atmosphere, and the rate of rise was of the order of 10,000 lbf/in^2 sec. The fact that the bubble collapse initially followed the analytic collapse governed by inertia, and then slowed down or rebounded indicated a pressure rise inside the bubble which is more rapid than an adiabatic or isothermal compression of gas. Heating and evaporation at the bubble wall[45] probably is of significance in the collapse even though the range of pressures and liquid properties suggests that inertia should control the collapse. It may be that deviations from thermal equilibrium causing the vapor within the bubble to act as a perfect gas is partly responsible for the reduced collapse rates.

Bubble collapse was asymmetric. The bubbles flattened on the downstream (high-pressure) side, and the indentation thus formed sometimes appeared to move in the upstream direction as a jet, giving the bubble a torus like shape.

APPENDICES

APPENDIX I

RUNGE-KUTTA METHOD FOR NUMERICAL SOLUTION OF ORDINARY DIFFERENTIAL EQUATIONS

Consider first a single first order equation of the form

$$\frac{dy}{dx} = y' = f(x, y) \tag{A-1}$$

where x is the independent variable and y' the derivative of the dependent variable y. If y_j is the known value of y at x_j, and Δx is the increment in x, $(x_{j+1} - x_j)$ then approximately

$$y_{j+1} = y_j + \Delta x\, y_j' \tag{A-2}$$

A more accurate approximation would involve a higher order expansion than the simple linear or first order expansion of Equation (A-2). Galler[87] describes one of the methods known as the Runge-Kutta process which is especially adapted to high speed electronic computers, and which is available as a subroutine at the Computing Center of the University of Michigan. Equation (A-2) gives a straight line approximation to the curve between (x_j , y_j) and $(x_j + \Delta x , y_j + k_o)$ where from Equation (A-2)

$$k_o = \Delta x\, f(x_j, y_j) \tag{A-3}$$

At the fractional distance m along the increment, make another estimate of the increment in y by using the derivative evaluated at this point

$$k_1 = \Delta x\, f(x_j + m\Delta x, y_j + m k_o) \tag{A-4}$$

Then, yet another estimate of the increment in y is made using k_o and k_1

$$k_2 = \Delta x\, f(x_j + n\Delta x,\ y_j + (n-r)k_o + r k_1) \qquad \text{(A-5)}$$

and also

$$k_3 = \Delta x\, f(x_j + p\Delta x,\ y_j + [p-s-t]k_o + s k_1 + t k_2) \qquad \text{(A-6)}$$

There are then four estimates of the increment in y, namely k_o, k_1, k_2, and k_3, based on the known increment Δx and on four calculations of the derivative y' at four different (x,y) coordinates between (x_j, y_j) and $(x_j + \Delta x,\ y_j + \Delta y)$. It remains to choose a suitable average of these four values of the increment in the dependent variable y. A weighted average is calculated such that

$$\Delta y = y_{j+1} - y_j = a k_o + b k_1 + c k_2 + d k_3 \qquad \text{(A-7)}$$

where

$$a + b + c + d = 1 \qquad \text{(A-8)}$$

It is desired to choose the coefficients so that an expansion of $f(x,y)$ in a Taylor's series is correct to fourth order terms, $(\Delta x)^4$. Therefore, expand y in a Taylor series about y_j, so that y_{j+1} is given by

$$y_{j+1} = y_j + \Delta x\, y_j' + \frac{(\Delta x)^2}{2!} y_j'' + \frac{(\Delta x)^3}{3!} y_j''' + \frac{(\Delta x)^4}{4!} y_j'''' + \cdots \qquad \text{(A-8)}$$

where the derivatives are total derivatives of a function of two variables, or in other words using Equation (A-1)

$$y_j' = f(x_j, y_j)$$

$$y_j'' = \frac{\partial f(x_j, y_j)}{\partial x} + f(x_j, y_j)\frac{\partial f(x_j, y_j)}{\partial y} \quad , \quad etc.$$

Also, expand each of the k's in Taylor's series using the given increments in x and y about x_j , y_j and substitute all of these expansions into Equation (A-7) for Δy and equate this to Δy obtained from the expansion of Equation (A-8). By comparing coefficients on the two sides of the resulting equation, eight equations are produced with ten unknowns, a , b , c , d , m , n , r , p , s , t . Gill[88] chooses two of the ten, thereby uniquely specifying the other eight, in order to best accomodate the solution by means of a digital computer, so that there will be a minimum amount of temporary storage of quantities during the analysis. He shows that the method can be extended to the solution of a series of n simultaneous differential equations of the form

$$y_1' = f_1(x, y_1, y_2, \cdots y_n)$$
$$y_2' = f_2(x, y_1, y_2, \cdots y_n)$$
$$- \quad - \quad - \quad - \quad - \quad - \quad - \quad -$$
$$y_n' = f_n(x, y_1, y_2, \cdots y_n)$$

This method has the advantage that the new value of the dependent variable at $(x + \Delta x)$ can be found using only the information available at x, namely the value of the function and its slope. Thus, if the initial values of dependent and independent variables are known, the integration then proceeds from that point without reference back to preceding values. Therefore, no special computer instructions are necessary to initiate the procedure if the derivatives can be calculated at the initial values. In addition, the increment Δx, can be changed to any arbitrary value prior to calculating the next value of y. This property is used to good advantage when the independent variable is the bubble radius in order to cover a several decade span by successively reducing the increment in radius at each decade.

APPENDIX II

NUMERICAL SOLUTION FOR INCOMPRESSIBLE LIQUID

The solutions for the bubble wall velocity and the time elapsed as functions of the bubble radius are obtained first. Selected values of the velocity and radius are stored in memory during the machine procedure. After the wall velocity curve is determined and printed, these stored values are used to determine the pressure and velocity field throughout the liquid at the selected bubble radii. This procedure is possible since the liquid is incompressible and therefore the pressure field is completely determined once the wall velocity (and acceleration as a function of velocity) is known.

The calculations necessarily involve dimensional quantities because of the scaling effect of the viscosity and surface tension parameters. In order to easily interpret the relative magnitude of the variables, the input data to the program was in mixed units as follows:

Variable	Units for input data
R_o - initial radius	mils (in. x 10^{-3})
p_∞, p_o - pressure	atmospheres
μ - viscosity	multiples of μ_o ., where μ_o = viscosity of water
σ - surface tension	multiples of σ_o , where σ_o = surface tension of water
ρ_∞ - density	multiples of density of water

The output format included the input data, and solution for the normalized variables, as previously defined, in tabular form. The equations which are solved by the Runge-Kutta method are

$$\frac{dU'}{dR'} = -\frac{1}{R'U'}\left\{\frac{3}{2}U'^2 + \frac{[P'_\infty(R') - P'_o(R')]}{[P_\infty(R_o) - P_o(R_o)]} + \frac{2\sigma'}{R'} + \frac{U'\mu'}{R'}\right\}$$

$$\frac{dt'}{dR'} = \frac{1}{U'}$$

The initial conditions that $U' = 0$ at $R' = 1$, cause difficulty in the calculation of the derivative dU'/dR'. Therefore, an approximation is made for values of $R' \geq 0.990$. Since the velocity is very small, the viscous term and the kinetic energy term are both small and the change in $[p'_\infty(R') - p'_o(R')]$ is assumed negligible. If they are neglected, the equation is

$$U'\frac{dU'}{dR'} = -\frac{1}{R'}\left\{1 + \frac{2\sigma'}{R'}\right\}$$

which can be solved to give

$$\frac{U'^2}{2} = -\left\{\ln R' - \frac{2\sigma'}{R'}\right\} + C$$

Using the initial conditions, the constant of integration is

$$c = -2\sigma'$$

and therefore

$$U' = \sqrt{-2\left[\ln R' + 2\sigma'\left(\frac{R'-1}{R'}\right)\right]} \qquad \text{(A-9)}$$

Equation (A-9) is used for values of $R' \geq 0.990$. Then R' is set equal to 0.999999 and the velocity is calculated from Equation (A-9). This velocity is used to start the Runge-Kutta procedure, and values of U' compared well with the approximate solution to a radius of 0.990. The increment in the independent variable R' is reduced as R' becomes small so that the current value of R' is always at least 100 times larger than the increment in R'. Only sufficient values of R' are printed, in order to produce a good curve, so there are actually many more steps made in the integration procedure than appear in the output. Even though the machine has eight digit accuracy, the roundoff in R' for a decrease from 1.0 to 10^{-6} causes the current values of R' to differ from exact multiples of the increment in R'. Therefore, a change in increment is made after each decade change in R', so that the printed values of R' are simple numbers and can conveniently be compared from one output to another at the same values of R'.

The pressure and velocity field require no integration once the bubble wall velocity and radius are obtained. The selected values are obtained from a table in memory and the pressure and velocity are simply calculated for a given instant of time from the following algebraic formulas

$$p'(r') = p_\infty'(R') + \frac{u'^2}{2r'} - \frac{u'^2}{2r'^4} - \frac{1}{r'}\left[1 + \frac{u'\dot{u}'}{R'} + \frac{2\sigma'}{R'}\right]$$

$$u'^2 = \frac{u'^2}{r'^2} \quad , \quad r' = \frac{r}{R}$$

Note that the liquid radius here is given in terms of the current bubble radius R. This will not be possible later, when the pressure field in the compressible case is considered because the pressure is calculated along a characteristic path and time (and therefore bubble radius) changes as this path is traveled. Therefore, the later liquid radius normalization is different.

The internal bubble pressure $p_o(R')$ and the pressure at infinity $p_\infty(R')$ are put into the program as external functions, so that they can be changed without changing any other part of the main program. Several special variables are specified in the input data for use as parameters in the external pressure functions so that some variation can be conveniently effected by merely changing the input data card.

The solution was programed in the MAD (Michigan Algorithm Decoder) language and run on the IBM 7090 computer. The following list compares the notation for the variables as used in the computer program given on the following pages.

COMPUTER NOTATION FOR INCOMPRESSIBLE LIQUID

Variable	Description	Computer Notation
	(primed quantities are normalized)	
$p_\infty(R_o)$	Initial pressure at infinity	PINF (atm)
$p_o(R_o)$	Initial internal pressure	PO (atm)
R_o	Initial bubble radius	RO (mils)
ρ	Liquid density (multiples of water)	RHO
R'	Bubble radius	R
dR'	Increment in radius	DELR
r'	Radius in liquid	RL
U'	Bubble wall velocity	U(1)
t'	Time	U(2)
σ	Surface tension (multiples of water)	SIGMA
σ'	Surface tension (normalized)	D
μ	Viscosity (multiples of water)	MU
μ'	Viscosity (normalized)	C
p'(R')	Pressure at bubble wall	LIQPRS.(R)
p'(r')	Pressure in liquid	P
$p_\infty'(R')$	Variable pressure at infinity	PEXT. (R,PINF,PO,Z1,Z2)
-	Constants read in as data to vary external function	Z1,Z2,Y1,Y2
$p'_o(R')$	Variable internal pressure	PINT. (R,PO,PINF,Y1,Y2)
dU'/dR'	Derivative of velocity	DU(1)
dt'/dR'	Derivative of time	DU(2)
u'	Velocity in liquid	V
-	Stored bubble wall velocity	SU (K)
-	Stored bubble radius	SR (K)

COMPUTER LISTING - INCOMPRESSIBLE LIQUID

```
      $COMPILE MAD,PUNCH OBJECT,PRINT OBJECT,FULL DUMP

MAD (24 SEP 1964 VERSION) PROGRAM LISTING ... ... ...


      START       READ DATA,PINF,SIGMA,MU,RO,RHO,PO,Y1,Y2,Z1,Z2
                  INCRMT=10000.
                  C=.720*MU/(RO*(((PINF-PO)*2116.22*RHO).P..5))
                  D=59.75*SIGMA/(RO*(PINF-PO)*2116.22)
                  PRINT FORMAT TABHD1,MU,SIGMA,PINF,RO,RHO,C,D
                  PRINT FORMAT TABHD3
                  EXECUTE SETRKD.(2,U(1),DU(1),Q(1),R,DELR)
                  TAG1=1
                  TAG2=10
                  THROUGH INITAL,FOR R=1.,DELR,TAG1.G.100
                  DELR=-1./INCRMT
                  U(1)=-(-2.*(ELOG.(R)+2.*D*((R-1.)/R))).P..5
                  WHENEVER TAG2.E.10
                      PRINT FORMAT OUT1,R,U(1),0.,0.,LIQPRS.(R),PEXT.(R,PINF,PO
                 1 ,Z1,Z2)
                      TAG2=0
                  END OF CONDITIONAL
                  TAG1=TAG1+1
                  TAG2=TAG2+1
      INITAL      CONTINUE
                  PRINT FORMAT TABHD2
                  DELR=-1.E-6
                  R=.999999
                  U(1)=-(-2.*(ELOG.(R)+2.*D*((R-1.)/R))).P..5
                  U(2)=DELR/U(1)
                  J=1
                    SR(J)=R
                    SU(J)=U(1)
                    J=J+1
                  PRINT FORMAT OUT1,R,U(1),0.,U(2),LIQPRS.(R),PEXT.(R,PINF,PO,Z
                 1 1,Z2)
                  TAG2=1
                  TAG1=2
                  I=3
                  DELR=.9999-R
      GO          TRANSFER TO LOC(RKDEQ.(0))
      LOC(1)      DU(1)=-(1.5*U(1)*U(1)*R+C*U(1)+2.*D+R*(PEXT.(R,PINF,PO,Z1,Z2)
                 1 -PINT.(R,PO,PINF,Y1,Y2)))/(U(1)*R*R)
                  DU(2)=1./U(1)
                  TRANSFER TO GO
      LOC(2)      CONTINUE
                  TRANSFER TO LOC(I)
      LOC(3)      WHENEVER TAG1.LE.10
                  DU(1)=-(1.5*U(1)*U(1)*R+C*U(1)+2.*D+R*(PEXT.(R,PINF,PO,Z1,Z2)
                 1 -PINT.(R,PO,PINF,Y1,Y2)))/(U(1)*R*R)
                      PRINT FORMAT OUT1,R,U(1),DU(1)*U(1),U(2),LIQPRS.(R),PEXT.
                 1 (R,PINF,PO,Z1,Z2)
                      WHENEVER TAG1.E.1
                    SR(J)=R
                    SU(J)=U(1)
                    J=J+1
                      END OF CONDITIONAL
                      TAG1=TAG1+1
```

```
            DELR=-1.E-4
                TRANSFER TO GO
            END OF CONDITIONAL
            I=4
            TAG1=1
            PRINT FORMAT TABHD2
            DU(1)=-(1.5*U(1)*U(1)*R+C*U(1)+2.*D+R*(PEXT.(R,PINF,PO,Z1,Z2)
           1 -PINT.(R,PO,PINF,Y1,Y2)))/(U(1)*R*R)
                PRINT FORMAT OUT1,R,U(1),DU(1)*U(1),U(2),LIQPRS.(R),PEXT.
           1 (R,PINF,PO,Z1,Z2)
              SR(J)=R
              SU(J)=U(1)
              J=J+1
            TRANSFER TO GO
LOC(4)      WHENEVER TAG1.L.10
                TAG1=TAG1+1
                TRANSFER TO GO
            OR WHENEVER TAG1.E.10.AND.TAG2.L.9
            DU(1)=-(1.5*U(1)*U(1)*R+C*U(1)+2.*D+R*(PEXT.(R,PINF,PO,Z1,Z2)
           1 -PINT.(R,PO,PINF,Y1,Y2)))/(U(1)*R*R)
                PRINT FORMAT OUT1,R,U(1),DU(1)*U(1),U(2),LIQPRS.(R),PEXT.
           1 (R,PINF,PO,Z1,Z2)
                TAG1=1
                TAG2=TAG2+1
                TRANSFER TO GO
            END OF CONDITIONAL
            I=5
            PRINT FORMAT TABHD2
            DU(1)=-(1.5*U(1)*U(1)*R+C*U(1)+2.*D+R*(PEXT.(R,PINF,PO,Z1,Z2)
           1 -PINT.(R,PO,PINF,Y1,Y2)))/(U(1)*R*R)
            PRINT FORMAT OUT1,R,U(1),DU(1)*U(1),U(2),LIQPRS.(R),PEXT.(R,P
           1 INF,PO,Z1,Z2)
              SR(J)=R
              SU(J)=U(1)
              J=J+1
            TAG1=1
            TAG2=1
            TRANSFER TO GO
LOC(5)      WHENEVER DU(1).L.0.,TRANSFER TO SLO(1)
            WHENEVER TAG1.L.100
                TAG1=TAG1+1
            WHENEVER DELR+R.L..90,DELR=.90-R
                TRANSFER TO GO
            OR WHENEVER TAG1.E.100.AND.TAG2.L.9
            DU(1)=-(1.5*U(1)*U(1)*R+C*U(1)+2.*D+R*(PEXT.(R,PINF,PO,Z1,Z2)
           1 -PINT.(R,PO,PINF,Y1,Y2)))/(U(1)*R*R)
                PRINT FORMAT OUT1,R,U(1),DU(1)*U(1),U(2),LIQPRS.(R),PEXT.
           1 (R,PINF,PO,Z1,Z2)
                TAG1=1
                TAG2=TAG2+1
            WHENEVER DELR+R.L..90,DELR=.90-R
                TRANSFER TO GO
            END OF CONDITIONAL
            PRINT FORMAT TABHD2
            DU(1)=-(1.5*U(1)*U(1)*R+C*U(1)+2.*D+R*(PEXT.(R,PINF,PO,Z1,Z2)
           1 -PINT.(R,PO,PINF,Y1,Y2)))/(U(1)*R*R)
            PRINT FORMAT OUT1,R,U(1),DU(1)*U(1),U(2),LIQPRS.(R),PEXT.(R,P
           1 INF,PO,Z1,Z2)
              SR(J)=R
              SU(J)=U(1)
```

```
            J=J+1
           I=6
           TAG1=1
           TAG2=1
           TAG3=100
           DELR=-1.E-4
           TRANSFER TO GO
LOC(6)     WHENEVER DU(1).L.0.,TRANSFER TO SLO(1)
           WHENEVER TAG1.L.TAG3
               TAG1=TAG1+1
           WHENEVER R+DELR.L..10,DELR=.10-R
               TRANSFER TO GO
           OR WHENEVER TAG1.E.TAG3.AND.TAG2.L.8
           DU(1)=-(1.5*U(1)*U(1)*R+C*U(1)+2.*D+R*(PEXT.(R,PINF,PO,Z1,Z2)
          1 -PINT.(R,PO,PINF,Y1,Y2)))/(U(1)*R*R)
               PRINT FORMAT OUT1,R,U(1),DU(1)*U(1),U(2),LIQPRS.(R),PEXT.
          1 (R,PINF,PO,Z1,Z2)
               WHENEVER TAG2.E.4
             SR(J)=R
             SU(J)=U(1)
             J=J+1
               END OF CONDITIONAL
               TAG1=1
               TAG2=TAG2+1
           WHENEVER R+DELR.L..10,DELR=.10-R
               TRANSFER TO GO
           END OF CONDITIONAL
           PRINT FORMAT TABHD2
           DU(1)=-(1.5*U(1)*U(1)*R+C*U(1)+2.*D+R*(PEXT.(R,PINF,PO,Z1,Z2)
          1 -PINT.(R,PO,PINF,Y1,Y2)))/(U(1)*R*R)
           PRINT FORMAT OUT1,R,U(1),DU(1)*U(1),U(2),LIQPRS.(R),PEXT.(R,P
          1 INF,PO,Z1,Z2)
             SR(J)=R
             SU(J)=U(1)
             J=J+1
           TAG1=1
           TAG2=1
           I=7
           TAG3=100
           DELR=-1.E-4
           TRANSFER TO GO
LOC(7)     WHENEVER DU(1).L.0.,TRANSFER TO SLO(1)
           WHENEVER TAG1.L.TAG3
               TAG1=TAG1+1
           WHENEVER R+DELR.L..01,DELR=.01-R
               TRANSFER TO GO
           OR WHENEVER TAG1.E.TAG3.AND.TAG2.L.9
           DU(1)=-(1.5*U(1)*U(1)*R+C*U(1)+2.*D+R*(PEXT.(R,PINF,PO,Z1,Z2)
          1 -PINT.(R,PO,PINF,Y1,Y2)))/(U(1)*R*R)
               PRINT FORMAT OUT1,R,U(1),DU(1)*U(1),U(2),LIQPRS.(R),PEXT.
          1 (R,PINF,PO,Z1,Z2)
               WHENEVER TAG2.E.5
             SR(J)=R
             SU(J)=U(1)
             J=J+1
               END OF CONDITIONAL
               TAG1=1
               TAG2=TAG2+1
           WHENEVER R+DELR.L..01,DELR=.01-R
               TRANSFER TO GO
```

```
            END OF CONDITIONAL
            PRINT FORMAT TABHD2
            DU(1)=-(1.5*U(1)*U(1)*R+C*U(1)+2.*D+R*(PEXT.(R,PINF,PO,Z1,Z2)
           1 -PINT.(R,PO,PINF,Y1,Y2)))/(U(1)*R*R)
            PRINT FORMAT OUT1,R,U(1),DU(1)*U(1),U(2),LIQPRS.(R),PEXT.(R,P
           1 INF,PO,Z1,Z2)
              SR(J)=R
              SU(J)=U(1)
              J=J+1
            TAG1=1
            TAG2=1
            I=8
            TAG3=100
            DELR=-1.E-4
            M=0
            THROUGH FINISH,FOR VALUES OF DELR=-1.E-5,-1.E-6,-1.E-7,-1.E-8
           1 ,-1.E-9,-1.E-10
            M=M+1
            PRINT FORMAT TABHD4,M,DELR
                TRANSFER TO GO
LOC(8)      CONTINUE
            WHENEVER DU(1).L.0.,TRANSFER TO SLO(1)
            WHENEVER TAG1.L.TAG3
                TAG1=TAG1+1
            WHENEVER  R+DELR.L.-100.*DELR,DELR=-(R+100.*DELR)
                TRANSFER TO GO
            OR WHENEVER TAG1.E.TAG3.AND.TAG2.L.9
            DU(1)=-(1.5*U(1)*U(1)*R+C*U(1)+2.*D+R*(PEXT.(R,PINF,PO,Z1,Z2)
           1 -PINT.(R,PO,PINF,Y1,Y2)))/(U(1)*R*R)
                PRINT FORMAT OUT1,R,U(1),DU(1)*U(1),U(2),LIQPRS.(R),PEXT.
           1 (R,PINF,PO,Z1,Z2)
                WHENEVER TAG2.E.5
              SR(J)=R
              SU(J)=U(1)
              J=J+1
                END OF CONDITIONAL
                TAG1=1
                TAG2=TAG2+1
            WHENEVER  R+DELR.L.-100.*DELR,DELR=-(R+100.*DELR)
                TRANSFER TO GO
            END OF CONDITIONAL
            PRINT FORMAT TABHD2
            DU(1)=-(1.5*U(1)*U(1)*R+C*U(1)+2.*D+R*(PEXT.(R,PINF,PO,Z1,Z2)
           1 -PINT.(R,PO,PINF,Y1,Y2)))/(U(1)*R*R)
            PRINT FORMAT OUT1,R,U(1),DU(1)*U(1),U(2),LIQPRS.(R),PEXT.(R,P
           1 INF,PO,Z1,Z2)
              SR(J)=R
              SU(J)=U(1)
              J=J+1
            TAG1=1
            TAG2=1
FINISH      CONTINUE
ALPHA       THROUGH PFIELD,FOR K=1,1,K.E.J
              PRINT FORMAT TABHD5,SR(K)
              I=1
              THROUGH PFIELD,FOR RL=1.,.1,I.G.50
            P=PEXT.(SR(K),PINF,PO,Z1,Z2)*(RL-1.)/RL+(SU(K)*SU(K))/(2.*RL)
           1 -(SU(K)*SU(K))/(2.*RL*RL*RL*RL)-(SU(K)*C+2.*D)/(SR(K)*RL)+PIN
           2 T.(SR(K),PO,PINF,Y1,Y2)/RL
                V=SU(K)/(RL*RL)
```

```
                PRINT FORMAT OUTP,RL,RL*SR(K),P,V
                I=I+1
PFIELD          CONTINUE
                TRANSFER TO START
SLO(1)          CONTINUE
                PRINT FORMAT TABHD2
                DU(1)=-(1.5*U(1)*U(1)*R+C*U(1)+2.*D+R*(PEXT.(R,PINF,PO,Z1,Z2)
              1 -PINT.(R,PO,PINF,Y1,Y2)))/(U(1)*R*R)
                PRINT FORMAT OUT1,R,U(1),DU(1)*U(1),U(2),LIQPRS.(R),PEXT.(R,P
              1 INF,PO,Z1,Z2)
                TAG1=1
                TAG2=1
                TAG3=1
                TEN=1.
                M=15
SLOC(6)         TEMU1=U(1)
                TEMU2=U(2)
                TEMR=R
                DELR=-R/(100.*TEN)
SLOC(4)         U(1)=TEMU1
                U(2)=TEMU2
                R=TEMR
                DELR=-R/(100.*TEN)
SLOC(5)         TRANSFER TO FRST(RKDEQ.(0))
FRST(1)         DU(1)=-(1.5*U(1)*U(1)*R+C*U(1)+2.*D+R*(PEXT.(R,PINF,PO,Z1,Z2)
              1 -PINT.(R,PO,PINF,Y1,Y2)))/(U(1)*R*R)
                DU(2)=1./U(1)
SLOC(3)         TRANSFER TO SLOC(RKDEQ.(0))
SLOC(1)         WHENEVER U(1).G.0.
                  U(1)=0.
                  TAG3=2
                  END OF CONDITIONAL
                DU(1)=-(1.5*U(1)*U(1)*R+C*U(1)+2.*D+R*(PEXT.(R,PINF,PO,Z1,Z2)
              1 -PINT.(R,PO,PINF,Y1,Y2)))/(U(1)*R*R)
                DU(2)=1./U(1)
                TRANSFER TO SLOC(3)
SLOC(2)         WHENEVER U(1).G.0.,TAG3=2
                WHENEVER TAG3.E.2
                  TEN=10.*TEN
                  WHENEVER TEN.G.1.E25,TRANSFER TO ALPHA
                  TAG3=1
                  TRANSFER TO SLOC(4)
                  END OF CONDITIONAL
                WHENEVER TAG1.L.10
                  TAG1=TAG1+1
                OR WHENEVER TAG1.E.10
                DU(1)=-(1.5*U(1)*U(1)*R+C*U(1)+2.*D+R*(PEXT.(R,PINF,PO,Z1,Z2)
              1 -PINT.(R,PO,PINF,Y1,Y2)))/(U(1)*R*R)
                PRINT FORMAT OUT1,R,U(1),DU(1)*U(1),U(2),LIQPRS.(R),PEXT.(R,P
              1 INF,PO,Z1,Z2)
                TAG1=1
                TAG2=TAG2+1
                END OF CONDITIONAL
                WHENEVER R.LE.1.E-8
                DU(1)=-(1.5*U(1)*U(1)*R+C*U(1)+2.*D+R*(PEXT.(R,PINF,PO,Z1,Z2)
              1 -PINT.(R,PO,PINF,Y1,Y2)))/(U(1)*R*R)
                PRINT FORMAT OUT1,R,U(1),DU(1)*U(1),U(2),LIQPRS.(R),PEXT.(R,P
              1 INF,PO,Z1,Z2)
                TRANSFER TO ALPHA
                END OF CONDITIONAL
```

```
   WHENEVER TAG2.E.M.OR.(TAG1.E.1.AND.TAG2.L.10)                                    *256
     SR(J)=R                                                                        *257
     SU(J)=U(1)                                                                     *258
     J=J+1                                                                          *259
   END OF CONDITIONAL                                                               *260
   WHENEVER TAG2.E.M,M=M+15                                                         *261
   WHENEVER TAG2.LE.150                                                             *262
   TRANSFER TO SLOC(6)                                                              *263
   OR WHENEVER TAG2.G.150                                                           *264
   TRANSFER TO ALPHA                                                                *265
   END OF CONDITIONAL                                                               *266
   INTEGER TAG1,TAG2,TAG3,I,M,J,K                                                   *267
   DIMENSION U(2),DU(2),Q(2)                                                        *268
   DIMENSION SR(75),SU(75)                                                          *269
   VECTOR VALUES TABHD1=$1H1,S9,69HSOLUTION TO PORITSKY BUBBLE C                    *270
  1 OLLAPSE IN VISCOUS,INCOMPRESSIBLE LIQUID/1HO,S9,86HTHE LIQUID                   *270
  2  CONSTANTS,NORMALIZED TO THE VALUES FOR WATER AT 1 ATM AND 20                   *270
  3  DEGREES C, ARE/1HO,S20,25HVISCOSITY              MU=,1E15.6/1                  *270
  4 H ,S20,25HSURFACE TENSION     SIGMA=,1E15.6/1H ,S20,25HPRES. A                  *270
  5 T INFINITY   PINF=,1E15.6/1H ,S20,25HINITIAL RADIUS (MILS) RO                   *270
  6 =,1E15.6/1H ,S20,25HDENSITY               RHO=,1E15.6/1HO,S9,6                  *270
  7 OHTHE CORRESPONDING VALUES OF THE DIMENSIONLESS PARAMETERS AR                   *270
  8 E/1HO,S20,9HVISCOSITY,S8,2HC=,1E12.6/1H ,S20,19HSURFACE TENSI                   *270
  9 ON  D=,1E12.6*$                                                                 *270
   VECTOR VALUES TABHD2=$1H-*$                                                      *271
   VECTOR VALUES TABHD3=$1H-,S5,4HR/RO,S9,8HVELOCITY,S5,12HACCEL                    *272
  1 ERATION,S7,4HTIME,S9,8HPRESSURE,S5,9HEXT.PRES.*$                                *272
   VECTOR VALUES TABHD4=$1H+,S91,2HM=,1I3,S5,5HDELR=,1E15.6*$                       *273
   VECTOR VALUES TABHD5=$1H1,S3,96HPRESSURE AND VELOCITY FIELDS                     *274
  1 IN THE LIQUID WHEN THE RATIO OF BUBBLE RADIUS TO INITIAL RADI                   *274
  2 US IS ,1E12.6/1H-,S12,14HRADIUS IN LIQ.,S1,14HLIQ. RADIUS/RO,                   *274
  3 S3,12HLIQUID PRES.,S2,13HLIQ. VELOCITY*$                                        *274
   VECTOR VALUES OUT1=$1E14.6,5E15.6*$                                              *275
   VECTOR VALUES OUTP=$1H ,S10,4E15.6*$                                             *276
   INTERNAL FUNCTION LIQPRS.(X)=PINT.(X,PO,PINF,Y1,Y2)-(2.*D+C*U                    *277
  1 (1))/X                                                                          *277
   END OF PROGRAM                                                                   *278

THE FIRST OCCURRENCE OF A FLOATING POINT VARIABLE USED AS A SINGLE OR DOUBLE SUBSCRIPT WAS IN THE STATEMENT ENDING
                          GO         TRANSFER TO LOC(RKDEQ.(0))          034
```

```
$COMPILE MAD,PUNCH OBJECT,PRINT OBJECT

MAD (24 SEP 1964 VERSION) PROGRAM LISTING ... ... ...


                EXTERNAL FUNCTION(R,PINF,PO,Z1,Z2)
                ENTRY TO PEXT.
                WHENEVER Z1.E.0.
                FUNCTION RETURN PINF/(PINF-PO)
                OR WHENEVER Z1.E.1.
                WHENEVER R.LE. .3
                FUNCTION RETURN 0.82/(PINF-PO)
                OR WHENEVER R.G. .3
                FUNCTION RETURN (.04/(R-.25)+.02)/(PINF-PO)
                END OF CONDITIONAL
                OR WHENEVER  Z1 .E. 2.0
                WHENEVER R .LE. 0.4
                  FUNCTION RETURN(0.787+(.4-R)*3.15)/(PINF-PO)
                OR WHENEVER R .G. 0.4
                  X=(0.72-R)/0.33
                  ALPHA=X
                  ANSWR=X
                COEF=1.
                THROUGH LOC1,FOR N=2,1,.ABS.ALPHA.L. .0001*.ABS.ANSWR
                  A=2.*N-1.
                  B=2.*N-2.
                  C=2.*N-3.
                  COEF=C/B*COEF
                  ALPHA=(COEF*X.P.A)/A
                  ANSWR=ANSWR+ALPHA
LOC1              CONTINUE
                  FUNCTION RETURN(0.255*ANSWR+0.45)/(PINF-PO)
                END OF CONDITIONAL
                END OF CONDITIONAL
                INTEGER N
                END OF FUNCTION
```

```
$COMPILE MAD,PUNCH OBJECT,PRINT OBJECT

MAD (24 SEP 1964 VERSION) PROGRAM LISTING ... ... ...


            EXTERNAL FUNCTION(R,PO,PINF,Y1,Y2)
            ENTRY TO PINT.
            FUNCTION RETURN (PO/(PINF-PO))*R.P.(-3.*Y1)
            END OF FUNCTION
```

APPENDIX III

NUMERICAL SOLUTION FOR COMPRESSIBLE LIQUID

The solution for the compressible liquid is similar to that for the incompressible liquid in that the bubble wall motion is completely determined first, and then the pressure and velocity fields are determined along an outgoing characteristic path for selected initial conditions at various bubble radii. Equations (36) through (40) for motion of the bubble wall are written as follows

$$\frac{dU}{dR} = -\frac{U}{2R}\left(\frac{U-3C}{U-C}\right) + \frac{H}{RU}\left(\frac{U+C}{U-C}\right) + \frac{1}{C}\frac{dH}{dR} \tag{A-10}$$

$$\frac{dT}{dR} = \frac{1}{U} \quad , \qquad \rho = \rho_r\left(\frac{P+B}{P_r+B}\right)^{1/n} \tag{A-12}$$

$$C(P) = \left(\frac{n(P+B)}{\rho_r}\right)^{1/2}\left(\frac{P+B}{P_r+B}\right)^{-1/2n} \tag{A-13}$$

$$H(P) = \frac{n(P_\infty+B)}{(n-1)\,\rho_\infty}\left[\left(\frac{P+B}{P_\infty+B}\right)^{\frac{n-1}{n}} - 1\right] \tag{A-14}$$

$$P(R) = P_0(R) - \frac{2\sigma}{R} - \frac{4\mu U}{R} \tag{A-15}$$

It is necessary to analytically obtain the term dH/dR in Equation (A-10) as follows.

$$\frac{dH}{dR} = \frac{dH}{dP}\frac{dP}{dR} = \frac{1}{\rho_\infty}\left(\frac{P_\infty + B}{P+B}\right)^{1/n}\left\{\frac{dP_o}{dR} + \frac{2\sigma}{R^2} - \frac{4\mu}{R}\frac{dU}{dR} + \frac{4\mu U}{R^2}\right\} \quad \text{(A-16)}$$

Equation (A-16) is substituted into Equation (A-10) resulting in

$$\frac{dU}{dR}\left\{1 + \frac{4\mu}{C\rho_\infty R}\left(\frac{P_\infty + B}{P+B}\right)^{1/n}\right\} = \quad \text{(A-17)}$$

$$-\frac{U}{2R}\left(\frac{U-3C}{U-C}\right) + \frac{H}{RU}\left(\frac{U+C}{C-U}\right) + \frac{1}{C\rho_\infty}\left(\frac{P_\infty + B}{P+B}\right)^{1/n}\left\{\frac{dP_o}{dR} + \frac{2\sigma}{R^2} + \frac{4\mu U}{R^2}\right\}$$

If the above equations were normalized in a manner similar to the incompressible equations, they would remain essentially unchanged, still containing the scaling parameters σ and μ, so there is no analytic advantage to such a procedure. Instead, it was decided to use a normalization similar to that of Flynn[60] which permits a convenient interpretation of the real magnitude of the normalized variables. The following constants for water at 1 atm and 20°C are used.

$$\rho_o = 62.31 \ \text{lbm/ft}^3 \quad (60)$$

$$C_o = 4865.5 \ \text{ft/sec} \quad (60)$$

$$\sigma_o = 4.982 \times 10^{-3} \ \text{lbf/ft} \quad (69)$$

$$\mu_o = 2.088 \times 10^{-5} \text{ lbf - sec/ft}^2 \qquad (90)$$

$$a_o = 1 \text{ atm} = 2116.2 \text{ lbf/ft}^2$$

The variables are then normalized for computation as in the following table, where again the primed quantities are normalized. For convenience, the notation used for these variables in the computer program is also given. Several dimensionless quantities occur in the normalized equations, involving the above constants for water. It is convenient to designate these as follows.

$$K_1 = \frac{\rho_o c_o^2}{a_o g} = 2.1666 \times 10^4$$

$$K_2 = \frac{\sigma_o}{a_o R_o} = \frac{2.8252 \times 10^{-2}}{R_o} \text{ (when } R_o \text{ is in mils, in. x } 10^{-3})$$

$$K_3 = \frac{\mu_o c_o}{a_o R_o} = \frac{0.57599}{R_o} \text{ (when } R_o \text{ is in mils)}$$

$$K_4 = \frac{\mu_o g}{c_o \rho_o R_o} = \frac{2.6584 \times 10^{-5}}{R_o} \text{ (when } R_o \text{ is in mils)}$$

Substitution of the normalized variables into the equations gives the following set of equations which were programed for computer solution.

$$\frac{dU'}{dR'} = \frac{\left\{ -\frac{U'}{2}\left(\frac{U'-3C'}{U'-C'}\right) + \frac{H'}{U'}\left(\frac{U'+C'}{C'-U'}\right) + \frac{1}{C'\rho_\infty' K_1}\left(\frac{P_\infty'+B'}{P'+B'}\right)^{1/n}\left[R'\frac{dP_0'}{dR'} + P_0' - P'\right]\right\}}{\left\{ R' + \frac{4\mu' K_4}{C'\rho_\infty'}\left(\frac{P_\infty'+B'}{P'+B'}\right)^{1/n}\right\}} \quad \text{(A-18)}$$

$$\frac{dT'}{dR'} = \frac{1}{U'} \quad , \quad \rho_\infty' = \left(\frac{P_\infty'+B'}{1+B'}\right)^{1/n} \quad , \quad C_\infty'^2 = \frac{n}{K_1}\frac{(P_\infty'+B')}{\rho_\infty'}$$

$$C'^2(P') = C_\infty'^2\left(\frac{P'+B'}{P_\infty'+B'}\right)^{\frac{n-1}{n}}$$

$$H'(P') = \frac{(P_\infty'+B')}{\left(\frac{n-1}{n}\right)K_1\rho_\infty'}\left\{\left(\frac{P'+B'}{P_\infty'+B'}\right)^{\frac{n-1}{n}} - 1\right\}$$

$$P'(R') = P_0'(R') - \frac{2K_2\sigma'}{R'} - \frac{4K_3\mu' U'}{R'}$$

The variables p_∞', p_0' and dp_0'/dR' are specified in external functions, and for a given function there are one or two parameters which will alter the bubble behavior, the values of which can be inserted as data without changing the program at all. Also, the external functions can be completely changed in form without altering the main program, just as in the solution for the incompressible liquid.

The initial conditions of U' and R' present some difficulty. It can be shown that for very small velocity and for $R' \cong 1$, the equation of motion is approximately

$$\frac{dU'}{dR'} \simeq \frac{H'}{R'U'}$$

Assume that for small U', the variation in H' with R' is small so that it may be assumed constant. Therefore,

$$U' \cong -\sqrt{2H' \ln R'} \tag{19}$$

where the velocity logarithmically approaches zero as R' approaches 1.0. In order to solve Equation (A-19), where H' is a function of U', a repetitive procedure was used at a fixed value of $R' = 0.9999$, and P' and then H' and U' were calculated. Several repetitions gave a set of values of U', P', and H' which satisfied (A-19) exactly. These values of U' and R' were used as initial conditions in the Runge-Kutta procedure. Also, Equation (A-19) was solved for ten increments in R' from 0.9999 to 0.9990 and the curve compared with that obtained from the Runge-Kutta solution and no significant difference in magnitude or slope of U' vs R' was apparent.

The bubble wall velocity and the time are obtained as functions of bubble radius with no reference to the velocity or pressure fields in the liquid. The Kirkwood-Bethe assumption on wave propagation permits such a procedure. At 97 selected values of the bubble radius a characteristic path originating on the bubble wall is traced through the liquid. The initial values for this procedure are obtained from a table of values of U', H', T', R', P' and C' at the bubble wall which is stored in memory during the solution for the wall motion. The equations for the characteristic path, 41, 46, 47, 48, are as follows

$$z(r,t) = r\left(h + \frac{u^2}{2}\right)$$

$$\left(\frac{du}{dt}\right)_c = \left[\frac{z}{r^2} + \frac{zu}{cr^2} - \frac{2cu}{r}\right]\frac{c}{c-u}$$

$$\left(\frac{dr}{dt}\right)_c = c+u$$

$$\left(P(r,t)\right)_c + B = (P_\infty + B)\left[\left(\frac{z}{r} - \frac{u^2}{2}\right)\left(\frac{(n-1)}{n}\frac{\rho_\infty}{(P_\infty + B)}\right) + 1\right]^{\frac{n}{n-1}}$$

The normalized form of these equations is unchanged except that the variables then represent normalized quantities.

The solution to these equations is sets of characteristic curves, as many sets as desired up to the total number of increments in bubble wall radius used in the solution for the bubble wall motion. A set of these curves was initiated from each of the 97 printed values of bubble radius (many more than 97 increments were actually used in computing bubble wall motion however). Since time is the independent variable used along a characteristic path, each set of curves consists of a table with five columns -- time, radial position, pressure, velocity, and Mach number -- arranged so that one can enter the table in computer storage with a given value of time and obtain the corresponding values of the other four variables. There are 56 values of these variables printed for each set of curves (although more intermediate values are calculated),

but only the first 40 of these are stored in memory. The 97 sets of curves, each set with five variables and 40 values, are stored as they are computed in a three dimensional array called URV (K, M, L) by the internal function STURV., giving a total of 19,400 stored values along characteristics.

After completion of the computation, printing and storage of the characteristic curves, the values of the variables throughout the liquid at a fixed instant of time were obtained, rather than the values along a path where time was continually changing. The value of time at the start of each path, which corresponded to the time at the bubble wall, was selected, and the table of each set of curves which originated at an earlier time was entered and the values corresponding to that time were selected and printed for each of the four variables; radial position, pressure, velocity, and Mach number. A library subroutine was used which provided a linear interpolation in the table. Up to a fifth order interpolation could have been specified as easily, but for computing time economy the first order was chosen. The printed values along the characteristic curves show that a linear interpolation between the available values provides a very good approximation to a smooth characteristic curve.

The very rapid change in variables with respect to time when the bubble wall velocity was large, necessitated careful consideration of numerical accuracy. The machine has inherently eight digit arithmetic accuracy, which was not sufficient for the later stages of bubble

collapse with the time normalization used. Since in the formulation of the problem for bubble wall motion, the variable, time, does not appear explicitly in any form but as the derivative, dT/dR , the actual numerical value of time may be changed at will during computation. Therefore, in computing the bubble wall motion, before time became of such a magnitude that there was no significant change in eight digits for each step, the time zero was changed. Similarly, along a characteristic curve time could be initialized starting at the bubble with the value zero thereby providing a much more significant numerical change as the path was computed. However, this method introduced some additional difficulties when the tables of characteristic curves are entered with a value of time based on the same normalization but with a different zero point. Nevertheless, this difficulty was overcome and the resulting characteristic curves could be plotted such that each curve had an accuracy to at least the eleventh significant digit, with the important interpretive convenience of being related to real time by a simple constant normalizing quantity.

NORMALIZATION AND COMPUTER NOTATION FOR COMPRESSIBLE LIQUID

Variable	Normalized Variable	Description	Computer Program Notation
U/C_o	U'	Bubble wall velocity	Y(1)
C/C_o	C'	Sonic velocity in liquid at wall	C
R/R_o	R'	Bubble radius	R
$T/R_o/C_o$	T'	Time	Y(2)
H/C_o^2	H'	Enthalpy	H1
P/a_o	P'	Pressure in liquid at wall	P
p_o/a_o	p_o'	Internal pressure	PINT.(R,A,GAMMA)
p_∞/a_o	p_∞'	Variable pressure at infinity	PINF.(R,X)
ρ_∞/ρ_o	ρ_∞'	Density at infinity	RHOINF
B/a_o	B'	Parameter in equation of state	B
μ/μ_o	μ'	Liquid viscosity	MU
σ/σ_o	σ'	Liquid surface tension	SIGMA
r/R_o	r'	Radius in liquid	V(2)
$z/R_oC_o^2$	z'	Characteristic quantity	Z
u/C_o	u'	Particle velocity of liquid	V(1)
C_∞/C_o	C_∞'	Sonic velocity at infinity	CINFSQ
c/C_o	c'	Sonic velocity in liquid	CL
p/a_o	p	Pressure in liquid away from wall	PL
$t\ c_o/R_o$	t'	Time from start of characteristic	TL
$dt\ c_o/R_o$	dt'	Increment in time on characteristic	DELTL

NORMALIZATION AND COMPUTER NOTATION FOR COMPRESSIBLE LIQUID (CONT'D)

Variable	Normalized Variable	Description	Computer Program Notation
TC_o/R_o	T'	Stored values of variables at bubble wall which are used to initiate characteristic path	ST
U/C_o	U'		SU
H/C_o^2	H'		SH
R/R_o	R'		SR
P/a_o	P'		SP
C/C_o	C'		SC
		Initial internal pressure (atm)	A
		Increment in bubble radius (negative)	DELR
n	n	Constant in equation of state (=7.)	N
$(n-1)/n$	-	Constants, evaluated for repetitive computational efficiency	E X 1
$(n-1)/2n$	-		E X 2
$1/n$	-		N X 3
$\rho_o C_o^2/a_o g$	K_1	Constant = 2.166634×10^4	K 1
$\sigma_o/a_o R_o$	K_2	Surface tension parameter	K 2
$\mu_o c_o/a_o R_o$	K_3	Viscosity parameter	K 3
$\mu_o g/c_o \rho_o R_o$	K_4	Viscosity parameter	K 4
dU/dR	dU'/dR'	Velocity derivative	F (1)
dT/dR	dT'/dR'	Time derivative	F (2)
γ	-	Exponent in internal pressure variation as $(R')^{-3}$	GAMMA
-	-	Input data to determine DELR	INCRMT
-	-	Variable pressure in equation of state expressions = PINF. (R,X)+B	P1

NORMALIZATION AND COMPUTER NOTATION FOR COMPRESSIBLE LIQUID (CONT'D)

Variable	Normalized Variable	Description	Computer Program Notation
R_o	1.	Initial bubble radius	RO
p_∞/a_o	p_∞'	Initial pressure in liquid	X
	-	Three dimensional array in which characteristic curves are stored	URV(K,M,L)
	-	Internal function for storing variables at bubble wall	CHARAC.
	-	Internal function for calculating wall pressure and printing wall variables	PRS.
	-	Internal function for storing values along characteristic for later use	STURV.

COMPUTER LISTING - COMPRESSIBLE LIQUID

```
      $COMPILE MAD,PUNCH OBJECT,PRINT OBJECT,FULL DUMP

MAD (24 SEP 1964 VERSION) PROGRAM LISTING ... ... ...


      NEW         CONTINUE
                  FLAG=1
                  DIM(1)=3
                  DIM(2)=1
                  DIM(3)=5
                  DIM(4)=40
                  EXECUTE FTRAP.
                  READ DATA,MU,SIGMA,B,N,X,RO,INCRMT,GAMMA
                  EX1=(N-1.)/N
                  EX2=(N-1.)/(2.*N)
                  EX3=1./N
                  EXECUTE SETRKD.(2,Y(1),F(1),Q(1),R,DELR)
                  K1=2.166634E4
                  K2=2.825187E-2/RO
                  K3=.575986/RO
                  K4=2.65843E-5/RO
                  R=1.
                  Y(1)=0.
                  Y(2)=0.
                  DELR=-1./INCRMT
                  P1=PINF.(R,X)+B
                  RHOINF=(P1/(B+1.)).P.EX3
                  J=1
                  CINFSQ=(N*P1)/(RHOINF*K1)
                  PRINT FORMAT TABHD1,MU,SIGMA,PINF.(R,X),RO,RHOINF
                  PRINT FORMAT TABHD2
                  TAG1=1
                  P=PINT.(R,A,GAMMA)-(2.*K2*SIGMA+4.*K3*Y(1)*MU)/R
                  C=SQRT.(CINFSQ*((P+B)/P1).P.EX1)
                  H1=(P1/(K1*EX1*RHOINF))*(((P+B)/P1).P.EX1-1.)
                  PRINT FORMAT OUT1,R,Y(1)/C,Y(1),0.0,Y(2),P,H1,PINT.(R,A,GAMMA
     1            ),PINF.(R,X)
                  THROUGH INITAL,FOR R=1.+DELR,DELR,TAG1.G.10
                  P1=PINF.(R,X)+B
                  RHOINF=(P1/(B+1.)).P.EX3
                  CINFSQ=(N*P1)/(RHOINF*K1)
                  P=PINT.(R,A,GAMMA)-(2.*K2*SIGMA+4.*K3*Y(1)*MU)/R
                  H1=(P1/(K1*EX1*RHOINF))*(((P+B)/P1).P.EX1-1.)
                  C=SQRT.(CINFSQ*((P+B)/P1).P.EX1)
                  Y(1)=-(2.*H1*ELOG.(R)).P..5
                  Y(2)=(R-1.)/Y(1)
                  F(1)=(((Y(1)/2.)*(Y(1)-3.*C)+(H1/Y(1))*(Y(1)+C))/(C-Y(1))+((P
     1            1/(P+B)).P.EX3/(K1*C*RHOINF))*(R*DPINT.(R,A,GAMMA)+PINT.(R,A,
     2            GAMMA)-P))/(R+(4.*K4*MU/(C*RHOINF))*(P1/(P+B)).P.EX3)
                  PRINT FORMAT OUT1,R,Y(1)/C,Y(1),F(1),Y(2),P,H1,PINT.(R,A,GAMM
     1            A),PINF.(R,X)
                  TAG1=TAG1+1
      INITAL      CONTINUE
                  PRINT FORMAT OUT2
                  TAG1=1
                  Y(1)=0.
                  R=1.+DELR
      OVER        CONTINUE
```

```
            P1=PINF.(R,X)+B
            RHOINF=(P1/(B+1.)).P.EX3
            CINFSQ=(N*P1)/(RHOINF*K1)
            P=PINT.(R,A,GAMMA)-(2.*K2*SIGMA+4.*K3*Y(1)*MU)/R
            H1=(P1/(K1*EX1*RHOINF))*(((P+B)/P1).P.EX1-1.)
            C=SQRT.(CINFSQ*((P+B)/P1).P.EX1)
            Y(1)=-(2.*H1*ELOG.(R)).P..5
            Y(2)=(R-1.)/Y(1)
            F(1)=(((Y(1)/2.)*(Y(1)-3.*C)+(H1/Y(1))*(Y(1)+C))/(C-Y(1))+((P
           1 1/(P+B)).P.EX3/(K1*C*RHOINF))*(R*DPINT.(R,A,GAMMA)+PINT.(R,A,
           2 GAMMA)-P))/(R+(4.*K4*MU/(C*RHOINF))*(P1/(P+B)).P.EX3)
            PRINT FORMAT OUT1,R,Y(1)/C,Y(1),F(1),Y(2),P,H1,PINT.(R,A,GAMM
           1 A),PINF.(R,X)
            TAG1=TAG1+1
            WHENEVER TAG1.G.10,TRANSFER TO GOSUB
            TRANSFER TO OVER
GOSUB       CONTINUE
            PRINT FORMAT OUT2
            EXECUTE CHARAC.
            I=3
            TAG1=1
            TAG3=1
GO          TRANSFER TO LOC(RKDEQ.(C))
LOC(1)      CONTINUE
            P1=PINF.(R,X)+B
            RHOINF=(P1/(B+1.)).P.EX3
            CINFSQ=(N*P1)/(RHOINF*K1)
            P=PINT.(R,A,GAMMA)-(2.*K2*SIGMA+4.*K3*Y(1)*MU)/R
            WHENEVER P.L.-3000.
                M=5
                TRANSFER TO FINISH
                END OF CONDITIONAL
            C=SQRT.(CINFSQ*((P+B)/P1).P.EX1)
            H1=(P1/(K1*EX1*RHOINF))*(((P+B)/P1).P.EX1-1.)
            F(1)=(((Y(1)/2.)*(Y(1)-3.*C)+(H1/Y(1))*(Y(1)+C))/(C-Y(1))+((P
           1 1/(P+B)).P.EX3/(K1*C*RHOINF))*(R*DPINT.(R,A,GAMMA)+PINT.(R,A,
           2 GAMMA)-P))/(R+(4.*K4*MU/(C*RHOINF))*(P1/(P+B)).P.EX3)
            F(2)=1./Y(1)
            TRANSFER TO GO
LOC(2)      CONTINUE
            TRANSFER TO LOC(I)
LOC(3)      WHENEVER TAG3.L.9
            EXECUTE PRS.
                TAG3=TAG3+1
                TRANSFER TO GO
            END OF CONDITIONAL
            PRINT FORMAT OUT2
            EXECUTE PRS.
            EXECUTE CHARAC.
            I=4
            TAG1=1
            TAG3=1
            TRANSFER TO GO
LOC(4)      WHENEVER TAG1.L.10
                TAG1=TAG1+1
                TRANSFER TO GO
            OR  WHENEVER TAG1.E.10.AND.TAG3.L.9
            EXECUTE PRS.
                TAG1=1
                TAG3=TAG3+1
```

```
                    TRANSFER TO GO
                END OF CONDITIONAL
                PRINT FORMAT OUT2
                EXECUTE PRS.
                EXECUTE CHARAC.
                I=5
                TAG1=0
                TAG3=1
LOC(5)          WHENEVER TAG1.L.100
                    TAG1=TAG1+1
                    TRANSFER TO GO
                OR WHENEVER TAG1.E.100.AND.TAG3.L.9
                EXECUTE PRS.
                EXECUTE CHARAC.
                    TAG1=1
                    TAG3=TAG3+1
                    TRANSFER TO GO
                END OF CONDITIONAL
                I=6
                PRINT FORMAT OUT2
                EXECUTE PRS.
                EXECUTE CHARAC.
                TAG1=1
                TAG3=1
                TRANSFER TO GO
LOC(6)          WHENEVER F(1).L.0.,TRANSFER TO SLO(1)
                WHENEVER TAG1.E.800.OR.TAG1.E.600.OR.TAG1.E.400.OR.TAG1.E.200
                EXECUTE PRS.
                EXECUTE CHARAC.
                END OF CONDITIONAL
                WHENEVER TAG1.L.1000
                    TAG1=TAG1+1
                WHENEVER .1.G.R+DELR,DELR=.1-R
                    TRANSFER TO GO
                OR WHENEVER TAG1.E.1000.AND.TAG3.L.8
                EXECUTE PRS.
                EXECUTE CHARAC.
                    TAG1=1
                    TAG3=TAG3+1
                WHENEVER .1.G.R+DELR,DELR=.1-R
                    TRANSFER TO GO
                END OF CONDITIONAL
                PRINT FORMAT OUT2
                PRINT COMMENT$ TIME PRINTED AFTER TIME REACHES 134.1 IS THE I
              1 NCREASE IN TIME BEYOND 134.0$
                EXECUTE PRS.
                EXECUTE CHARAC.
                TAG1=1
                TAG3=1
                DELR=-1./INCRMT
                I=7
                TRANSFER TO GO
LOC(7)          WHENEVER F(1).L.0.,TRANSFER TO SLO(1)
                WHENEVER TAG1.L.100
                    TAG1=TAG1+1
                    TRANSFER TO GO
                OR WHENEVER TAG1.E.100.AND.TAG3.L.9
                EXECUTE PRS.
                EXECUTE CHARAC.
                    TAG1=1
```

```
            TAG3=TAG3+1
          WHENEVER .01.G.R+DELR,DELR=.01-R
            TRANSFER TO GO
          END OF CONDITIONAL
          PRINT FORMAT OUT2
          EXECUTE PRS.
          EXECUTE CHARAC.
          TAG1=1
          TAG3=1
          DELR=-1./INCRMT
          I=8
          THROUGH FINISH,FOR M=1,1,M.G.4
          DELR=-10..P.(-M-4)
            TRANSFER TO GO
LOC(8)    WHENEVER F(1).L.0.,TRANSFER TO SLO(1)
          WHENEVER TAG1.L.100
            TAG1=TAG1+1
          WHENEVER 10..P.(-M-2).G.R+DELR,DELR=10..P.(-M-2)-R
            TRANSFER TO GO
            OR WHENEVER TAG1.E.100.AND.TAG3.L.9
          EXECUTE PRS.
          EXECUTE CHARAC.
            TAG1=1
            TAG3=TAG3+1
          WHENEVER 10..P.(-M-2).G.R+DELR,DELR=10..P.(-M-2)-R
            TRANSFER TO GO
            END OF CONDITIONAL
          PRINT FORMAT OUT3,M+1,DELR/10.
          WHENEVER M.E.2,PRINT COMMENT$ TIME WHICH IS PRINTED AFTER R=1
        1 X10-4 IS THE CHANGE IN TIME FOR PRINTED CHANGE IN BUBBLE RADI
        2 US$
          EXECUTE PRS.
          EXECUTE CHARAC.
            TAG1=1
            TAG3=1
FINISH    CONTINUE
          EXECUTE SETRKD.(2,V(1),F(1),Q(1),TL,DELTL)
          THROUGH PFIELD,FOR K=1,1,K.E.J
          PRINT FORMAT TABHD4,SR(K)
          M=3
          TAG1=1
          TAG2=1
          TAG3=1
          TEN=10.
          TEMV1=SU(K)
          TEMV2=SR(K)
          TEMP=SP(K)
          TEMC=SC(K)
          TEMT=0.0
          TL=0.0
          V(2)=SR(K)
          PL=SP(K)
          V(1)=SU(K)
          CL=SC(K)
          DELTL=SR(K)/(20.*SC(K))
          P1=PINF.(SR(K),X)+B
          RHOINF=(P1/(B+1.)).P.EX3
          CINFSQ=(N*P1)/(RHOINF*K1)
          Z=SR(K)*(SH(K)+SU(K)*SU(K)/2.)
          EXECUTE STURV.(K,1)
```

```
            PRINT FORMAT OUTCH,SR(K),SP(K),SU(K),SU(K)/SC(K),ST(K),DELTL
            TAG2=2
LOCP(4)     V(1)=TEMV1
            V(2)=TEMV2
            PL=TEMP
            CL=TEMC
            TL=TEMT
              DELTL=V(2)/(TEN*CL)
LOCP(5)     TRANSFER TO GOP(RKDEQ.(0))
GOP(1)      F(1)=(Z*(CL+V(1))/V(2)-2.*CL*CL*V(1))/(V(2)*(CL-V(1)))
            F(2)=CL+V(1)
LOCP(3)     TRANSFER TO LOCP(RKDEQ.(0))
LOCP(1)     WHENEVER V(1).G.0..OR.((Z/V(2)-V(1)*V(1)/2.)*(N-1.)/CINFSQ+1.
          1 ).L.0..OR.V(2).L.0.
               V(1)=0.
               V(2)=1.
               TAG1=2
               END OF CONDITIONAL
            PL=P1*((Z/V(2)-V(1)*V(1)/2.)*(N-1.)/CINFSQ+1.).P.(N/(N-1.))-B
            CL=SQRT.(CINFSQ*((PL+B)/P1).P.EX1)
            F(1)=(Z*(CL+V(1))/V(2)-2.*CL*CL*V(1))/(V(2)*(CL-V(1)))
            F(2)=CL+V(1)
            TRANSFER TO LOCP(3)
LOCP(2)     WHENEVER V(1).G.0..OR.((Z/V(2)-V(1)*V(1)/2.)*(N-1.)/CINFSQ+1.
          1 ).L.0..OR.V(2).L.0.,TAG1=2
            WHENEVER TAG1.E.2
                TEN=10.*TEN
            WHENEVER TEN.G.1.E25.OR.DELTL.L.1.E-25,TRANSFER TOPFIELD
               TAG1=1
               TRANSFER TO LOCP(4)
               END OF CONDITIONAL
            WHENEVER TAG2.LE.20
            PL=P1*((Z/V(2)-V(1)*V(1)/2.)*(N-1.)/CINFSQ+1.).P.(N/(N-1.))-B
            CL=SQRT.(CINFSQ*((PL+B)/P1).P.EX1)
            EXECUTE STURV.(K,TAG2)
            PRINT FORMAT OUTCH,V(2),PL,V(1),V(1)/CL,TL,DELTL
               TEMV1=V(1)
               TEMV2=V(2)
               TEMP=PL
               TEMC=CL
               TEMT=TL
              DELTL=V(2)/(TEN*CL)
               TAG2=TAG2+1
               TRANSFER TO LOCP(5)
            OR WHENEVER TAG2.LE.56.AND.TAG3.E.5
            PL=P1*((Z/V(2)-V(1)*V(1)/2.)*(N-1.)/CINFSQ+1.).P.(N/(N-1.))-B
            CL=SQRT.(CINFSQ*((PL+B)/P1).P.EX1)
            WHENEVER TAG2.LE.40,EXECUTE STURV.(K,TAG2)
            PRINT FORMAT OUTCH,V(2),PL,V(1),V(1)/CL,TL,DELTL
               TEMV1=V(1)
               TEMV2=V(2)
               TEMP=PL
               TEMC=CL
               TEMT=TL
            DELTL=V(2)/(TEN*CL)
            WHENEVER TAG2.E.56,TRANSFER TO PFIELD
            TAG2=TAG2+1
            TAG3=1
            TRANSFER TO LOCP(5)
               END OF CONDITIONAL
```

```
            TAG3=TAG3+1
            TRANSFER TO LOCP(5)
PFIELD       CONTINUE
            THROUGH PRPRNT ,FOR K=1,1,K.E.J
              PRINT FORMAT TABHD3,URV(K,1,1),SR(K)
            WHENEVER FLAG .G. 1 .AND. K .L. FLAG
            PRINT FORMAT OUTP,URV(K,2,1),URV(K,3,1),URV(K,4,1),URV(K,5,1)
            THROUGH PRT1,FOR L=K-1,-1,L.L.1
            TIP=URV(L,1,1)
            URV(L,1,1)=0.0
            WHENEVER URV(K,1,1)-TIP.G.URV(L,1,40),TRANSFER TO PRT1
              THROUGH PRT2,FOR M=2,1,M .G. 5
            PT(M)=TAB.(URV(K,1,1)-TIP,URV(L,1,1),URV(L,M,1),1,1,1,40,SW(M
           1 ))
              WHENEVER SW(M) .E. 2.,PT(M)=0.
PRT2          CONTINUE
              PRINT FORMAT OUTP,PT(2)...PT(5)
PRT1        URV(L,1,1)=TIP
            PRINT COMMENT$ NO ADDITIONAL VALUES POSSIBLE,BUBBLE WALL HAS
           1 NOT PROGRESSED FAR ENOUGH.$
            OR WHENEVER FLAG .G. 1 .AND. K .GE. FLAG
            PRINT FORMAT OUTP,URV(K,2,1),URV(K,3,1),URV(K,4,1),URV(K,5,1)
            THROUGH PRT3,FOR L=K-1,-1,L.L.1
              WHENEVER L .L. FLAG
            TIP=URV(L,1,1)
            URV(L,1,1)=0.
            FLGT=134.+URV(K,1,1)-TIP
            WHENEVER FLGT .G. URV(L,1,40),TRANSFER TO PRT3
              THROUGH PRT4,FOR M=2,1,M .G. 5
              PT(M)=TAB.(FLGT,URV(L,1,1),URV(L,M,1),1,1,1,40,SW(M))
              WHENEVER SW(M) .E. 2.,PT(M)=0.
PRT4          CONTINUE
              OR WHENEVER L .GE. FLAG
            TIP=URV(L,1,1)
            URV(L,1,1)=0.
            WHENEVER URV(K,1,1)-TIP.G.URV(L,1,40),TRANSFER TO PRT3
              THROUGH PRT5,FOR M=2,1,M .G. 5
            PT(M)=TAB.(URV(K,1,1)-TIP,URV(L,1,1),URV(L,M,1),1,1,1,40,SW(M
           1 ))
              WHENEVER SW(M) .E. 2.,PT(M)=0.
PRT5          CONTINUE
              END OF CONDITIONAL
              PRINT FORMAT OUTP,PT(2)...PT(5)
PRT3        URV(L,1,1)=TIP
            PRINT COMMENT$ NO ADDITIONAL VALUES POSSIBLE,BUBBLE WALL HAS
           1 NOT PROGRESSED FAR ENOUGH.$
            END OF CONDITIONAL
PRPRNT      CONTINUE
            THROUGH PRT7,FOR ADDTL=.0001*URV(J-1,1,1),.0001*URV(J-1,1,1),
           1 ADDTL.G. .00055*URV(J-1,1,1)
            PRINT FORMAT TABHD3,URV(J-1,1,1)+ADDTL,0.0
            THROUGH PRT8,FOR L=J-1,-1,L .L. 1
            WHENEVER L .L. FLAG
            TIP=URV(L,1,1)
            URV(L,1,1)=0.0
            FLGT=134.+URV(J-1,1,1)+ADDTL-TIP
            WHENEVER FLGT .G. URV(L,1,40),TRANSFER TO PRT8
              THROUGH PRT9,FOR M=2,1,M .G. 5
              PT(M)=TAB.(FLGT,URV(L,1,1),URV(L,M,1),1,1,1,40,SW(M))
              WHENEVER SW(M) .E. 2.,PT(M)=0.
```

```
PRT9          CONTINUE
              OR WHENEVER L .GE. FLAG
              TIP=URV(L,1,1)
              URV(L,1,1)=0.0
              WHENEVER URV(J-1,1,1)+ADDTL-TIP.G.URV(L,1,40),TRANSFER TO PRT
             1 8
                THROUGH PRT10,FOR M=2,1,M .G. 5
              PT(M)=TAB.(URV(J-1,1,1)+ADDTL-TIP,URV(L,1,1),URV(L,M,1),1,1,1
             1 ,40,SW(M))
                WHENEVER SW(M) .E. 2.,PT(M)=0.
PRT10         CONTINUE
              END OF CONDITIONAL
              PRINT FORMAT OUTP,PT(2)...PT(5)
PRT8          URV(L,1,1)=TIP
              PRINT COMMENT$ NO ADDITIONAL VALUES POSSIBLE,BUBBLE WALL HAS
             1 NOT PROGRESSED FAR ENOUGH.$
PRT7          CONTINUE
               TRANSFER TO NEW
SLO(1)         CONTINUE
               PRINT FORMAT OUT2
              EXECUTE PRS.
              EXECUTE CHARAC.
              TAG1=1
               TAG2=1
              TAG3=1
              TEN=1.
              M=1
SLOC(6)       TEMY1=Y(1)
              TEMY2=Y(2)
              TEMR=R
              DELR=-R/(100.*TEN)
SLOC(4)       Y(1)=TEMY1
              Y(2)=TEMY2
              R=TEMR
              DELR=-R/(100.*TEN)
SLOC(5)       TRANSFER TO FRST(RKDEQ.(0))
FRST(1)       CONTINUE
              P1=PINF.(R,X)+B
              RHOINF=(P1/(B+1.)).P.EX3
              CINFSQ=(N*P1)/(RHOINF*K1)
              P=PINT.(R,A,GAMMA)-(2.*K2*SIGMA+4.*K3*Y(1)*MU)/R
              WHENEVER P.L.-3000.
                  M=5
                  TRANSFER TO FINISH
                  END OF CONDITIONAL
              C=SQRT.(CINFSQ*((P+B)/P1).P.EX1)
              H1=(P1/(K1*EX1*RHOINF))*(((P+B)/P1).P.EX1-1.)
              F(1)=(((Y(1)/2.)*(Y(1)-3.*C)+(H1/Y(1))*(Y(1)+C))/(C-Y(1))+((P
             1 1/(P+B)).P.EX3/(K1*C*RHOINF))*(R*DPINT.(R,A,GAMMA)+PINT.(R,A,
             2 GAMMA)-P))/(R+(4.*K4*MU/(C*RHOINF))*(P1/(P+B)).P.EX3)
              F(2)=1./Y(1)
SLOC(3)       TRANSFER TO SLOC(RKDEQ.(0))
SLOC(1)       WHENEVER Y(1).G.0.
                Y(1)=0.
                TAG3=2
                END OF CONDITIONAL
              P1=PINF.(R,X)+B
              RHOINF=(P1/(B+1.)).P.EX3
              CINFSQ=(N*P1)/(RHOINF*K1)
              P=PINT.(R,A,GAMMA)-(2.*K2*SIGMA+4.*K3*Y(1)*MU)/R
```

```
      WHENEVER P.L.-3000.
          M=5
          TRANSFER TO FINISH
          END OF CONDITIONAL
      C=SQRT.(CINFSQ*((P+B)/P1).P.EX1)
      H1=(P1/(K1*EX1*RHOINF))*(((P+B)/P1).P.EX1-1.)
      F(1)=(((Y(1)/2.)*(Y(1)-3.*C)+(H1/Y(1))*(Y(1)+C))/(C-Y(1))+((P
     1 1/(P+B)).P.EX3/(K1*C*RHOINF))*(R*DPINT.(R,A,GAMMA)+PINT.(R,A,
     2 GAMMA)-P))/(R+(4.*K4*MU/(C*RHOINF))*(P1/(P+B)).P.EX3)
      F(2)=1./Y(1)
      TRANSFER TO SLOC(3)
SLOC(2)  WHENEVER Y(1).G.0.,TAG3=2
      WHENEVER TAG3.E.2
        TEN=TEN*10.
        WHENEVER TEN .G.1.E25
          PRINT RESULTS TEN,R,DELR,Y(1),Y(2)
          M=5
          TRANSFER TO FINISH
          END OF CONDITIONAL
        TAG3=1
        TRANSFER TO SLOC(4)
        END OF CONDITIONAL
      WHENEVER TAG1.L.10
      TAG1=TAG1+1
       OR WHENEVER TAG1.E.10
      EXECUTE PRS.
       TAG1=1
       TAG2=TAG2+1
      END OF CONDITIONAL
      WHENEVER R.LE.1.E-6
      EXECUTE PRS.
      M=5
      TRANSFER TO FINISH
      END OF CONDITIONAL
      WHENEVER TAG1.E.1.AND.TAG2.L.10.AND.J.L.98
        EXECUTE CHARAC.
      OR WHENEVER TAG2.E.M.AND.J.L.98
       EXECUTE CHARAC.
       M=M+15
       END OF CONDITIONAL
      WHENEVER TAG2.LE.300
        TRANSFER TO SLOC(6)
      OR WHENEVER TAG2.G.300
      M=5
       TRANSFER TO FINISH
       END OF CONDITIONAL
      INTEGER TAG1,TAG2,TAG3,I,J,K,L,M,FLAG,O
      DIMENSION Y(2),F(2),Q(2),V(2),SU(100),SR(100),ST(100),SH(100)
     1 ,SP(100),SC(100)
      DIMENSION URV(19400,DIM(1)),DIM(4)
      DIMENSION SW(5),PT(5)
      DIMENSION TIM(100)
      VECTOR VALUES TABHD1=$1H1,S9,92HSOLUTION OF GILMORE'S BUBBLE
     1 WALL MOTION FOR COMPRESSIBLE,VISCOUS WATER WITH SURFACE TENSI
     2 ON/1HO,S9,36HTHE NORMALIZED LIQUID PARAMETERS ARE/1HO,S20,25H
     3 VISCOSITY          MU     =,1E15.6,/1H ,S20,25HSURFACE TENSION
     4    SIGMA=,1E15.6/1H ,S20,25HPRESS. AT INFINITY  PINF=,1E15.6/
     5 1H ,S20,25HINITIAL RADIUS (MILS) RO=,1E15.6/1H ,S20,25HDENSIT
     6 Y AT INF.   RHOINF=,1E15.6*$
      VECTOR VALUES TABHD2=$1H-,S7,4HR/RO,S9,8HMACH NO.,S7,8HVELOCI
```

```
     1 TY,S8,5HDU/DR,S9 ,4HTIME,S11,8HPRESSURE,S7,8HENTHALPY,S6,8HIN
     2 T.PRS.,S9,5HPINF.*$
       VECTOR VALUES TABHD3=$1H1,S3,70HPRESSURE AND VELOCITY FIELDS
     1 IN THE LIQUID WHEN THE NORMALIZED TIME IS,1E15.8,26H  AND THE
     2  BUBBLE RADIUS IS,1E13.6/1H-,S12,14HLIQ. RADIUS/RO,S3,12HLIQU
     3 ID PRES.,S2,13HLIQ. VELOCITY,S5,8HMACH NO.*$
       VECTOR VALUES TABHD4=$1H1,S3,80HPATH OF A CHARACTERISTIC STAR
     1 TING FROM THE BUBBLE WALL WHEN THE BUBBLE RADIUS IS,E17.8/1H-
     2 ,S11,14HLIQ. RADIUS/RO,S4,12HLIQUID PRES.,S2,13HLIQ. VELOCITY
     3 ,S5,8HMACH NO.,S9,4HTIME,S10,10HDELTA TIME*$
       VECTOR VALUES OUT1=$1H ,E14.6,3E15.6,E15.8,3E15.6,E12.5*$
       VECTOR VALUES OUT2=$1H0*$
       VECTOR VALUES OUT3=$1H /1H ,S10,2HM=,I3,5HDELR=,E13.6/*$
       VECTOR VALUES OUTP=$1H ,S8,E15.8,3E15.6*$
       VECTOR VALUES OUTCH=$1H ,S10,E15.8,3E15.6,E17.8,E15.6*$
        INTERNAL FUNCTION
        ENTRY TO CHARAC.
       SU(J)=Y(1)
       SH(J)=H1
        SR(J)=R
        SP(J)=P
        SC(J)=C
       WHENEVER J.L. 80
       ST(J)=Y(2)
       TIM(J)=ST(J)
       OR WHENEVER J.GE.80
       TIP=(R-SR(J-1))/Y(1)
       TIM(J)=TIP
       THROUGH TIPPO,FOR O=J-1,-1,O.L.79
       TIP=TIP+TIM(O)
TIPPO  CONTINUE
       ST(J)=TIP
       END OF CONDITIONAL
        J=J+1
        FUNCTION RETURN
        END OF FUNCTION
       INTERNAL FUNCTION
       ENTRY TO PRS.
       WHENEVER Y(2) .G. 134.
         Y(2)=Y(2)-134.
         FLAG=J
         END OF CONDITIONAL
       P1=PINF.(R,X)+B
       RHOINF=(P1/(B+1.)).P.EX3
       CINFSQ=(N*P1)/(RHOINF*K1)
       P=PINT.(R,A,GAMMA)-(2.*K2*SIGMA+4.*K3*Y(1)*MU)/R
       H1=(P1/(K1*EX1*RHOINF))*(((P+B)/P1).P.EX1-1.)
       C=SQRT.(CINFSQ*((P+B)/P1).P.EX1)
       F(1)=(((Y(1)/2.)*(Y(1)-3.*C)+(H1/Y(1))*(Y(1)+C))/(C-Y(1))+((P
     1 1/(P+B)).P.EX3/(K1*C*RHOINF))*(R*DPINT.(R,A,GAMMA)+PINT.(R,A,
     2 GAMMA)-P))/(R+(4.*K4*MU/(C*RHOINF))*(P1/(P+B)).P.EX3)
       WHENEVER R .G. .99E-4
       PRINT FORMAT OUT1,R,Y(1)/C,Y(1),F(1),Y(2),P,H1,PINT.(R,A,GAMM
     1 A),PINF.(R,X)
       OR WHENEVER R .L. .99E-4
       PRINT FORMAT OUT1,R,Y(1)/C,Y(1),F(1),(R-SR(J-1))/Y(1),P,H1,PI
     1 NT.(R,A,GAMMA),PINF.(R,X)
       END OF CONDITIONAL
       FUNCTION RETURN
       END OF FUNCTION
```

```
                INTERNAL FUNCTION (K,TAG2)                                      *489
                ENTRY TO STURV.                                                 *490
                WHENEVER TAG2.E. 1,URV(K,1,TAG2)=ST(K)                          *491
                WHENEVER TAG2 .G. 1,URV(K,1,TAG2)=TL                            *492
                URV(K,2,TAG2)=V(2)                                              *493
                URV(K,3,TAG2)=PL                                                *494
                URV(K,4,TAG2)=V(1)                                              *495
                URV(K,5,TAG2)=V(1)/CL                                           *496
                FUNCTION RETURN                                                 *497
                END OF FUNCTION                                                 *498
                END OF PROGRAM                                                  *499

THE FOLLOWING NAMES HAVE OCCURRED ONLY ONCE IN THIS PROGRAM.
COMPILATION WILL CONTINUE.

     EX2

THE FIRST OCCURRENCE OF A FLOATING POINT VARIABLE USED AS A SINGLE OR DOUBLE SUBSCRIPT WAS IN THE STATEMENT ENDING
                                GO          TRANSFER TO LOC(RKDEQ.(0))          069
```

```
      $COMPILE MAD,PRINT OBJECT,PUNCH OBJECT

MAD (24 SEP 1964 VERSION) PROGRAM LISTING ... ... ...


                    EXTERNAL FUNCTION(R,A,GAMMA)
                    ENTRY TO PINT.
                    FUNCTION RETURN A*(R.P.(-3*GAMMA))
                    ENTRY TO DPINT.
                    FUNCTION RETURN -3.*GAMMA*A/(R.P.(3.*GAMMA+1.))
                    END OF FUNCTION
```

```
$COMPILE MAD,PRINT OBJECT,PUNCH OBJECT

MAD (24 SEP 1964 VERSION) PROGRAM LISTING ... ... ...


          EXTERNAL FUNCTION(R,X)
          ENTRY TO PINF.
          FUNCTION RETURN X
          END OF FUNCTION
```

REFERENCES

1. Euler, Leonhard, "Théorie plus complète des machines, qui sont mises en mouvement par la réaction de l'éau", Historie de l'Academie Royale des Sciences et Belles Lettres, Classe de Philosophie Experimentale, pp 227-295, Mém 10, 1754, Berlin, 1756.

2. Reynolds, Osborne, "Experiments Showing the Boiling of Water in an Open Tube at Ordinary Temperatures", Scientific Papers, 2, (1901) 578-587.

3. Thornycroft, Sir John, and Barnaby, S. W., "Torpedo-boat Destroyers", Proc. Inst. Civ. Eng., 122, (1895) 51-103.

4. Barnaby, S. W., "On the Formation of Cavities in Water by Screw Propellers at High Speeds", Trans. Inst. Nav. Arch., 39, (1898) 139-144.

5. Parsons, Sir Charles, "The Application of the Compound Steam Turbine to the Purpose of Marine Propulsion", Trans. Inst. Nav. Arch., 38, (1897) 232-42.

6. Burrill, L. C., "Sir Charles Parsons and Cavitation", Trans. Inst. Marine Engrs., 43, No. 8, (1951) 149-167.

7. Parsons, Sir Charles A., and Cook, S. S., "Investigations into the Causes of Corrosion or Erosion of Propellers", Trans. Inst. Nav. Arch., 61, (1919) 222-247.

8. Eisenberg, P., On the Mechanism and Prevention of Cavitation, DTMB - 712, 1950.

9. Eisenberg, P., "Cavitation", International Sci. and Tech., Feb. 1963, 77-84.

10. Eisenberg, P., "Modern Developments in the Mechanics of Cavitation", Applied Mech. Rev., 10, No. 3 (1957) 85-89.

11. Cavitation in Hydrodynamics, Proc. of Symp. at Nat'l. Phy. Lab., H. M. Stationery Office, London, 1956.

12. "Cavitation in Hydraulic Structures: A Symposium", Proc. Amer. Soc. Civ. Eng., 71, No. 7, 1945.

13. Besant, W., A Treatise on Hydrodynamics, Cambridge Univ. Press, Cambridge, (1859) 198.

14. Lord Rayleigh, "On the Pressure Developed in a Liquid During the Collapse of a Spherical Cavity", Phil. Mag., 34, (1917) 94-98.

15. Lamb, Sir Horace, Hydrodynamics, Dover Publ., 6th Ed., New York, (1945) 122.

16. Lamb, Sir Horace, "The Early Stages of a Submarine Explosion", Phil. Mag., S.6., 45, No. 266, (1923) 257-265.

17. Beeching, R., "Resistance to Cavitation Erosion", Trans. Inst. Eng. and Shipbuilders in Scotland, 85, (1942) 210-276.

18. Noltingk, B. E. and Neppiras, E. A., "Cavitation Produced by Ultrasonics", Proc. Phy. Soc. (London), 63, (1950) 674-685.

19. Poritsky, H., "The Collapse or Growth of a Spherical Bubble or Cavity in a Viscous Fluid", Proc. First Nat'l. Congress Appl. Mech., ASME, (1952) 813-821.

20. Shu, S. S., "Note on the Collapse of a Spherical Cavity in a Viscous Incompressible Fluid", Proc. First Nat'l, Congress Appl. Mech., ASME, (1952) 823-825.

21. Silver, R. S., "Theory of Stress Due to Collapse of Vapour Bubbles in Liquid", Engineering, (Dec. 25, 1942) 501-502.

22. Plesset, M. S., "The Dynamics of Cavitation Bubbles", Trans. ASME, Jour. Appl, Mech., (Sept. 1949) 277-282.

23. Plesset, M. S., Bubble Dynamics, Report No. 85-23, Calif. Inst. Tech., 1963.

24. Novotny, H., Werkstoffzertorung dursch Kavitation, V. D. I. Verlag Gimbh, Berlin N W 7, 1942 (Also Edwards Brothers, Ann Arbor, Mich., 1946).

25. Becker, A., Roellig, L. O., and Wilson, S. S., Experimental Evidence for the Persistence of Microbubbles, unpublished notes.

26. Thomson, Sir William, "On the Equilibrium of Vapour at a Curved Surface of a Liquid", Phil. Mag., S. 4, 42, (1871) 448-452.

27. Keenan, J. H., Thermodynamics, John Wiley & Sons Inc., New York, 1941, Ch. XXIII.

28. Paul, M. A., Principles of Chemical Thermodynamics, McGraw-Hill Book Co., Inc., New York, (1951) 264-276.

29. Reynolds, O., "On the Internal Cohesion of Liquids and the Suspension of a Column of Mercury to a Height more than Double that of the Barometer", Scientific Papers, I, Cambridge Univ. Press, (1900) 231-243.

30. Fisher, J. C., "The Fracture of Liquids", J. Appl. Phys., 19, (1948) 1062-1067.

31. Harvey, E. N., McElroy, W. D., and Whiteley, A. H., "On Cavity Formation in Water", Jour. Appl. Phys., 18, (1947) 162-172.

32. Zivi, S. M., Gas Microbubble Dilation -- A Reactor Shutdown Mechanism, Space Tech. Labs, 897-6017-RU-001, 1962.

33. Birkhoff, G., and Zarantonello, E. H., Jets, Wakes and Cavities, Academic Press Inc., New York, (1957) 236.

34. Herring, C., Theory of the Pulsations of the Gas Bubble Produced by an Underwater Explosion, Report C4-sr20-010, Columbia Univ., (1941) 67.

35. Oza, H. P., "On the Collapse of a Hemispherical Cavity Seated on a Surface", Trans. ASME, J. Appl. Mech., 69, (1947) A-39-A-42.

36. Naudé, C. F., and Ellis, A. T., "On the Mechanism of Cavitation Damage by Nonhemispherical Cavities Collapsing in Contact with a Solid Boundary", Trans. ASME, J. Basic Eng., Series D, 83, (1961) 648-656.

37. Naudé, C. F., and Ellis, A. T., On the Mechanism of Cavitation Damage by Non-Hemispherical Cavities Collapsing in Contact with a Solid Boundary, CIT Rpt. No. E-108.7, 1960.

38. Kornfeld, M. and Suvorov, L., "On the Destructive Action of Cavitation", J. Appl. Phy., 15, (1944) 495-506.

39. Shutler, N. D. and Mesler, R. B., A Photographic Study of the Dynamics and Damage Capabilities of Bubbles Collapsing Near Solid Boundaries, Dept. of Chem. and Petrol. Eng., Univ. of Kansas, 1964.

40. Smissaert, G. E., Two-Component Two-Phase Flow Parameters for Low Circulation Rates, ANL - 6755, 1963.

41. Vogrin, J. A., Jr., An Experimental Investigation of Two Phase, Two Component Flow in a Horizontal, Converging-Diverging Nozzle, ANL - 6754, 1963.

42. Lamb, Ref. 15, p. 600.

43. Elliott, D. G., A Two-Fluid Magnetohydrodynamic Cycle for Nuclear-Electric Power Conversion, Calif. Inst. Tech., JPL - TR - 32 - 116, 1961.

44. Clark, J., A New Method for Detecting Cavitation and Turbulence in Cryogenic Fluids, Rept. No. AE-6826-R, Rev.-1, The Garrett Corp., Air Research Manuf. Div., 1958, also paper at 1958 Annual Cryogenic Eng. Conf.

45. Florschuetz, L. W. and Chao, B. T., On the Mechanics of Vapor Bubble Collapse -- A Theoretical and Experimental Investigation, ME Technical Report 1069-2 Eng. Expt. Station, Univ. of Ill., 1963, also ASME paper No. 64-HT-23.

46. Underwater Explosion Research, 3 vols., Office of Naval Research, U. S. Navy Dept., Washington, D. C., 1950.

47. Walters, J. K. and Davidson, J. F., "The Initial Motion of a Gas Bubble Formed in an Inviscid Liquid, Part 2., The Three-Dimensional Bubble and the Toroidal Bubble", J. Fluid Mech., 17, (1963) 321-336.

48. Trilling, L., "The Collapse and Rebound of a Gas Bubble", J. Appl. Phys., 23, No. 1, (1952) 14-17.

49. Hickling, R., Effects of Thermal Conduction in Sonoluminescence, Calif. Inst. Tech., Rpt. No. 85-21, Pasadena, Calif., 1962.

50. Chambers, L. A., "The Emission of Visible Light from Cavitated Liquids", J. Chem. Phys., 5, (1937) 290-292.

51. Jarman, P., "Sonoluminescence: A Discussion", J. Acous. Soc. America, 32, No. 11, (1960) 1459-1462.

52. Jarman, P., "Measurements of Sonoluminescence from Pure Liquids and Some Aqueous Solutions", Proc. Phys. Soc. (London), 73, (1959) 628-640.

53. Jarman, P. and Taylor, K. J., "Light Emission from Cavitating Water", Brit. Jour. Appl. Phys., 15, (1964) 321-322.

54. Treaster, A. L., Cavitation Hysteresis, M. S. Thesis, Dept. Aero. Eng., Penn State Univ., 1964.

55. Kaplan, W., Advanced Calculus, Addison-Wesley Publ. Co, Inc., Reading, Mass., 1959.

56. Bird, R. B., Stewart, W. E. and Lightfoot, E. N., Transport Phenomena, John Wiley and Sons, 1960.

57. Knapp, R. T., and Hollander, A., "Laboratory Investigations of the Mechanism of Cavitation", Trans. ASME, 70, (1948) 419.

58. Gilmore, F. R., The Growth or Collapse of a Spherical Bubble in a Viscous Compressible Liquid, Calif. Inst. Tech. Rpt. No. 26-4, Pasadena, Calif., 1952.

59. Gilmore, F. R., The Growth or Collapse of a Spherical Bubble in a Viscous Compressible Liquid, 1952 Heat Transfer and Fluid Mechanics Inst., Stanford Univ. Press, pp. 53-64.

60. Flynn, H. G., Collapse of a Transient Cavity in a Compressible Liquid, Tech. Mem. No. 38, Acous. Res. Lab., Harvard Univ., Cambridge, Mass., 1957.

61. Mellen, R. H., An Experimental Study of the Collapse of a Spherical Cavity in Water, USL Res. Rpt. No. 279, U.S. Navy Underwater Sound Lab., Ft. Trumbull, New London, Conn., 1955.

62. Mellen, R. H., Spherical Pressure Waves of Finite Amplitude from Collapsing Cavities, USL Res. Rpt. No. 326, U.S. Navy Underwater Sound Lab., Ft. Trumbull, New London, Conn., 1956.

63. Schneider, A. J. R., Some Compressibility Effects in Cavitation Bubble Dynamics, PhD Thesis, Calif. Inst. Tech., 1949.

64. Brand, R. S., The Collapse of a Spherical Cavity in a Compressible Liquid, PhD Thesis, Brown Univ., 1960.

65. Brand, R. S., The Shock Wave Produced by Collapse of a Spherical Cavity, Tech. Rpt. No. 1, Mech. Eng. Dept., Univ. of Conn., Storrs Conn., 1962.

66. Hickling, R. and Plesset, M. S., The Collapse of a Spherical Cavity in a Compressible Liquid, Calif. Inst. Tech. Rpt. No. 85-24, Pasadena, Calif., 1963.

67. Kirkwood, J. G. and Bethe, H. A., The Pressure Wave Produced by an Underwater Explosion, I, OSRD No. 588, 1942.

68. Cole, R. H., Underwater Explosions, Princeton Univ. Press, 1948.

69. Burdon, R. S., Surface Tension and the Spreading of Liquids, Univ. Press, Cambridge, 1949.

70. Fox, F. E. and Herzfeld, K. F., "Gas Bubbles with Organic Skin as Cavitation Nuclei", J. Acous. Soc. America, 26, No. 6, 1954.

71. Kemball, C., "On the Surface Tension of Mercury", Trans. Faraday Soc., 42, (1946) 526.

72. Nowak, E. S., A Rational Equation of State for Water and Water Vapor in the Critical Region, ASME Paper No. 63-HT-35.

73. Oldroyd, J. G., "Complicated Rheological Properties", in Rheology of Disperse Systems, C. C. Mill (editor), Pergamon Press, New York, (1959) 1-15.

74. Bridgman, P. W., "The Effect of Pressure on the Viscosity of Forty-three Pure Liquids", Proc. Am. Acad. Arts Sci., 61, No. 3, (1926) 57-99.

75. Suciu, S. N., Zoss, L. M. and Sibbitt, W. L., The Solubility of Nitrogen and Hydrogen in Water, ASME Paper No. 53-A-64, 1953.

76. Caw, W. A. and Wylie, R. G., "Effect of Dissolved Air on the Viscosity of Water", Nature, 198, (1961) 995-996.

77. Lamb, Ref. 15, pp 571-578.

78. Tisza, L., "Supersonic Absorption and Stokes' Viscosity Relation", Phy. Rev., 61, (1942) 531-536.

79. Liebermann, L. N., "The Second Viscosity of Liquids", Phy. Rev., 75, (1949) 1415-1422.

80. Karin, S. M. and Rosenhead, L., "The Second Coefficients of Viscosity of Liquids and Gases", Revs. Modern Phys., 24, (1952) 108-113.

81. Eckart, C., "Vortices and Streams Caused by Sound Waves", Phys. Rev., 73, (1948) 68.

82. Litovitz, T., "Properties of Matter. The Liquid State", J. Acous. Soc. America, 30, (1958) 383-384.

83. Hammitt, F. G., Cavitation Damage and Performance Research Facilities, ORA Technical Report No. 03424-12-T, Laboratory for Fluid Flow and Heat Transport Phenomenon, Nuc. Eng. Dept., Univ. of Mich., 1963.

84. Fitzpatrick, H. M. and Strasberg, M., "Hydrodynamic Sources of Sound", Chap. X in Naval Hydrodynamics, Publication 515, Nat'l. Academy of Sciences, Nat'l. Res. Council, (1957) 247-276.

85. Benjamin, T. B., in Proc. Second Symp. on Naval Hydrodynamics, (1958) 207-233.

86. Maxwell, J. C., "On the Dynamical Theory of Gases", Phil. Trans., clvii, 49 (1866) also Papers, 2, p. 26.

87. Galler, B. A., Notes on the Runge-Kutta Methods for Numerical Solution of Ordinary Differential Equations, Univ. of Mich. Computing Center, 1960.

88. Gill, S., "A Process for the Step-By-Step Integration of Differential Equations in an Automatic Digital Computing Machine", Proc. Cambridge Phil. Soc., 47, (1951) 96-108.

89. International Critical Tables, IV, as quoted in Ref. 69, p. 10.

90. Streeter, V. L., Fluid Dynamics, McGraw Hill Book Co., New York, 1948.

91. Gongwer, C. A., Aerojet Gen'l Corp., Azusa, Calif., in discussion to Ref. 85, and also personal communication of film to F. G. Hammitt, the Univ. of Mich.

92. Hammitt, F. G., Liquid-Metal Cavitation -- Problems and Desired Research, ASME paper 60-HYD-13, 1960.

93. Parkin, B. R. and Kermeen, R. W., The Roles of Convective Air Diffusion and Liquid Tensil Stresses During Cavitation Inception, Presented at the IAHR Symp. on Cavitation and Hydraulic Machinery at Sendai, Japan, Sept. 3-8, 1962.